The European Cancer Stem Cell Research Institute
Y Sefydliad Ymchwil Bôn-gelloedd Canser Ewropeaidd

Characterising the role of *Cbx3*/HP1γ in Normal Intestinal Homeostasis and Tumorigenesis

Ka Ian Lio

Thesis submitted for the degree of

Doctor of Philosophy

European Cancer Stem Cell Research Institute

Cardiff University, United Kingdom

March 2015

Declarations

This work has not previously been accepted in substance for any degree and is not concurrently submitted in candidature for any degree.

Signed …… (candidate) Date ……

STATEMENT 1

This thesis is being submitted in partial fulfillment of the requirements for the degree of PhD.

Signed …… (candidate) Date ……

STATEMENT 2

This thesis is the result of my own independent work/investigation, except where otherwise stated. Other sources are acknowledged by explicit references.

Signed …… (candidate) Date ……

STATEMENT 3

I hereby give consent for my thesis, if accepted, to be available for photocopying and for inter-library loan, and for the title and summary to be made available to outside organisations.

Signed …… (candidate) Date ……

STATEMENT 4: PREVIOUSLY APPROVED BAR ON ACCESS

I hereby give consent for my thesis, if accepted, to be available for photocopying and for inter-library loans **after expiry of a bar on access previously approved by the Graduate Development Committee.**

Signed …… (candidate) Date ……

Acknowledgements

This PhD study has been an amazing journey that has given me the opportunities to experience intellectual, professional and personal growth. There are so many people I would like to thank and express my sincere gratitude to because without their help and support this PhD thesis would not have been possible.

To My Supervisors

First of all, I would like to express my deepest thanks to Dr. Karen Reed, who is not only my supervisor but also my friend, for all of her invaluable help and support (both academic and emotional) since I started my PhD. She has inspired me not only to be a good scientist in the lab, but also in the public. I have benefited greatly from participating in Karen's public engagement events and she has been a source of inspiration in encouraging me to be creative in teaching science to public. Karen is like a compass that activates the magnets of curiosity and knowledge, or perhaps I should say she is like a 'human' Olympic relay torch, lighting up the passion towards science in our next generations. I also would like to give a heartfelt thanks to my secondary supervisor Professor Alan Clarke for all his invaluable and constructive advices in my research. A lab meeting or a brief conversation with Alan would reinvigorate my enthusiasm for science immeasurably. I feel incredibly privileged and deeply honoured to have both wonderful supervisors like Karen and Alan in my life.

To My Colleagues

My acknowledgements also go to former and current members of ARC lab, Madeleine Young, Liliana Ordonez, Joanna Krzystyniak, Sophie Wang, Valerie Meniel, Trevor Hay, Victoria Marsh, Mark Bishop, Mattew Zverev, Boris Shorning, James Mattews, Kirsty Greenow, Lee Parry, Aliaksei Hollik and Meera Raja. This thesis owes much to this outstanding group of scholars and I am very lucky to have the opportunity to be a part of this big family. They are all very supportive, passionate, dedicated, talented, and knowledgeable – in short, they were all amazing colleagues to be with in every sense. I also would like to thank my CUROP summer student Keziah Rose and my final year project student Katharine Weetman for helping me alleviating some of my workloads. They provided me with opportunities to learn how to deliver complicated ideas clearly and they made my time in the lab more joyful and productive. I am very grateful to them for all of their help.

To My Financial Supporters

I would like to thank Tenovus scholarship for sponsoring my PhD research and providing me with generous financial support to attend conferences. I particularly would like to thank Anita Howman for organising various communication events, including Tenovus Communication meeting and the Tenovus Conference, providing invaluable learning and teaching experiences that I believe would be useful for life. I also gratefully acknowledge the postgraduate scholarship funding received towards my PhD writing up period from the Tertiary Education Services Officer, Macau Government. Finally I would also like to thank The British Association for Cancer Research (BACR) and European Association for Cancer Research (EACR) for providing me with bursaries to attend various conferences.

To My Friends

I wish to thank all my friends who have supported me over the last few years: Ling Yue, Xin Lewis, Minae Yoshida, Hayley Chan, Fion Si Kei Lai, Cherry Li, Dr. Shun Ming Yuen, Dr. Rhiannon French, Ikran Abdi Abshir, Jin Huang, Dr. Lei Shi, Ian Walker, Jo Walker, Simon Ewens, Dr. Jamal Ibrahim, Dr. Ricky Sharma, Prof. Barbara Pedley, Dr. Susan Short, Dr. Nita Maihle, Dr. Katerina Politi and so many have helped and supported me, on so many levels, and I hope they will forgive me for not mentioning them all by name.

I must acknowledge with tremendous gratitude to my remarkable friend Dr. Jikta Soukupova, she is someone who could see the truth and pain in me and never leave my side. Thanks Jitka for all her unconditional kindness, constant support and encouragement, and insightful advice over the past few years.

I also owe a deep thank you to Dr. Marisa Alcaide who has taught me to look at life from a different perspective, who and what are truly important in my life and thank her for all her love, passion, wisdom and help.

I also must express my deep gratitude to my University soul mate Shiyi Wang for walking this academic path with me by my side from the beginning; together we have made all our summer research internships and this entire PhD journey possible.

I also must thank my life soul mate Philip Tsu Lap Law for being the sunshine and cheerleader of my life. I am very grateful that he has seen me through the ups and downs of this roller coaster PhD journey and I owe him huge thanks not only for taking care of me during this writing up period, but also for being such a wonderful soul mate, and for his constant and unwavering support.

I would also like to thank Kelson Ho, Alex Seven Wong, Lu Chan and Zoe Chio who have been incredible and caring friends to me over the last decade. Having friends like these made everything possible and I have been touched and honoured by their willingness to share their life experiences and valuable opinions with me. Also, their spiritual support has made all the difference.

To My Family

I have been blessed with a very loving, caring, warm, helpful and supportive family. My beloved grandmother, Yao Lan, took intense care of my mum before my arrival to earth and she had been a source of constant and unconditional love and spiritual support for as long as I could remember. She always stressed the importance of education since I was young and in some unconscious way, this respect for education shaped my values and made me the person that I am today.

I am also grateful to my beloved mother, Rica In Fong Leong and the two important men in my life: my brother Alan Wai Hou Lio and my boyfriend David Hok for their unconditional love, support and encouragement. This journey would not have been possible without the support of my family. My mother, the person who has been the strong positive role model in my life, who has been a constant and consistent source of love, strength, support and encouragement throughout my life. She has been striving her best to work extremely hard in Macau just for my brother's and my overseas education in the U.K., I really deeply appreciate all the sacrifices that my mum has made for me. There is a Chinese saying 《親恩深似海，母愛重如山》 that is literally translated as 'Family love is profound as a deep sea, Motherhood is heavy as a mountain'. This is one of my favorite Chinese sayings that closely describe the importance of my family to me. Although no words could be used to express how thankful I am for everything my mother has done for me and she is a true gift that I could never repay. As for my brother, I also find it difficult to express my appreciation because it is so boundless. He is my most important source of joy and laughter; he is my best friend; he is my cheerleader; he is my dream-rekindler; and he

is an amazing brother. I have learnt so much from my dear brother and I appreciate all of his kindness, care, love, supports and encouragements. Finally, it is a pleasure to express my deep and sincere gratitude to my beloved boyfriend David Hok for coming into my life and all his enthusiastic supports, unconditional love and much more. I am grateful to have him always being there for me and he has taught me that trust and love cannot be found, but built. Lao Tzu once said: 'Being deeply loved by someone gives you strength, while loving someone deeply gives you courage'. I see in David both my strength and courage. Let's embrace our present, with lessons learnt from yesterday and dreams planned for tomorrow. Family love will forever be the fuel of my life. Thanks for sharing this life journey with me and this thesis is dedicated to my family.

Table of Contents

List of Figures

List of Tables

Abbreviations and Definitions

Symbols	
°C	Degrees Celsius
µg	Micrograms
µl	Microlitres
µm	Micrometer
µM	Micromolar
A	
Ab	Antibody
ABC	Avidin-Biotin Complex
Apc	Adenomatous Polyposis Coli
Ascl2	Achaete Scutelike 2
Apc^{MIN}	Multiple Intestinal Neoplasia (MIN) mutation of the Adenomatous polyposis coli gene
Axin	Axis Inhibitor
B	
Beta-Gal	Beta-Galatosidase
Bmi-1	B-lymploma Mo-MLV insetion region 1 polycomb ring-fiber oncoprotein
BMP	Bone Morphogenic Protein
bp	Base pair
BrdU	5-Bromo-2-deoxyuridine
BSA	Bovine Serum Albumin
C	
CBC cells	Crypt Base Columnar cells
CBX	Chromobox protein homolog
cDNA	Complimentary deoxyribonucleic acid
CK	Casein kinase
Cm	Centrimetres
c-Myc	Cellular-Myelocyomatosis oncogene
CRC	Colorectal Cancer
Cre	Causes recombination
$CreER^T$	Causes recombination-Estrogen receptor fusion transgene
C_T	Cycle time
D	
DAB	3,3'-diaminobenzidine
ddH_2O	Double distilled water
dH_2O	Deionised water
Dhh	Desert Hedgehog
DNA	Deoxyribonucleic acid
DNase	Deoxyribonuclase
Dsh	Dishevelled
DTT	Dithiothretinol
E	
E-cadherin	Epithelial Cadherin
ECL	Electrochemiluminescence
EDTA	Ethylenediamine Tetra-acetic Acid
EpCAM	Epithelial Cell Adhesion Molecule
ER	Estrogen Receptor
Erk	Extracellular regulated MAP kinase
F	
FAP	Familial Adenomatous Polyposis
FBS	Foetal Bovine Serum
G	
GEF	Guanine Nucleotide Exchange Factor
GSK-3	Glycogen Synthase Kinase-3
Gli	Glimoa-associated oncogene homolog
GTP	Guanosine Triphosphate
GTPase	Guanosine Triphosphatase
H	
H&E	Haematoxylin and Eosin
HDAC1	Histone deacetylase 1
Hh	Hedgehog
HNPCC	Hereditary Nonpolyposis Colorectal Cancer
HP1	Heterochromatin Protein 1
hr	Hour
HRP	Horseradish peroxidase
I	
Ig	immunoglobulin
IHC	Immunohistochemistry
Ihh	Indian hedgehog

IP	Intraperitoneal
ISC	Intestinal stem cell
J	
JPS	Juvenile Polyposis Syndrome
K	
KDa	Kilodaltons
Kg	Kilograms
K-Ras	Kirsten Rat sarcoma viral oncogene homolog
KS	Kolmogorov-Sirnov
L	
l	Litre
Lgr5	Leucine-rich repeat-containing G-protein coupled receptor 5
LOH	Loss of heterozygosity
LoxP	Locus of crossover of Bacteriophage P1
LRP	Low density lipoprotein receptor related protein
M	
M	Molar (moles per litre)
mAb	Monoclonal antibody
MAPK	Mitogen Activated Protein Kinase
MEK	Mitogen Acitvated Erk Kinase 1/2
mg	milligrams
Min	Minutes
miRNAs	Micro-RNAs
mm	Millimetre
MMR	Mismatch Repair
MSI	Microsatellite instability
MSH2	MutS E.Coli homolog of 2
mRNA	Messenger Ribonucleic Acid
N	
NCID	Notch Receptor Intracellular Domain
NFκB	Nuclear Factor of kappa light polypeptide gene enhancer in B-cell
NGS	Normal Goat Serum
NRS	Normal Rabbit Serum
O	
Olfm4	Olfactomedin 4
O/N	Overnight
P	
pAb	Polyclonal antibody
pAkt	Phosphor-Akt
PBS	Phosphate Buffered Saline
PBS/T	0.1% TWEEN-20 in Phosphate Buffered Saline
PCR	Polymerase Chain Reaction
PI	Post induction
PKA	Protein Kinase A
PI3K	Phosphatidylinositol 3-kinase
PLL	Poly-L-Lysine
Ptch	Patched
PTEN	Phosphatase and Tensin homolog mutated on chromosome ten
PVDF	Polyvinylidene difluoride
Q	
qRT-PCR	Quantitative Reverse-transcription PCR
R	
Ras	Rat sarcoma viral oncogene homolog
RNA	Ribonucleic Acid
RNase	Ribonuclease
RPM	Revolutions Per Minute
RT	Room Temperature
S	
SD	Standard deivation
SDS	Sodium Dodecyl Sulphate
SDS-PAGE	Sodium Dodecyl Sulphate-Polyacrylamide Gel Electrophoresis
Sec	Seconds
Shh	Sonic hedgehog
siRNA	Small interfering RNA
Smo	Smoothened
T	
TA cells	Transit-Amplifying cells
TACE	Tumour Necrosis Factor Converting Enzyme

TBS	Tris Buffered Saline
TBS/T	Tris Buffered Saline with TWEEN-20
TCF	T-cell factor
TCF-4	Transcription factor 4
Tcf/Lef	T-cell factor and Lymphoid enhancer factor
TEMED	N,N,N,N-Tetramethylethylenediamine
	Tetracycline
TGF-β	Transforming Growth Factor-β
TTM	Non-fat milk powder in Tris buffered saline containing 0.1% TWEEN-20
V	
V	Volts
VillinCreERT	Villin Cre recombinase ER transgene
v/v	Volume per Volume
W	
W	Watts
w/v	Weight per Volume
WT	Wild Type
Wnt	Wingless-type murine mammary tumour virus integration site family
X	
x g	Times gravity
X-Gal	5-bromo-4-4-chloro-3-indolyl beta-D-galatopyranoside

Abstract

Epigenetic modifications are being increasingly recognised to contribute to colorectal cancer formation. Emerging evidence has demonstrated that HP1γ (coded by the gene *Cbx3*) has an important role in carcinogenesis by regulating several mechanisms, such as heterochromatin formation, gene silencing and DNA replication and repair. The aim of this study was to characterise the role of HP1γ in normal intestinal homeostasis and cancer progression.

The *Cbx3* gene was conditionally deleted in the murine small intestinal epithelium under normal intestinal homeostasis and in the context of aberrant Wnt signalling using transgenic mouse models. Furthermore, the long-term consequence of *Cbx3* loss in Wnt-driven tumorigenesis was examined using a mouse model possessing a heterozygous mutation of the *Apc* gene.

The results presented in this thesis demonstrate that *Cbx3* has subtle effects on the histone epigenome, although these do not confer any noticeable manifestation in intestinal homeostasis. Upon aberrant Wnt-activation, *Cbx3* loss resulted in prolonged survival potentially via attenuation of Wnt activation at the receptor level and RNA splicing defects. Furthermore, the long-term *Cbx3* deficiency accelerates both Wnt-driven tumour development and progression, and reduces survival of male mice with heterozygous loss of *Apc.* Additionally, marked epigenetic alternations were observed in association patterns of HP1γ and the heterochromatin markers (H3K9me3 and H4K20me3) between wild-type and *Apc*-deficient intestines, suggesting the multifaceted roles of HP1γ in maintaining a gene-repressive environment in heterochromatin for normal intestinal homeostasis, and providing a gene permissive environment in euchromatin for carcinogenesis.

The findings of this study demonstrate for the first time the functional versatility of HP1γ in intestinal homeostasis and tumorigenesis. *Cbx3* plays a novel role in positive regulation of Wnt signaling and RNA splicing in the aberrant Wnt-activated intestine and a role in heterochromatin formation and gene silencing in long-term Wnt-activated tumorigenesis. These data contribute to the body of knowledge how colorectal cancer progresses and provide a critical foundation for further investigation of the role of HP1γ in Wnt signaling, RNA splicing, tumour progression, and its interaction with histone marks in mouse models of colorectal cancer.

Chapter One

General Introduction

1. General Introduction

1.1. The Mammalian Small Intestine

1.1.1. General Intestinal Morphology and Physiology

The mammalian digestive tract consists of the mouth and salivary glands, the stomach, the small intestine, the liver, the pancreas, the gallbladder and the large intestine. The main function of the digestive tract is to enable nutrients from consumed food and beverages to gain access to the circulatory system and the body. The gastrointestinal tract, the largest part of the digestive tract, is comprised of the stomach and the intestines. The stomach acts as a short-term storage reservoir for consumed food and serves the function of mechanical processing mixing with hydrolytic enzymes, pH change and digestion (Guyton A.C., 1996).

The mammalian intestine is divided anatomically into two major parts – the small and large intestines. The small intestine is comprised of three regions: the duodenum, jejunum and ileum. Apart from the two papillae that serve as entry points for pancreatic and bile ducts and the presence of the mucus-secreting Brunner's glands in the submucosa of the duodenum, all three regions of the small intestine share a similar structure. The wall of the intestine is structured into four layers: serosa, muscle layers, submucosa and mucosa (as illustrated in Figure 1.1) (Crane, 1968).

The outermost layer of the intestine is represented by the serosa, which is composed of visceral peritoneum merging with connective tissue. Secondly, the muscularis externa is comprised of a thin outer layer of longitudinal muscle and a thicker inner region of circular muscle. Thirdly, the submucosal layer consists of connective tissues, blood vessels and lymphatics. Last but not least, the mucosal layer is composed of a muscularis mucosae, a lamina propria and the simple columnar epithelium. The small intestine incorporate three modifications that account for its 600-fold increased absorptive surface area. Firstly, both mucosa and submucosa are formed into plicae circulares (circular folds) perpendicular to the intestinal axis. Secondly, the surface of the mucosa is organised into finger-like projections called villi. At the base of the villi, the epithelium forms pocket-like invaginations into the lamina propria termed crypts of Lieberkuhn (intestinal crypts). Lastly, the apical

membrane of the absorptive columnar epithelium lining the surface of villi forms microscopic cytoplasmic protrusions called microvilli, forming the brush border of the small intestine and further increasing the epithelial surface area. Progressing from the duodenum towards the ileum, the thickness of the intestinal wall and the number of the circular folds decrease, so does the density and the size of the villi. In contrast, the Peyer's patches containing lymph nodes in the ileum are larger and more numerous than those of the duodenum and jejunum (Guyton A.C., 1996).

The primary function of the small intestine is to facilitate digestion of consumed food and nutrient absorption. The majority of the water, electrolytes, vitamins and minerals are absorbed in the small intestine (primarily in the duodenum and jejunum) while the remaining is absorbed in the large intestine. The large intestine consists of four regions: the caecum, colon, rectum and anal canal. The colon is the largest part of the large intestine. The mucosa of the large intestine differs from the small intestinal mucosa through the absence of circular folds and villi. The colonic mucosa is organised into crypts similar to those found in the small intestine. However, there is a shift of cell type abundance between small and large intestine. Absorptive cells predominate in the small intestine whereas the mucus-secreting cells incorporate the majority of the large intestinal epithelium (Pitman and Blumberg, 2000).

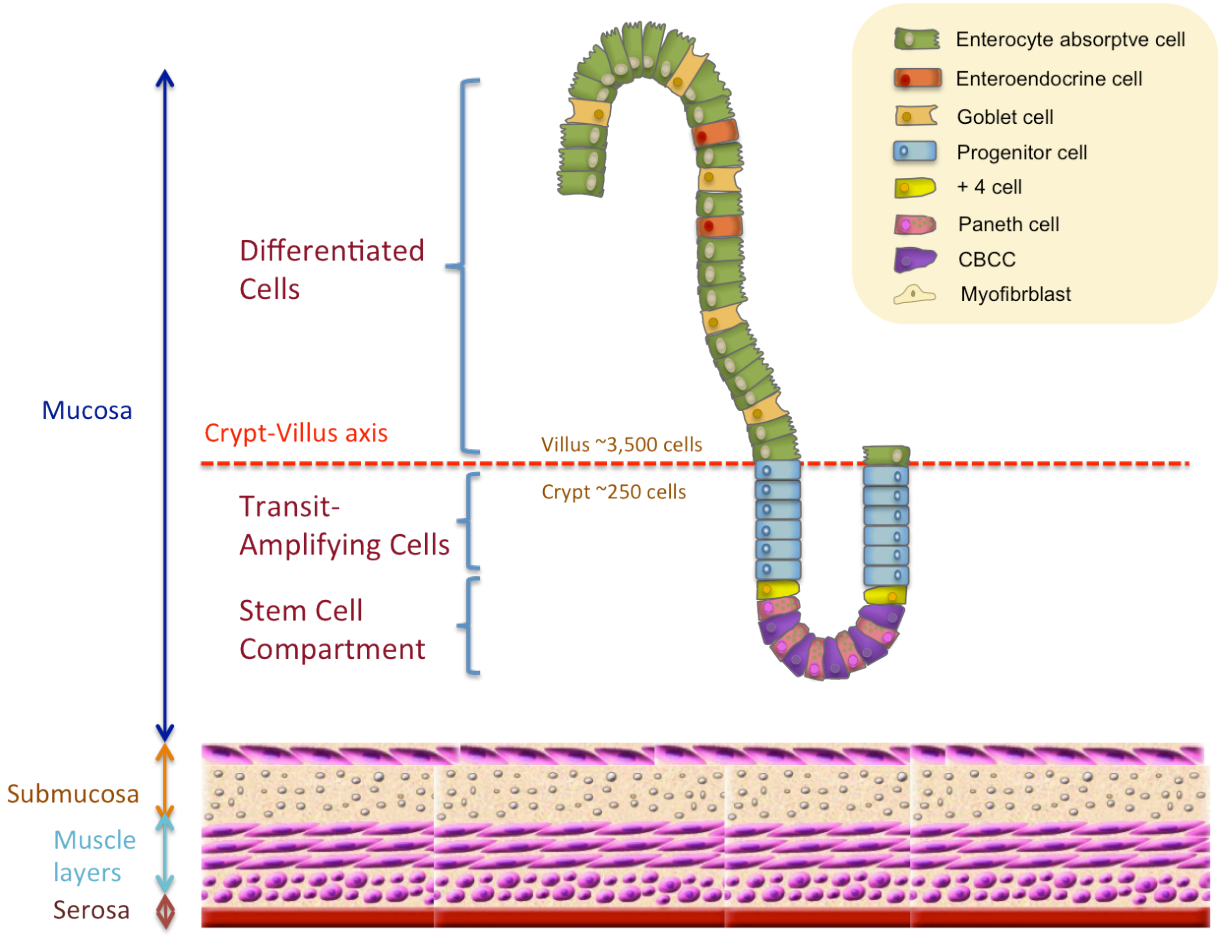

Figure 1.1: Schematic representation of the crypt-villus unit in the small intestine.
The outermost layer of the intestine is represented by the connective tissue of the serosa. Underneath the serosa, the muscle layers surrounding the submucosa composed of connective tissue containing blood vasculature and nerves. The mucosa is composed of a muscularis mucosae, a lamina propria and the simple columnar epithelium.

1.1.2. Histology of the small intestinal epithelium

As mentioned in the previous section, the primary function of the small intestine is to facilitate nutrient absorption and therefore, the epithelium is organized into distinct crypt-villus structure to maximise the surface area for absorption (Figure 1.1). Both lysozyme-producing Paneth cells and intestinal stem cells reside within the base of crypts. The intestinal stem cells are capable of self-renewal and also give rise to the transit-amplifying (TA) cells, which function to rapidly expand epithelial renewal and initiate lineage differentiation. The differentiated cell lineages consist of absorptive enterocytes, mucin-secreting goblet cells, hormone-producing enteroendocrine cells and anti-microbial secreting Paneth cells. Apart from downward migrating Paneth cells, the differentiated cells are in continual upward migration towards the apex of the villus where they undergo apoptosis and are exfoliated within 4 to 8 days (Cheng, Merzel and Leblond, 1969; Hall *et al.*, 1994). As a result of the continuous migration towards the villus apex, the entire intestinal epithelium is renewed every 5 days in humans and every 3 days in mice (Marshman, Booth and Potten, 2002).

The mucosa of the small intestine is lined by a simple columnar epithelium that consists primarily of enterocytes representing the absorptive lineage, with scattered goblet, enteroendocrine and Paneth cells constituting the secretory linages (as illustrated in Figure 1.1).

The majority of the cells in the villus (80%) are represented by the only member of the absorptive lineage – enterocytes. They are positioned along the top of the crypt and over the whole of the villus and are actively renewed with an average turnover time of 3 days. The enterocyptes are characterised by the presence of a tight array of microvilli on their apical membrane that constitute a brush border, which facilitate the final stages of digestion and provides a site of attachment for pathogens (Cheng and Leblond, 1974; Cheng, 1974). The apical and basal membranes of the enterocytes contain various channel proteins responsible for transporting nutrients from the intestinal lumen into the blood and lymphatic vasculature, while also transporting certain ions into the lumen (Smith, 1992).

The second most abundant cell types in the small intestinal epithelium are goblet cells, which are the most abundant cell type in the secretory lineage. Mature goblet cells

are scattered among the enterocyptes from mid-crypt to the villus apex and are renewed at a similar turnover rate to that of the enterocytes (Troughton and Trier, 1969). Goblet cells are distinguished by the presence of large mucus containing granules and enlarged rough endoplasmic reticulum. The mucus secreted by the goblet cells serves as a lubricant for promoting movement and effective diffusion of gut contents, and protecting the lining of the intestine from mechanical abrasion or damage by acidic stomach contents and auto-digestion by the digestive enzymes (Cheng and Leblond, 1974).

The Paneth cells represent the second most abundant member in the secretory lineage. They are located at the base of the crypts and they differ from all the other mature cell types in their downward migration, maintenance of active Wnt signalling and slower turnover time of 57 days (Ireland *et al*., 2005). The Paneth cells are distinguished by the presence of a large number of apical secretory granules that contain a number of substances with antimicrobial activity and therefore they are considered to play a critical role in the regulation of the intestinal microflora. Previous studies suggested that Paneth cells provide a niche for the intestinal stem cells (Sato *et al.*, 2011).

The enteroendocrine cells represent less than 1% of the terminally differentiated cells in the intestinal epithelium and consists a family of at least 15 different cell types. These cells differ in the morphology of their secretory granules and the unifying feature of all the enteroendocrine cells is expression and secretion of a range of polypeptide hormones that regulate secretion into the gastrointestinal tract (Hocker and Wiedenmann, 1998).

In addition to the main cell types, two minor cell lineages are present in the small intestinal epithelium. Firstly, Membranous or Microfold (M) cells are located in the epithelium adjacent to the Payer's patches. Their basolateral membrane forms invaginations occupied by the immune cells: macrophages, T and B-lymphocytes. M cells are able to internalise particles and microorganisms from the lumen by phagocytosis and transport them across the epithelial border, where they are processed by the immune cells (Neutra, Frey and Kraehenbuhl, 1996). Secondly, Tuft cells (also known as brush or fibrillovesicular cells) are scattered throughout the gastrointestinal tracts. They are characterised by a goblet-shaped body, the presence of long microvilli on the apical membrane and vesicles in the apical cytoplasm. Although their role in the small intestine is still undefined, the

abundance of the vesicles in the cytoplasm indicates that tuft cells may be involved in the secretion or absorption of certain substances (Sato, 2007).

1.1.3. Maintenance of the small intestinal homeostasis

The intestinal homeostasis has a critical function within this perpetually renewing tissue, the balance of proliferation, cell death, differentiation, migration and cell positioning must be closely regulated in order to ensure the proper maintenance and function of the intricate cellular architecture described previously. Regulation of these processes is precisely orchestrated by a number of important signalling pathways, including Wnt signalling, Notch/Delta signalling, transforming growth factor-beta (TGFβ) and bone morphogenetic protein (BMP) signalling, and Hedgehog signalling. Each of these pathways and the role they play in maintaining the intestinal homeostasis are briefly described in this section (also see Figure 1.2).

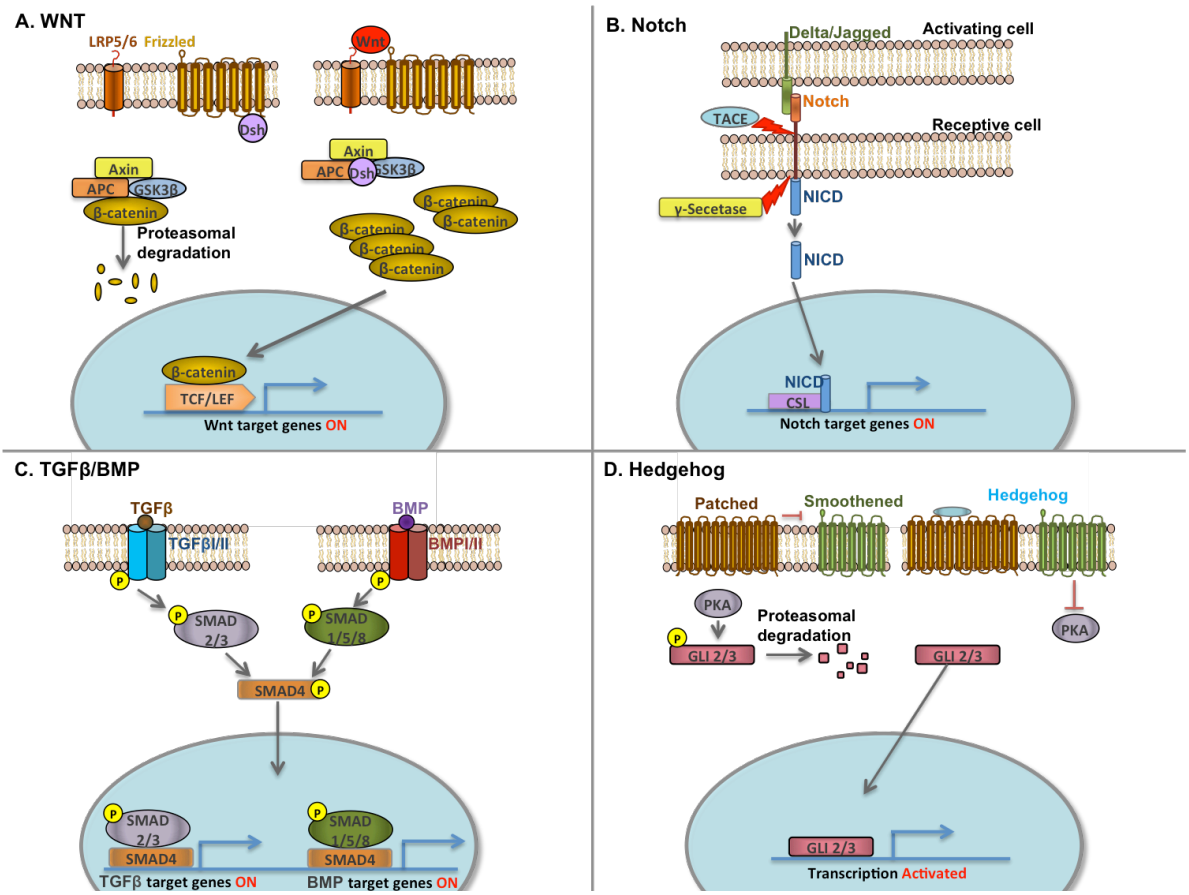

Figure 1.2: The main signalling pathways regulating homeostasis of the intestinal epithelium.
A: Wnt signalling. In the absence of Wnt ligand, β-catenin destruction complex is formed consisting of Axin, Apc and GSK3β, which binds β-catenin and mediates its phosphorylation and proteasomal degradation. In the presnce of Wnt ligand, Wnt ligand binds to Frizzled receptor and LRP5/6 co-receptor results in activation of Dishevelled (Dsh) and phosphorylation of LRP5/6, which together inhibit the β-catenin destruction complex, allowing accumulation and translocation of β-catenin to the nucleus, where it docks on TCF/LEF factors and activates transcription of Wnt target gene expression. B: Notch signalling. Binding of notch receptor cell surface ligands of the Delta/Jagged family stimulates cleavage of the Notch receptor by TACE and γ-secretase. Cleavage by γ-secretase releases the notch intracellular domain (NICD), which translocates to the nucleus and binds to transcription factor CSL to activate expression of Notch target genes. C: TGFβ/BMP signalling. TGFβs or BMPs bind to their type I/II receptors, resulting in phosphorylation of the type I receptor. TGFβ signals through SMAD2/3 and BMP signals are transduced through SMAD1/5/8. Both result in activation of SMAD4, which translocates to the nucleus and modulates target gene expression. D: Hedgehog signalling. In the absence of Hedgehog ligands, unbound Patched receptors inhibit the Smoothened signal transducer, allowing PKA to phosphorylate GLI2/3 transcription factor, sequestering it away from the nucleus and targeting its cleavage. Binding of Hedgehog to Patched releases repression of Smoothened, which in turn suppressed PKA, thereby allowing full-length GLI2/3 to accumulate and translocate to the nucleus, where it activates target gene expression.

1.1.3.1. The canonical Wnt pathway

The β-catenin-dependent pathway, referred to as the canonical Wnt signalling pathway, plays a key role in regulation of morphology, proliferation, motility and cell fate (Archbold *et al.,* 2012). The canonical Wnt signalling pathway was discovered by genetic analysis in Drosophila (Rijsewijk *et al.,* 1987), and subsequently, this signaling cascade was found to be highly conserved between Drosophila and vertebrates (Miller and Moon, 1996). Mutations and epigenetic alternations of this pathway lie at the heart of many human diseases, including colorectal cancer.

Wnt signalling in adult intestine regulates the fine balance between stem cell maintenance and differentiation. Figure 1.2A shows a schematic representation of the canonical Wnt signalling pathway. In the absence of a Wnt ligand, the tumour suppressor proteins adenomatous polyposis coli (APC) and axis inhibitor (Axin) form the scaffold of the destruction complex and bind free β-catenin enabling its phosphorylation by Casein Kinase 1 (CK1) at the Ser45 residue (Amit *et al.,* 2002; Liu *et al.,* 2002). Subsequently, Glycogen synthase kinase-3β (GSK3β) in the Axin complex phosphorylates β-catenin (Rubinfeld *et al.*, 1996) which is then recognised by the E3 ubiquitin ligase β-transducing repeat-containing protein (β-TrCP), which triggers the ubiquitination of β-catenin and its subsequent degradation by proteasomes, reducing the level of cytosolic β-catenin (Hart *et al.*, 1999).

In the presence of a Wnt ligand, the signalling pathway is activated through the binding of the Wnt ligand to the seven transmembrane serpentine receptor, Frizzled (Huang and Klein, 2004), and low density lipoprotein receptor related protein (LRP5/6) complex (Pinson *et al*., 2000), activating the cytoplasmic protein dishevelled (Dsh). Dsh then inhibits the activity of the Axin complex ((β-catenin-APC)-GSK3β), GSK3β is no longer functional. The overall result is accumulation of cytosolic β-catenin (Tamai *et al*., 2004) and stabilized β-catenin will then translocate into the nucleus and bind to members of the T-cell factor (Tcf)/Lymphoid enhancing factor (Lef) family (Waterman, 2002). In a Wnt-inactive cell, Tcf proteins are associated with general transcriptional repressors, such as Groucho, and repress the expression of Tcf-reponsive genes (Roose *et al*., 1998). On the activation of Wnt signalling, β-catenin binding of Tcf proteins displaces Groucho and leads to transcription of Wnt target genes (Daniels and Weis, 2005).

The canonical Wnt signalling pathway drives proliferation in the intestine and maintains homeostasis. A number of studies in which the Wnt signalling was inhibited at various points in the pathway, have demonstrated that loss of Wnt signalling perturbs normal intestinal structure and proliferation. Transgenic ectopic overexpression of the Wnt antagonist *Dickkopf-1* (Dkk1) in adult small intestine resulted in reduced proliferation and loss of all the secretory cell lineages, and a rapid degeneration of the crypt-villus architecture (Pinto *et al*., 2003). Likewise, conditional homozygous deletion of β-catenin and the Wnt target gene cellular-Myelocytomatosis oncogene (*c-Myc*) in adult mouse intestine resulted in catastrophic disruption of normal intestinal homeostasis, with loss of proliferative zone and ablation of the crypts (Muncan *et al.*, 2006; Ireland *et al.,* 2004), Inhibition of Wnt signalling by deletion of Wnt transcription factor Tcf-4 in murine models resulted in loss of proliferation in embryonic intestines (Korinek *et al*., 1998). These studies highlight the importance of Wnt signalling in controlling cell proliferation and guiding progenitor cells towards the secretory lineage.

In a similar but opposite fashion, aberrant activation of the Wnt pathway by deletion of *Apc* or by overexpression of a dominant stable form of β-catenin have resulted in dramatic increase in proliferative cells within the crypt, coupled with a complete block in cell migration and impaired apoptotic response (Sansom et al., 2004; Harada *et al*., 1999). The same studies have shown that activation of Wnt signalling by deletion of *Apc* impairs cell migration along the crypt-villus axis, resulting in the proliferative zone being poorly organised and causing mis-localisation of Paneth cell throughout the crypt rather than restricted to the crypt base. Overall, aberrant activation of the Wnt signalling resulted in a general failure to differentiate as evident by the loss of all but Paneth cell differentiation markers (Andreu *et al.*, 2005). Together, these studies demonstrate that Wnt signalling plays a role in regulating cell proliferation, cell differentiation and directing cells towards the secretory lineage.

1.1.3.2. The Notch/Delta Pathway

Notch signalling plays a range of important roles in the homeostasis of self-renewing tissues, including regulation of apoptosis, proliferation, differentiation, spatial patterning and cell fate determination (Artavanis-Tsakonas, Rand and Lake, 1999). Notch signalling is a cell-to-cell signalling pathway, indicating that signal transduction can only occur between adjacent cells. The Notch signalling cascade is initiated by binding of the Notch cell surface receptors, Notch1 and Notch2 (coexpressed on stem cells and TA cells), to one of the Delta-like or Jagged family of membrane-bound ligands (expressed by Paneth cells) on an adjacent cell (Figure 1.2B). As a result of this receptor-ligand interaction, the Notch receptor undergoes two successive proteolytic cleavage events. The first cleavage takes place in the extracellular domain and is mediated by Tumour necrosis factor (TNF)-alpha-converting enzyme (TACE). The second cleavage occurs intracellularly within the trans-membrane domain and is carried out by γ-secretase. The second cleavage releases the Notch intracellular domain (NICD). The NICD then translocates to the nucleus where, together with the Notch downstream transcription factor CSL, it activates transcription of its target gene (reviewed in (Wilson and Radtke, 2006).

In the adult intestine, a number of studies have demonstrated the importance of Notch signalling pathway in intestinal homeostasis and maintenance of the undifferentiated state of TA cells. Conditional inactivation of the essential Notch transcription factor CSL in the mouse intestine results in complete loss of all proliferative cells within the crypt and their conversion into goblet cells. An identical phenotype was achieved by blocking Notch signalling with γ-secretase inhibitors (van Es *et al*., 2005).

In a reverse approach, excessive activation of Notch signaling by overexpression of a constitutively active form of NICD resulted in severe deficiency of secretory cell types in the intestine, while an expansion of the proliferative compartment was observed (Fre *et al.*, 2005). Together, these data suggests that Notch signalling is essential for maintenance of the crypt progenitors in the undifferentiated state within the crypt and for determination of the cell fate towards the absorptive lineage.

1.1.3.3. The TGF-β and BMP pathway

Transforming growth factor (TGF)-β signalling regulates a number of biological processes such as embryogenesis, wound healing, cell proliferation and differentiation (Sancho, Batlle and Clevers, 2004). Bone morphogenic proteins (BMPs) are part of the TGF-β superfamily. BMP signalling is known to play a role in development and maintenance of the intestinal epithelium. In addition, it is responsible for the regulation of the interaction between epithelial cell and the underlying mesenchyme (Ishizuya-Oka, 2005) (Figure 1.2C). Both TGF-βs and BMPs are soluble and extracellular signalling proteins. TGF-βs bind preferentially to TGF-β type II receptor, which then dimerise with type I receptor. Conversely, BMPs bind preferentially to BMP type I receptors, which then associate with the BMP type II receptor. In both cases, the type II receptors phosphorylate the cytoplasmic domain of the type I receptor which then recruits and phosphorylates members of Mothers Against Decapentaplegic homolog (SMAD) family of signal transducers. SMAD2 and 3 are preferentially phosphorylated by the TGF-β type I receptor, whereas BMP signalling the type I receptor recruits and phosphorylates SMAD1, SMAD5 or SMAD8. The SMADs that are recruited to the receptors and phosphorylated are collectively known as the Receptor associated SMADs (R-SMADs). The activated R-Smads then dissociate from the receptor and form a complex with SMAD4 (also known as co-SMAD), which then enables the translocation of the complex into the nucleus where these active SMAD complexes bind to TGF-β or BMP target genes and recruit regulatory proteins to the genes promoters to allow transcription (reviewed in Shi and Massague, 2003).

In the intestine, conditional deletion of the BMP type I receptor (BMPRI) in the epithelial cells of mouse intestine resulted in an increase in proliferation within the epithelium and development of intestinal polyps that were characterised by an expanded proliferative compartment (He *et al*., 2004). A further study overexpressed the BMP inhibitor Noggin in the submucosa around the crypt region of mouse intestine, thus blocking BMP signals from mesenchyme in this region, resulted in abnormal villus structure and the development of ectopic crypt structures (Haramis *et al*., 2004). These observations demonstrate that BMP signalling is important for interactions between overlying epithelium and underlying mesenchyme to coordinate the development of epithelial structures in the correct context.

1.1.3.4. The Hedgehog pathway

Hedgehog signalling plays an important role in a variety of biological processes, including embryonic development of the gastrointestinal tract, maintenance of tissue homeostasis, carcinogenesis and tissue repair (reviewed in van den Brink, 2007). Hedgehog signalling is governed by two transmembrane proteins called Patched and Smoothened (see Figure 1.2D). In the absence of Hedgehog proteins, the signalling pathway is inactive. Unbound cell surface receptor of Patched suppresses the activation of Smoothened. When Smoothened is inactive, protein kinase A (PKA) is able to phosphorylate the cytoplasmic transcription factor Glioblastoma-associated oncogene homolog (Gli)2/3, which serves to sequester Gli away from the nucleus, as well as to target its proteolytic cleavage and inactivation. There are three Hedgehog ligands found in vertebrates, Sonic hedgehog (Shh), Indian hedgehog (Ihh) and Desert hedgehog (Dhh). These are able to bind to Patched receptors and in doing so prevent the suppression of Smoothened, which when activated prevents the phosphorylation and subsequent partial degradation of Gli2/3. This leads to accumulation of full-length Gli, which then translocate to the nucleus and activate transcription of its target gene (reviewed in van den Brink, 2007).

In the small intestine, loss of either Shh or Ihh (both are expressed throughout the epithelium) results in gross malformation of the gut epithelium (Ramalho-Santos, Melton and McMahon, 2000). Loss of Shh results in overgrown villi in the duodenum suggesting an increase in proliferation whereas loss of Ihh results in reduced proliferation in the crypt region, disruption of the intestinal mesenchymal architecture and deterioration of the extracelluar matrix. In addition, loss of either Shh or Ihh results in post-natal lethality (Ramalho-Santos, Melton and McMahon, 2000). Together, these data imply Hedgehog ligands exhibit distinct roles in the small intestine. To explore the combined role of both Shh and Ihh ligands in adult intestinal homeostasis, complete abrogation of hedgehog signalling in the intestine by overexpression of the hedgehog inhibitor (Hhip) resulted in hyperproliferation of the epithelium with ectopic crypt development and abnormal branching of villi (Madison *et al.*, 2005). Thus, the secretion of Shh and Ihh in the crypt region, acts as paracrine signals for mesenchymal stromal cells to inhibit proliferation in the villus epithelium, highlighting the importance of epithelial-mesenchymal interactions in tissue homeostasis.

1.1.4. The small intestinal stem cell

The intestinal epithelium represents the most rapidly self-renewing tissues in adult mammals. The constant renewal of the epithelium is regulated and maintained by a population of intestinal stem cells, which give rise to all the intestinal epithelial cell lineages. By definition, stem cells are able to proliferate and self-renew indefinitely, while generating phenotypically diverse progeny specific to the given tissue (Potten and Loeffler, 1990). Considering how stem cells play a critical role in intestinal epithelial homeostasis, a better understanding of intestinal stem cell function and regulation will provide insights into intestinal pathologies.

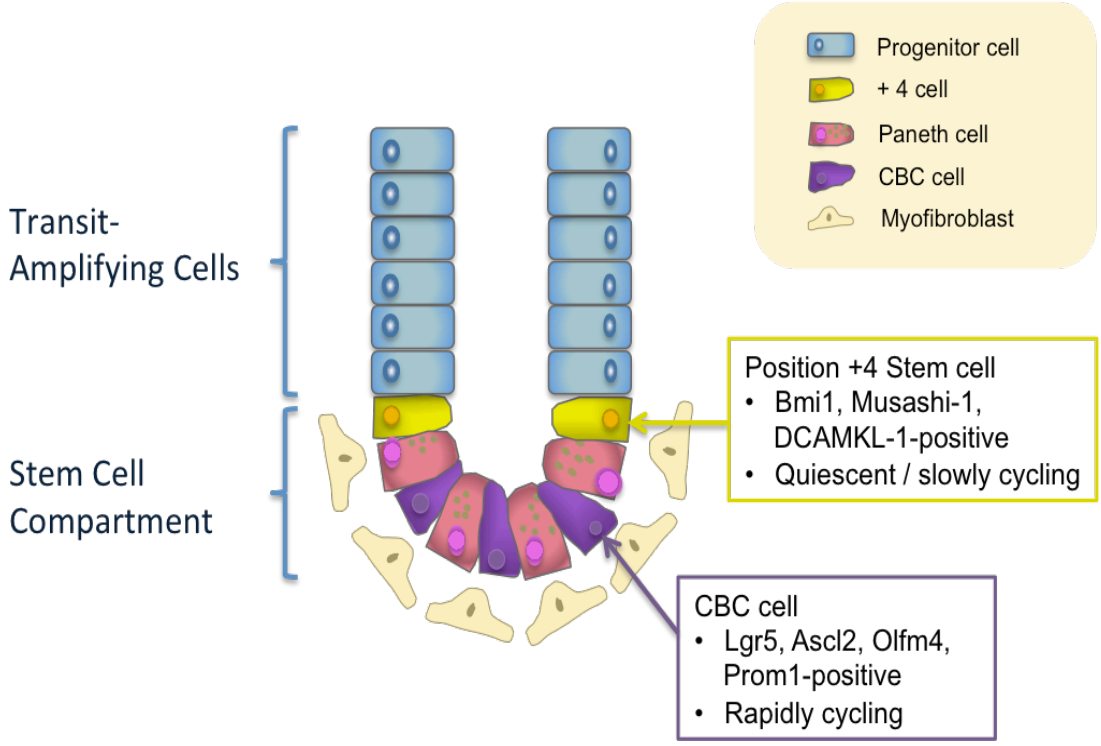

Figure 1.3: Schematic representation of the small intestinal crypt and candidate locations of the intestinal stem cell.
The small intestinal stem cell locations have been proposed to be the crypt base columnar (CBC) cell population and position +4 stem cell population. Putative markers of the intestinal stem cells have been proposed for both candidate locations (boxes). Paneth cells, mesenchymal cells and stromal components are proposed to constitute the stem cell niche.

1.1.4.1. Intestinal stem cell identify, marker and location

There has been much debate over the identity and location of the intestinal stem cell within the crypt (Figure 1.3). The historic views on the stem cell position within the crypt and identification of candidate intestinal stem cell markers will be discussed in this section.

A number of early DNA labelling studies have suggested that the intestinal stem cell is located approximately 4 cell positions from the base of the crypt, directly above the Paneth cell compartment. The rational for these experiments lies in the differential kinetics of cell proliferation and migration occurring within the crypt. Labelling of the replicating intestinal cells was achieved by using tritiated thymidine (^{3}HTdR) or Bromodeoxyuridine, which are incorporated into newly synthesized DNA of replicating cells during S phase of the cell cycle. This approach will label an expending stem cell population, as the stem cells are able to incorporate and retain the label due to their low proliferation rate. Conversely, TA cells rapidly proliferate and migrate out of the crypt and the label is rapidly diluted and lost. Thus, the slowly cycling label-retaining cells (LRCs) can be used to identify the position of the stem cell. Christopher Potten and colleagues revealed that the LRC is normally found at position +4, immediately above the Paneth cells. These cells cycled once a day on average, at half the rate of the rest of the rapidly proliferating crypt cells, and were therefore proposed as intestinal stem cells (Potten, 1974).

An alternative location for the intestinal stem cell was proposed in the same year as for the +4 position cells. This alternative position is within the slender cells intercalated between mature Paneth cells at crypt base, and is known as crypt base columnar (CBC) cells (Cheng and Leblond, 1974). This model proposes that cells below position 4 in the crypt are slowly cycling and capable to maintain an undifferentiated state. This study is further supported by a number of clonal analysis experiments that suggested the stem cell zone at positions 1-4 in the crypt base (Bjerknes and Cheng, 1981).

The ability to reliably identify and isolate intestinal stem cells would undoubtedly accelerate our understanding of stem cells roles in normal intestinal homeostasis and cancer. Many efforts have been focused on the identification of stem cell-specific molecular marker that would distinguish the stem cell from other cells in the crypt (proposed markers listed in Figure 1.3).

One of the first intestinal stem cell markers to be proposed was the RNA-binding protein Musashi-1. Musashi-1 has been found to be highly expressed in developing and regenerating crypts, as well as in adenomas of Apc^{MIN} mice (carrying a nonsense-mutation in codon 850 of *Apc* resulting in a truncated protein), all of which potentially contains expanded stem cell populations. However, expression of Musashi-1 has been shown to be high in both +4 and CBC intestinal stem cells as well as in early progenitor cells and therefore cannot be used exclusively as an intestinal stem cell marker (Potten *et al*., 2003).

The microtubule-associated kinase Doublecortin and Calmodulin-kinase like-1 (DCAMKL-1) has been proposed to mark more specifically to intestinal stem cell based on its ability to stain individual cells around +4 position (May *et al.*, 2008). However, a number of characteristics have undermined DCAMKL-1 being a specific marker for the intestinal stem cell. DCAMKL-1 positive cells were frequently found to be present among the villus cells, they were radiation-resistant and did not seem to contribute to crypt cell regeneration (May *et al.,* 2008). Furthermore, DCAMKL-1 positive cells expressed typical tuft cell markers, such as cyclooxygenase 1 and 2, and therefore DCAMKL-1 was in fact a marker of differentiated tuft cells rather than an exclusive stem cell marker of the adult intestine (Gerbe *et al.*, 2009).

The leucine-rich-repeat-containing G-protein-coupled receptor 5 (Lgr5) was identified as a candidate marker of the intestinal stem cell based on a screen of Wnt-target genes (Barker *et al.*, 2007). Localisation of Lgr5 revealed positively stained cells are confined to the crypt base and *Lgr5* expression specifically marks the CBC cell population. Barker and colleagues further investigated the functional properties of Lgr5-positive cells using an inducible Cre-recombinase transgene expressed under the control of the endogenous *Lgr5* promoter and the *LacZ* reporter allele. They demonstrated that the entire crypt-villus was populated with LacZ-expressing cells, suggesting that *Lgr5*-positive CBC cells are capable of generating all the cell lineages of the intestinal epithelium. This provides functional evidence that Lgr5-positive cells are intestinal stem cells as they are capable to maintain self-renewal and pluripotency for long periods of time. Three additional stem cell markers, Aschaete scute-like 2 (*Ascl2*), Olfactomedin-4 (*Olfm4*) and *CD133/Prominin1 (Prom1*), have been revealed based on a gene expression analysis of Lgr5-EGFP cells (van der Flier e*t al.*, 2009; van der Flier *et al*., 2009; Snippert *et al.,* 2009). *Ascl2* is a Wnt target gene that belongs to a member of the basic helix-loop-helix family of transcription factors; *Olfm4* encodes an anti-

apoptotic factor that associated with tumour growth, cell adhesion and metastasis whereas *Prom1* encodes CD133 protein, which is a cell surface marker of intestinal stem cells. Since all these genes (*Ascl2*, *Olfm4* and *CD133)* have been found to be co-expressed with *Lgr5* and therefore they have been established as highly specific and robust marker of *Lgr5*-positive CBC cells (Jubb *et al.,* 2006; Barker *et a*l., 2007; van der Flier *et al*., 2009; van der Flier *et al.*, 2009).

Despite the fact that Barker and colleagues provided convincing evidence of the nature of CBC stem cells, a study conducted by Sangiorgi and Capecchi (2008) demonstrated that *Bmi1* (the polycomb group oncogene) also marks true intestinal stem cells, but is mainly expressed in position +4 and +5 cells in the crypt, therefore adding a further layer of complexity to research aimed at identifying the key intestinal stem cell markers. The authors investigated the functional properties of *Bmi1*-positive cells using an inducible Cre-recombinase transgene expressed under the control of the *Bmi1* promoter and the Rosa26-*LacZ* or *Rosa26-YFP* transgene, they demonstrated that *Bmi1*-positive cells were capable of forming long-lived cell clones that contained all of the differentiated epithelial cell linages of the epithelium. Consistent with this, ablation of the stem cell population via selective expression of diphtheria toxin in *Bmi1*-positive cells resulted in a complete loss of crypt structures (Sangiorgi and Capecchi, 2008). Therefore, these studies provide robust evidence that *Bmi*-expressing cells play a crucial role in the repopulation of the crypt-villus.

The current understanding proposes that *Lgr5* specifically marks the rapidly dividing CBC cell population which is responsible for intestinal homeostasis, while *Bmi1* expression mainly detects the more slowly dividing, label retaining +4 position cells, which are considered as quiescent stem cells and are activated in response to radiation-induced tissue injury or apoptotic cell death (Barker *et al*., 2007; Sangiorgi and Capecchi, 2008). Thus, based on the observed differences in cell cycle kinetics and locations between *Lgr5*-positive and *Bmi*-postive cells, over the recent years it has been proposed that these *Lgr5* and *Bmi1* label distinct populations of stem cells, with *Lgr5* being a marker of active CBC stem cells and *Bmi1* labeling a quiescent or slow cycling cell population (Tian et al., 2011;Yan et al., 2012).

However, the precise identity and location of the intestinal stem cell is still a matter of debate and a recent study by Buczachi and colleagues demonstrated that the quiescent stem cells gradually committed to the absorptive or secretory cell lineages and matured into Paneth and enteroendocrine cells during homeostasis. Upon intestinal injury by radiation, hydroxyurea or doxorubicin, these quiescent cells can undergo rapid proliferation and self-renewal to regenerate all of the epithelial linages, suggesting that the quiescent cells can be recalled to the active stem cell state (Buczacki *et al.*, 2013) (reviewed in Barker, 2014).

Although the intestinal stem cell field has progressed at an extraordinarily rapid pace, the precise identity and location of intestinal stem cells continues to remain under intense debate. There has not yet been a consensus regarding the ideal marker for intestinal stem cells, there is however a growing support for Lgr5, Ascl2 and Olfm4 to be the key intestinal stem cell markers.

1.1.4.2. Maintenance and homeostasis of the intestinal stem cell

The lack of definitive stem cell markers has hindered the progress in understanding the roles of various factors and signaling pathways involved in intestinal stem cell homeostasis. However, a number of indirect evidence has provided insights into the factors and pathways required for stem cell maintenance (Sato *et al*., 2009). Sato and colleagues generated an *in vitro* system that allows the growth of intestinal organoids in culture, from single mouse intestinal crypt. The intestinal crypts were seeded singly in the laminin-rich Matrigel, which provides the three-dimensional growth mimicking the nature architecture of the intestine and the laminin prevent detachment induced apoptosis (anoikis) in culture (Sato *et al.,* 2009). In order to sustain the long-term growth of the organoid culture the intestinal stem cells require the presence of a number of factors: Wnt agonist R-spondin, Notch ligand Jagged, epidermal growth factor (EGF) and the BMP antagonist Noggin. These named components are sufficient to support the growth of the organoids from single Lgr5 positive cells, therefore further supporting the use of Lgr5 as a marker of the intestinal stem cell population (Sato *et al.*, 2009).

The intestinal stem cell niche, the cellular components in which the intestinal stem cells reside, is thought to provide a range of signals in establishing or maintaining stem cell homeostasis. The mesenchymal cells express a number of basal membrane components such as collagen IV, laminin and nidogen, providing mechanical support and cellular adhesion (Paulsson, 1992). Paneth cells have long been thought to provide stem cell permissive environment due to their expression of Wnt ligands Wnt3 and Wnt11, the EGF receptor ligands EGF and TGFα, the Notch ligand Dll4 and the production of protective antimicrobial factors (Sato *et al*., 2011a). Factors produced by the mesemchyme and Paneth cells provide an essential niche to support intestinal stem cell *in vivo* and in *in vitro* culture of intestinal stem cells as outlined earlier (Bevins and Salzman, 2011; Sato *et al.*, 2011a; Sato *et al.*, 2011b). Notably, Lgr5 positive cells intercalated with Paneth cells at the bottom of crypts suggesting that the Paneth cells play a critical role for maintenance of the Lgr5 positive intestinal stem cells (Sato *et al*., 2011b). Consistent with the notion that Paneth cells are critical for the maintenance of the intestinal stem cell niche, ablation of Paneth cells via conditional knockout of *Sox9* gene has resulted in crypt loss occurring with the Paneth cell turnover rate (Sato *et al.,* 2011b). It may seem clear that Paneth cells in the crypt base are the sole niches to provide factors that regulate stem cell populations. However, it has been demonstrated that the knockout of Wnt3 from intestinal epithelium *in vivo* had no obvious effect on intestinal morphology and phenotype, whereas the loss of Wnt3 in intestinal organoid cultures resulted in organoid death, which is then rescued when co-cultured with mesenchymal cells (Farin, Van Es and Clevers, 2012). This indicates that other functionally important Wnts produced by extraepithelial or stromal niche cells other than the Paneth cell also contribute an essential role in the maintenance of the intestinal stem cell homeostasis.

Despite the contradictory evidence indicating that intestinal stem cells do not solely rely on the presence of Paneth cells to maintain intestinal homeostasis, recent evidence demonstrated that Paneth cells play an important role in supporting intestinal stem cell to repair epithelium after damage. Parry and colleagues generated two conditional mouse models (VillinCre and AhCre, described in section 1.3.2.2) to delete the transcription factor β-catenin within the intestinal epithelium. Rapid recovery and repopulation of the intestine

was demonstrated when the Paneth cells were retained, whereas loss of intestinal epithelial architecture was observed in the absence of Paneth cells, indicating the role of Paneth cells within the in vivo intestinal stem cell niche in aiding damage repair (Parry *et al*., 2013). Therefore, Paneth cells are an essential niche component that plays a crucial role in governing stem cell behavior not only during intestinal epithelial homeostasis but also during tissue repair and regeneration following injury.

1.2. Colorectal Cancer

1.2.1. Colorectal cancer in humans

1.2.1.1. Colorectal cancer statistics

"Cancer does not discriminate. It knows no nationality, no creed, no gender, no age. It affects all of us alike, not discriminating who or where you are; rich or poor alike."

(John Kanzius 1944-2009)

It is estimated that more than one in three people will be diagnosed with some form of cancer during their lifetime. Colorectal cancer (CRC) is the third most common cancer type across both genders, after lung and breast cancer in the U.K. (excluding non-melanoma skin cancer). Over 40,700 new cases are diagnosed per year in the U.K., and the incidence of CRC has remained relatively stable for over a decade. Despite the fact that the five-year survival rates for CRC have doubled in the past 40 years, CRC is still the second most common cause of cancer death in the U.K. after lung cancer (Cancer Research UK, 2013).

1.2.1.2. Environmental risk factors

The high incidence of CRC is often attributed to unhealthy lifestyles. Studies have shown CRC risk is positively associated with high consumption of red and processed meats, and inversely associated with fishes, fresh vegetables, dietary fibres and folic acid intake (Norat *et al.*, 2002; Park *et al.,* 2005). Physical inactivity is also known to be a contributory factor, increasing the risk of CRC by up to 24% (Wolin, Yan and Colditz, 2011). Related to the westernised diet and lack of exercise, obesity is also known to be an important risk factor, around 13% of CRC in the U.K. are obesity-related (Murphy *et al*., 2000) (Cancer Research UK, 2013). Furthermore, smoking and high alcohol consumption has also linked to increase the risk of developing CRC.

1.2.1.3. Genetic risk factors and predisposition

CRCs can be divided into three categories: sporadic, familial and hereditary cases. Over 80% of the CRC cases are sporadic, which is a multistep process caused by accumulation of both acquired genetic and epigenetic mutations in multiple genes such as Adenomatous Polyposis Coli (*APC)*, Kiresten-Ras (*K-ras)* and Tumour Protein 53 (*TP53)* (Fearon and Vogelstein, 1990). However, a significant proportion of CRC has a clear genetic background, patients with two or more first-degree (e.g. brothers and sisters) or second-degree (e.g. grandparents) relatives with CRC are considered to be at an increased risk of the disease and this is known as familial CRC. Lastly, hereditary CRC occurs in less than 10% of the CRC cases and the best-known syndromes are familial adenomatous polyposis (FAP), caused by inherited mutation in *APC* gene, and hereditary non-polyposis colorectal cancer (HNPCC) or Lynch syndromes, caused by mutation in one of the DNA mismatch repair (MMR) genes (Stoffel, 2010; Groden et al., 1991)

1.2.1.4. Therapeutic strategies

The course of treatment a patient undergoes is largely dependent on the severity of the tumour stage. Surgery is the cornerstone treatment for early-stage cancer that has not spread to distant sites (stage I-III), additional treatment with radiation and chemotherapy may also be used pre- or post-operation. Chemotherapy is the first treatment option for metastatic disease (stage IV) when tumour lesions are not fully resectable by surgery (NICE Guidelines, 2011). The available treatment modalities for metastatic CRC include cytotoxics (5-Flurouracil, oxaliplatin and irinotecan) and anti-epidermal growth factor agents (cetuximab and panitumumab) (Abad *et al.*, 2008). These are used in combination or sequentially to treat CRC patients. Despite the mortality rates from colon cancer decreasing over the past 30 years, there is still a huge heterogeneity in survival rates (Cancer Research UK 2013). Basic research into intestinal tumorigenesis is critically important for improving future drug designs and development and treatment strategy.

1.2.2. Multi-step development of colorectal cancer

The development of CRC is a step-wise process in which the acquisition of multiple genetic mutations leads to transformation of normal glandular epithelium into invasive adenocarcinoma. This multi-step model was proposed in the study conducted by Fearon and Vogelstein in 1990, in which they comprehensively reviewed the genetic alterations present at various stages of the CRC and they proposed that 4 to 5 mutational steps are necessary to result in colorectal malignancy. These steps involve the gradual accumulation of oncogenes activation and tumour suppressor genes inactivation. This model has become the classical view of CRC initiation and progression and is now commonly referred to as the 'Chromosomal instability' (CIN) pathway. The first mutations involved in the stepwise model are in 'gatekeeper' tumour suppressor gene, APC, leading to formation of a benign lesion, then subsequent activation of the oncogene *KRAS*, allelic loss of chromosome 18q locus, and loss of expression of the tumour suppressor *p53*, all contributing to the progression of a benign tumour to malignant disease (Figure 1.4). However, not all CRCs follow the Fearon-Vogelstein progression pathway as other pathways of colorectal carcinogenesis have also been identified, including the 'microsatellite instability' pathway (Kim *et al*., 1999; Jass, Young and Leggett, 2002). In this report the chromosomal instability pathway will be focused, as it is known to be the most common mutational pathway of colorectal disease.

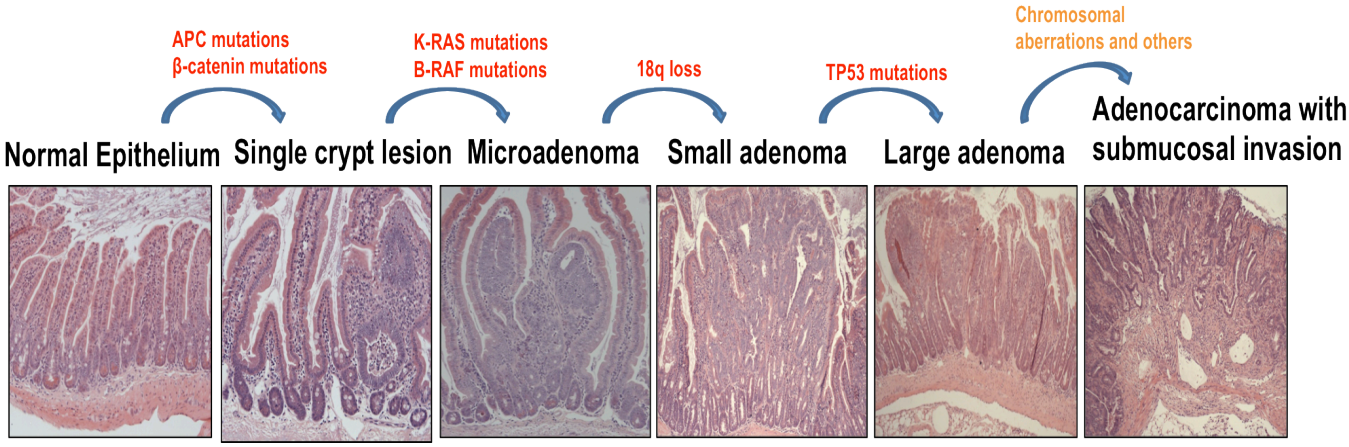

Figure 1.4: Colorectal Cancer is a multi-step process.
The transformation of normal glandular epithelium into invasive adenocarcinoma is a multi-step process accompanied by the accumulation of genetic and epigenetic mutations.

1.2.2.1. APC and the canonical-Wnt signalling

The 'gatekeeper' tumour suppressor gene, *APC*, was discovered by genetic linkage analysis in FAP families (Bodmer *et al*., 1987; Groden *et al*., 1991; Joslyn *et al.*, 1991). Mutation in the *APC* gene appears in aberrant crypt foci and early adenomas (Figure 1.2), suggesting that inactivation of *APC* occurs very early in adenoma formation (Levy *et al*., 1994; Hocker and Wiedenmann, 1998). As described previously, *APC* plays a central role in the canonical Wnt signaling pathway, a pathway that provides a key driving force behind sustained proliferation in the crypt and intestinal homeostasis. Although FAP represent a small proportion of all CRC cases, the majority of sporadic CRC show activation of the Wnt pathway and more than 80% of CRC cases are attributed to mutational inactivation of *APC* (Kinzler and Vogelstein, 1996). Apart from loss of *APC* function, mutations that stabilize β-catenin have also been observed in 10% of CRC (Morin *et al*., 1997).

In order to recapitulate FAP symptoms and CRC development in a controlled environment, a number of animal models targeting Wnt pathway components have been generated (reviewed in Heyer et al., 1999). The most well-known animal model, *Min (Multiple intestinal neoplasia)* mice, have been found to carry a nonsense-mutation in codon 850 of *Apc* resulting in a truncated protein. Mice heterozygous for the APC^{Min} allele have a shortened lifespan and develop multiple adenomas across the gastrointestinal tract (Su *et al.*, 1992). Notably, mouse models with *Apc* inactivation predominantly develop tumours in the small intestine, whereas the majority of *APC*-induced intestinal tumorigeneisis arise in the large intestine in human.

1.2.2.2. Kras and the RAS-RAF-MAPK signalling

Mutations in components of the RAS-RAF-MAPK pathway are required for the next step in progression from early adenoma to intermediate adenoma. The Rat Sarcoma viral oncogene homology (RAS) family is comprised of Harvey (H-RAS), Kirsten (K-RAS) and Neuroblastoma (N-RAS). RAS proteins are a group of small G-proteins that is commonly found to be activated in many cancers (reviewed in Bos, 1989). RAS proteins become activated when bound by GTP, which is stimulated by a number of Guanine nucleotide exchange factors (GEFs) that facilitate exchange of GDP for GTP. Once bound by GTP, the

active form of RAS is able to phosphorylate and trigger numerous downstream pathways. The most characterized pathway downstream of RAS is the RAF-MEK-ERK mitogen-activated protein kinase (MAPK) cascade. Phosphorylated MARK kinases are translocated into nucleus where they activate a range of transcription factors resulting in response that drives tumorigenesis.

In human, mutations resulting in constitutively activated K-RAS have been found to occur in approximately 50% of all CRC cases (Figure 1.4) (van Engeland et al., 2002;Sancho, Batlle and Clevers, 2004). Additionally, activating mutations in B-RAF gene have been found in 20% of CRC with functional K-RAS (Rajagopalan *et al*., 2002). Mutations in either K-RAS or B-RAF are commonly regarded to be involved in tumour progression (Fearon and Vogelstein, 1990; Rajagopalan *et al.*, 2002). This notion of K-RAS and B-RAF mutations as drivers of cancer progression has been supported by a number of studies. The study from Sansom showed that following loss of *Apc* and activation of the Wnt signaling cascade, *k-Ras* activation accelerated Wnt-driven tumorigenesis and conferred a more invasive phenotype compared to tumours with native *k-Ras* (Sansom *et al*., 2006). This study supports the notion that activation of RAS-RAF-MAPK pathway plays a crucial role in cancer progression.

1.2.2.3. Allelic loss of 18q and TGFβ / BMP signalling

The allelic loss of the 18q chromosomal region is the next step toward malignancy, which is found in 70% of carcinomas and 50% of late adenomas (Fearon and Vogelstein, 1990b). The candidate for involvement in colorectal cancer progression found at this locus is the tumour suppressor Deleted in Colorectal Carcinoma (*DCC*). The *DCC* gene encodes a receptor for the ligand Netrin that controls axonal growth and cellular migration (Keino-Masu *et al*., 1996). The role of *DCC* in cancers remains unclear. Studies of $DCC^{-/-}$ mice exhibited marked neuronal abnormalities and died shortly after birth consistent with the previously proposed role of *DCC* in axon guidance, however $DCC^{+/-}$ mice survived into adulthood were found to have no predisposition for intestinal tumours. Furthermore, heterozygous *DCC* loss had no effect on tumour progression or multiplicity in Apc^{Min} mice (Fazeli *et al*., 1997). Fazeli *et al* suggested that the loss of *DCC* in human CRC may only be a

consequence of loss of part of chromosome 18q and therefore *DCC* may not play a role either in initiation or in progression of intestinal disease.

Another gene, which is present in very close proximity (at 18q21.1) to the *DCC*-encoding gene (at 18q21.3) on chromosome 18 is Smad4 and may link to CRC (Thiagalingam *et al*., 1996). As previously described in section 1.1.3.3, SMAD4 is the effector protein involved in the downstream signaling of the TGF-β and BMP signaling pathway. Mutations in *SMAD4* have been implicated in Juvenile polyposis syndrome (JPS) associated with increased risk of CRC. Approximately 20-25% of JPS cases were attributed to *SMAD4* mutation (Howe *et al.*, 2004; Chow and Macrae, 2005). In murine studies, Takaku et al. deleted *Smad4* alone and in the context of *Apc* mutation (*Apc* is also on chromosome 18 in the mouse). Homozygous loss of *Smad4* was found to be embryonic lethal, whereas *Smad4* heterozygous mice exhibited little phenotypic differences compared to wild-type littermates. However, mice with heterozygous deletion of *Smad4* and *Apc* enhanced the malignancy of tumours compared to *Apc* heterozygous control mice. Tumours were found to be increase in size and were more invasive, suggesting that the evidence for the role of *Smad4* as a tumour suppressor in CRC is more compelling than that for *DCC*, especially in the aspect of cancer progression (Takaku *et al*., 1998).

1.2.2.4. Mutation of p53 and malignancy

Fearon and Vogelstein proposed the loss of short arm of chromosome 17, which harbours the *TP53* gene, encoding the tumour suppressor p53, as a final step required for cancer progression towards malignant disease (Fearon and Vogelstein, 1990b). As the first tumour suppressor gene discovered, *p53* responds to cellular stresses that cause DNA damage allowing the cell to either repair the damaged DNA, or undergo apoptosis. In normal conditions *p53* is rendered inactive by mouse double minute 2 homolog (MDM2), which binds to *p53* and mediates *p53* ubiquitination causing it to be degraded. Translational modifications of *p53* (e.g. phosphorylation and acetylation) induced by cellular stress or damage to DNA cause conformational changes in *p53* preventing its association with MDM2, which allow it to translocate into the nucleus and activate transcription of target genes, resulting in cell cycle arrest, stimulation of DNA repair, senescence or cell death by

apoptosis (Vousden and Lane, 2007; Helton and Chen, 2007). Loss of *p53* function therefore removes its role as "guardian of the genome", abolishing the normal regulation for the cell to carry out DNA damage repair or undergo apoptosis before proceeding to proliferate, thereby predisposing the cell to mutation accumulation and neoplastic transformation. Germline mutations of *p53* are known to cause the hereditary condition, Li-Fraumeni syndrome (Li *et al.*, 1988). Mutations of *p53* are seen in approximately 50% of CRC (reviewed in Iacopetta, 2003). Consistent with the model proposed by Fearon and Vogelstein, *p53* mutations have been reported in nearly 50% of carcinomas, while in less than 10% of adenomas, suggesting that the loss of *p53* function is normally associated with late-stage carcinomas rather than early adenomas in human (Figure 1.4) (Purdie *et al*., 1991). Despite the strong association of *p53* mutations with CRC in human, mouse models of *p53* loss in the context of intestinal tumorigenesis have produced conflicting results. Clarke *et al* demonstrated that deficiency of *p53* in Apc^{Min} mice (which are predisposed to intestinal tumour formation) did not result in an increase in tumour progression compared to *p53* proficient Apc^{Min} mice (Clarke, Cummings and Harrison, 1995). Consistent with this, Reed *et al.* showed that conditional loss of *p53* has very little effect on the acute activation of the Wnt pathway in the intestine, suggesting no role in early adenoma formation (Reed et al., 2008b). Petitjean et al. observed that in humans, *p53* gene often acquires point mutations rendering it unable to activate gene transcription (Petitjean *et al*., 2007). Therefore Muller *el al.* compared mice bearing a mutated allele of *p53* with heterozygous *Apc* loss and mice with heterozygous loss of *p53* and *Apc*. They found that the number of intestinal tumours were similar in both the mice with the mutated *p53* allele and mice deficient for *p53*. However in the mice expressing a mutant form of *p53*, the tumours were found to be more advanced, suggesting that some mutations in *p53* cause a gain-of-function in which the mutated *p53* is capable of promoting invasion, explaining the reason why the lack of gain-of-function mutation do not establish more malignant tumours in *p53* deficient mice (see diagram Figure 1.4) (Muller *et al.*, 2009).

1.3. Modeling colorectal cancer in mouse using conditional transgenesis

Mouse models have provided an important understanding into the development and progression of CRC, these models have also been useful in elucidating molecular pathways and served as important preclinical platforms to verify efficacy of potential novel therapeutic agents. Progress in transgenic technology led to the development of a new generation of models that recapitulate the initiation and progression of CRC in human.

The classic example of the mouse models to demonstrate intestinal tumorigenesis is the *Min (Multiple Intestinal Neoplasia)* mouse. This model was derived using a random mutagenesis approach by treating a line of mice with the mutagen ethynitrosurea (ENU), which predisposed them to the formation of intestinal tumours (Moser, Pitot and Dove, 1990a). Following the establishment of the Min mouse line, the gene mutation responsible for the phenotype was sequenced and discovered to bear a mutation in the *Apc* gene, at codon 850 (Su *et al*., 1992). As aforementioned, *Apc* mutation is commonly found in human FAP, therefore the Apc^{Min} mouse has since become a model of human hereditary CRC predisposition syndrome FAP. This Apc^{Min} mouse model has made an invaluable contribution to our understanding of the effect of environmental changes, genetic and epigenetic alterations and therapeutic agents on CRC initiation and development (Shoemaker *et al*., 1997). However, there are substantial differences on tumour distribution and extent of progression to advanced stages between carcinogenesis in Apc^{Min} and human intestine (Heyer *et al.*, 1999). Therefore, more sophisticated mouse models combining mutations in different genes are being constantly developed in order to model the more comprehensive aspects of tumour development and progression in human.

1.3.1. Constitutive transgenesis

Targeted transgenic technology in mice came in 1987 with the generation of targeted deletion of the hypoxanthine-guanosine phosphoribosyl transferase (HPRT) gene (Kuehn *et al*., 1987). Since then, numerous mouse models of constitutive gene deletion have been generated providing insights into the *in vivo* function of a number of genes in various conditions. Although constitutive transgenesis has been a valuable research tool allowing studies into the physiological role of numerous genes, some important limitations associated with constitutive gene loss also exist.

One of the biggest limitations of constitutive models is that the absolute requirement of many genes in the germ line for normal embryonic development. Around 15% of gene knockouts are embryonic lethal, which means the generation of an adult mouse deleted for these genes is impossible. This makes it difficult to study cancer biology, as many known tumour suppressor genes and oncogenes are vital for embryonic development. The second limitation is that constitutive knockout approach produces complete targeted gene deletion in the whole organism. This causes issues to study the effects of gene loss in a particular tissue if severe phenotypes occurring elsewhere in the organism. Finally, constitutive gene deletion is likely to affect the interaction between different cell types and also it may potentially mask the true cellular role of a gene in specific cell types due to gene redundancy or a compensatory mechanism within the organism.

In order to overcome the limitations imposed by approaches utilizing constitutive transgenesis, conditional transgenic models have been developed, thereby enabling an array of genes to be targeted in specific tissues.

1.3.2. Conditional transgenic models

The use of conditional transgenic models allows temporo-spatial control of gene deletion or expression in transgenic animals. The ability to switch gene expression ‘on’ or ‘off’ in targeted tissues at specific times allows unprecedented flexibility for exploring gene function in cancer initiation, development and progression.

A number of conditional transgenic approaches have been designed to provide the temporally 'switchable' mechanism that consists of two principal elements: an inducible 'effector' transgene and a 'target' transgene. Examples of these approaches used in murine models include Cre-loxP (Causes recombination (Cre) – Locus of crossover of bacteriophage P1 (loxP)), Flp-Frt (Flp-Flp recognition target) and TetO (tetracycline operator) techniques. The Cre-loxP system will be the focus of this thesis, and is described in detail below.

1.3.2.1. The Cre-loxP system

The Cre-loxP system operates as a binary mechanism. The effector component is represented by Cre recombinase, which is a 34 bp long nucleotide sequences isolated from bacteriophage P1 (Abremski and Hoess, 1984). It is a site-specific DNA recombinase which binds to DNA recognitions sequences called loxP (Hoess, Ziese and Sternberg, 1982; Sternberg and Hamilton, 1981), yielding the recombined DNA product. Depending on the loxP sites orientation, recombination results in either inversion or excision of the DNA fragment surrounding between the loxP sites. When loxP sites are inserted unidirectionally surrounding the entire gene, those genes have been targeted for recombination. When the gene is exposed to Cre recombinase, the region between loxP sites is excised or floxed out, rendering the gene completely inactive. Activation of a transgene can also be achieved using the Cre-loxP system; in this case, a transcription terminating Stop-cassette flanked by loxP sites is inserted before the gene of interest. Upon exposure to Cre recombinase, the loxP flanked Stop cassette is eliminated and the expression of the transgene of interest is resumed.

The versatility of this approach does come with some limitations. While the traditional constitutive knockout system produces complete gene deletion in the organism, the Cre-loxP approach may result in incomplete targeted gene excision. The quality of gene excision reflects not only the extent of Cre recombinase expression but also the chromosomal environment of the targeted gene. Epigenetically, floxed loci in the open and active chromatin state will be more accessible to Cre recombinase and therefore susceptible to site-specific recombination than loci in the condensed and inaccessible state. Partial gene excision produces an animal that is mosaic, although in some cases this Cre-mediated

mosaicism has been exploited and it has been believed to be one of the benefits of the system (Betz *et al.*, 1996). On the other hand, it has been proposed that expression of Cre recombinase in mammalian cells may promote genomic instability by introducing DNA double-stranded breaks (Thyagarajan *et a*l., 2000).

1.3.2.2. Post-translational regulation of Cre recombinase activity in the intestine

Post-translational regulation of Cre recombinase activity allows the combination of cell-type or tissue-specificity with inducibility under temporal control. The most common approach to this is the use of a fusion protein of Cre and a modified Estrogen receptor (ER) (el Marjou *et al.*, 2004a; Feil *et al*., 1996). In general, the fusion CreER protein is sequestered in the cytoplasm preventing it from accessing loxP sites in the nucleus. However, in the presence of the ER antagonist Tamoxifen, the ER domain of the fusion protein is bound by Tamoxifen, thereby exposing the nuclear localisation signal. This facilitates the CreER fusion protein to translocate into the nucleus, where it recognises and recombines the loxP sites.

Expression of CreER fusion protein under the control of a tissue-specific promoter provides a sophisticated means of tissue-specific inducible deletion or activation of a targeted gene of interest. For example, in the intestine, the Villin promoter has been coupled to a CreER fusion protein to allow temporal control over Cre recombinase expression within the intestinal epithelium (el Marjou *et al.*, 2004a). Another promoter also used in the intestine is AhCreER, in which control of Cre recombinase expression is regulated at two levels: by transcriptional control of the Ah promoter (activated by β-napthoflavone) and by a requirement for Tamoxifen binding. Expression of Cre recombinase from AhCreER mice was detected in the intestine, liver, pancreas, gallbladder, and stomach (Kemp *et al.*, 2004).

1.4. Epigenetics and Cancer

"The major problem, I think, is chromatin. What determines whether a piece of DNA along the chromosome is functioning, since it's covered with the histones? You can inherit something beyond the DNA sequence. That's where the real excitement of genetics is now"

(Watson and Crick 2003)

Although genetic mutations have been the focus of cancer research for many years, epigenetic alterations have been increasingly recognised to also play a major role in tumorigenesis. The progression from a microadenoma to carcinomadenoma in CRC may take decades, supporting the notion that accumulated genetic and epigenetic alterations underlie the multistep developmental process of CRC (Figure 1.4). Epigenetic modifications have been proposed to contribute to CRC formation through the activation on oncogenes (gain of gene function) and the inactivation of tumour suppressor genes (loss of gene function) that regulate signalling pathways that control hallmark behaviours of cancers. Among all the epigenetic alternations in CRC, the most extensively characterised are promoter hypermethylation of *MLH1, APC, RB1, VHL, MGMT, GSTP1,* and *BRCA1* genes, representing paradigmatic cancer-related epigenetic silencing of tumour suppressor genes (Knudson, 2001).

The term 'epigenetics' was first proposed by Conrad Waddington in 1939 to describe 'the causal interactions between genes and their products, which bring the phenotype into being' (Waddington, 1939). The current definition of epigenetics refers to the study of heritable changes in gene expression occurring without changes in primary DNA sequence (Sharma, Kelly and Jones, 2010). Three different yet highly interdependent epigenetic mechanisms have been recognised: (1) histone modification, (2) RNA interference and (3) DNA (de)methylation (Figure 1.5). In the context of this thesis, we mainly foucs on histone modification.

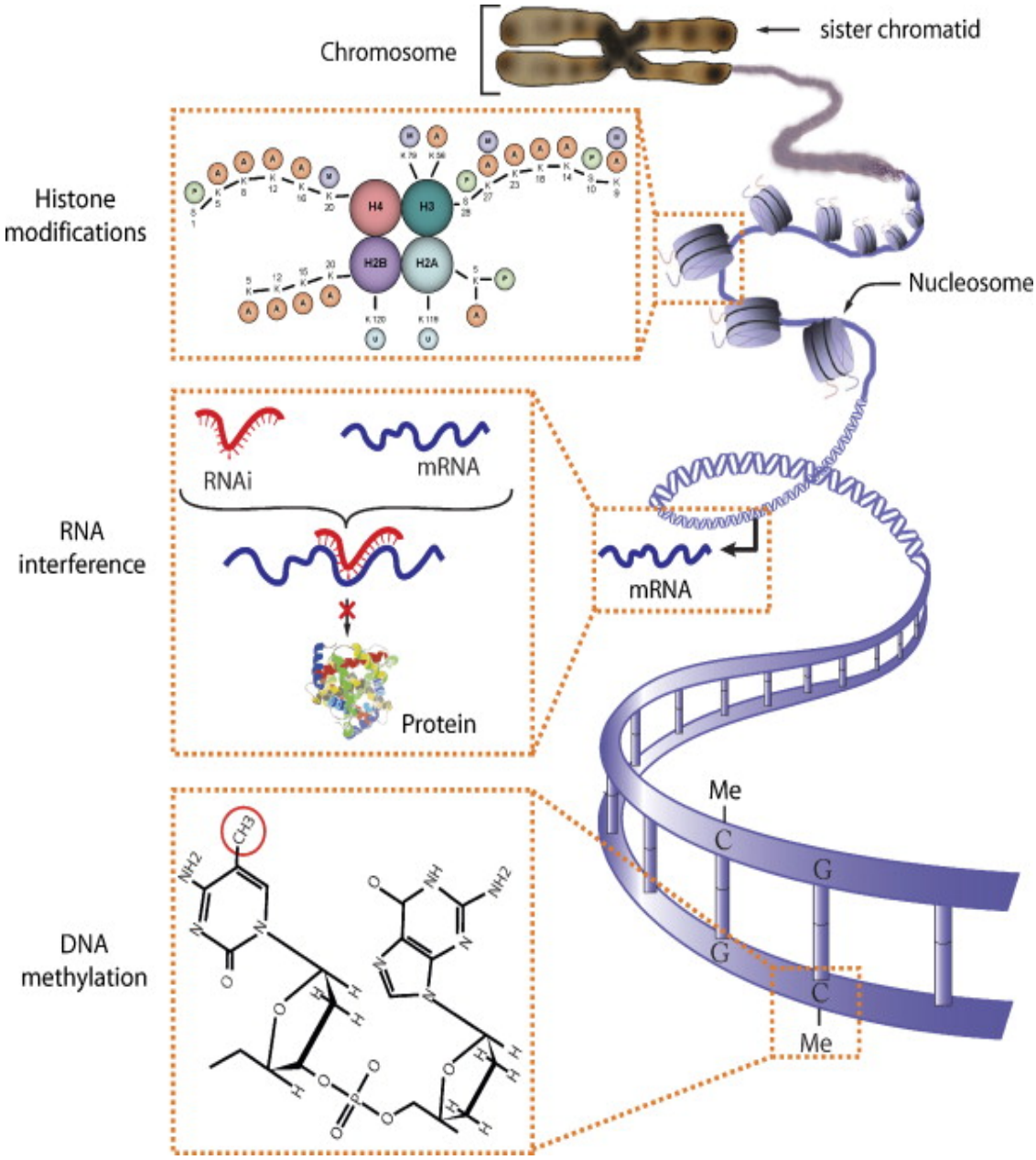

Figure 1.5: Epigenetic modifications.
Top: Histone modifications, covalent modifications of N-terminal tails of histones; Middle: RNA interference, maintenance of gene transcription in a heritable way in the form of small RNAs (microRNA); Bottom: DNA methylation, a covalent modification of the cytosine in a CpG dinucleotide (Sawan *et al*., 2008).

1.4.1. Nucleosome and Post-translational Histone Modifications

In eukaryotic cells, DNA is packaged into a compact chromatin structure. The basic chromatin unit, the nucleosome, comprises approximately 147 base pairs of super-helical DNA wrapped around an octamer of two histone H2A/H2B dimers and two histone H3/H4 dimers. The linker histone H1 binds to short linker DNA between nucleosomes. These can then be further packed into higher order chromatin structures. The crystal structure of the nucleosome core has been resolved, revealing that the N-terminal histone tails emanating from the core (Luger *et al.*, 1997), making them subject to a variety of reversible covalent post-translational modifications which alter their interaction with DNA and other nuclear proteins.

Nucleosome density and access to the genomic DNA in eukaryotic cells is highly regulated in order for processes such as DNA damage repair, replication, transcription, and mitosis to occur at the right time and place (Sawan *et al.*, 2008). One of the primary mechanisms regulating access to the DNA is post-translational histone modification (PTM) (Goldberg, Allis and Bernstein, 2007). The PTMs identified so far include acetylation and methylation of lysines (K) and arginines (R), phosphorylation of serines (S) and threonines (T), ubiquitination, sumoylation and biotinylation of lysines, ADP ribosylation, deimination and proline isomerisation (Kouzarides, 2007) (Figure 1.6). Histone modifications are effected by 'writer' enzymes: Histone acetyltransferases (HATs), histone methyltransferase (HMTs), and histone kinases; whereas Histone deacetylases (HDACs), histone demethylases (HDMs) and histone phosphatases are 'eraser' enzymes reversing the modification marks.

The combination of histone modifications constitutes the histone ''code'', which influences chromatin condensation and the ability of various chromatin interacting proteins to recognise the presence and absence of specific PTMs, thereby inducing distinct downstream effects (Sawan and Herceg, 2010).

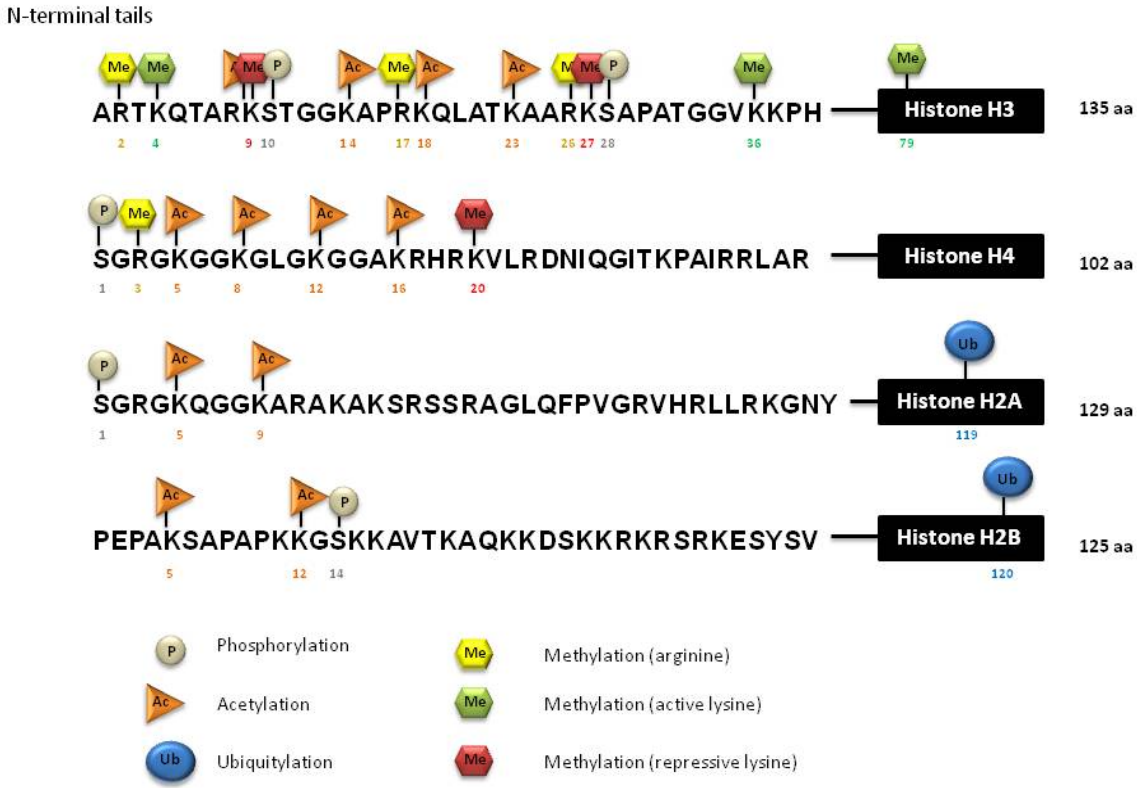

Figure 1.6: Schematic representation of core histone post-translational modifications (Adapted from Shechter *et al*., 2007).

1.4.2. The Role of Histone modification in Transcriptional control: Euchromatin and Heterochromatin

Histone modifications help to subdivide the genome into distinct domains such as euchromatin, characterised as opened and accessible state of the DNA, and heterochromatin, described as condensed and repressive state of the DNA, which is in general transcriptionally inactive (Jenuwein and Allis, 2001). There are two major subtypes of heterochromatin: constitutive and facultative. Constitutive heterochromatin describes regions that contain a high density of repetitive DNA elements and transposable elements, such as centromeres and telomeres (Grewal and Jia, 2007). Facultative heterochromatin, in contrast, refers to developmentally regulated regions where states can be converted between euchromatin and heterochromatin. This therefore can switch on or off transcription at specific times, such as during certain developmental phases of the cell cycle

(Trojer and Reinberg, 2007). Besides the roles in gene silencing, heterochromatin also plays a role in genomic stability. Previous studies have demonstrated that animal with mutated genes that regulate heterochromatin structure increased spontaneous DNA damage in heterochromatin of somatic and meiotic cells (Peng and Karpen, 2009). Heterochromatin formation is also essential for maintaining the stability of repeat DNA sequences, presumably by suppressing inappropriate homologous recombination (Peng and Karpen, 2007). Reduced levels of heterochromatin in mice and *Drosophila* have also been demonstrated to have higher levels of spontaneous DNA damage, chromosomal instability, and exhibit defects in chromosomal compaction and segregation during mitosis (Yan *et al.*, 2011).

Transcriptionally active euchromatin has been found to be associated with methylation of lysines 4, 36, and 79 on histone H3 (Gerber and Shilatifard, 2003). On the contrary, methylation of lysines 9 and 27 on histone H3 and lysine 20 of histone H4 has been strongly linked with less transcriptionally active and more condensed heterochromatin (Kouzarides, 2007).

Mutations in various factors involved in chromatin formation and maintenance have been associated to the development of disease, in particular cancer (Ko, 2008). These mutations either result in the repression of normally active genes (e.g. tumour suppressor genes) or the activation of normally silent genes (e.g. oncogenes).

Connections have been identified for various modification and at all levels of chromatin formation and maintenance: for 'writiers' such as H3K27 methyltransferase EZH2 which is overexpressed in metastatic prostate cancer (Varambally *et al.,* 2002), 'readers' such as HP1γ which is upregulated in various tumours and is identified as a putative biomarkers for osteosarcoma and prostate cancer (Slezak *et al.,* 2013; Saini *et al.,* 2012), 'erasers' such as HDAC1 which is aberrantly recruited to promoters due to fusion with DNA-binding proteins (Lin *et al.,* 1998), and for chromatin remodelers such as NuRD complex where its ATPase subunit is deleted in certain neuroblastomas (Bagchi *et al.,* 2007). The multitude and variety of these connections foreshadows the enormous potential that intervention with these processes may have for the treatment of cancer. However, it is clear at this point that a deeper understanding of the epigenetic mechanisms regulating

chromatin structure and function and the specific mechanisms of chromatin-dependent tumourigenesis is required, and much basic research will be absolutely necessary to achieve the full potential of chromatin-based therapeutics. The close relationships between chromatin and cancer make such research imperative.

Having outlined the basic principles of chromatin biology, the following section is a more detailed view of one specific non-histone component of chromatin: Heterochromatin protein 1, the chromatin effector protein that was at the centre of my PhD research.

1.4.3. Structure and Function of Heterochromatin Protein 1

Heterochromatin protein 1 (HP1) was first identified by screening a monoclonal antibody panel generated against a fraction of *Drosophila* non-histone chromosomal proteins associated with heterochromatin. Immunofluorescence staining of polytene chromosome revealed that HP1 localised to centric heterochromatin, telomeres and approximately 200 euchromatic regions (James and Elgin, 1986). A few years later the gene encoding HP1, SU(VAR)2-5, was found as a suppressor of position-effect variegation (PEV) (Eissenberg *et al.*, 1990). HP1 is phylogenetically highly conserved among all eukaryotes including *S. pombe, M. muscuculus and H. sapiens* (Eissenberg *et al.*, 1990; Singh *et al.,* 1991; Ye and Worman, 1996). Mammalian cells contain at least three different isoforms of HP1, in humans these are named HP1α, HP1β and HP1γ (Lomberk *et al.*, 2006). The three human HP1 proteins are encoded by the *chromobox homolog* (*CBX*) genes: *CBX5* (HP1α), *CBX1* (HP1β) and *CBX3* (HP1γ) (Ye and Worman, 1996). The translated human HP1α, HP1β and HP1γ amino acid sequences are 191, 185 and 173 residues in length respectively, and in general, HP1α and β are localised in heterochromatin, whereas HP1γ is present in both heterochromatin and euchromatin (Minc, Courvalin and Buendia, 2000) (Table 1.1).

Isotype	Gene	Location(s)	Knock-out
HP1α	*CBX5*	Heterochromatin	Same as wildtype
HP1β	*CBX1*	Heterochromatin	Lethal when born
HP1γ	*CBX3*	Heterochromatin and Euchromatin	Lack of germ cells

Table 1.1: The localisation of HP1 family (Brown *et al*., 2010a).

All HP1 proteins identified in eukaryotes share a well-conserved architecture consisting of an amino-terminal chromodomain (CD) and a carboxy-terminal chromoshadow domain (CSD) linked by a flexible hinge region (Aasland and Stewart, 1995; Kellum, 2003). The CD is a chromatin-binding module that specifically recognises and binds to heterochromatin (Ball *et al.*, 1997). The CSD is primarily involved in homo- and/or heterodimerisation and interaction with other proteins (Thiru *et al.*, 2004) (Figure 1.7).

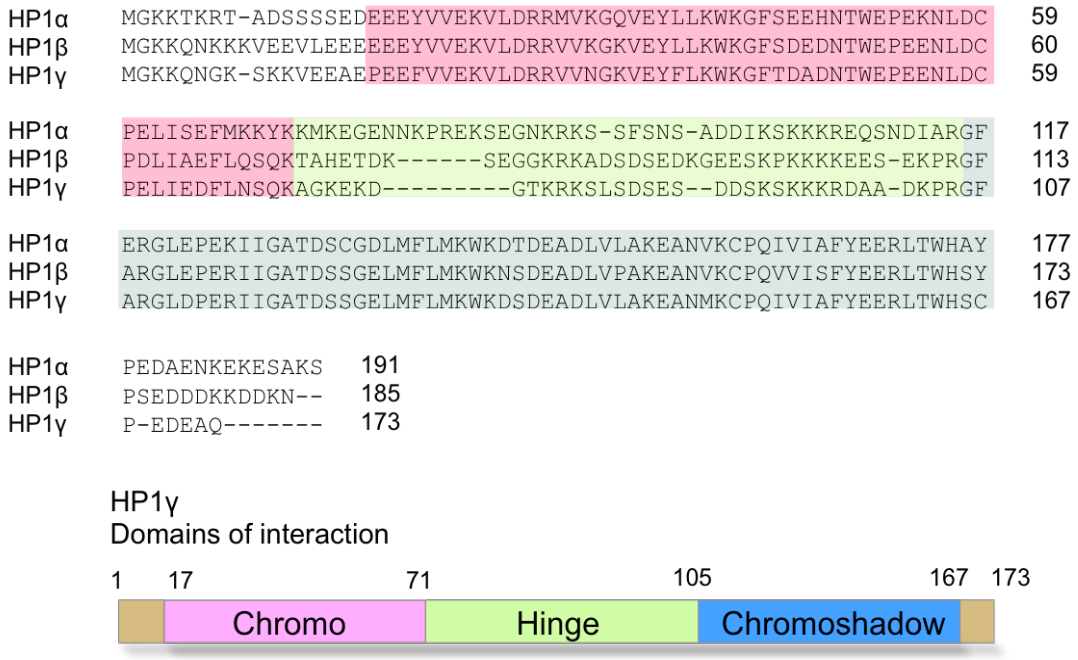

Figure 1.7: The amino-acid sequence of mouse heterochromatin protein 1 (HP1) isoform α, β and γ.
The amino-terminal chromodomain (Red), the central hinge region (Green) and the chromoshadow domain (Blue) are distinguished. Diagram adapted from (Maison and Almouzni, 2004a).

1.4.3.1. The chromo domain

The amino-terminal chromodomain (chromatin organisation modifier) is identified in MOF (Males Absent on the First), HP1, Pc (Polycomb) and CHD1 (chromo-ATPase / helicase-DNA-binding protein) (Pearce, Singh and Gaunt, 1992). The functions of the CDs are diverse between different proteins. For instance, MOF associates with the X-chromosome via the interaction of its CD with roX2 RNA that is enriched on the male X-chromosome

(Akhtar, Zink and Becker, 2000). On the other hand, the CD of HP1, Pc and CHD1 interact with methylated lysine residues on histone tails in heterochromatin, while the most studied CD is that of HP1, which has been demonstrated to interact specifically with the di- and tri-methylated lysine 9 of histone H3 (H3K9m2 and H3K9me3) (Bannister *et al.,* 2001; Jacobs and Khorasanizadeh, 2002). Previous studies support that HP1 and H3K9me2 co-localise extensively, but not exclusively on polytene chromosomes (Li, Yi and Makova, 2002). In addition, mutations in a conserved valine 26 to methionine in the CD in Drosophila abolished the ability of HP1 to bind to the H3K9me2. Consequently, this resulted in delocalization of HP1 from the chromosome, leading to disruption of gene silencing and late larval lethality (Jacobs *et al.*, 2001; James *et al.*, 1989).

The interaction with the methylated H3K9 is not the only binding partner of the HP1 CD. Mouse HP1β was demonstrated to interact with the nuclear envelope proteins through the CD, and the interaction with lamina-associated polypeptide 2β (LAP2β) and lamin B receptor (LBR) was mapped to the CD, suggesting HP1 may play a role in nuclear envelope reassembly and architecture (Kourmouli *et al*., 2000). Furthermore, the CD of mammalian HP1γ binds to the retinoblastoma protein (Rb) as demonstrated by yeast-two-hybrid analysis and immunoprecipitation (Williams and Grafi, 2000). Therefore, the HP1γ is thought to target to the CyclinE promoter to silence gene expression (Nielsen *et al.,* 2001a; Nielsen *et al.*, 2001b)

1.4.3.2. The hinge region

The hinge region is highly flexible and allows the CD and the CSD to move independently to each other. The hinge of HP1 interacts with RNA and histone H1 in Drosophila (Nielsen *et al*., 2001a) and mouse, and histone deacetyltransferase (HDACs) in humans (Zhang, McKinsey and Olson, 2002). Interaction between the hinge of HP1 with H1 and HDACs may correlate with the formation of higher order chromatin structures, gene repression and silencing. In addition, phosphorylation of the hinge region is dynamic through the cell cycle and is believed to play a role in HP1-mediated gene silencing (Zhao, Heyduk and Eissenberg, 2001). Furthermore, phosphorylation of serine 83 in HP1γ confers an interaction with Ku70 (involved in DNA double stranded break repair and telomere

maintenance) and disrupts silencing when tethered by GALA-DNA binding domain suggesting an important role of dynamic phosphorylation and dephosphorylation in HP1 binding and gene silencing (Lomberk, Wallrath and Urrutia, 2006).

1.4.3.3. The chromo shadow domain

The Carboxy-terminal CSD is structurally similar to the CD and it is reported to be responsible for homodimerization of HP1 through an alpha-helical region (Brasher *et al*., 2000; Jacobs *et al*., 2001). Homodimerisation also creates a hydrophobic platform for interaction with a variety of nuclear proteins such as the pentapeptide motif PxVxL-containing proteins (Cowieson *et al.,* 2000). Many proteins interact with the HP1 family through the PxVxL, including KRAB-associated protein (Kap1) and chromatin assembly factor 1 subunit p150 (CAF1) involved in gene silencing. These PxVxL-containing proteins possess a diverse range of functions including chromatin remodeling, DNA replication and transcription regulation.

On the other hand, there are also several nuclear proteins that interact with the HP1 CSD through non-PxVxL motifs. For example, Brg1 (ATPase subunit in SW1/SNF chromatin remodeling complexes) has been shown to interact with mammalian HP1γ by co-immunoprecipition (Nielsen *et al.*, 2002a). In addition, the histone methyltransferase SU(VAR)3-9 associates with HP1 both *in vitro* and *in vivo* through a CSD dimer. Ku70 interacts with HP1α through a 28 amino acid leucine-serine (LS) repeat of Ku70 and the CSD of HP1α. Therefore, the CSD of HP1 allows interaction with different pentapeptide-motif proteins as well as non-PxVxL containing proteins ranging from chromatin modifiers, transcriptional activators and transcriptional repressors (Thiru *et al,* 2004).

1.4.4. Localisation and function of HP1 family

In recent years, great progress has been made in our understanding of the general principles how chromatin is organised and functions within the cell. However, there are still many functional questions in HP1 biology that have not been understood. For example, a full understanding of the different roles of the three HP1 isofoms, of the regulation of HP1's diverse molecular interactions, or of the exact molecular mechanism(s) of HP1-mediated gene silencing or activation, splicing, DNA damage repair and telomere maintenance will still require plenty of research.

It has been established that each HP1 isoform exhibits distinct localization patterns on chromatin. HP1α and β are generally localised in heterochromatin, whereas HP1γ is present in both heterochromatin and euchromatin (Minc, Courvalin and Buendia, 2000). The localisation of HP1 appears to be dynamic and cell cycle dependent (Dialynas *et al.*, 2007). The main mechanism localising HP1 within centric heterochromatin is via its CD interaction with H3K9me3. Studies have demonstrated that this HP1-methylated-H3K9 binding can be abolished by either phosphorylation of H3S10 or phosphorylation of H3S10 associated with acetylation of H3K14 (Hirota *et al.*, 2005; Fischle *et al*., 2005; Mateescu *et al.,* 2004). It has been reported that HP1α specifically binds to the H3Y41 region via its CSD and phosphorylation of H2Y41 by JAK2 leads to dissociation of HP1α from chromatin (Dawson *et al*., 2009). The versatile and dynamic localisation behaviour of HP1 remains unclear and further complexities occur in relation to the length of time that HP1 binds to different regions in different contexts. Alternative mechanisms defining the sub-nuclear localisation of HP1 comprised of post-translational modification of the HP1 protein itself, interactions between the CSD and other transcription factors, and direct binding of HP1 to DNA and RNA transcripts (Badugu, Shareef and Kellum, 2003; Piacentini *et al*., 2003).

The most studied function of HP1 is in the heterochromatin formation. The underlying basis for formation of heterochromatin and gene silencing revolves around interactions between the SU(VAR)3-9, HP1 and the H3K9me3 modification. Trimethylation of Histone H3K9 is mediated by SU(VAR)3-9, the CD of HP1 is a binding module for H3K9me3 while SUR(VAR)3-9 itself interacts with HP1 via the CSD. Once formed, this complex then allows the spreading of heterochromatic states and mediates silencing and proper

chromatin compaction (reviewed in Fanti and Pimpinelli, 2008). Evidence implicates a pivotal role for HP1 proteins in the assembly and spread of heterochromatin containing H3K9 methylation. In the study, Canzio and colleagues demonstrated that the *S. pombe* HP1 homolog, Swi6, recognises the H3K9me3 site at the interface of two CDs. This binding causes Swi6 to tetramerise on a nucleosome, generating two CD sticky ends, which can bridge nearby methylated nucleosomes, enhancing silencing and heterochromatin spread *in vivo* (Canzio *et al*., 2011).

In addition to being required for heterochromatin formation and gene silencing, HP1 proteins are reported to play roles in the regulation of gene expression at multiple euchromatic regions. Evidence has accumulated to implicate HP1 proteins as a positive regulator of gene expression at a subset of euchromatic loci. In *Drosophila*, high-resolution genome-wide mapping experiments have revealed HP1 is associated with transcriptionally active chromatin (de Wit, Greil and van Steensel, 2007). Detailed mapping studies of HP1 have demonstrated its enrichment at developmentally regulated genes and at heat-shock-induced chromosomal puff loci, which are structures with intense gene activity (Piacentini *et al., 2003; Cryderman et al., 2005)*. Furthermore, *Drosophila* HP1γ homolog, HP1c, has been shown to interact with Facilitates Chromatin Transcription (FACT), which is a histone chaperone complex. It was demonstrated that HP1c guides the recruitment of FACT to active genes and links FACT to active forms of RNA polymerase II. The recruitment of FACT into heat-shock loci is impaired in the absence of HP1c and subsequently causes a defect in heat-shock gene expression (Kwon *et al.*, 2010). In murine cells, HP1γ was observed to localise to the coding regions of several genes (Vakoc *et al.*, 2005a). In addition, HP1γ has been implicated in alternative splicing for a subset of genes (Saint-Andre *et al.*, 2011). Recent published data has indicated a role for HP1γ in aiding in efficient co-transcriptional RNA processing through recruitment of the splicing machinery. Depletion of *Cbx3* diminished the recruitment of splicing factors such as SNRNP70 and SRSF1 to gene bodies, resulting in RNA processing defect and subsequently leading to an increase in unspliced transcripts of its target genes (Smallwood *et al*., 2012). Collectively, these studies implicate a role of HP1 proteins in positive gene expression and RNA splicing.

Furthermore, emerging evidence indicates that HP1 proteins play roles in the DNA damage response (DDR). A number of studies have established that the compact

architecture of heterochromatin is structurally inhibitory to DDR. Decreasing the levels of HP1 results in relaxation of the chromatin structure, thereby allowing a chromatin dynamic that facilitates bypassing the requirement for ATM signalling and enhances the efficiency of DNA repair (Ayoub *et al*., 2008). All three isoforms of HP1 have been shown to be recruited to UV-induced DNA lesions in both human and mouse cells (Dinant and Luijsterburg, 2009), and *C. elegans* possessing HP1 knockout are more susceptible to UV-induced DNA damage (Luijsterburg and van Attikum, 2011). It is the CD of HP1 that appears to be the most important component for this function (Dinant and Luijsterburg, 2009).

Although the majority of information from the literature studied the members of HP1 family as a whole this could be misleading, as there is little redundancy among the HP1 family. Knockout of HP1β, but not HP1α, was associated with genome instability in mice while depletion of HP1γ, but not HP1α or β, led to mitotic defects in human tissue culture cells (Aucott *et al.,* 2008). In addition, dysfunction of HP1α and HP1β but not HP1γ plays a crucial role during the process of tumorigenesis (Sharma *et al*., 2003a) and the down-regulation of HP1α but not HP1β and HP1γ is implicated in invasive and metastatic phenotype of breast cancer (Kirschmann *et al*., 2000). Thus, there are substantial functional differences among HP1 variants. Furthermore, in many cases, the same HP1 variant is implicated in multiple functions.

1.4.5. Heterochromatin protein 1 gamma and Cancer

In the past few years, several studies have implicated genetic alteration of HP1γ in the development of several types of human cancers. HP1γ is frequently up-regulated in many cancer cell lines, including colon, cervix, stomach, lung and myxoid liposarcoma (Takanashi *et al.,* 2009). Enhanced expression of HP1γ was detected in peripheral blood leukocytes of patients with advanced leukaemia compared to those from normal donors (Popova *et al.*, 2006). Similar increases in HP1γ protein level were observed in seminoma tumours, which are germ cell cancers of the testes (Bartkova *et al.*, 2011). Additionally, expression level of *Cbx3*, the gene that encodes for HP1γ, was markedly increased in lung cancer tissues compared to normal lung tissues, suggesting that *Cbx3* may be a promising candidate gene in lung adenocarcinoma (Han *et al*., 2014). Silencing of *Cbx3* in selected

cancer cell lines causes the inhibition of growth. Consistent with this, the deletion mutant of HP1γ lacks tumorigenesis activity in a mouse xenograft model (Sharma *et al.*, 2003). Recent evidence has shown that HP1γ is absent in differentiated cells of various normal human tissues, suggesting that the loss of HP1γ is required for cell differentiation to occur (Takanashi *et al.*, 2009). In HP1γ$^{-/-}$ mutant embryos, the number of primordial germ cells (PGCs) was reduced dramatically and this could be caused by inhibition of G1/S phase transition, suggesting that HP1γ plays an important role in maintaining enough germ cells by regulating the PGC cell cycle (Abe *et al*., 2011). *Cbx3* has been documented to negatively regulate adipocyte differentiation from preadipocyte cells and is required for male germ cell survival and spermatogenesis (Brown *et al*., 2010). HP1γ has been implicated to be associated with Suv4-20h1 and Suv4-20h2 (Schotta *et al.*, 2004) and directly affects the methylation level of histone H4K20 and consequently regulates gene expression epigenetically. Molecular interaction between HP1γ and histone H4K20 is expected to be a key mechanism of cell differentiation. In addition, HP1γ is reported to have a role in alternative splicing through recruitment of the splicing machinery and defective mRNA splicing contribute to cancer development (Saint-Andre *et al.*, 2011). A summary of the proposed functions of HP1γ is outlined in Figure 1.8. The studies mentioned here demonstrate that HP1γ in cancer is often up-regulated and absence of HP1γ is required for cells to differentiate, together these may suggest that the expression of HP1γ may contribute to cancer progression.

The involvement of HP1γ in human cancer underlines the importance of learning more about this important chromatin protein. A better understanding of the multiple roles that HP1γ plays in the process of cancer development will not only enormously contribute to our understanding of chromatin but may also lead to insights that could one day be translated for the benefit of human patients in the clinic.

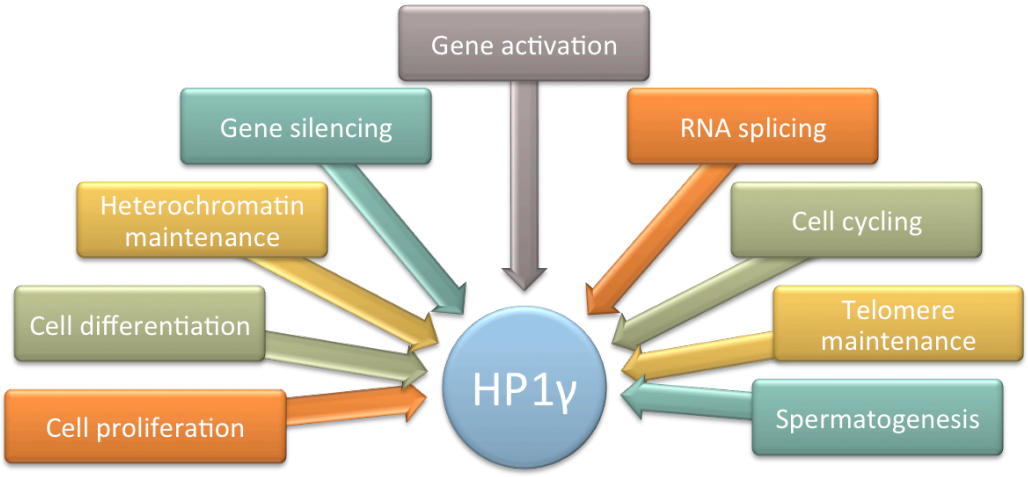

Figure 1.8: A summary of the proposed functions of HP1γ.

1.4.6. Preliminary results of HP1 gamma studies

Prior to my PhD project, preliminary work conducted by Dr. Karen Reed and Dr. John Jenkins (Liverpool University) examining *Cbx3* expression by qRT-PCR analysis using samples from human colorectal cancer patients, demonstrated a significant increase in *Cbx3* expression (3.03 medium fold change) compared to normal tissues (Figure 1.9).

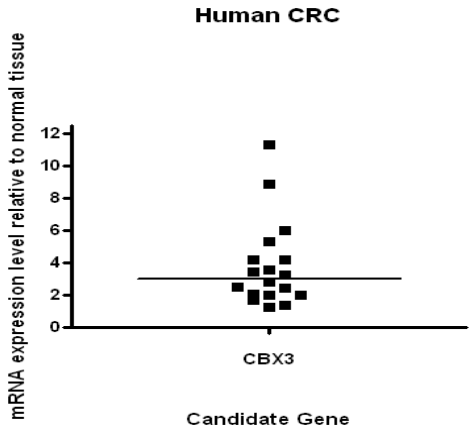

Figure 1.9: *Cbx3* specific qRT-PCR expression analysis.
qRT-PCR expression analysis using tumour samples from 18 CRC patients compared to matched normal tissues, shows a significant increase in *Cbx3* expression tumour samples (Medium fold change 3.03, Wilcoxon Signed Rank Test: Significant with P = 0.0001). Data generated by Dr. Karen Reed and Dr. John Jenkins.

Additionally, a microarray expression analysis and differential iTRAQ-QSTAR protein profiling was carried out and identified *Cbx3* / HP1γ to be up-regulated in the mouse model of colorectal cancer (Hammoudi *et al.*, 2013). *Cbx3*-specific qRT-PCR expression revealed a significant increase in *Cbx3* expression (2.5 medium fold change) following the conditional loss of *Apc* in intestinal tissues. Consistent with this result, HP1γ-specific Western blot analysis demonstrated an increase in the level of HP1γ protein following the conditional loss of *Apc* in intestinal tissues (Figure 1.10).

Furthermore, the *Cbx3* gene is over-expressed and ranked within the top 10% of gene changes in all but one of the colorectal cancer data sets on the online cancer microarray database, Oncomine. Collectively, these data highlight an interesting increased

trend in HP1γ levels in colorectal cancer, suggesting that HP1γ may be an effective target for gene therapy against human colorectal cancer.

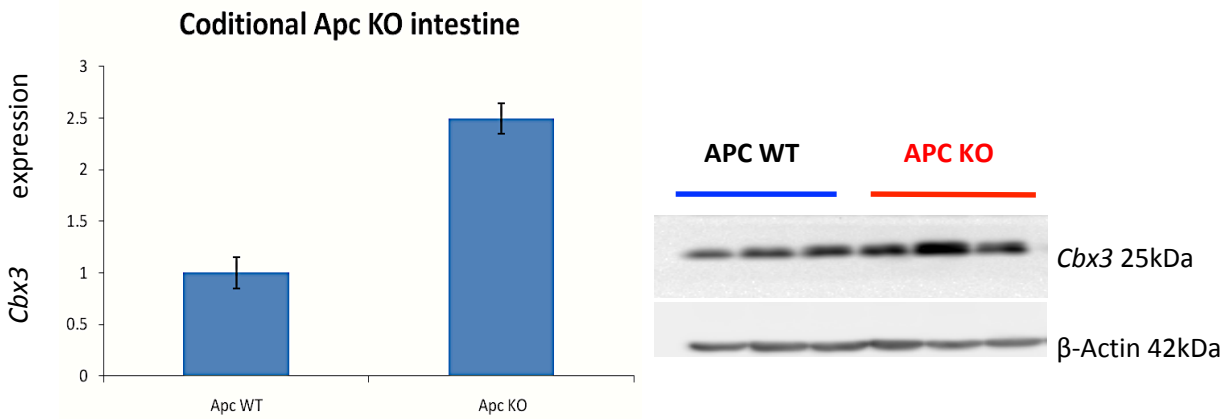

Figure 1.10: Over-expression of *Cbx3*/HP1γ following the conditional loss of *Apc* in intestinal tissues of mice models.
LEFT: *Cbx3*-specific qRT-PCR expression analysis in normal and *Apc*-deficient intestinal tissues from mice model. *Cbx3* is significantly increased in intestinal tissues of *Apc*-deficient models compared to wildtype (Medium fold change 2.5-fold over-expression). RIGHT: HP1γ-specific Western Blot Analysis in wilttype and *Apc*-deficient intestinal tissues from mice model. Data generated by Dr. Karen Reed.

1.5. Project aims

A growing body of evidence indicates that *Cbx3* functions as a driver in cancer cell growth. This is supported by our preliminary observations that over-expression of HP1γ (coded by the gene *Cbx3*) was detected in tumour samples of colorectal cancer patients compared to matched normal tissues. In concordance, marked increase in HP1γ level was observed in mouse models of colorectal cancer. Thus accumulating evidence strongly implicates HP1γ in cancer development. The principle aim of this study is to characterise the effects of homozygous *Cbx3* deletion on normal intestinal homeostasis and acute Wnt-activated intestines, and the long-term implications of *Cbx3* loss on Wnt-driven tumorigenesis to assess if *Cbx3* loss would attenuate Wnt-driven cancer progression in mouse models of colorectal cancer. Project plans are summarised in Figure 1.11. It is envisaged that more can be learned about the role of HP1γ in colorectal cancer progression and this research will contribute to our knowledge of the phenotypic and mechanistic basis of colorectal cancer progression, and could potentially pave the way for more effective treatments to be developed.

Strategy	**To study the immediate intestinal phenotypes following Cbx3 loss**		**To study the effect of Cbx3 loss in the Wnt-activated small intestines**		**To study the delayed phenotypes, including adenoma formation in $APC^{fl/+}$, in conjunction with the loss of Cbx3**		
Genotype	Cre^+ $LacZ^+$ **$Cbx3^{fl/fl}$** **$APC^{+/+}$**	Cre^+ $LacZ^+$ $Cbx3^{+/+}$ $APC^{+/+}$	Cre^+ $LacZ^+$ **$Cbx3^{fl/fl}$** **$APC^{fl/fl}$**	Cre^+ $LacZ^+$ $Cbx3^{+/+}$ $APC^{fl/fl}$	Cre^+ $LacZ^+$ **$Cbx3^{fl/fl}$** **$APC^{fl/+}$**	Cre^+ $LacZ^+$ $Cbx3^{fl/+}$ $APC^{fl/+}$	Cre^+ $LacZ^+$ $Cbx3^{+/+}$ $APC^{fl/+}$
Induction	4 daily inter-peritoneal injections of 80mg/kg Tamoxifen at 8 weeks of age						
Endpoints	Day 4 Day 7 Day 22 Day 366		Day 4 Various time points		Various time points Age to Day 500		
Phenotype Characterisations	A. Histological and immunohistochemical status: Crypt and villus size, levels of apoptosis, mitosis and S-phase incorporation of BrdU and stem cell olfm4 in situ hybridisation . B. Differentiation status: Numbers and localisation of paneth, goblet, enterocytes and enteroendocrine cells. C. Migration rates along the crypt-villus axis: Comparison of the position of cells labeled 2 Hrs and 24 Hrs post BrdU administration. D. QRT-PCR and immunohistochemistry expression analysis for: A panel of intestinal stem cell markers and Wnt, Noth, TGF-β, PI3K signaling target genes.						
Mechanistic studies	A. Transient knock down of *Cbx3* using siRNA and Topflash assay. B. Co-localisation studies using immunofluorescence. C. RNA-sequencing						

Figure 1.11: Summary of project plan.

Chapter Two

Materials and Methods

2. Materials and Methods

2.1. Generation of Experimental Mouse Models

The *Cbx3* transgenic mice with the loxP flanked *Cbx3* alleles (*Cbx3*$^{fl/fl}$) (Brown *et al*., 2010) were obtained from Prim B. Singh (Research Center Borstel, Germany) and crossed with *VillinCreER*$^{+}$*APC*$^{fl/fl}$ mice (Shibata *et al.,* 1997) to investigate their compound effects on intestinal homeostasis and tumorigenesis (Figure 2.1). The Cre-LoxP (Cause Recombination Locus Of X-over P1) recombinase system allows recombination of DNA in the intestine at a specified time point and therefore was employed for this study. The *VillinCreER* transgene (el Marjou *et al*., 2004) was induced through the intraperitoneal (IP) injection of Tamoxifen once daily, for four consecutive days, at a dose of 80 mg/kg dissolved in corn oil (Sigma). The extent of *Cbx3* deletion was confirmed using the *Rosa26-floxed-stop-LacZ* surrogate reporter and by Western blot and immunohistochemistry. All experimental procedures were conducted in accordance with the UK Animals Act 1986 and current UK Home Office regulations under valid personal (PIL: 30/9727) and project licenses (PLL: 30/2737).

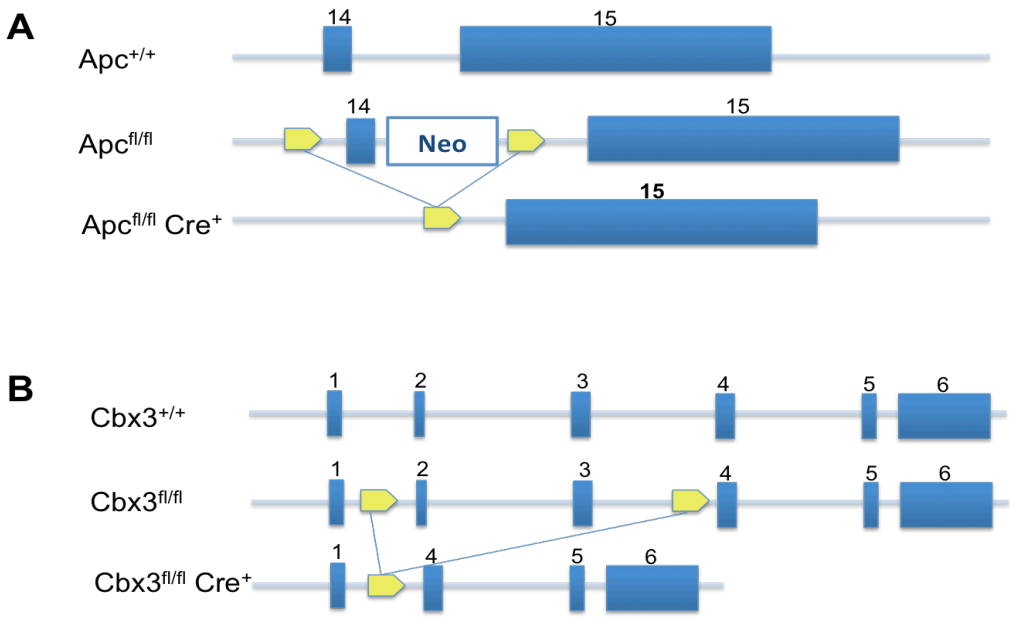

Figure 2.1: Graphical representation of Cre-LoxP targeted alleles.
(A) Two loxP sites are placed either side of exon 14 of the *Apc* gene. (B) Two loxP sites are placed in the *Cbx3* gene so that they flank exons 2 and 3. In this inducible Cre recombinase system, intraperitoneal injection of Tamoxifen will cause excision of the floxed sites.

2.1.1. Animal Husbandry

2.1.1.1. Colony maintenance

Mice were housed in a standard facility and had access to the standard diet (Special Diets Service UK, RM3(E)) and fresh drinking water.

2.1.1.2. Breeding

All mice were maintained on an outbred background. Adult animals (6 weeks and older) of known genotype were generally bred in trios (one male with two females). After birth, pups were left with their mothers until capable of feeding independently then they were weaned, usually at four weeks of age.

2.1.1.3. Identification and ear biopsies

At weaning age, mice were sexed and separated. Ear clipping was carried out for identification purposes. I would like to acknowledge Matt Zverev and Elaine Taylor for their technical assistance with ear clipping. The resulting ear pinna was used for DNA extraction and genotyping (see below).

2.1.2. Experimental Procedures

2.1.2.1. Injection of Tamoxifen

Expression of Cre recombinase from the *VillinCre* transgene was induced using Tamoxifen (Sigma) delivered in corn oil (Sigma). Powdered Tamoxifen was added to corn oil in an amber bottle to give a concentration of 10 mg Tamoxifen per 1 ml corn oil. The solution was heated to 80°C with regular shaking to ensure complete dissolution of Tamoxifen. Once completely dissolved, the Tamoxifen solution was aliquoted and stored at -20°C until needed. Prior to injection, aliquots of Tamoxifen were defrosted, reheated to approximately 80°C to re-dissolve the Tamoxifen and kept at this temperature until immediately before injection to prevent precipitation. Animals were then injected IP at a dose of 80 mg Tamoxifen per kg body weight once a day for 4 days (Figure 2.2).

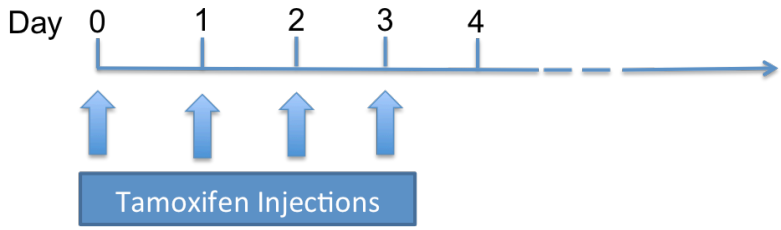

Figure 2.2: Timeline of Tamoxifen injection routine.

2.1.2.2. Injection of 5'-Bromo-2-deoxyuridine

Where indicated, animals were administered 0.25 ml of 10 mg/ml 5'-Bromo-2-deoxyuridine (BrdU, Biosciences) IP either 2 or 24 hours prior to harvesting in order to label cells in S-phase of the cell cycle.

2.1.3. PCR Genotyping

PCR genotyping was performed on all transgenic animals prior to experimental use by PCR using DNA extracted from ear biopsies at weaning age (four weeks). I wish to acknowledge Mark Bishop for all his assistance with genotyping. All PCR genotyping primers were designed using the Primer3 web-based software at http://bioinfo.ut.ee/primer3/ unless provided by earlier publications. Sequences were verified using BLAST engine against Ensembl database at http://www.ensembl.org/Multi/blastview and synthesised by Sigma Genosys.

2.1.3.1. DNA purification

Ear biopsy samples were stored at -20°C until analysis to prevent degradation. For DNA isolation 250 µl of Cell Lysis Solution (Gentra) and 5 µl of 20 mg/ml Proteinase K (Roche) were added to the tissue and digested overnight at 37°C with vigorous agitation. The next day, the digested samples were cooled to room temperature and 100 µl of Protein Precipitation Solution (Gentra) added. Tubes were inverted to mix and centrifuged at 13000 rpm in a microcentrifuge for 10 min to pellet all protein and insoluble material. The supernatant was removed into a clean tube containing 250 µl isopropanol and the mixture

was centrifuged at 13000 rpm for 15 min. The supernatant was carefully discarded, and the DNA pellet allowed to air-dry at room temperature for 1 hour. The dried DNA pellet was then dissolved in 250 µl of PCR-grade water (Sigma) at 37°C with agitation.

2.1.3.2. Generic protocol for PCR genotyping

All PCR reactions were performed in thin-wall 96-well plates or in thin-wall 0.2 ml strip tubes (Greiner Bio-One) and run on either PTC-100 Peltier (MJ Research), Techne Flexigene (Krackeler Scientific) or GS1 (G-Storm) thermal cycler. Pipetting of all DNA samples and reagents was carried out using filtered pipette tips to avoid aerosol contamination of samples. 2.5 µl of crude genomic DNA extract was loaded into wells using a multi-channel pipette. A master mix for all samples was then prepared containing all other reaction components (distilled water, GoTaq 5X PCR buffer (Promega), 25mM Magnesium Chloride (Promega), 25 mM dNTPs (Bioline), Primers (Sigma-Genosys) and either GoTaq (Promega) or DreamTaq (Fermentas) DNA polymerase). 47.5 µl of the appropriate master mix were added to each well to make the reaction volume up to 50 µl. 96-well plates were sealed with aluminium foil tape and strip tubes with appropriate caps (Greiner Bio-One). Samples were then gently tapped on the bench to remove air bubbles and ensure the mixture was at the bottom of the well. Reactions were then run using cycle conditions outlined in Table 2.1. The primer sequences used for genotyping of the particular transgenes and their corresponding product sizes are provided in Table 2.2.

2.1.3.3. Visualisation of PCR products

Upon completion of PCR reactions the products were visualised by agarose gel electrophoresis. To each sample, 5 µl DNA loading dye (50% Glycerol (Sigma), 50% distilled water, 0.1% (w/v) Bromophenol Blue (Sigma)) was added. All samples were then loaded with an appropriate marker (e.g. 100 bp ladder (Promega)) onto 2% agarose gel (4 g agarose (Eurogentech), 200 ml 1X Tris-Borate-EDTA (TBE) buffer (Sigma), 10 µl of 10 mg/ml ethidium bromide (Sigma) or 10 µl Safeview (NBS Biologicals)). Gels were run in 1X TBE buffer at 120 V for approximately 30 minutes. Products were then visualised in UV light using GelDoc apparatus (BioRad).

	Cre/LacZ	ApcLoxP	Cbx3LoxP
PCR Reaction Components:			
DNA extract	2.5 µl	2.5 µl	2.5 µl
Master Mix:			
PCR-grade Water (Sigma)	31.5 µl	31.7 µl	31.7 µl
Go Taq PCR Buffer (5X, Promega)	10 µl	10 µl	10 µl
Magnesium Chloride (25 mM, Promega)	5 µl	5 µl	5 µl
dNTPs (25 mM, Bioline)	0.4 µl	0.4 µl	0.4 µl
Forward Primer (100 mM, Sigma Genosys)	0.2 µl	0.1 µl	0.1 µl
Reverse Primer (100 mM, Sigma Genosys)	0.2 µl	0.1 µl	0.1 µl
Taq DNA Polymerase	0.2 µl	0.2 µl	0.2 µl
Brand of Taq DNA Polymerase	Go Taq	Dream Taq	Go Taq
Total Reaction Volume:	50 µl	50 µl	50 µl
Cycling conditions (Time; Temperature):			
Initial denaturation	3 min; 94°C	3 min; 94°C	4 min; 94°C
Cycle number	30	30	35
Step 1: Denaturation	30 sec; 95°C	30 sec; 95°C	1 min; 94°C
Step 2: Annealing	30 sec; 55°C	30 sec; 60°C	1 min; 60°C
Step 3: Elongation	1 min; 72°C	1 min; 72°C	1 min; 72°C
Final Extension	5 min; 72°C	5 min; 72°C	5 min; 72°C
Hold	15 °C	15 °C	15 °C

Table 2.1 PCR Genotyping reaction conditions

Target	Forward Primer Sequence (5' to 3')	Reverse Primer Sequence (5' to 3')	Product Size
Cre	TGA CCG TAC ACC AAA ATT TG	ATT GCC CCT GTT TCA CTA TC	100 bp
LacZ	CTG GCG TTA CCC AAC TTA AT	ATA ACT GCC GTC ACT CCA AC	500 bp
ApcLoxP	GTT CTG TAT CAT GGA AAG ATA GGT GGT C	CAC TCA AAA CGC TTT TGA GGG TTG ATT C	WT: 226 bp; Targeted: 314 bp
Cbx3LoxP	AGT CCC AGT ACT GAG AGT TC	CTC TAC CTC CTG AGT ACT AG	WT: 200 bp Targeted: 400 bp

Table 2.2 Primer Sequences used for PCR Genotyping

2.2. Tissue harvesting and processing

2.2.1. Tissue Harvesting

Animals were sacrificed using a schedule 1 approved method of culling (cervical dislocation or carbon dioxide) and were dissected using a micro-dissection kit. The fur was sprayed with 70% ethanol and an incision made along the mid-line of the abdomen through both skin and peritoneal wall. Tissue samples were collected after animal sacrifice and placed in appropriate fixatives as quickly as possible to avoid RNA and protein degradation. The small intestine (SI) and colon were flushed with ice-cold 1X phosphate-buffered solution (PBS; Invitrogen). Selected regions of intestine were either bundled using surgical microtape (Micropore) or 'swiss-rolled' (intestine was opened longitudinally, rolled from end to end using forceps and secured with a 23G syringe needle (BD Microlance)). Epithelial cell extracts were collected from 10 cm session of small intestinal tissue in ice-cold Weiser solution (section 2.2.6). Fresh frozen tissues of liver and small intestine were preserved in dry ice before long-term storage at -80^{o}C freezer and the tissues were used for RNA (Section 2.8.1) and protein (section 2.7.1) isolation. The large intestine was flushed with ice-cold 1X PBS and 'swiss-rolled'.

2.2.2. Tissue Fixation

Once the tissue samples were collected, they were fixed in ice-cold 10% neutral buffered formalin (Sigma) and incubated for 12-24 hours at 4^{o}C. Following fixation, samples were either processed straight away or transferred into ice cold 70% ethanol and stored at 4^{o}C until processing.

Fixation method used for intestinal wholemounts and β-galactosidase staining is outlined in section 2.2.5.

2.2.3. Tissue processing and sectioning

2.2.3.1. Tissue dehydration

Tissue was processed using an automatic processor (Leica TP1050). Tissue was dehydrated in increasing concentrations of ethanol (70% for 1 hour, 95% for 1 hour, 100% 2 x 1 hour 30 min, 100% for 2 hours), Xylene 2 x 1 hour and paraffin 1 x 1 hour and 2 x 2 hours. After dehydration, tissue was embedded in paraffin wax.

2.2.3.2. Tissue sectioning

Paraffin blocks were sectioned on a microtome (Leica RM2135) at a thickness of 5 µm. Sections were then floated onto slides coated with poly-L-lysine (PLL) (Polysine, Thermo Fisher) and baked at 58°C for 24 hours. I would like to thank Derek Scarborough and Mark Isaac for their histology services on tissue dehydration and sectioning.

2.2.4. Tissue preservation for RNA, DNA or protein extraction

2.2.4.1. For RNA extraction

Intestinal tissues or epithelial extracts were placed in screw-cap tubes containing 1.4 mm ceramic beads (Lysing Matrix D tubes, MP biomedical) and 1 ml of Trizol reagent (Invitrogen). Samples were then either stored at 4°C (for several weeks) or -20°C (for several months).

2.2.4.2. For DNA extraction

Small samples were removed from tissues intended for DNA extraction and were placed in 1.5 ml eppendorf tube and stored at -20°C until DNA extraction (usually within 2 weeks).

2.2.4.3. For Protein extraction

Tissue samples or intestinal epithelial extracts were transferred into 1.5 ml eppendorf tube and quickly immersed in liquid nitrogen or dry ice to snap freezes tissue.

Tissues were removed from liquid nitrogen or dry ice at convenience and stored at -80°C until needed.

2.2.5. Analysis of beta-galactosidase activity

2.2.5.1. Intestinal tissue wholemount

Mice bearing the Rosa26/LacZ reporter transgene were used to assess levels of recombination in small and large intestinal tissues. Defined regions of the intestine were removed and flushed with ice-cold 1 X PBS (Invitrogen) and ice-cold X-Gal fixative solution (2% formaldehyde (Sigma), 0.1% glutaraldehyde (Sigma) in 1 X PBS). Intestines were placed on a set paraffin wax in 15 cm plastic Petri dish (paraffin wax (Sigma), with 10% mineral oil (Sigma)). The intestines were cut opened longitudinally and pinned epithelial side facing up using entomological pins (Watkins & Doncaster).

2.2.5.2. Fixation and demucification of the intestinal wholemounts

Intestinal wholemounts were fixed in X-Gal fixative for at least 1 hour at room temperature. Plates were then washed with 1 X PBS before adding demucifying solution (10% glycerol (Sigma), 0.01 M Tris-HCl (pH 8.2), 20% ethanol (Fisher Scientific), 0.9% NaCl, 0.003% (w/v) Dithiothreitol (DTT, Sigma)). Intestines were incubated with demucifying solution with agitation for 1 hour. The plate then was flooded with 1 X PBS and any adhering mucin was washed off the tissue by pipetting the 1 X PBS with force onto the intestine using a Pasteur pipette, and examined under a dissection microscope to ensure complete removal of mucins. This procedure was repeated using fresh 1 X PBS until intestines were clean.

2.2.5.3. Staining with X-Gal substrate

The wholemounts were stained using X-Gal staining solution: 1 mM $MgCl_2$ (Sigma), 3 mM potassium ferricyanide (Sigma), 3 mM potassium ferrocyanide (Sigma) in 1 X PBS. The solution was prepared in advance and stored in the dark at 4°C and X-Gal solution (5% in DMF, Promega) was added to a concentration of 0.02% immediately prior to staining. The intestines were incubated with the staining solution overnight or until the sufficient level of staining was achieved in the dark with agitation. Once stained, tissues were washed with 1 X PBS and fixed with formalin to avoid further staining. Stained wholemounts were illuminated with Leica CLS50X light source and visually analysed under Olympus SZX12 low-

magnification stereomicroscope. Pictures were taken with Olympus C-4040ZOOM 4.1 Megapixel digital camera. When required, formalin-fixed intestines were 'swiss-rolled' and processed for histology as described in section 2.2.3.

2.2.6. Isolation of intestinal epithelium

2.2.6.1. Isolation of intestinal epithelial cells using Weiser solution

A method for enrichment of intestinal epithelial cells was adapted from (Flint, Cove and Evans, 1991). An approximately 10 cm of the small intestine was flushed with ice-cold 1 X PBS (Invitrogen) opened longitudinally and placed into a 50 ml Falcon tube (Greiner Bio-One) containing 15 ml of freshly prepared ice-cold modified Weiser epithelial extraction buffer (5.6 mM disodium hydrogen orthophosphate (Sigma), 8 mM potassium dihydrogen orthophosphate (Sigma), 96 mM sodium chloride (Sigma), 1.5 mM potassium chloride (Sigma), 27 mM tri-Sodium citrate (Sigma), 0.5 mM dithiothreitol (DTT, Sigma), 1.5% sucrose (Sigma), 1% D-sorbitol (Sigma), 6.07 mM EDTA (Sigma), 4 mM EGTA (Sigma), pH 7.3). The intestine was washed by gentle shaking in three changes of ice-cold Weiser solution. The tube was then attached to the vortex mixer and shaken at the lowest setting for 15 min, generating the first 'fraction' of epithelial cell extract that were transferred into a fresh tube. Fresh 15 ml of Weiser solution was added to the tube containing the intestine and the shaking steps were repeated twice. Three 15 ml fractions were joined together and the intestine was discarded.

2.2.6.2. Processing of crude epithelial cell suspensions

Epithelial cell suspensions in the 45 ml Weiser buffer were centrifuge at 1500-2000 rpm for 5 min. The supernatant was aspirated and the resulting pellet was resuspended in 20 m of ice-cold 1 X PBS and centrifuged. The wash in 1 X PBS was repeated twice, the pellet was finally resuspended in 3 ml of 1 X PBS and aliquoted into three 1.5 ml eppendorf tubes. The tubes were subsequently centrifuged for 1 minute and the pellet was stored at -80°C until needed.

2.3. Histological analysis

2.3.1. Haematoxylin and Eosin (H&E) staining of tissue sections

Tissue sections were de-waxed and rehydrated as described in section 2.4. Sections were then stained for 5 min in Mayer's Haemalum (R.A. Lamb) followed by washing in running tap water for 5 min. Sections were then stained in 1% aqueous Eosin (R.A. Lamb) for 5 mins followed by two 15 second washes in water. Stained sections were then dehydrated and mounted as described in section 2.4.

2.3.2. Quantitative histological analysis of H&E-stained tissue sections

Quantification of histological sections was performed on an Olympus BX41 light microscope fitted with a Colorview III (5 megapixel, Soft Imaging Systems) camera aided with AnalySIS software (Version 3.2, Build 831, Soft Imaging Systems) or Moticam 5000 camera (5 megpixel, Motic Instruments) aided with Motic Images Advanced Software (Version 3.2, Motic China Group). Quantitative and statistical analysis of histological parameters was performed as described in section 2.10.

2.3.2.1. Scoring of crypt length

Crypt length was scored by counting the total number of epithelial cells from the base to the crypt-villus junction. This was performed for 50 half-crypts per section and average of 50 crypts were scored per mouse.

2.3.2.2. Scoring of villus length

Villus length was scored by counting the total number of epithelial cells from the crypt bottom to the villus tip. Scoring was carried out for 50 half-villi per section. The average villus length was calculated as average total crypt-villus length minus average crypt length for each mouse.

2.3.2.3. Scoring of Mitotic index

Mitotic cells were identified on H&E stained sections based on their morphological appearance. Number of mitotic figures was scored in 50 half-crypts per section. Mitotic index was calculated as average number of mitotic figures per half-crypt for each mouse.

2.3.2.4. Scoring of Apoptotic index

Apoptotic cells were identified on H&E stained sections bashed on their distinctive morphological appearance. The number of apoptotic bodies was counted in 50 half-crypts per slide. The apoptotic index was calculated as average number of apoptotic bodies per half-crypt for each mouse. Where applicable, the position of apoptotic bodies in the crypt was scored to examine the distribution of apoptosis within the crypt. The positional analysis was conducted as described in section 2.10.

2.3.3. Use of special stains for quantification of intestinal histological traits

2.3.3.1. Grimelius staining

The Grimelius staining method was used to identify acgyrophilic enteroendocrine cells. Prior to staining, all glassware used for the staining was rinsed with ultrapure double-distilled (dd) H_2O. Tissue sections were de-waxed and rehydrated as described in section 2.4. 1% (w/v) silver nitrate (Sigma) was dissolved in Acetate buffer (0.02 M acetic acid (Fisher Scientific), 0.02 M sodium acetate (Sigma) in ddH_2O) and preheated to 65°C in a coplin jar in a water bath. Once slides were immersed in this solution, the coplin jar was sealed, wrapped in tin foil and incubated at 65°C for 3 hours. Meanwhile, reducing solution (0.04 M sodium sulphite (Fisher Scientific), 0.1 M hydroquinone (Sigma) in ddH_2O) was freshly prepared and preheated to 45°C. The slides were then transferred from sliver solution into reducing solution where they were incubated for 5 minutes or until the tissue developed yellow colour. Stained slides were then dehydrated and mounted as described in section 2.4.

Stained sections were examined and the number of enteroendocrine cells was scored in 50 half crypt-vills axes per section. The average number of enteroendocrine cells

per half crypt-villus axis was calculated for each mouse and analysed as described in section 2.10.

2.3.3.2. Staining with Alcian Blue

Alcian Blue staining for mucins was used to identify mucin-secreting Goblet cells. Tissue sections were de-waxed and rehydrated as described in section 2.4. Slides were then immersed in Alcian Blue staining solution (1% (w/v) Alcian Blue (Sigma) in 3% (v/v) acetic acid (Fisher Scientific)) for 30 seconds followed by washing in running water for 5 minutes. Tissue sections were then counterstained with 0.1% nuclear fast red (Sigma) for 5 minutes. Sections were washed well in running tap water for 5 minutes and then dehydrated and mounted as described in section 2.4.

Stained sections were analysed and the number of goblet cells were counted in 50 half crypt-villus axes per section. The average number of goblet cells per half crypt-villus axis was calculated for each mouse and analysed as described in section 2.10.

2.3.3.3. Alkaline phosphatase staining

Staining for brush border-specific Alkaline phosphatase was used as a marker of enterocytes. Slides were de-waxed and rehydrated as described in section 2.4. Fast red substrate (DAKO), prepared as described in the manufacturer's instructions, was applied to slides for 20 minutes at room temperature. Slides were rinsed in dH_2O and counterstained in Mayer's Haemalum for 30 seconds followed by a 5 minutes wash in running water. As Fast Red staining is not stable in solvents, slides were mounted using glycerol (Sigma).

The intensity and thickness of the brush border staining were visually analysed using light microscopy.

2.3.3.4. Lysozyme staining

Immunohistochemistry with an anti-lysozyme antibody (see section 2.4) was employed to identify Paneth cells. Both Paneth cell number and position were scored. The number of Paneth cell was counted as the number of lysozyme-positive cells in 50 half-crypts per section. The average number of Paneth cells per half-crypt was calculated for

each mouse and analysed as described in section 2.10. Paneth cell position was scored from the base of the crypt and the positional analysis was carried out as described in section 2.10.

2.3.3.5. Ki67 staining

Immunohistochemistry with an anti-Ki67 antibody (see section 2.4) was used to identify proliferating cells to confirm the morphology-based Mitotic index score. Both Ki67 cell number and position was scored to assess the size and distribution of proliferative compartment within the crypt. The number of Ki67-positive cells was scored as the number of proliferating cells in 50 half-crypts per section. The average number of Ki67-positive cells per half-crypt was calculated for each mouse and analysed as described in section 2.10. Position of Ki67-positive cell were scored from the base of the crypt and the positional analysis was performed as described in section 2.10.

2.3.3.6. Cleaved Caspase-3 staining

Immunohistochemistry with an anti-cleaved Caspase-3 antibody (see section 2.4) was used to identify programmed cell death as a supplement to the Apoptotic index. Both the number and position of Caspase-3 positive cells were scored to assess the quantity of cell death and distribution of apoptosis within the crypt. The average number of apoptotic cells per half-crypt was calculated for each mouse and analysed, and the positional analysis was carried out as described in section 2.10.

2.3.3.7. BrdU staining

Intestinal tissue samples harvested from mice injected with BrdU at 2 or 24 hours before dissection were stained with an anti-BrdU antibody as described in section 2.4. Both the number and position of BrdU positive cells at 2 and 24 hours post-labelling were used to assess proliferation activity and cell migration respectively. The number of BrdU positive cells was counted in 50 half-crypts per section and the average number of BrdU positive cells per half-crypt was calculated for each mouse and analysed as described in section 2.10. The position of BrdU labelled cells was scored from the base of the crypt and cell positional analysis was carried out as described in section 2.10.

2.4. Immunohistochemistry (IHC)

2.4.1. Generic immunohistochemistry protocol

All IHC was performed following the generic protocol described below with specific conditions and modifications for particular antibodies outlined in Table 2.3. All incubation steps were carried out at room temperature (approximately 18-22°C) in a humidified chamber to prevent tissue sections drying out.

2.4.1.1. De-waxing and rehydration of tissue sections

Tissue sections were de-waxed/deparaffinised by washing for 2 x 5 min in Xylene (Fisher Scientific) followed by rehydration washes in decreasing concentrations of ethanol (Fisher Scientific): 2 x 3 min washes in 100% and 1 x 3 min wash in 95% and 1 x 3 min wash in 70% ethanol. Tissue sections were then washed in dH_2O.

2.4.1.2. Antigen retrieval

Antigen retrieval was achieved by heat treatment in a boiling water bath or microwave in either 1 X citrate buffer (LabVision) or a custom citrate buffer (10 mM Sodium Citrate (Sigma), pH 6.0). For retrieval in a boiling water bath, slides were immersed in preheated buffer in a Coplin jar (R.A. Lamb) and incubated at 99°C for the time specified in Table 2.3. For microwave antigen retrieval, adequate buffer was preheated in a plastic container or a plastic pressure cooker for 5 min in a domestic microwave at high power (850W). Slides held in a plastic slide rack were then immersed in preheated buffer and further heated according to conditions specified in Table 2.3. Slides were allowed to cool in antigen retrieval buffer at room temperature for at least 30 min followed by 5 min wash in dH_2O. Slides were then washed in washing buffer (either 1 X PBS (Invitrogen) or 1 X TBS (Sigma) in dH_2O with 0.1% (v/v) TWEEN-20 (Sigma) as specified in Table 2.3).

2.4.1.3. Blocking of endogenous peroxidases

Endogenous peroxidase activity was blocked by incubating tissue sections with hydrogen peroxide. Either 30% hydrogen peroxide (Sigma) diluted in dH_2O to appropriate concentration or a commercial peroxidase blocking solution (Envision+ Kit (Dako)) was used. The appropriate hydrogen peroxide concentrations and incubation times for specific

antibodies are detailed in Table 2.3. Tissue sections were circled with water-resistant wax pen (DAKO), placed in a slide chamber and peroxidase-blocking solution was applied to cover the tissue. Following incubation, slides were briefly rinsed in dH_2O and washed 1 X 5 min in washing buffer.

2.4.1.4. Blocking of non-specific antibody binding

Non-specific binding of antibody was blocked by treating tissue sections either with normal serum (DAKO) or BSA (Sigma) diluted in wash buffer as described in Table 2.3. Typically, the serum used for blocking was derived from the species in which the secondary antibody was raised (i.e. if the secondary antibody was raised in goat, normal goat serum was used to block non-specific binding). Normal serum was applied and slides incubated for the times indicated in Table 2.3. Following incubation, blocking solution was removed and primary antibody was applied without washing of slides.

2.4.1.5. Primary antibody incubation

Primary antibody was appropriately diluted before use in serum block solution. The dilutions and incubation times used with specific antibodies are outlined in Table 2.3. After incubation, primary antibody was removed from the section, the slides were washed 3 X 5 min in washing buffer.

2.4.1.6. Secondary antibody incubation

Tissue sections were incubated with secondary antibody following the optimised protocols outlined in Table 2.3. When signal amplification step was required by the protocol, an appropriate biotinylated secondary antibody (Dako) was diluted 1:200 in serum block. Otherwise, an appropriate Horseradish perosidase (HRP)-conjugated secondary antibody (Envision+ Kit (Dako)) was used undiluted. Appropriate secondary antibodies and incubation times for specific primary antibodies are indicated in Table 2.3. After incubation, slides were washed 3 X 5 min in wash buffer.

2.4.1.7. Signal amplification

When the protocol required the incorporation of a signal amplification step, the Avidin-Biotin Complex reagent (Vectastain ABC kit, Vector labs) was prepared according to

manufacturer's instructions 30 min before used and stored at room temperature. The ABC reagent was then applied to slides for 30 min at room temperature, followed by 3 X 5 min washes in washing buffer.

2.4.1.8. Signal detection using 3,3'-diaminobenzidine (DAB)

The 3,3'-diaminobenzidine (DAB) method was used for colourimetric detection of signal. The (DAB) reagents (Envision+ kit (DAKO)) were prepared according to the manufacture's protocol before incubation (2 drops of DAB chromogen mixed with 1 ml of DAB substrate). Tissue sections were incubated with DAB reagents until adequate brown staining was visible under a microscope. Slides were then washed 1 X 5 min in dH_2O.

2.4.1.9. Counterstaining, dehydration and slide mounting

Nuclei were counter-stained in Mayer's Haemalum (R.A. Lamb) for 30 seconds and washed in tap water for 2 minutes. Slides were dehydrated by immersion in a gradient of ethanol (1 X 3 min 70%, 1 X 3 min 95%, 2 x 3 min 100%) and then in 2 x 5 min washes in Xylene. Sections were mounted in DPX-mountant (R.A. Lamb), covered with 24 x 50mm slips and left to air-dry in a fume hood.

Primary Antibody	BrdU	Lysozyme	Beta-Catenin	Caspase-3	Ki67
Manufacturer	Becton-Dickinson N357580	Neomarkers RB-372	Transduction Labs 610154	R&D systems AF835	Vector labs VPK452
Antigen retrieval	20 min, 100°C water bath, citrate buffer (Thermo)	20 min, 100°C water bath, citrate buffer (Thermo)	20 min, 100°C water bath, citrate buffer (Thermo)	30 min, 100°C water bath, citrate buffer (Thermo)	30 min, 100°C water bath, citrate buffer (Thermo)
Non-specific signal block	peroxidase block (Dako), 5min, RT; 1% BSA, 30 min, RT	1.5% H_2O_2, 15 min, RT; 10% NGS, 30 min, RT	1.5% H_2O_2, 30 min, RT; 1% BSA, 30 min, RT	2% H_2O_2, 10 min, RT; 10% NGS, 30 min, RT	0.5% H_2O_2, 20 min, RT; 20% NRS, 30 min, RT
Wash buffer	3 X5 min PBS/T	3 X 5 min TBS/T	3 X5 min PBS	3 X 5 min PBS	3 X 5 min TBS/T
Primary antibody conditions	1:200 in 1%BSA, 1 h at RT	1:100 in 10% NGS, 1 h at RT	1:300 in 1%BSA, 2 h at RT	1:400 in 10% NGS, O/N at 4°C	1:20 in 20% NRS, O/N at 4°C
Secondary antibody conditions	Envision + HRP-conjugated anti-mouse (DAKO), 30 min at RT	Envision + HRP-conjugated anti-rabbit (DAKO), 30 min at RT	Envision + HRP-conjugated anti-mouse (DAKO), 1 hat RT	Envision + HRP-conjugated anti-Rabbit (DAKO), 30 minat RT	Biotinylated anti-mouse (DAKO), 30 min at RT
Signal amplification	N/A	N/A	N/A	N/A	ABC kit (Vector Labs)

Table 2.3. Part I: Summary of IHC conditions.
Key: NRS – normal rabbit serum, NGS – normal goat serum, BSA – bovine serum albumin, RT – room temperature, O/N – overnight, TBS/T – tris buffered saline with tween, PBS – phosphate buffered saline.

Primary Antibody	HP1γ	HP1γ (phosphor S83)	Akt (phosphor S473)	Pten	Smad2/3
Manufacturer	Millipore 05-690	Abcam Ab45270	Cell Signalling 3787	Cell Signalling 9559	Santa Cruz SC11769
Antigen retrieval	30 min, 100°C water bath, citrate buffer (Thermo)	20 min, 100°C water bath, citrate buffer (Thermo)	30 min, 100°C water bath, citrate buffer (Thermo)	30 min, 100°C water bath, citrate buffer (Thermo)	30 min, 100°C water bath, citrate buffer (Thermo)
Non-specific signal block	0.5% H_2O_2, 20 min, RT; 10% NRS, 30 min, RT	peroxidase block (Dako), 5min, RT; 10% NGS, 30 min, RT	3% H_2O_2, 20 min, RT; 5% NGS, 45 min, RT	3% H_2O_2, 20 min, RT; 5% NGS, 30 min, RT	3% H_2O_2, 20 min, RT; 5% NRS, 35 min, RT
Wash buffer	3 X 5 min PBS	3 X 5 min TBS/T	3 X 5 min TBS/T	3 X 5 min TBS/T	3 X 5 min PBS
Primary antibody conditions	1:1000 in 10% NRS, O/N at 4°C	1:500 in 10% NGS, O/N at 4°C	1:50 in 5% NGS, O/N at 4°C	1:100 in 5% NGS, O/N at 4°C	1:500 in 10% NRS, O/N at 4°C
Secondary antibody conditions	Envision + HRP-conjugated anti-mouse (DAKO), 30 min at RT	Envision + HRP-conjugated anti-rabbit (DAKO), 30 min at RT	Biotinylated anti-rabbit (DAKO), 30 min at RT	Biotinylated anti-Rabbit (DAKO), 30 minat RT	Biotinylated anti-mouse (DAKO), 1:200 in 20% NRS, 30 min at RT
Signal amplification	N/A	N/A	ABC kit (Vector Labs)	ABC kit (Vector Labs)	ABC kit (Vector Labs)

Table 2.3 Part II: Summary of IHC conditions.
Key: NRS – normal rabbit serum, NGS – normal goat serum, BSA – bovine serum albumin, RT – room temperature, O/N – overnight, TBS/T – tris buffered saline with tween, PBS – phosphate buffered saline.

2.5. Immunofluorescence

2.5.1. Deparaffinising and rehydration of tissue sections

Tissue sections were deparaffinised for 2 x 5 minutes in Xylene (Fisher Scientific) followed by rehydration washes in decreasing concentrations of ethanol (Fisher Scientific): 2 x 3 minutes washes in 100% and 1 x 3 minutes wash in 95% and 1 x 3 minutes wash in 70% ethanol. Tissue sections were then washed in dH_2O.

2.5.2. Antigen retrieval

Antigen retrieval was achieved by heat treatment in a boiling water bath in citrate buffer (Thermo). Slides were immersed in preheated buffer in a Coplin jar (R.A. Lamb) and incubated at 100°C for 30 minutes as outlined in Table 2.4. Slides were then allowed to cool in antigen retrieval buffer at room temperature for at least 30 minutes followed by 5 minutes wash in dH_2O. Slides were then washed in 1x PBS (Invitrogen) for 5 minutes.

2.5.3. Blocking of endogenous peroxidases

Endogenous peroxidase activity was blocked by incubating tissue sections with hydrogen peroxide. A commercial peroxidase blocking solution (Envision+ Kit (Dako)) was applied on each slide for 5 minutes at room temperature as outlined in Table 2.4. Following incubation, slides were briefly rinsed in dH_2O and washed in 1x PBS washing buffer for 5 minutes.

2.5.4. Blocking of non-specific antibody binding

Non-specific binding of antibody was blocked by treating tissue sections with normal serum (DAKO) diluted in wash buffer as described in Table 2.4. Normal serum was applied and slides incubated for the times indicated in Table 2.4. Following incubation, blocking solution was removed and primary antibody was applied without washing of slides.

2.5.5. Primary antibody incubation

Primary antibody was appropriately diluted before use in serum block solution. The dilutions and incubation times used with specific antibodies are outlined in Table 2.4. After

incubation, primary antibody was removed from the sections, the slides were washed 3 x 5 minutes in washing buffer.

2.5.6. Secondary antibody incubation

Tissue sections were incubated with fluorescent secondary antibodies in a moist and dark chamber for 60 minutes. Appropriate secondary antibodies and incubation times for specific primary antibodies are indicated in Table 2.4. After incubation, slides were washed 3 x 5 minutes in wash buffer.

2.5.7. Nuclear staining

DAPI (4', 6-Diamidino-2-Phenylindole, Dilactate (DAKO)) solution was applied on each slide and sections were subsequently covered with 24 x 50mm slips. Slides were stored in the dark at -20^{o}C.

Primary Antibody	HP1γ	HP1α	H3K4me3	H3K9me3	H4K20me3
Manufacturer	Millipore 05-690	Abcam Ab77256	Abcam Ab8580	Abcam Ab8898	Active Motif 39180
Antigen retrieval	30 min, 100°C water bath, citrate buffer (Thermo)	30 min, 100°C water bath, citrate buffer (Thermo)	30 min, 100°C water bath, citrate buffer (Thermo)	30 min, 100°C water bath, citrate buffer (Thermo)	30 min, 100°C water bath, citrate buffer (Thermo)
Non-specific signal block	peroxidase block (Dako), 5min, RT; 10% NGS, 30 min, RT	peroxidase block (Dako), 5min, RT; 10% NMS, 30 min, RT	peroxidase block (Dako), 5min, RT; 10% NGS, 30 min, RT	peroxidase block (Dako), 5min, RT; 10% NGS, 30 min, RT	peroxidase block (Dako), 5min, RT; 10% NGS, 30 min, RT
Wash buffer	3 X 5 min PBS	3 X 5 min PBS	3 X 5 min PBS	3 X 5 min PBS	3 X 5 min PBS
Primary antibody conditions	1:1000 in 10% NGS, O/N at 4°C	1:500 in 10% NMS, O/N at 4°C	1:500 in 10% NGS, O/N at 4°C	1:500 in 10% NGS, O/N at 4°C	1:500 in 10% NGS, O/N at 4°C
Secondary antibody conditions	1:400 Anti-mouse 594 (Invitrogen), 60 min at RT	1:400 Anti-goat 488 (Invitrogen), 60 min at RT	1:400 Anti-rabbit 488 or 594 (Invitrogen), 60 min at RT	1:400 Anti-rabbit 488 or 594 (Invitrogen), 60 min at RT	1:400 Anti-rabbit 488 or 594 (Invitrogen), 60 min at RT
Nuclear stain	DAPI (Dako)	DAPI (Dako)	DAPI (Dako)	DAPI (Dako)	DAPI (Dako)

Table 2.4: Summary of Immunofluorescence conditions.

Key: NRS – normal rabbit serum, NGS – normal goat serum, NMS – normal mouse serum, RT – room temperature, O/N – overnight, PBS – phosphate buffered saline.

2.6. *In situ* hybridisation

In situ hybridisation was performed to assess the expression of the intestinal stem cell marker *Olfm4*. This technique uses digoxigenin (DIG) labelled RNA probes (riboprobes) complementarily bind to *Olfm4* mRNA sequence. Probe binding can be detected using an anti-digoxigenin alkaline phosphatase-conjugated antibody by the development of a purple stain. The probe for *Olfm4,* cloned into a pBluescript II SK+ vector, was provided by Hans Clever's group (Hubrecht Institute, Netherlands). All solutions were made using RNase-free water (Sigma) or DEPC treated water. All glassware used in the protocol was heat-treated by baking at 200^{o}C overnight and sterile filtered pipette tips were used throughout.

2.6.1. Probe synthesis

The *Olfm4* probe was synthesised by linearization of plasmid DNA for the transcription of DIG-labelled riboprobes using T7 promoter. 30 µg of plasmid DNA was linearised for probe preparation using NotI restriction enzyme (NEB) according to manufacturer's instructions. The resultant digestion product was analysed on an agarose gel to confirm complete linearisation. The *Olfm4* digest was approximately 700 bps after digest. Linearised DNA was subsequently purified using DNA purification columns (Qiagen). The DNA was quantified using a NanoDrop machine (Thermo Scientific) and adjusted to a concentration of 1 µg/µl using 10 mM Tris (pH 8.0) as required. The linearised plasmid DNA was used as a template for the transcription of DIG-labelled riboprobes using T7 RNA polymerase (Roche). The components of the DIG-labelling reaction are listed in Table 2.5.

Component	**Volume (µl)**
RNase Free H_2O	12
Transcription Buffer (10x) (Roche)	2
DIG RNA Labelling mix (Roche)	2
RNasin (Promega)	1
T7 RNA Polymerase (Roche)	2
DNA (1 µg/µl)	1

Table 2.5: The constituents required for DIG labelling

The labelling reaction was performed for 2 hours at 37°C, followed by DNA template digestion by incubation with 20 units of DNaseI (Ambion) for 15 minutes at 37 °C. Riboprobes were then purified using the RNeasy Mini kit (Qiagen) according to manufacturer's protocols. Probes were eluted with 100 µl of Ultrapure RNase-free H_2O and stored at -80 °C in 10 µl aliquots until use.

2.6.2. Probe hybridisation

Sections were dewaxed in 2 x 10 minutes changes of xylene, and rehydrated by 1 minute washes in ethanol of decreasing concentration: 2 x 100%, 95%, 75%, 50% and 30%. Endogenous alkaline phosphatase activity was blocked in 6% hydrogen peroxide (in 1x PBS) at room temperature for 30 minutes. Slides were then washed 2 x 5 minutes in 1x PBS and digested in Proteinase K (Roche) solution for 5 minutes (200 µg/ml proteinase K, 50 mM Tris, 5 mM EDTA in dH_2O), washed for 5 minutes in 1x PBS, post-fixed in 4$ paraformaldehyde for 5 minutes followed by 2 minutes wash in DEPC treated H_2O. To minimise non-specific probe binding, slides were treated in acetic anhydride solution (0.01 M acetic anhydride (Sigma) in 0.1 M triethanolamine hydrochloride (Sigma)) for 10 minutes at room temperature while stirring, washed once in 1x PBS and once in 1x saline then dehydrated through 1 minutes washes in 30%, 50%, 75%, 95% and 2 x 100% ethanol solutions. Slides were allowed to air-dry for 30 minutes. The *Olfm4* probe was diluted in 1 in 100 in hybridisation buffer (5 x SSC, 50% formamide, 5% SDS, 1 mg/ml heparin, 1 mg/ml calf liver tRNA (Merck) in dH_2O), which was heated at 80°C for 3 minutes. 100 µl of this was then applied to each slide, which was covered in parafilm to prevent probe mixture evaporation, and incubated overnight in a dark and moist chamber at 65°C overnight.

2.6.3. Post-hybridisation treatment

Slides were removed from the chamber and incubated in 5x SSC buffer at 65°C for 15 minutes then washed 2 x 30 minutes in 50% formamide, 5x SSC and 1% SDS (Sigma) for 30 minutes at 65°C. Post hybridisation washes were followed by 2 x 10 minutes washes in 0.5 M NaCl (Sigma), 10 mM Tris pH 7.5 (Sigma), 0.1% Tween-20 (Sigma) at room temperature. Sections were then incubated for 45 minutes in 0.5 M NaCl, 10 mM Tris pH 7.5, 0.1% Tween-20 with 25 µg RNase A (Qiagen) at 37°C. Sections were washed 2 x in 50% formamide, 5x SSC for 30 minutes at 65°C and pre-blocked in 10% heat-inactivated sheep

serum (DAKO) in PBS/T for 2-3 hours. Anti-DIG alkaline phosphatase conjugated antibody (Roche) was pre-absorbed in 1% heat-inactivated sheep serum in PBS/T containing 5 mg/ml mouse intestinal powder for 3 hours at 4°C and diluted to a final concentration of 1:2000 in 1% sheep serum in PBS/T. Slides were overlaid with 100 µl of antibody solution and were then covered in parafilm and incubated in a dark and moist chamber at 4°C overnight.

2.6.4. Signal detection

Slides were washed 3 x in PBS/T for 5 minutes, followed by 3 x 30 minutes wash in PBS/T. Slides were then preconditioned to inhibit endogenous alkaline phosphatase by washing 3 x in NTMT buffer (0.1 M NaCl, 0.1 M Tris pH 9.5, 0.05 M $MgCl_2$ (Sigma), 0.1% Tween, 2 mM Levamisole (Sigma)). The BM Purple substrate (Roche) was added to the slides and incubated in the dark at room temperature until desired level of signal was developed. Slides were then washed in PBS/T for 10 minutes and counterstained with Eosin (Sigma) for up to 10 seconds. Excess Eosin was washed off under running tap water and slides were dipped in xylene prior to air-drying and mounting using DPX mounting media (R.A. Lamb).

2.7. Quantitative Protein Analysis

2.7.1. Protein extraction from tissue samples

Epithelial cell extract samples and whole tissue samples (prepared as described in section 2.2.6 and 2.2.4, respectively) in eppendorf tubes were removed from storage at -80°C and placed on dry ice. 200 µl of cell lysis buffer (20 mM Tris-HCl pH 8.0, 2 mM EDTA pH 8.0, 0.5% (v/v) NP-40 (Sigma)) containing protease inhibitors (Complete mini protease inhibitor cocktail tablets (Roche)) and phosphatase inhibitors (25 mM sodium β-glycerophosphate (Calbiochem), 100 mM sodium fluoride (Sigma), 20 nM Calyculin A from *Discodermia calyx* (Sigam), 10 mM sodium pyrophosphate (Sigma)) were added. Cells were sheared by passing through a 23-gauge needle using a syringe at least 20 times. Tubes were then centrifuged in a refrigerated centrifuge (Legend Micro 17R, Thermo Scientific) at 9500 x g for 10 min at 4°C to remove residual insoluble material. The supernatant was then aliquoted into clean tubes and stored at -80°C until needed.

2.7.2. Quantification of protein concentration

The relative amount of total protein in each protein extract was determined using the Pierce BCA (Bicinchoninic acid) kit (Thermo Scientific). Serial dilutions of BSA (from 5 µg/ml to 35 µg/ml) in 1 X PBS (Invitrogen) were prepared along with serial dilutions of protein extract samples (1:100, 1:200, 1:400 and 1: 800 in 1 X PBS) and blank solutions containing 1 X PBS. All solutions were loaded in duplicates onto a 96-well plate. BCA kit reagents A and B were mixed in 50:1 ratio according to the manufactory guidelines. 100 µl of the mix was added to each well and mixed gently by pipetting. The plate was then incubated at 37°C for 1 hour or at room temperature overnight. After incubation, the plate was read at 590 nm on an appropriate colourimeter or a microplate reader (BioTek). A standard curve was generated using serial dilutions of BSA and respective protein concentrations in extracted samples were calculated. The standard curve was then used to extrapolate the relative concentration of protein in each experimental sample.

2.7.3. Western-blotting analysis

2.7.3.1. Preparation of protein samples

Samples were removed from storage at -80°C, defrosted on ice and appropriate amount of protein extract containing 30 µg of protein was transferred into a clean eppendorf tube. Samples were made up to 25 µl using Laemmli buffer (see Table 2.7 for composition). Samples were denatured by heating to 95°C for 5-10 min and then quenched on ice just prior to loading.

2.7.3.2. Casting of polyacrylamide gels

SDS-PAGE gels consist of resolving and stacking phases. Solutions for resolving (10%) and stacking (5%) gels were prepared according to conditions laid out in Table 2.6, but without addition of TEMED. SDS-PAGE gels were set using Mini-Protean III (Bio-Rad) gel casting apparatus with 1.5 mm spacers. Casting plates were cleaned with 70% ethanol (Fisher Scientific) before being assembled in a gel casting apparatus and filled to

approximately two thirds with the resolving gel. Once set, the stacking gel was poured over the resolving gel and a 10 or 15-well comb was inserted immediately. After the stacking gel had set, the combs were removed and the wells were rinsed with ddH_2O water.

5% Stacking polyacrylamide gel (2 gels)	**10% Resolving polyacrylamide gel (2 gels)**
6.9 ml distilled water	6.8 ml distilled water
1.7 ml 30% Acrylamide (Sigma)	8.4 ml 30% Acrylamide (Sigma)
100 µl 10% (w/v) Sodium dodecyl sulphate (SDS, Sigma)	250 µl 10% (w/v) Sodium dodecyl sulphate (SDS, Sigma)
1.3 ml 1M Tris-HCl pH 6.8 (Sigma)	9.4 ml 1M Tris-HCl pH 8.8 (Sigma)
66 µl 25% (w/v) Ammonium persulphate (APS, Sigma)	72 µl 25% (w/v) Ammonium persulphate (APS, Sigma)
13.2 µl N,N,N,N-tetramethylethylenediamine (TEMED, Sigma)	13.2 µl N,N,N,N-tetramethylethylenediamine (TEMED, Sigma)

Table 2.6 Composition of gels for SDS-PAGE.

Laemmli Buffer	**5x running buffer（1L）**	**1x Tris-Glycine transfer buffer (1L)**	**Stripping buffer**
0.125 M Tris-HCl pH 6.8 (Sigma)	950 ml deionized H2O	800 ml deionized H2O	62.5 mM Tris-HCl pH 6.8 (Sigma)
4%（w/v） SDS (Sigma)	15.1 g Tris base (Sigma)	200 ml methanol (Fisher Scientific)	2% w/v SDS (Sigma)
40% v/v glycerol (Sigma)	94 g Glycine (Sigma)	2.9 g Tris base (Sigma)	0.7% v/v beta-mercaptoethanol (Sigma)
0.1% w/v Bromophenol Blue (Sigma)	50 ml 10% (w/v) SDS (Sigma)	14.5 g Glycine (Sigma)	
6%（v/v） beta-mercaptoethanol (Sigma)			

Table 2.7 Composition of buffers used in Western analysis.

2.7.3.3. Protein separation by SDS-PAGE

Protein separation was performed using the Mini-Protean III (Bio-Rad) electrophoresis tank containing sufficient amount of SDS-PAGE running buffer (see Table 2.7 for composition). Full-range Rainbow molecular weight marker (Amersham) was loaded into the first lane of each gel and prepared protein samples were loaded into the appropriate remaining wells and gels were run at 120-200V until the dye front reached the end of the gel.

2.7.3.4. Transfer of proteins to nitrocellulose membranes

Before transfer, Amersham Hybond-ECL nitrocellulose membrane (GE Healthcare) was cut to a required size and soaked in transfer buffer prior to use. The membrane sandwich was assembled according to manufacturer's instructions in a wet electroblotting system (Flowgen Biosciences) using sponges, 3MM blotting paper (Whatman), membrane and the prepared gel as shown in Figure 2.3. Air bubbles were carefully rolled out after the addition of each layer. The blotting tank was fitted with blots so that current runs through gel towards the filter, filled with transfer buffer and placed in ice and run at 100V for 1 hour.

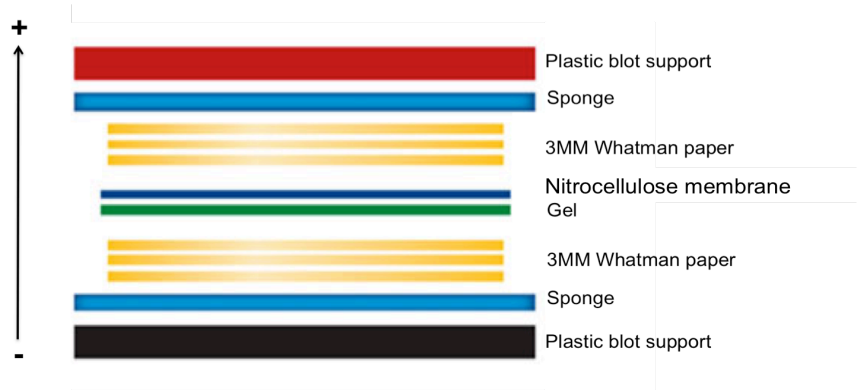

Figure 2.3. Blotting apparatus set-up for Western Analysis

2.7.3.5. Generic protocol for probing of membranes

Upon completion of the transfer, membranes were washed briefly in PBS/T. To prevent non-specific binding, blots were incubated in 5% skimmed milk powder in TBS/T under agitation for at least 1 hour at room temperature. Membranes were incubated with

agitation in blocking solution containing the appropriate dilution of primary antibodies under conditions specified in Table 2.8. After cultivation, membranes were then washed in PBS/T 3 x 5 min followed by cultivation with appropriate secondary antibody under conditions detailed in Table 2.8. Subsequently, membranes were washed again in PBS/T 3 X 5 min prior to protein detection. Appropriate amount of ECL reagent kit (Amersham) was used to develop membranes according to manufacturer's instructions. After incubation, blots were then wrapped in cling film prior to signal detection.

Primary Antibody	HP1γ	β-Actin
Manufacturer	Millipore 05-690	Sigma A5316
Primary Antibody conditions	1:1000 in 1% BSA in PBS, O/N at 4°C	1:5000 in 5% milk in TBS/T, 1 h at RT
Secondary Antibody	HRP-conjugated anti-mouse (GE Healthcare) 1:3000 in 1% BSA in PBS, 1 h at RT	HRP-conjugated anti-mouse (GE Healthcare) 1:2000 in 5% milk in TBS/T, 1 h at RT
Detection Reagents	ECL Advance (GE Healthcare)	ECL
Target Protein Size	25 kDa	48 kDa

Table 2.8: Antibody-specific conditions for Western blotting analysis.

2.7.3.6. Visualisation of protein bands

Immobilised immuno-labelled proteins were detected using ECL/ECL+ reagent (GE Healthcare, UK) according to manufacturer's instruction. Prepared ECL/ECL+ solutions were mixed well and cultivated for 1 minute, before addition on the membrane (1 ml per membrane). After removal of excess reagent, the membrane was placed in a molecular imager system (Gel Doc XR, Biorad) and exposed for varying lengths of time. Pictures of protein bands and molecular weight marker were captured and realigned and the target protein was identified by comparison to the molecular weight marker.

2.7.3.7. Stripping and reprobing of membranes

Membranes were stripped before being incubated with subsequent antibody of interest. Membranes were washed in PBS/T and incubated in stripping buffer (see Table 2.7 for composition) for 30 min at 55°C under gentle agitation. Membranes were washed in

PBS/T, blocked in milk blocking solution and probed with required antibodies overnight. The visualisation was performed as described in section 2.7.3.6.

2.8. Gene expression analysis

2.8.1. Isolation of RNA

To prevent degradation of RNA, care was taken during RNA isolation to ensure that all plastic and glassware was RNase-free. All solutions were made using RNase-free water (Sigma) or Diethyl pyrocarbonate (DEPC, Sigma)-treated water. Working surfaces and pipettes were treated with RNaseZAP (Sigma). Sterile filtered pipette tips were used throughout.

2.8.1.1. Homogenisation of whole tissues and epithelial cell extracts

Small intestine or epithelial cell extracts were placed in homogenising lysing matrix D tubes (MP Biomedicals) containing 1 ml Trizol reagent (Invitrogen) and 1.4 mm ceramic beads, and were homogenised using Precellys 24 homogeniser (Bertin Technologies) at 6500 RPM for 2 x 45 second cycles. The samples were then centrifuged at 13,000 rpm for 10 minutes at 4°C to pellet the cell debris and the ceramic beads.

2.8.1.2. RNA extraction

After homogenisation and centrifugation of samples, the supernatants were placed in a fresh set of RNase/DNase free 1.5 ml eppendorf tubes and 200 µl of chloroform (Fisher scientific) was added to each tube in a fume hood. The samples were then placed on ice with occasional shaking. The tubes were then centrifuged at 13,000 rpm for 15 min at 4°C to separate the solution phases. The top, aqueous phase containing RNA was removed and transferred into clean 1.5 ml eppendorf tubes containing 400 µl of the pre-chilled isopropanol (Fisher scientific). Tubes were then shaken well and incubated at 4°C for 1 hour or overnight to precipitate RNA. The samples were then centrifuged as aforementioned to collect RNA pellets, which were washed with 500 µl of ice-cold 75% ethanol (Fisher scientific), then the ethanol was discarded and the pellets were left to air-dry at room temperature for 10 minutes. To dissolve the pellet, 100 µl of RNase-free water (Sigma) was added and tubes were heated to 65°C for 10 minutes.

2.8.1.3. RNA Purification

Purification of RNA was achieved using the RNeasy Mini kit (Qiagen). All centrifugation steps were performed at 13,000 rpm in a refrigerated bench top centrifuge at 4°C. The 100 µl RNA from the previous step was used for purification and the kit was used according to the manufacturer's instructions. The concentration and purity of RNA was assessed in a 1 µl sample using NanoDrop 1000 (Thermo Scientific), then the samples were stored at -80°C until usage.

2.8.1.4. Determination of RNA quality

The quality of RNA was checked using denaturing agarose gel electrophoresis. RNA samples containing 2 µg of RNA were mixed with the appropriate amount of RNA 5 X loading buffer (See Table 2.9), incubated at 65°C for 10 min and then quenched on ice before being loaded onto the gel. Samples were loaded onto a denaturing gel (1% agarose (Eurogentech), in 1 X FA gel buffer. The gel was then run in FA gel running buffer at 120 V for 30 min. RNA was visualised under UV light on a GelDoc (BioRad). Assessment of RNA quality was determined by the sharpness of 18S and 28S ribosomal RNA bands.

5 X RNA Loading Buffer	1 X FA Gel Buffer	1 X FA Gel Running Buffer
0.25% Bromophenol blue (Sigma) 4 mM EDTA (Sigma) 0.9 M formaldehyde (Sigma) 20% glycerol (Sigma) 30% formamide (Sigma) 1 X FA gel buffer	20 mM 3-(N-Morpholino) propanesulfonic acid (MOPS, Sigma) 5 mM sodium acetate (Sigma) 1 mM EDTA (Sigma) 0.25 M formaldehyde (Sigma) 0.1 µg/ml Ethidium bromide (Sigma)	20 mM 3-(N-Morpholino) propanesulfonic acid (MOPS, Sigma) 5 mM sodium acetate (Sigma), 1 mM EDTA (Sigma) 0.25 M formaldehyde (Sigma)

Table 2.9: Composition of FA gel buffers

2.8.2. Preparation of cDNA for quantitative analysis

2.8.2.1. DNase treatment of RNA samples

The purified RNA samples were DNase treated to eliminate any remnants of trace DNA. A total of 10 µg of RNA was treated 10 µl of RQ1 enzyme (Invitrogen) and 5 µl RQ1 buffer (Invitrogen) and the total volume were made up to 50 µl with RNase free-water. The mix was incubated at 30°C for half an hour and the reaction was stopped by adding 5 µl of stop solution and heating to 65°C for 10 minutes.

2.8.2.2. Reverse transcription

For the cDNA synthesis, the DNase treated RNA yielded at a concentration of 1 µg/5.5 µl was used. The reverse transcription enzyme mix was prepared by adding 2 µl of random primers (100 ng/µl (Invitrogen)), 2 µl of dNTP (10mM (Invitrogen)), 12 µl of DNase treated RNA and 11 µl of RNase free-water. The mix was heated at 65°C for 5 min before returning to ice, 8 µl of First strand buffer (5x (Invitrogen)) and 4 µl of 0.1 M Dithiothreitol (DTT, Invitrogen) was added to tubes and incubated at room temperature for 2 min prior adding 1 µl of Superscript II or III reverse transcriptase (Invitrogen). Reverse transcription was carried out under following conditions: 25°C for 10 min, 42°C for 50 min and the enzyme was inactivated at 70°C for 15 min. After cDNA preparation was complete, 160 µl of RNase-free water was added to each sample to make up to 200 µl total cDNA solution. Negative control cDNA samples were prepared in the same way but excluding Superscript enzyme to the enzyme mix.

2.8.3. Quantitative real-time (qRT) PCR analysis

2.8.3.1. Primer design for qRT-PCR

Primer sets for qRT-PCR analysis were designed to ensure the PCR product yield was between 100-200 bp in size and have an annealing temperature close to 60°C, and where possible, primers were designed to reside across exon boundaries to avoid amplification of genomic DNA. Primers (Rac1, Rac1b, ATM, CDC25C, CCNE1, DDX11, PIM1 and CAV2) were designed using Primer3 web-based program (http://bioinfo.ut.ee/primer3/) and primer sequences were checked for mis-priming using BLAST engine against Ensembl database (http://www.ensembl.org/Multi/blastview) and synthesised by Sigma-Genosys. Madeleine Young kindly provided the Notch-targeted primer sequences (Delta1, nRarp, Hes1, mTert, Lrig1, Jagged1 and Jagged2). Primer sequences (Axin-2, CD44, c-Myc, Cyclin D1, E-cadherin and Beta-Actin) were obtained from the literature (Reed *et al.*, 2008b). The primer sequences used are provided in Table 2.10.

Target	Forward Primer Sequence (5' to 3')	Reverse Primer Sequence (5' to 3')
Axin-2	GCT CCA GAA GAT CAC AAA GAG C	AGC TTT GAG CCT TCA GCA TC
CD44	ATC GCG GTC AAT AGT AGG AGA A	AAA TGC ACC ATT TCC TGA GAC T
c-Myc	CTA GTG CTG CAT GAG GAG ACA C	GTA GTT GTG CTG GTG AGT GGA G
Cyclin D1	ACG ATT TCA TCG AAC ACT TCC T	GGT CAC ACT TGA TGA CTC TGG A
E-cadherin	CAG ATG ATG ATA CCC GGG ACA A	GGA GCC ACA TCA TTT CGA GTC A
Beta-Actin	TGT TAC CAA CTG GGA CGA CA	GGG GTG TTG AAG GTC TCA AA
EphB3	TAA CGC TGT GGA GGT CTC TGT A	CCT TGC TTT GCT TTG TAA CTC C
Msi-1	CCT GGT TAC ACC TAC CAG TTC C	AGA GCC TGT CCC TCG AAC TAC
Rac1	TTG CCG AGC TTT CCC GAA AG	CGG CCA TTT CCT GTT TTC TCT
Rac1b	GAC GGA GCT GTA GGT AAA ACT TG	ATC GGC AAT CGG CTT GTC TT
ATM	AGA ACC AGC TGC TAG ATC CG	GGG ACT TCT GTG AGG GGG AA
CDC25C	AGG TTG TTG AGA GAG TGG AAG G	TCA TTC TGT GGA GTC TTC GCT
CCNE1	TCT AGC CCC ACC CCT TTA GT	TTT AAA TGT CCC GCT CGA AGC
DDX11	GTG AGT GTG AGG GAT GAG GG	CTA AAC GCA GCA CCG TGG
PIM1	GCG ACA TCA AGG ACG AGA AC	TCA GAG CTG GCA GGG GTG
CAV2	GTT CGG ACT GCA AGC CAA G	GAG GCT AGG CAG GGC GAA
Delta1	CAA CTG TCC ATA GTG CAA TGG	CTG AGG TGT AAG ATG GAA GCG
nRarp	GCG TGG TTA TGG GAG AAA GAT	GGG AGA GGA AAA GAG GAA TGA
Hes1	GTG GGT CGT AAC GCA GTG TC	TCA GAA GAG AGA GGT GGG CTA
mTert	TGG CTT GCT GCT GGA CAC TC	TGA GGC TCG TCT TAA TTG AGG TC
Lrig1	GGG TCC ACG GCT ATC ATC AGC TC	CCG CCT CTG AGG ACT GAA AAC GC
Jagged1	TGC AGC TGT CAA TCA CTT CG	CAG AAT GAC GCT CCT GTC G
Jagged2	GTC CTT CCC GAT GGG AGT T	GTT TCC ACC TTG ACC TCG GT

Table 2.10: QRT-PCR primer sequences

2.8.3.2. qRT-PCR reaction

All qRT-PCR reactions were run on StepOnePlus real-time PCR system in conjunction with StepOne software v2.1 (Applied Biosystems). Each reaction was performed in a minimum of three technical and three biological replicates. In addition to this, control samples devoid of cDNA served as negative controls were run to ensure no contaminants were present in cDNA samples. A housekeeping gene (typically β-actin) was used on each plate as a reference gene.

The traditional qRT-PCR reaction reagent SYBR Green qPCR mix (Fast Mix, Applied Biosystems) that fluoresces when bound to double stranded DNA was used. qRT-PCR reactions were carried out in triplicate in MicroAmp 96-well PCR plates 0.1 ml wells (Applied Biosystems), and sealed with MicroAmp heat activated optical adhesive film lids (Applied Biosystems). Each reaction contained 10 ng of cDNA, 10 µl Fast Mix SyBR green mix (Applied Biosystems), 0.5 µl of 10 nM Primers (forward and reverse) and made up to 20 µl with DNase/RNase-free water. qRT-PCR reactions were performed using the StepOne Plus Real-Time PCR System (Applied Biosystems), all reaction were carried out under the same cycling conditions: 95^{o}C for 15 min for initial denaturing cDNA, followed by 30 cycles of a denaturation step at 95^{o}C for 30 seconds, and an annealing step at 60^{o}C for 30 seconds followed by an elongation step at 72^{o}C for 30 seconds. qRT-PCR reactions for the intestinal stem cell markers (*Lgr5, Ascl2, Olfm4, Bmi1* and *β-actin*) were performed using TaqMan assay (Applied Biosystems) following the manufacturer's instructions and using custom design TaqMan probes (Applied Biosystems). Forward and reverse primers (100 mM) were mixed and diluted to 10 mM concentration. TaqMan reactions were run using the following conditions 50 ^{o}C for 2 min, 95 ^{o}C for 10 min followed by 40 cycles of 95 ^{o}C for 15 seconds and 60 ^{o}C for 1 min. The experimental data was collected automatically using StepOne software (Applied Biosystems).

2.8.3.3. Analysis of qRT-PCR data

Data was initially visually examined using Step One Plus software. Melting curves were briefly analysed to confirm that each reaction yielded only one product at the expected melting temperature and formation of primer dimers was minimal.

Data was analysed using the $2^{\Delta\Delta CT}$ method (Livak and Schmittgen, 2001). Cycle time (C_T) values for each reaction was recorded and duplicates averaged. ΔC_T values were calculated using C_T value of the reference gene from the same sample for target gene of interest. The average ΔC_T across all biological replicates was then calculated, and $\Delta\Delta C_T$ was calculated as the difference in ΔC_T average between genotypes. The average $\Delta\Delta C_T$ from each biological group was then transformed into fold change according to the formula $2^{\Delta\Delta CT}$.

2.9. Cell culture maintenance and storage

2.9.1. Maintenance of cell line

The human embryonic kidney cells (HEK-293) were kindly provided by Prof. Trevor Dale's lab (School of Bioscience, Cardiff University). HEK-293 cell line was cultured in Dulbecco's modified Eagle's medium (DMEM, Invitrogen), supplemented with L-glutamine (2 mM, Invitrogen), 10% v/v foetal bovine serum (FBS, Sigma), penicillin (50 µg/ml, Invitrogen) and streptomycin (50 µg/ml, Invitrogen). The cell line was incubated at 37°C and 5% CO_2 in T25 or T80 tissue culture flasks (Nunc, Leics, U.K.) and were routinely passage every 2-3 days at a split ratio of 1:2 - 1:5 once they became 80 - 90% confluent. Growth media was aspirated and the cells were washed with 1 X PBS (Invitrogen) to remove any remaining media. The wash was removed and 2 ml for T25 or 4 ml for T80 tissue culture flasks of 0.25% Trypsin/EDTA (Invitrogen) was added to the flask followed by 5-10 minutes incubation at 37°C and the detachment of cells was observed under microscope. An appropriate volume of growth medium was added to the cells and these were then split at an appropriate ratio by the removal of excess cell suspension into waste. The remaining volume of cell suspension was made up to 5 ml for T25 or 15 ml for T80 tissue culture flasks with complete growth medium.

2.9.2. Long term cell storage

To maintain sufficient aliquots of same passage number cell lines, cells were frozen and cryo-stored using Mr. Frosty (Fischer Scientific). Respective cells were detached using 0.25% Trypsin/EDTA (Invitrogen) and re-suspended in 10 ml of growth medium in a 15 ml falcon tube, followed by centrifugation at 1100 rpm for 5 minutes at room temperature. The supernatant was aspirated and the pellet of cell was re-suspended in 1 or 2 ml of freezing medium (complete medium containing 10% v/v dimethyl sulfoxide (DMSO, Sigma)) and aliquoted into two 1 ml or one 2 ml Cryo-tube vials (Nunc, Leics, U.K.). The tube(s) were then placed into Mr. Frosty with Iso-propanol (Fischer Scientific) to facilitate slow freezing at -80°C for 24 hours before being transferred into either -80°C freezer for up to 2 weeks or liquid nitrogen storage for long-term storage. When cells were retrieved from Cryo-storage,

they were quickly defrosted in a 37°C water bath to avoid DMSO toxicity before being re-suspended in 10 ml of complete growth media and centrifuged at 1100 rpm at room temperature for 5 minutes. The cell pellet was re-suspended in 5 ml of complete growth medium and transferred to a T25 or T80 flask.

2.9.3. Cell counting

In order to allow the seeding of cells at appropriate density, cells were counted using an Improved Neubauer Counting Chamber (Hawksley). Cells were detached using 0.25% Trypsin/EDTA (Invitrogen) and re-suspended in an appropriate volume of complete growth medium and 10 µl of cell suspension was loaded into the counting chamber. Cells were counted under a microscope in four 1 mm^2 squares and the number of cells per ml of suspension was determined by calculating the average count per square and multiplying it by 1 x 10^4.

2.9.4. Transfection and Luciferase reporter assays

2.9.4.1. Transient siRNA transfection

In order to achieve *CBX3* knock down in HEK-293 cells, siCBX3 (FlexiTube, QIAGEN) were used. The negative control siRNA (AllStar Negative Control siRNA, QIAGEN) was designed to have minimal targeting of known genes in human. The siRNA (total amount of 5 nmol) was re-suspended according to manufacturer protocol in 250 µl of RNase-free water to obtain required concentration of 20 µM.

Cells were transfected with siRNA using lipofectamine RNAiMAX (Invitrogen). Volumes and concentrations of the reagents used in different tissue culture plates are outlined in Table 2.11. The appropriate volume of siRNA was diluted in serum-free OPTIMEM (Invitrogen) in the well of a tissue culture plate and mixed gently to cover the entire well surface. Appropriate volume of Lipofactamine RNAiMAX was subsequently added to each well containing the siRNA in OPTIMEM. The complex was mixed and incubated for 20 minutes at room temperature to allow the siRNA-Lipofectamine complexes

to form. Meanwhile, cells were diluted in antibiotic-free growth medium (for seeding concentrations see Table 2.12.). Cells were then carefully added to each well containing siRNA-Lipofactamine complexes and were incubated at 37°C in a 5% CO_2 incubator for 48 hours before being harvested and analysed.

Tissue culture vessel	Number of cells	Volume of Complete medium (ml)	Opti-MEM dilution medium	Final siRNA conc. (nM)	Volume of 20 µM siRNA	Lipofectamin RNAiMAX
96-well	2 x 10^4	0.1	20 µl	20	0.06 µl	0.3 µl
24-well	1 x 10^5	0.5	100 µl	20	0.8 µl	1.0 µl
6-well	5 x 10^5	2.0	500 µl	20	4.5 µl	7.0 µl

Table 2.11. Volumes and concentration of reagents for transient siRNA transfection in different culture plates.

Tissue culture vessel	Number of cells	Volume of Complete medium (ml)	Opti-MEM dilution medium	Plasmid DNA	Volume of Transfectin Reagent
96-well	2 x 10^4	0.1	25 µl	0.1 µg	0.3 µl
24-well	1 x 10^5	0.5	50 µl	0.6 µg	1.8 µl
6-well	5 x 10^5	2.0	250 µl	2.9 µg	8.7 µl

Table 2.12. Volumes and concentration of reagents for transient transfection for cells with plasmid DNA.

2.9.4.2. Transfection of cells with reporter plasmids

The TCF/LEF reporter plasmid, TOP-flash, and its mutant control, FOP-flash, were provided by Trevor Dale's lab (School of Bioscience, Cardiff University). For measuring transfection efficiency, cells were co-transfected with a non–Tcf/Lef-dependent β-gal coding vector, pcDNA-LacZ. In brief, HEK-293 cells were transfected with appropriate amount of siRNA (see Table 2.11) cultured in a 96-well plate to reach 60-80% confluence at the time of DNA plasmid transfection. The next day, cells were transfected in triplicates with 0.1 µg (100 ng) total DNA per well. Each of the plasmids were transfected at 0.033 µg/well, for pTOP-flash (which contains consensus sequence of Tcf/Lef enhancer upstream of the luciferase enzyme-coding region), pFOP-flash (control), pcDNA-lacZ (transfection control), ΔNLRP6, TCF4 or pcDNA3.1. Vector alone was included in the experiments. Transfection was carried out using Transfectin (BioRad) as described in Table 2.12. After four hours incubation, media

and DNA complexes were aspirated and replaced with fresh antibiotic-free medium and the cells were incubated for 48 hours at 37°C in 5% CO_2 before being lysed.

2.9.4.3. TCF/LEF luciferase reporter assays

After 48 hours post-transfection with luciferase reporter plasmids, cells were lysed in 50 µl GLO-lysis buffer (Promega) per well for 30 minutes on a rocker at room temperature. The lysates were equally aliquoted into two replicate white-walled and clear-bottomed plates (Corning). BrightGLO substrate and BetaGLO substrate (Promega) were used on each plate for the quantification of luciferase and β-gal activity respectively. Both activities were measured using a BMG Fluostar multi-platform plate reader using the luminescence mode. Tcf-mediated gene transcription was determined by the ratio of pTOP-flash/pFOP-flash luciferase activity, each normalized to β-gal enzymatic activity levels. The mean values of the normalized ratios were compared.

2.10. Statistical analysis

2.10.1. Kaplan-Meier survival analysis

Survival analysis and generation of survival curves was performed using the Kaplan-Meier method. All analyses were performed with the aid of SPSS software (Version 20). Statistical significance between survival times of different experimental cohorts was examined using the Log-Rank method. A significant difference between survival probabilities was accepted if p value was less or equal 0.05.

2.10.2. Kolmogorov-Smirnov analysis

Kolmogorov-Smirnov test was used to determine if two data sets differ significantly. All analyses were performed using the SPSS software (Version 20). The two-tailed test was used throughout and significant difference between distributions was accepted when p value was less or equal 0.05.

2.10.3. Mann-Whitney U-test

The Mann-Whitney U-test was used to determine statistical differences between non-parametric data sets. This was performed using the SPSS software (Version 20). A significant difference between means was accepted when p value was less or equal 0.05.

2.10.4. Student's t-test

The Student's T-test was used to test statistical differences between normally distributed data sets and between data sets with sample sizes of n = 3. This test was performed in Excel 2010 software.

Chapter Three

Investigating the effects of *Cbx3* loss in the small intestine

3. Investigating the effects of *Cbx3* loss in the small intestine

3.1. Introduction

HP1γ plays a critical role in chromatin organisation and gene expression and a growing body of evidence has implicated HP1γ as a novel prognostic and therapeutic target in various types of cancer (Slezak *et al*., 2013; Takanashi *et al*., 2009). Furthermore, a number of studies have implicated HP1γ in the regulation of cell differentiation and cancer development. Decreased expression of HP1γ is observed during cell differentiation, which is unique to this isoform compared to HP1α and HP1β. In differentiated cells of various normal human tissues, HP1γ is absent or not detectable, suggesting that the loss of HP1γ is required for cell differentiation to occur (Takanashi *et al.,* 2009). HP1γ has been documented to play a role in regulating cell proliferation, differentiation (Takanashi *et al.,* 2009), male germ cell survival and spermatogenesis (Brown *et al.,* 2010). Furthermore, upregulation of HP1γ is frequently observed in many cancer cell lines (including colon cell lines) and repression of HP1γ expression in selected cancer cell lines, which results in growth inhibition (Takanashi *et al.*, 2009). Consistent with this, the deletion mutant of HP1γ lacks tumorigenesis activity in a mouse xenograft model (Sharma *et al.,* 2003), suggesting that the expression of HP1γ may be important in the process of tumorigenesis. Given that HP1γ is closely linked to cell proliferation, differentiation and tumorigenesis, and little is known about the functional involvement of HP1γ in colorectal cancer development, it is of great interest to investigate the role of HP1γ in colorectal cancer initiation, progression and tumour development. The murine small intestinal epithelium is commonly used as a model tissue to study human CRC, particularly the early stages of this disease, because this tissue has been proven to be an excellent *in vivo* model system to study stem cell renewal (Fevr *et al.*, 2007), cell differentiation and proliferation, (i.e. intestinal homeostasis) that is maintained by Wnt signalling (Korinek *et al.*, 1997). It is of great interest to study the role of HP1γ in Wnt signalling therefore, it appears to be appropriate to investigate the consequences of *Cbx3* loss in normal intestinal epithelium in order to further explore its role in cancer development.

Conditional deletion of *Cbx3* was achieved using conditional transgenesis, involving LoxP-targeted *Cbx3* alleles combined with the inducible *VillinCreER* transgene. In this

chapter the effects of epithelial-specific *Cbx3* deletion both on epithelial homeostasis and on the intestinal stem cell were characterised and discussed.

3.2. Results

3.2.1. *VillinCreER* drives recombination in the small intestine with high efficiency

In order to examine the effects of *Cbx3* loss in the small intestinal epithelium, animals bearing the *VillinCreER* transgene were crossed with animals bearing LoxP-targeted *Cbx3* alleles (*Cbx3*$^{fl/fl}$). The VillinCreER is expressed along the entire length of the small and large intestine and its recombination is induced by treatment regime of 4 consecutive daily intraperitoneal administration of tamoxifen at a dose of 80 mg/kg (el Marjou *et al*., 2004).

Expression of *VillinCreER* recombinase in the small intestinal epithelium was confirmed using the ROSA26R LacZ reporter allele (abbreviated here as LacZ). The reporter construct consists of the LacZ β-galatosidase transgene with a LoxP flanked Stop-cassette (Soriano, 1999). In unrecombined cells, the Stop-cassette attenuates expression of the LacZ transgene. Following exposure to Cre recombinase, the LoxP flanked Stop-cassette is removed and the expression of β-galatocidase from the LacZ transgene is mediated. X-Gal substrate can be used as an indicator for cells expressing LacZ which results in a colourimetirc change from colourless to blue, therefore allowing identification of cells expressing Cre recombinase (See Figure 3.1).

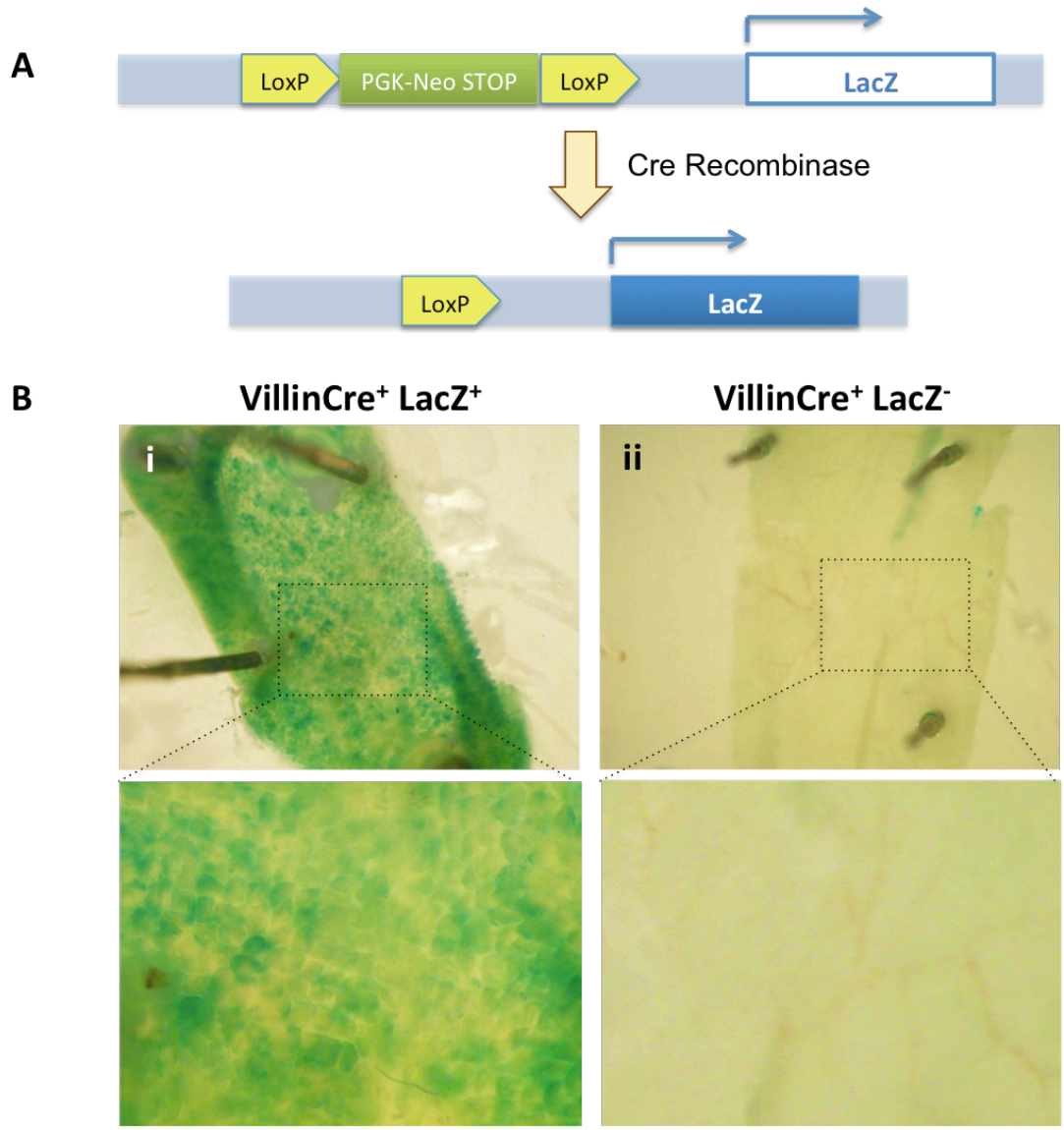

Figure 3.1: Assessment of *VillinCreER*-mediated recombination in the small intestinal epithelium. **(A) The ROSA26R transgene was used to report recombination within the small intestine. LoxP sites flank a PGK-Neo-STOP cassette inserted in the LacZ transgene. Induction of Cre recombinase activity results in PGK-Neo-Stop cassette excision and expression of the LacZ transgene. Cells expressing β-galactosidase can be visualised by exposure to X-Gal substrate, which results in a colourimetric change from colourless to blue. (B) Treatment of mice with 4 consecutive daily doses of Tamoxifen at 80 mg/kg results in a high levels of X-Gal staining, indicating a high level of recombination of the small intestinal epithelium. (i) The LacZ positive staining is demonstrated in intestine of *VillinCreER*$^{+}$*LacZ*$^{+}$ mice 4 days post-induction. (ii) Absence of the LacZ transgene results in no staining. The pictures show 2x magnification in the upper panels and 4x magnification in the lower panels.**

3.2.2. *Cbx3* loss under the control of *VillinCreER* recombination

Following the confirmation that the induction of *VillinCreER* activity results in efficient recombination within the intestinal epithelium, the loss of *Cbx3*, driven by *VillinCreER* mediated recombination, was examined and the immediate effects of *Cbx3* loss on small intestinal homeostasis assessed. Cohorts of experimental *VillinCreER*$^{+}$*Cbx3*$^{fl/fl}$ and control *VillinCreER*$^{+}$*Cbx3*$^{+/+}$ (where $^{+/+}$ denotes an absence of loxP sites) animals were induced with daily intraperitoneal injections of tamoxifen at 80 mg/kg for 4 days and animals were sacrificed 24 hours after the last dose and small intestines harvested. Loss of HP1γ protein from the epithelium following recombination was assessed qualitatively using immunohistochemistry and semi-quantitatively using western analysis. Immunohistochemical studies of HP1γ expression revealed strong staining in a mosaic pattern for HP1γ in the epithelium and stroma of tissue sections from control animals 4 days post-induction. In contrast, staining for HP1γ was absent from the epithelium of intestines *VillinCreER*$^{+}$*Cbx3*$^{fl/fl}$ animals whilst the mosaic-staining pattern in the stroma was retained (Figure 3.2).

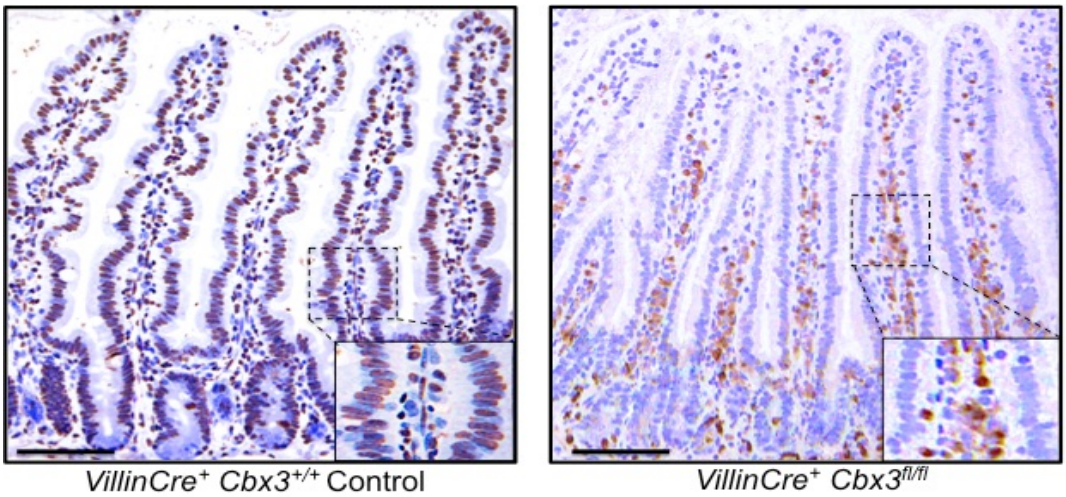

Figure 3.2: Induction of *VillinCreER* recombinase drives complete intestinal epithelial loss of *Cbx3*. *VillinCreER*$^{+}$*Cbx3*$^{fl/fl}$ mice were induced with 4 daily intraperitoneal injection of 80 mg/kg Tamoxifen along with *VillinCreER*$^{+}$*Cbx3*$^{+/+}$ controls. Immunohistochemical analysis of HP1γ expression revealed close to complete loss of *Cbx3* expression in the small intestinal epithelium of *VillinCreER*$^{+}$*Cbx3*$^{fl/fl}$ mice at day 4 post-induction. Scale bars represent 200 µm.

Given that *VillinCreER* recombination mainly occurs within the epithelium of the intestine, Western analysis on protein extracted from epithelium was used to examine the loss of HP1γ protein in the *VillinCreER*$^{+}$*Cbx3*$^{fl/fl}$ animals. A substantial reduction of HP1γ protein is observed in the *VillinCreER*$^{+}$*Cbx3*$^{fl/fl}$ animals at 4, 7, 14, 22 and 366 days post-induction compared to the *VillinCreER*$^{+}$*Cbx3*$^{+/+}$ control animals (Figure 3.3).

Overall, these data indicate that induction of *VillinCreER* results in recombination within the intestinal epithelium. In addition, *Cbx3* is excised specifically and efficiently from the small intestinal epithelium, resulting in dramatic loss of HP1γ protein 4 days post induction.

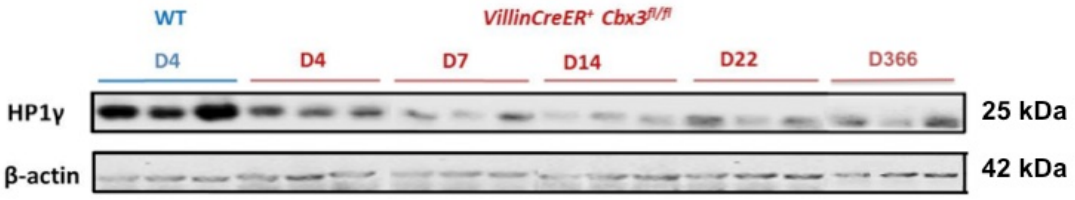

Figure 3.3: Western analysis showed substantial reduction of HP1γ protein from 4 days onwards post induction.
Western analysis of epithelial cell extract samples from *VillinCreER*$^{+}$*Cbx3*$^{fl/fl}$ animals confirms reduction of HP1γ protein at 4, 7, 14, 22 and 366 days post-induction. HP1γ protein (25kDa) is present in all control *VillinCreER*$^{+}$*Cbx3*$^{+/+}$ animals. β-actin (42kDa) was used as a loading control.

3.2.3. Intestinal epithelial Cbx3 deficiency does not impair survival

Before studying the effect of *Cbx3* loss in Wnt-activated intestines, it is critical to examine the effect of *Cbx3* deletion on the lifespan of the animals. A cohort of *VillinCreER*$^{+}$*Cbx3*$^{fl/fl}$ (n = 5) animals was aged along with *VillinCreER*$^{+}$*Cbx3*$^{+/+}$ control cohorts (n = 3). Mice from both groups were induced with 4 daily intraperitoneal injections of 80 mg/kg Tamoxifen and they were regularly inspected for health status. All mice were aged to the expected end point 366 days post induction and the health status from the experimental cohort *VillinCreER*$^{+}$*Cbx3*$^{fl/fl}$ animals looked indistinguishable from the control animals. Survival analysis of *VillinCreER*$^{+}$*Cbx3*$^{fl/fl}$ (n = 5) and control (n = 3) animals demonstrated no significant difference between the cohorts ($p > 0.1$ Log-Rank test, $n \geq 3$).

3.2.4. *Cbx3* deficiency has little immediate effects on small intestinal homeostasis

Although the loss of *Cbx3* from the intestinal epithelium did not affect survival, a more detailed characterisation of intestinal homeostasis was conducted at various time points (Day 4, 7, 14, 22 and 366). Upon dissection the phenotypic presentation of the intestinal epithelia from all the Cbx3 deficient cohorts was indistinguishable from the controls. Consequently, a quantitative analysis of histological and functional parameters of the intestinal epitheliums was performed to assess parameters of intestinal homeostasis. The data revealed subtle differences between *Cbx3* deficient and control animals (results are collated in Table 3.1).

Parameter	Genotype	Mean	±Standard Deviation	p Value (to WT)
Crypt Length (cells)	Control WT	18.73	2.19	
	Cbx3$^{fl/fl}$ D4	19.73	3.81	0.667
	Cbx3$^{fl/fl}$ D7	31.37	0.59	0.001
	Cbx3$^{fl/fl}$ D14	25.14	4.99	0.077
	Cbx3$^{fl/fl}$ D22	29.04	2.98	0.002
	Cbx3$^{fl/fl}$ D366	22.58	1.09	0.051
Villus Length (cells)	Control WT	62.27	6.78	
	Cbx3$^{fl/fl}$ D4	63.04	12.17	0.916
	Cbx3$^{fl/fl}$ D7	84.53	18.89	0.169
	Cbx3$^{fl/fl}$ D14	68.59	10.78	0.366
	Cbx3$^{fl/fl}$ D22	74.52	10.59	0.108
	Cbx3$^{fl/fl}$ D366	70.41	11.27	0.482
Apoptosis per half-crypt	Control WT	0.30	0.24	
	Cbx3$^{fl/fl}$ D4	0.54	0.17	0.103
	Cbx3$^{fl/fl}$ D7	0.21	0.06	0.428
	Cbx3$^{fl/fl}$ D14	0.20	0.13	0.585
	Cbx3$^{fl/fl}$ D22	0.26	0.09	0.707
	Cbx3$^{fl/fl}$ D366	0.21	0.01	0.059
Caspase3 positive cells per half-crypt	Control WT	1.37	0.37	
	Cbx3$^{fl/fl}$ D4	0.99	0.22	0.148
	Cbx3$^{fl/fl}$ D7	0.93	0.06	0.097
	Cbx3$^{fl/fl}$ D14	1.72	1.18	0.605
	Cbx3$^{fl/fl}$ D22	1.00	0.09	0.159
	Cbx3$^{fl/fl}$ D366	0.89	0.18	0.053
Mitosis per half-crypt	Control WT	0.17	0.11	
	Cbx3$^{fl/fl}$ D4	0.16	0.06	0.892
	Cbx3$^{fl/fl}$ D7	0.17	0.09	0.937
	Cbx3$^{fl/fl}$ D14	0.12	0.02	0.024

	Cbx3$^{fl/fl}$ D22	0.22	0.17	0.618
	Cbx3$^{fl/fl}$ D366	0.09	0.03	0.035
Ki67 positive cells per half-crypt	Control WT	18.98	2.73	
	Cbx3$^{fl/fl}$ D4	18.00	4.08	0.706
	Cbx3$^{fl/fl}$ D7	28.26	4.11	0.037
	Cbx3$^{fl/fl}$ D14	22.30	3.25	0.171
	Cbx3$^{fl/fl}$ D22	28.64	3.57	0.006
	Cbx3$^{fl/fl}$ D366	19.99	1.01	0.513

Table 3.1. Quantitative analysis of histological parameters between small intestinal tissues from control and *VillinCreER*$^{+}$*Cbx3*$^{fl/fl}$ animals.
Quantitative analysis of histological parameters such as crypt and villus length, apoptosis and proliferation were quantified and compared between small intestinal tissues from *VillinCreER*$^{+}$*Cbx3*$^{+/+}$ (marked here as Control WT) and *VillinCreER*$^{+}$*Cbx3*$^{fl/fl}$ animals at various time points post induction.

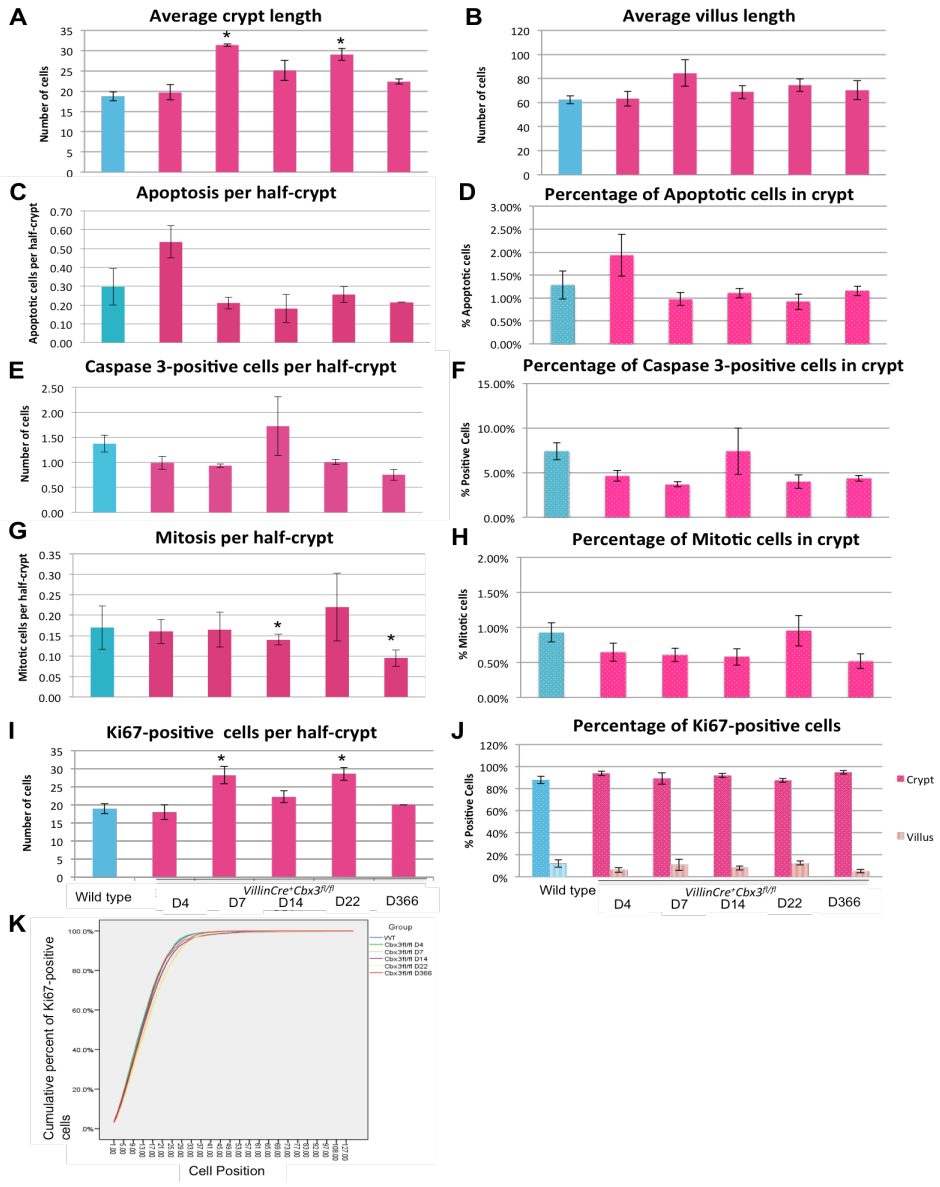

Figure 3.4: Quantitative analysis of the morphological and functional parameters of small intestinal epithelium following *Cbx3* deletion.
Experimental *VillinCreER^{+}Cbx3$^{fl/fl}$* animals along with controls were induced with 4 daily i.p. 80 mg/kg Tamoxifen and samples of the small intestine were harvested at day 4, 7, 14, 22 and 366 post induction. Histological parameters such as crypt length (A), villus length (B), apoptosis (C), percentage of apoptotic cells in crypt (D), mitosis (G) and percentage of mitotic bodies in crypt (H), were scored on H&E stained sections from control and *VillinCreER^{+}Cbx3$^{fl/fl}$* small intestines. The average number of cleaved Caspase 3 (E), Percentage of Caspase 3-positive cells in crypt (F), Ki67 (I) and percentage of Ki67 positive cells in crypt or villus were scored on respective immunostained sections. The positioning of Ki67 positive cells (K) in control and *VillinCreER^{+}Cbx3$^{fl/fl}$* small intestines at different time points were analysed by cumulative frequency analysis (Kolmogorov-Smirnov Z test, $p = 0.297$, $n \geq 3$). Error bars represent standard deviation.

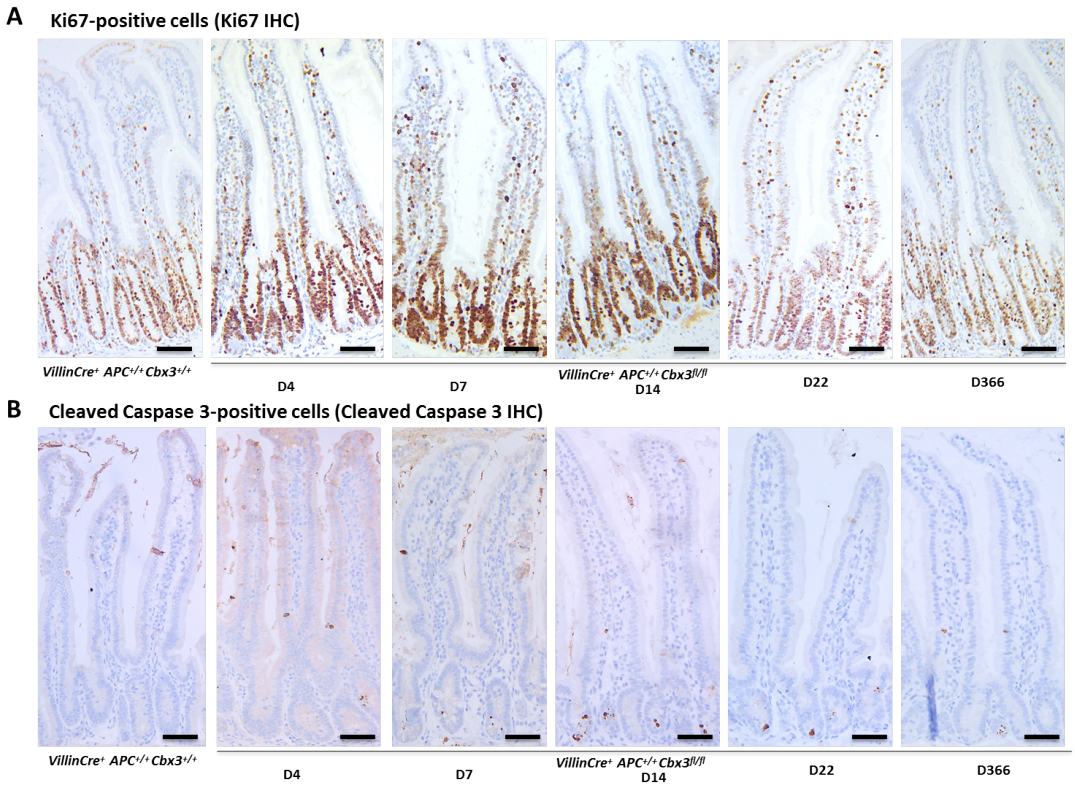

Figure 3.5: Immunohistochemical staining of Ki67 and cleaved Caspase-3.
Immunohistochemical staining of (A) Ki67 and (B) cleaved Caspase-3 positive cells were performed in control and *VillinCreER^{+}Cbx3$^{fl/fl}$* small intestines at different time points and selected representative sections are shown. Scale bars indicate 100 µm.

The crypt and villus sizes were scored as the average number of epithelial cells from the base of the crypt to the crypt-villus junction and from the crypt-villus junction to the top of villus respectively. Although no differences were observed in the crypt length 4 days post induction, a significant increase in the number of cells within the crypt was observed at both 7 and 22 days post induction (Figure 3.4A). However, the lack of significant differences at days 14 and 366 renders it difficult to draw an easy conclusion about the role of *Cbx3* in regulating crypt length. Conversely, the length of villus was not significantly changed at any of the time points (Figure 3.4B).

To gain a clearly understanding, markers of cell proliferation and cell death were also examined in detail. Levels of apoptosis and mitosis within the crypt were scored from H&E stained sections and quantified as average number of apoptotic bodies and mitotic

figures per half-crypt respectively. No significant alteration in the numbers of apoptotic bodies was observed in any of the time points analysed Figure 3.4C and Figure 3.5B). Furthermore, the numbers of apoptotic bodies were quoted as percentage of total crypt cells to take account of the differences in crypt length. No significant changes in the percentage of apoptotic index in crypt regions were detected in any of the time points examined (Figure 3.4D). In order to validate apoptotic levels obtained from quantification of apoptotic bodies, sections of the *Cbx3*-deficient and control intestine were stained with the cell death marker cleaved Caspase-3. Scoring of cleaved Caspase-3 positive cells detected no significant differences following *Cbx3* loss at any of the time points (Figure 3.4E). Further examination of the percentage of cleaved Caspase-3 positive cells in crypt revealed no significant differences following *Cbx3* loss at all time points examined.

Quantification of mitotic figures revealed no difference in mitosis levels in *Cbx3*-deficient animals on 4, 7 and 22 days post-induction versus control animals. Whereas analysis of mitotic figures between *Cbx3*-deficient epitheliums on 14 days and 366 days post induction and control intestines demonstrated a significant increase in the average number of mitotic bodies (Figure 3.4G). Further examination of the percentage of mitotic cells in crypt showed no significant difference across all time points examined. In order to validate mitosis levels obtained from quantification of mitotic figures, sections of the *Cbx3*-deficient and control intestine were stained with Ki67, a cell proliferation marker. Quantification of the Ki67 positive cells detected no change in the average number of proliferating cells per half-crypt *Cbx3*-deficient samples on day 4, 14 and 366 post-induction verses control. However, a significant increase in the average number of Ki67 positive cells was detected in *Cbx3*-deficient epithelium on day 7 and 22 post induction (Figure 3.4I and Figure 3.5A), which correlates with the increase in crypt length shown in (Figure 3.4A). Furthermore, the relative distribution of Ki67 positive cells in crypt or villus as a percentage of the total Ki67 positive cells in the small intestines of wildtype control and *VillinCreER*$^{+}$*Cbx3*$^{fl/fl}$ small intestines were examined at different time points. The data revealed no significant difference between the distribution patterns between the control and *Cbx3*-deficient samples, all of which were with the majority of proliferative cells confined to the crypt (Figure 3.4J). This observation, therefore, further confirmed that the increase in Ki67 expressing cells on Day 7 and Day 22 samples compared to control samples was attributed

to the increase in crypt sizes solely but not an increase in proliferative activity in the epithelium. Additionally, distribution of the cells stained positive for Ki67 was analysed in order to examine the shape of the proliferative compartment. Analysis of the cumulative frequency of Ki67 positive cells in the crypt demonstrated no difference in distribution of proliferating cells across all *Cbx3*-deficient and control samples (Kolmogorov-Smirnov Z test, $p = 0.297$, $n \geq 3$, Figure 3.4K).

Overall, quantitative analysis of the histological and functional parameters of the small intestinal epithelium showed that *Cbx3* loss is tolerated within the small intestinal epithelium and does not perturb the normal architecture of the intestinal epithelium.

3.2.5. *Cbx3* deficiency has no effect on cell migration of the intestinal epithelium

In order to examine the effects of *Cbx3* loss on epithelial cell migration a BrdU pulse-chase experiment was performed. Cohorts of *VillinCreER*$^{+}$*Cbx3*$^{fl/fl}$ and control mice (n = 4) were administrated with BrdU reagent on day 4 post-induction and one group of mice from both cohorts was sacrificed 2 hours and another group of mice was sacrificed 24 hours post-BrdU treatment to assess cell migration. The positions of the BrdU-labelled cells was then scored and their cumulative frequency was analysed as an indicator of migratory ability of the epithelial cells in *Cbx3*-deficient and control intestine.

Positional quantification of BrdU-positive cells 2 hours post-labelling revealed no significant difference in the distribution of BrdU positive cells between control and experimental animals, with positive cells being confined to the crypt (Kolmogorov-Smirnov Z test, p = 0.771, n = 4, Figure 3.6). Similarly, cumulative frequency analysis of BrdU-labelled cells 24 hours post-labelling displayed no significant changes in the migratory ability of the *Cbx3*-deficient epithelium (Kolmogorov-Smirnov Z test, p = 0.997, n = 4, Figure 3.6).

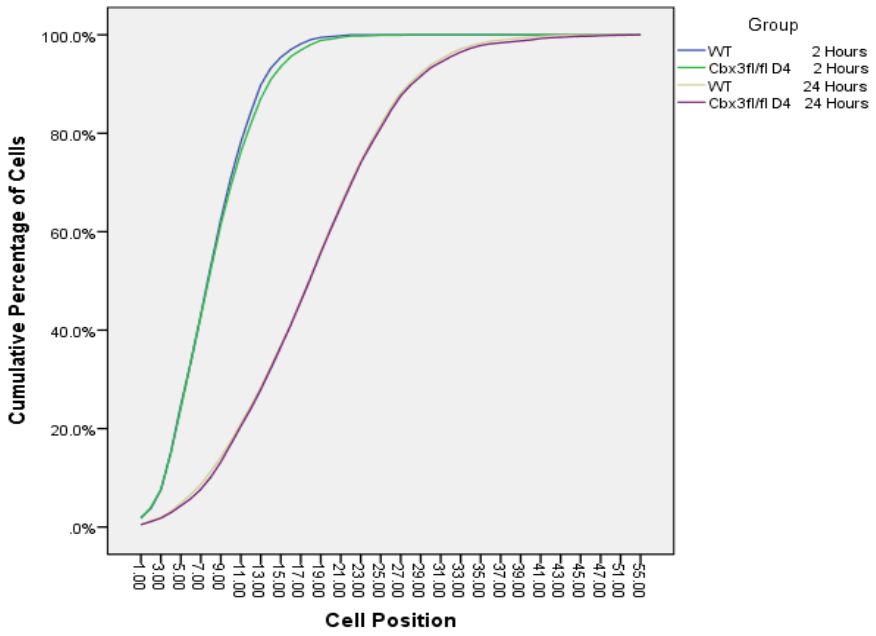

Figure 3.6: *Cbx3* deficiency in small intestinal epithelium had no effects on cell migration.
Cumulative frequency analysis of BrdU immunostaining 2 hours and 24 hours post-labelling revealed no significant changes in cell migration in the small intestinal epithelium of *VillinCreER^{+}Cbx3$^{fl/fl}$* compared to control mice 4 days post-induction (Kolmogorov-Smirnov Z test, 2 hours p = 0.771, n = 4; 24 hours p = 0.997, n = 4).

3.2.6. Intestinal epithelial cells differentiate normally in the absence of *Cbx3*

Intestinal homeostasis is highly regulated and maintained between cell proliferation and differentiation. In order to further characterise the effects of *Cbx3* loss on small intestinal homeostasis the major differentiated cell types present in the small intestinal epithelium in *Cbx3*-deficient and control mice at day 4, 7, 14, 22 and 366 post induction were examined. The results of quantitative analysis of differentiated cells in control and *Cbx3*-deficient animals are collated in Table 3.2.

Parameter	Genotype	Mean	Standard Deviation	p Value (to WT)
Goblet cells per half crypt and villus	Control WT	6.24	0.95	
	Cbx3$^{fl/fl}$ D4	5.42	0.53	0.196
	Cbx3$^{fl/fl}$ D7	6.72	0.51	0.469
	Cbx3$^{fl/fl}$ D14	5.85	1.09	0.609
	Cbx3$^{fl/fl}$ D22	7.11	0.21	0.169
	Cbx3$^{fl/fl}$ D366	5.22	0.08	0.120
Enteroendocrine cells per half crypt and villus	Control WT	0.44	0.22	
	Cbx3$^{fl/fl}$ D4	0.43	0.22	0.978
	Cbx3$^{fl/fl}$ D7	0.44	0.16	0.976
	Cbx3$^{fl/fl}$ D14	0.42	0.15	0.900
	Cbx3$^{fl/fl}$ D22	0.43	0.08	0.968
	Cbx3$^{fl/fl}$ D366	0.45	0.01	0.919
Paneth cells per half crypt and villus	Control WT	7.26	0.83	
	Cbx3$^{fl/fl}$ D4	6.01	0.17	0.116
	Cbx3$^{fl/fl}$ D7	4.77	2.47	0.217
	Cbx3$^{fl/fl}$ D14	6.07	1.11	0.219
	Cbx3$^{fl/fl}$ D22	5.95	0.37	0.097
	Cbx3$^{fl/fl}$ D366	5.41	2.14	0.424

Table 3.2: Quantitative analysis of *Cbx3*-deficient epitheliums reveals no significant difference on cell differentiation compared to controls.
Small intestinal epitheliums from *VillinCreER*$^{+}$*Cbx3*$^{+/+}$ (marked here as Control WT) and *VillinCreER*$^{+}$*Cbx3*$^{fl/fl}$ animals at various time points post-induction were examined and demonstrated no signification alternations on cell differentiation compared to controls (n ≥ 3).

In the small intestine, enterocytes responsible for absorption constitute the majority of the cells in the villus. Using alkaline phosphatase, which specifically stains the brush border of the enterocytes, insight into the state of the enterocytes in the *Cbx3*-deficient epitheliums compared to the controls could be gained. Alkaline phosphatase staining patterns revealed no alteration in the location of the brush border or differentiation of enterocytes in the context of *Cbx3* deficiency (Figure 3.8A).

Goblet cells represent the second most abundant cell type in the small intestinal epithelium. Alcian blue staining was carried out to access changes in Goblet cell differentiation upon *Cbx3* loss (Figure 3.8B). Quantification of the positively stained cells revealed no significant changes in number of Goblet cells between experimental and control animals (Figure 3.7A).

Enteroendocrine cells represent another secretory cell lineage of the small intestinal epithelium. In order to assess the frequency of the positively stained enteroendocrine cells, Grimelius staining was carried out on small intestinal sections from *Cbx3*-deficient intestine and controls (Figure 3.8C). Scoring of the cells stained for Grimelius showed no difference between experimental and control animals (Figure 3.7B).

The last member of the secretory cell lineage studied is Paneth cell. Tissue from control and *Cbx3*-deficient animals at various time points were stained immunohistochemically against lysozyme, a marker of Paneth cells (Figure 3.8D). Positively stained cells were scored and showed no difference in the Paneth cell numbers between experimental and control animals (Figure 3.7C). The staining of Paneth cells were found to be located at the base of the crypt and their position of the lysozyme positive cells showed no changes in the loss of *Cbx3*.

Overall, these observations demonstrates that small intestinal epithelial cells are capable to differentiate normally in the absence of *Cbx3* from day 4 to day 366 post-induction, as all mature cell types revealed no differences between *Cbx3*-deficient and control intestines.

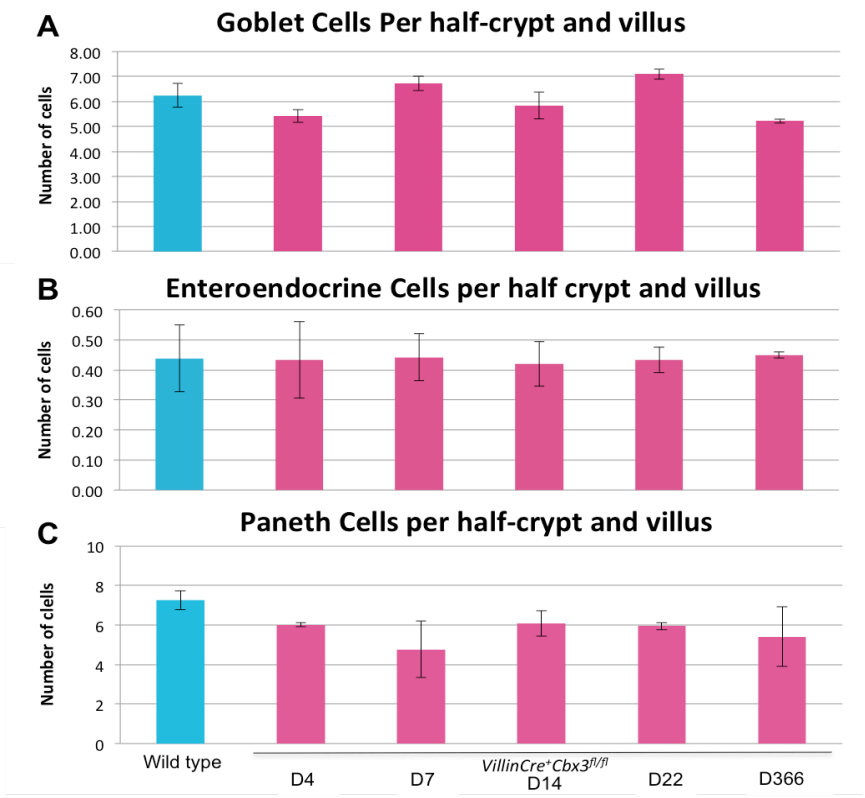

Figure 3.7: Quantification analysis of cell differentiation upon loss of *Cbx3* within the small intestine.

The average number Goblet (A), Enteroendocrine (B) and Paneth (C) cells per half-crypt and villus was scored in both the wildtype control and *VillinCreER^{+}Cbx3$^{fl/fl}$* animals at day 4, 7, 14, 22 and 366 post induction. No significant difference was observed in the number of all the parameters tested above between control and experimental mice. Error bars represent standard deviation. Exact values, standard deviations, respective p values are provided in Table 3.2.

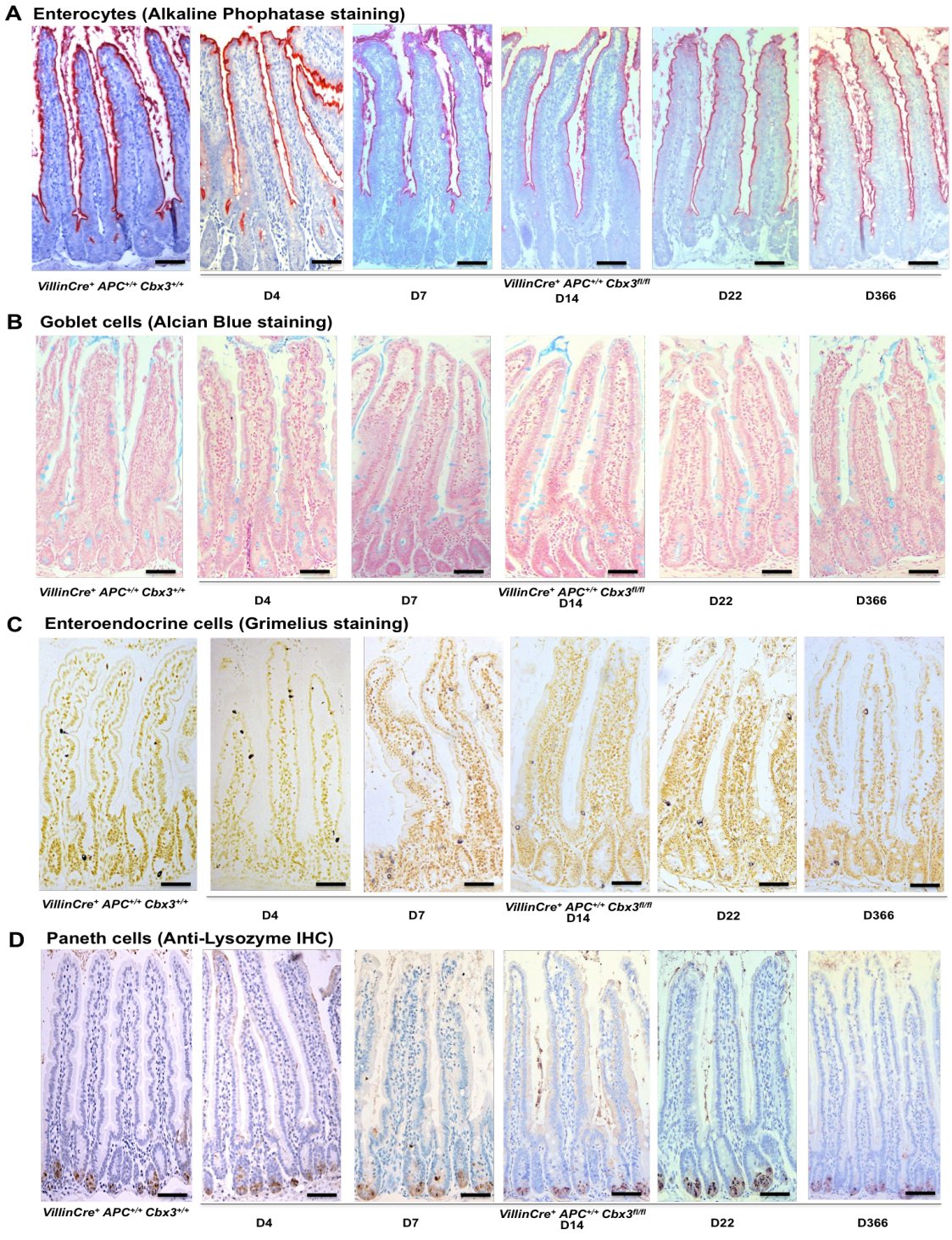

Figure 3.8: Identification of differentiated epithelial cell types following *Cbx3* loss.
Small intestinal sections of *Cbx3*-deficient and control animals were subjected to cell type-specific stains to visualise Enterocytes (A), Goblet cells (B), Enteroendocrine cells (C) and Paneth cells (D). The presence of Enterocytes, Goblet, enteroendocrine and Paneth cells were not affected by *Cbx3* loss. Scale bars indicate 100 µm.

3.2.7. *Cbx3* loss alters intestinal stem cell gene expression

Previous evidence suggested that loss of *Cbx3* is required for cell differentiation to occur; therefore it would be of great interest to investigate the consequences of *Cbx3* loss on the normal intestinal stem cell population.

To assess the effects of *Cbx3* loss on the small intestinal stem cell population, the expression levels of the intestinal stem cell markers *Ascl2*, *Lgr5*, *Bmi1, Msi1* and *Olfm4* were analysed (Potten et al., 2003;Barker et al., 2007b;Sangiorgi and Capecchi, 2008;van der Flier et al., 2009a;van der Flier et al., 2009b). Epithelium cell extracts from the small intestine of *VillinCreER*$^{+}$*Cbx3*$^{fl/fl}$ and control mice at day 4 post-induction were used for qRT-PCR analysis to minimise interference from the stromal compartments of the intestine. The qRT-PCR expression analysis revealed a significant increased expression of *Ascl2* in *Cbx3* deficient epithelium compared to wildtype epithelium ($p = 0.04$, $n = 3$, Figure 3.9). However, this observation is not detected in the expression of *Lgr5* ($p = 0.287$), *Bmi1* ($p = 0.344$), *Msi1* ($p = 0.803$) and *Olfm4* ($p = 0.696$) following loss of *Cbx3* from the intestinal epithelium (Figure 3.9). Thus the differences in the profiles of these surrogate markers of stem cell function do not paint an entirely clear picture of *Cbx3* deficiency on intestinal stem cell compartment. One limitation is that three biological replicates may not be sufficient to yield accurate data, therefore increasing the sample size in future qRT-PCR analysis could be performed in order to improve the statistical power of the candidate intestinal stem cell genes.

In situ hybridisation using RNA probes for *Olfm4* was performed to investigate further the effect of *Cbx3* loss on the intestinal stem cell compartment. The *in situ* hybridisation revealed no alteration of *Olfm4* staining of the *VillinCreER*$^{+}$*Cbx3*$^{fl/fl}$ and control epithelium (Figure 3.10), consistent with the qRT-PCR data and indicate that loss of *Cbx3* has no effect on *Olfm4* expression.

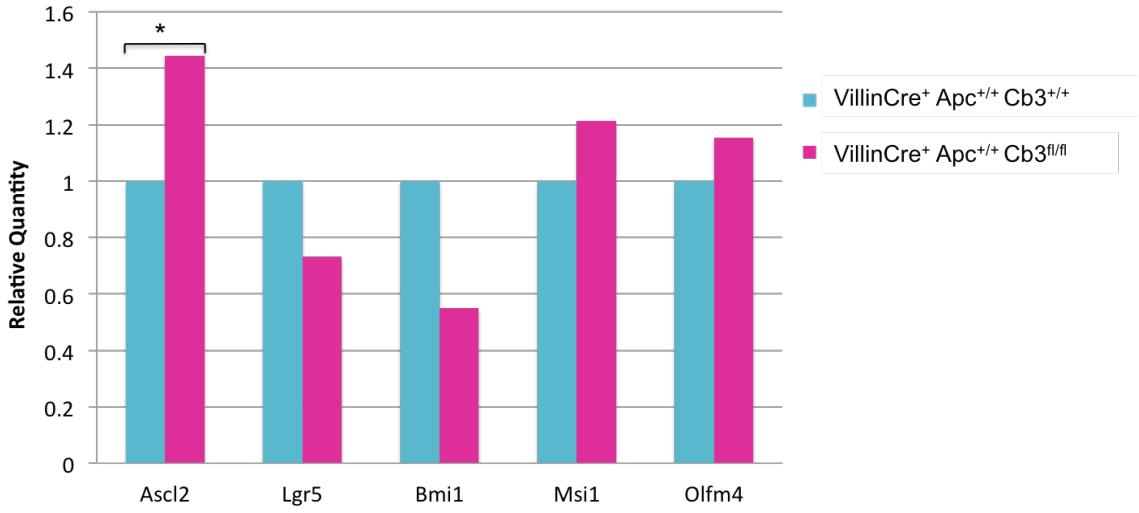

Figure 3.9: *Cbx3* loss in the small intestinal epithelium increases *Ascl2* expression.
Quantitative RT-PCR analysis of the small intestinal epithelium 4 days post-induction revealed significantly increased expression level of *Ascl2* in the small intestinal epithelium of *VillinCreER^{+}Cbx3$^{fl/fl}$* mice compared to control animals ($p = 0.04$, $n = 3$). No significant changes in the level of *Lgr5, Bmi1, Msi1* and *Olfm4* markers was observed in *Cbx3*-deficient intestinal epithelium compared to controls (Two-tailed T-test, $p > 0.05$, $n = 3$).

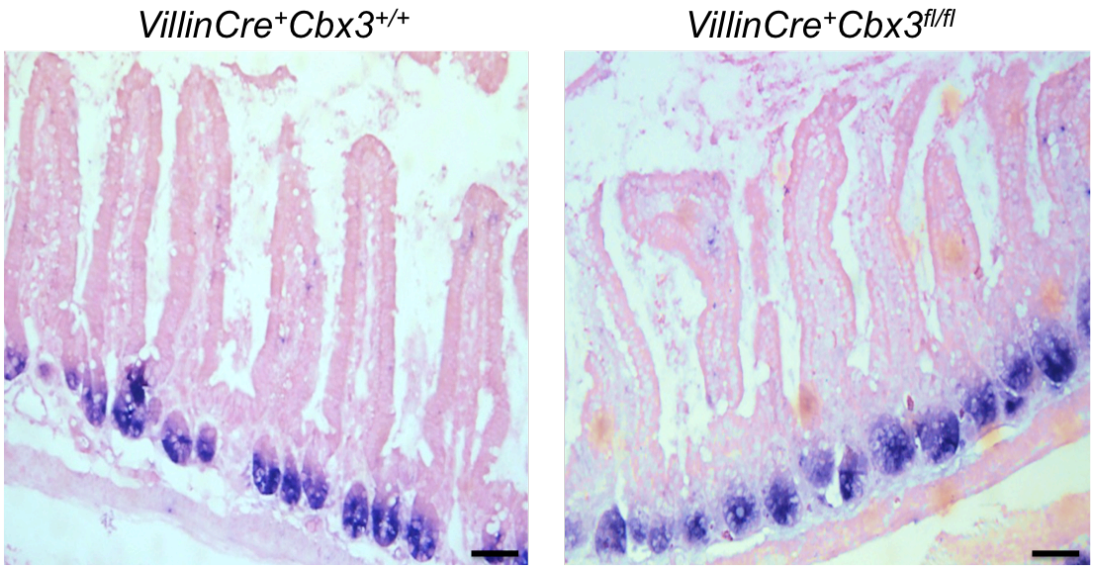

Figure 3.10: *In situ* hybridisation for *Olfm4* expression in control and *VillinCreER^{+}Cbx3$^{fl/fl}$* intestines.
***In situ* hybridisation analysis of the stem cell marker *Olfm4* in the small intestine of *VillinCreER^{+}Cbx3$^{fl/fl}$* mice compared to control mice at day 4 post-induction demonstrated no alteration of *Olfm4* expression following *Cbx3* loss. Scale bars represent 100 µm.**

3.2.8. *Cbx3* deficiency leads to reduced heterochromatic marks

It is known that *Cbx3* is a regulator of the epigenome, with critical roles in establishing, spreading and maintaining heterochromatin (Maison and Almouzni, 2004b). HP1γ, coded by the gene *Cbx3*, has been reported to be the reader of repressive methylation at histone H3K9 trimethylation, and mediate heterochromatin spread (Jacobs and Khorasanizadeh, 2002b; Nielsen *et al.,* 2002b). It is therefore hypothesized that depletion of *Cbx3* would result in a complete loss of H3K9me3 marks in intestines. Immunofluorescence analysis was performed in small intestinal tissue sections of control wildtype and *VillinCreER*$^{+}$*Cbx3*$^{fl/fl}$ animals. Fluorescence microscopy images of intestines stained with antibodies against HP1γ (red) and H3K9me3 (green) revealed that both HP1γ and H3K9me3 signals overlapped substantially with that of DNA (DAPI, blue) (Figure 3.11A). The level of H3K9me3 was substantially lowered in the absence of *Cbx3* in the *VillinCreER*$^{+}$*Cbx3*$^{fl/fl}$ intestinal epithelium compared to the control intestinal epithelium (Figure 3.11B), suggesting HP1γ plays some role in establishing and / or maintaining H3K9me3 in the intestinal homeostasis.

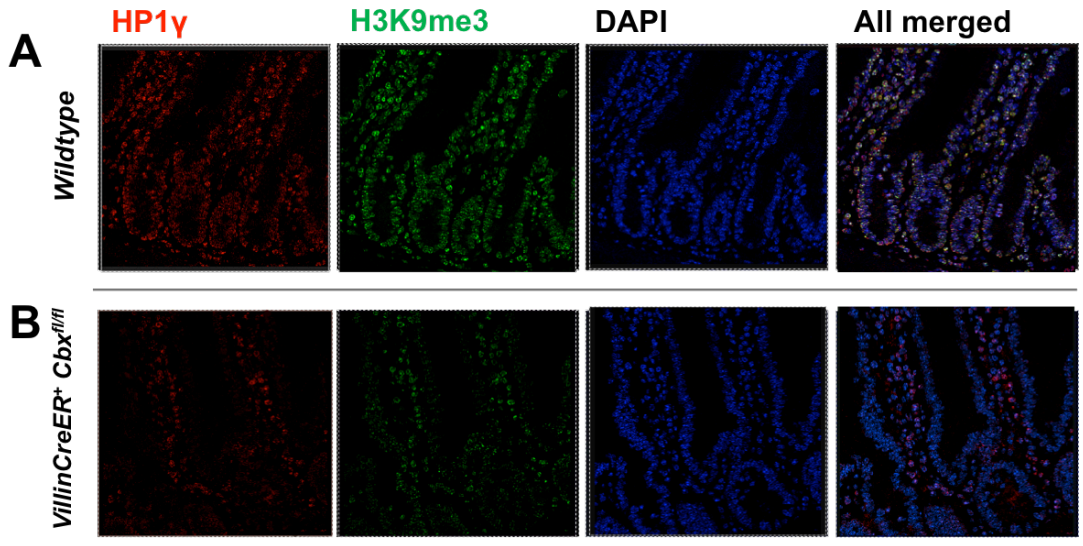

Figure 3.11: Immunofluorescence analysis of HP1γ and H3K9me3 in small intestine of wildtype and *VillinCreER*$^{+}$*Cbx3*$^{fl/fl}$ day 4 post induction.
Confocal analysis of HP1γ and H3K9me3 in wildtype (A) and *VillinCreER*$^{+}$*Cbx3*$^{fl/fl}$ (B) are illustrated in Red (Alexi 594) and Green (Alexi 488), respectively. These images are representative of small intestines analysed in each cohort (n = 3). Nuclei were counterstained with DAPI (4', 6-diamidino-2-phenylindole; blue).

After identifying that *Cbx3* loss causes reduction in H3K9me3 level in the *VillinCreER*$^{+}$*Cbx3*$^{fl/fl}$ intestines, it would be interesting to investigate whether another heterochromatic marker H4K20me3 would also be affected in the absence of *Cbx3*. H4K20me3, together with H3K9me3 and HP1γ, were found to be essential for proper establishment of a compact heterochromatin structure (Dambacher, Hahn and Schotta, 2013). Therefore immunofluorescence analysis was performed on small intestinal tissue sections from wildtype and *VillinCre*$^{+}$*Cbx3*$^{fl/fl}$ mice. Fluorescence microscopy images of intestines stained with antibodies against H4K20me3 correlated with the staining patterns observed in H3K9me3, with intense signals on the large matter of DAPI-dense facultative heterochromatin in the wildtype intestine (Figure 3.12A) and marked reduction of signals in *Cbx3*-deficient intestinal epitheliums (Figure 3.12B). These findings suggest that HP1γ is involved in the establishment of both H3K9me3 and H4K20me3 signatures at heterochromatin in intestinal homeostasis.

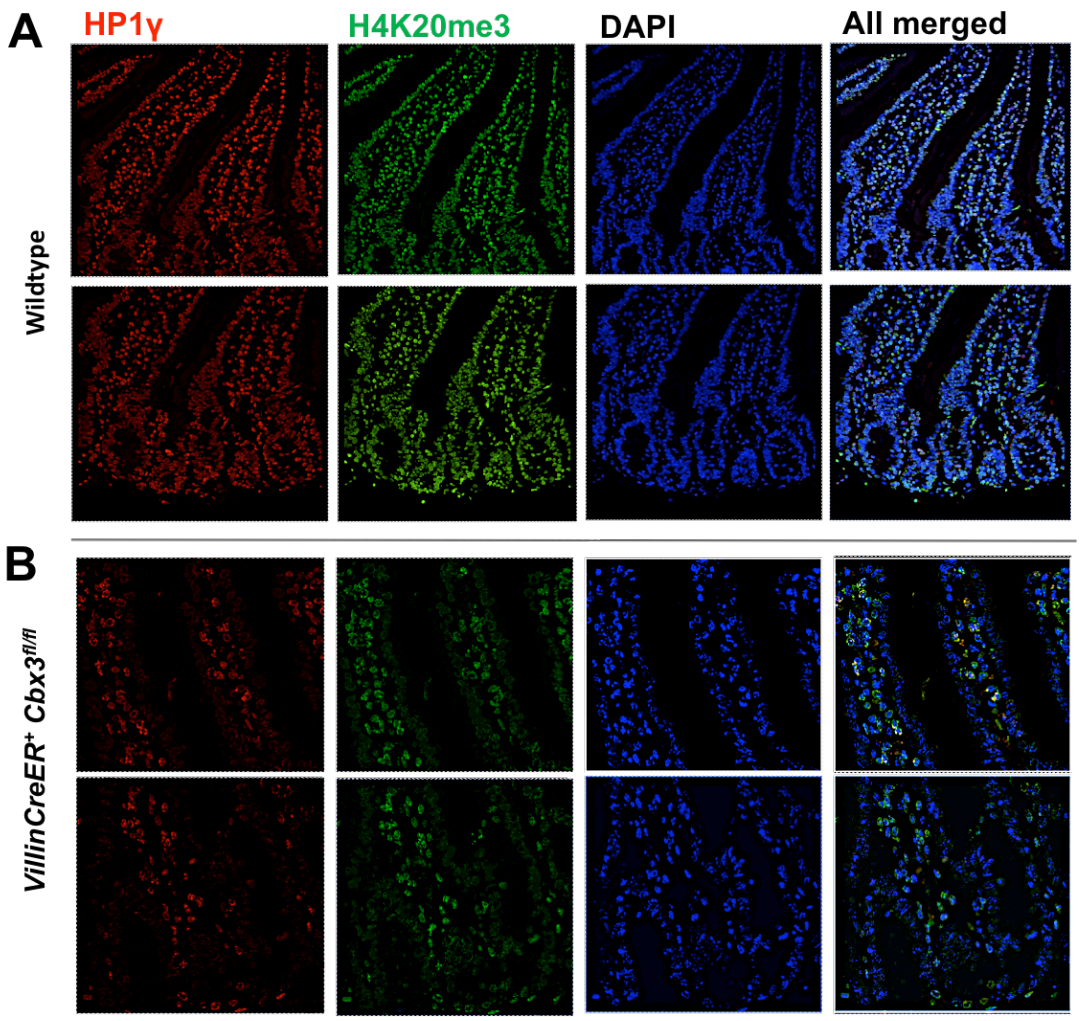

Figure 3.12: Immunofluorescence analysis of HP1γ and H4K20me3 in small intestine of wildtype and *VillinCreER^{+}Cbx3$^{fl/fl}$* mice day 4 post-indcution.
Confocal images of control (A) and *VillinCreER^{+}Cbx3$^{fl/fl}$* (B) small intestines stained with anti-HP1γ antibody (red) and anti-H4K20me3 antibody (green). Presented images are representative of small intestinal tissues analysed in each cohort (n = 3). Nuclei were stained with DAPI (4', 6-diamidino-2-phenylindole; blue).

Despite the fact that the most common of HP1γ functions is the formation of heterochromatin, HP1γ is present in both heterochromatin and euchromatin (Minc, Courvalin and Buendia, 2000), it would be of great interest to investigate the importance of HP1γ to a euchromatic marker, H3K4me3. H3K4me3 is an active marker associated with actively transcribed genes (Hon, Hawkins and Ren, 2009). Therefore, immunofluorescence analysis of HP1γ and H3K4me3 was performed in the small intestine of the wildtype and

VillinCreER^{+}*Cbx3*$^{fl/fl}$ animals. In contrast to the heterochromatic markers, the staining pattern of H3K4me3 was found to be mostly unchanged following the loss of *Cbx3* (Figure 3.13), suggesting the active euchromatic marker H3K4me3 is present in small intestinal homeostasis, regardless of the presence or absence of *Cbx3*.

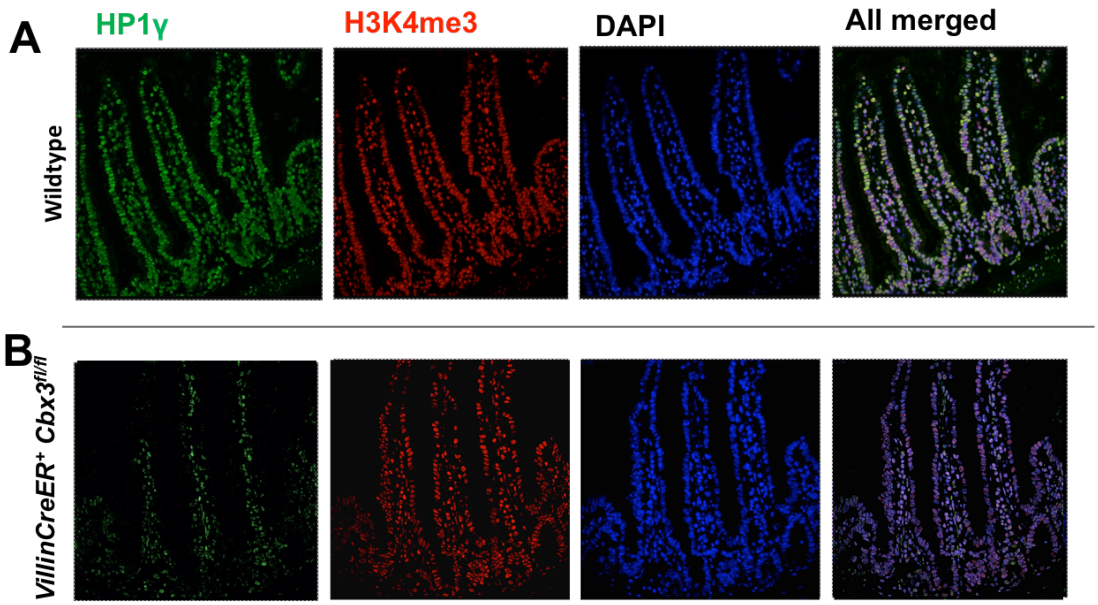

Figure 3.13: Immunofluorescence analysis of HP1γ and H3K4me3 in small intestine of (A) wildtype and (B) *VillinCreER*$^{+}$*Cbx3*$^{fl/fl}$ mice day 4 post-induction. Confocal images of small intestines stained with anti-HP1γ antibody (green) and anti-H3K4me3 antibody (red). These images are representative of small intestinal tissues analysed in each cohort (n = 3). Nuclei were stained with DAPI (4', 6-diamidino-2-phenylindole; blue).

3.3. Discussion

Previous studies have suggested a role for *Cbx3* (encoding the HP1γ protein) in cell lineage differentiation. *Cbx3* negatively regulates adipocyte differentiation from preadipocyte cells and is required for male germ cell survival and spermatogenesis. Another study also suggested *Cbx3* plays a critical role in the epigenetic regulation of both cell differentiation and cancer development. However, little is known about the functional involvement of *Cbx3* in intestinal epithelial cell differentiation and development (Cammas *et al*., 2002; Cammas *et al.,* 2004; Takanashi *et al.*, 2009). This chapter describes for the first time, to our knowledge, the phenotypes of *Cbx3* deficiency in small intestinal homeostasis, using conditional transgenics, involving LoxP-targeted *Cbx3* alleles together with the inducible *VillinCreER* transgene.

Following generation of *VillinCreER*$^{+}$*Cbx3*$^{fl/fl}$ and control animals, the loss of *Cbx3* has been confirmed from the intestinal epithelium following induction of Cre recombinase activity by treatment with 4 consecutive daily doses of Tamoxifen at 80 mg/kg. Recombination within the small intestinal epithelium was assessed using the ROSA26R transgene reporter and visualised by X-Gal staining for β-galatosidase activity. This confirmed that the induction of *VillinCreER* activity resulted in efficient recombination within the intestinal epithelium. The loss of HP1γ protein from epithelium of *VillinCreER*$^{+}$*Cbx3*$^{fl/fl}$ animals following recombination was also confirmed, both by Immunohistochemical studies and western analysis. Immunohistochemical studies of HP1γ revealed near-100% loss of HP1γ from the epithelium, whilst mosaic-staining pattern of HP1γ still remained in the stroma. Western analysis on protein extracted from epithelium further supported the fact that induction results in a substantial reduction of HP1γ protein 4 days post induction. This therefore indicates that induction of *VillinCreER* results in efficient recombination within the intestinal epithelium, resulting in dramatic loss of HP1γ protein 4 days post-induction.

Furthermore, the effect of *Cbx3* deletion on the lifespan of the mice was also examined. A cohort of *VillinCreER*$^{+}$*Cbx3*$^{fl/fl}$ was aged along with control *VillinCreER*$^{+}$*Cbx3*$^{+/+}$ mice and both groups were induced with 4 daily intraperitoneal injections of 80 mg/kg

Tamoxifen and were regulated checked for health status. The epithelial *Cbx3* deficiency did not affect health status of the experimental mice 366 days after induction.

3.3.1. Epithelial *Cbx3* is not required for normal intestinal homeostasis

Having established that *Cbx3* is lost from the intestinal epithelium in *VillinCreER*$^{+}$*Cbx3*$^{fl/fl}$ animals, and that the loss of *Cbx3* from the intestinal epithelium did not affect survival in our mouse models, the effect of *Cbx3* deletion at various time points (Day 4, 7, 14, 22 and 366) on intestinal homeostasis were then examined. As *Cbx3* has been demonstrated to play an important role in cell proliferation and differentiation, one could predict that *Cbx3* loss would result in dramatic changes in the intestinal homeostasis.

In contrast to this hypothesis, deletion of *Cbx3* from the epithelium has no dramatic effect upon homeostasis up to 366 days post-induction. No perturbations in gross histology were identified, and no change in proliferative and apoptotic status were observed, either from immunohistochemical studies or from scoring of mitotic or apoptotic index from H&E-stained sections. Furthermore, analysis of the migratory ability of *Cbx3*-deficinet epithelial cells revealed no alteration in migration. Although majority of the histological and quantitative analysis revealed no abnormalities in the general crypt-villus architecture despite the loss of *Cbx3* from the epithelial cells. One notable difference is on the crypt sizes, which were quantified as significantly larger at both 7 and 22 days post-induction although these increases were not prominent under histological inspection. Despite this finding, *Cbx3*-deficient intestines displayed no significant changes in the villus sizes at any of the time points. The increase in crypt size observed at day 7 and 22 is therefore likely to be attributed to high variation and lower sample size. In addition, the lack of age-matched controls (data from all the experimental cohorts were compared with data from the day 4 control cohort) and the lack of significant differences at days 14 and 366 render it difficult to draw an easy conclusion about the role of *Cbx3* in regulating crypt length. Using age-matched controls and increasing the sample number in each cohort in future studies would reduce variation in data and increase the statistical power of the experiment.

Takanashi and colleagues have demonstrated that the loss of *Cbx3* is required for cell differentiation to occur (Takanashi *et al*., 2009). Therefore it might be predicted that

Cbx3 loss would result in increased differentiation of stem cell to mature epithelial cell types. However, qualitative and quantitative analysis of the normal differentiation of epithelial cells revealed that the presence, location and frequency of mature cell types was unaffected by *Cbx3* loss across all time points. These data therefore indicate that *Cbx3* is not necessary for normal development of the epithelium and deletion of *Cbx3* from the epithelium exhibits no effect on the normal intestinal homeostasis.

3.3.2. *Cbx3* loss in the epithelium alters *Ascl2* stem cell gene expression

Previous studies from the literature indicate that *Cbx3* plays a role in stem cell maintenance in adipocyte, male germ cell and cardiovascular system (Xiao *et al.,* 2011; Brown *et al.*, 2010). However, little is known about the functional involvement of *Cbx3* in intestinal stem cell maintenance.

To examine the effects of *Cbx3* loss on the small intestinal stem cell population, the expression levels of a number of the intestinal stem cell markers *Ascl2, Lgr5, Bmi1, Msi1* and *Olfm4* were assessed using qRT-PCR. The qRT-PCR analysis expression analysis showed no change of expression level in the crypt base columnar stem cell markers (*Lgr5, Msi1* and *Olfm4*) and the +4 stem cell marker (*Bmi1*) following *Cbx3* loss, Furthermore, *In situ* hybridisation using RNA probes for *Olfm4* was performed and this confirmed that there was no alteration in the stem cell compartment of the epithelium.

However, *Cbx3* loss up-regulated one of the stem cell markers, *Ascl2*, in the small intestinal epithelium. *Ascl2*, one of the CBC stem cell markers, was identified as an important regulator of intestinal stem cell fate, as its conditional deletion in the intestinal epithelium resulted in a rapid and selective loss of the *Lgr5*$^{+}$ stem cell compartment, suggesting *Ascl2* is essential for the maintenance of Lgr5 stem cells in the adult intestinal epithelium (van der Flier *et al*., 2009). *Ascl2* expression level was significantly increased following the loss of *Cbx3*, indicating *Cbx3* plays an active role on regulating *Ascl2* expression and keeping a balance between stem cell maintenance and differentiation to maintain epithelial homeostasis. Previous data from this chapter demonstrated that the deletion of *Cbx3* has no effect on cell differentiation and intestinal homeostasis, despite the fact that *Cbx3* loss results in a significant increase in *Ascl2* expression, this does not translate into any

cellular or phenotypic effects. This may be due to the highly plastic system operates between the intestinal stem cell populations, the effect of *Ascl2* up-regulation following *Cbx3* loss is likely to be diluted by the niche environment at the crypt base. Similarly, *Ascl2* upregulation in normal intestinal homeostasis and in a Wnt-activated intestines has been reported to result in no alternation in the stem cell compartment of the intestine and no changes in survival in the Apc^{min} mouse suggesting that elevated levels of *Ascl2* does not have an impact on the overall intestinal homeostasis and overall survival (Reed *et al.*, 2012). Furthermore, *Ascl2* is a Wnt target gene and it promotes cell growth and migration in colon cancer (Kwon *et al.*, 2013). This observation raises a number of interesting questions with regard to the role of *Cbx3* on colon cancer development and therefore provides directions for further investigation in the next chapter.

3.3.3. *Cbx3*-deficient intestinal epithelium displays diminished heterochromatic marks

Extensive studies have revealed that *Cbx3* is a regulator of the epigenome, with roles in establishing, spreading and maintaining heterochromatin, through its ability to bind to H3K9me3, which is an epigenetic marker for gene silencing in the context of a histone code (Eissenberg, 2001; Bannister *et al.,* 2001; Lachner *et al.,* 2001; Maison and Almouzni, 2004). In this study, immunofluorescence analysis was performed in small intestinal tissue sections of control wildtype and $VillinCreER^{+}Cbx3^{fl/fl}$ animals and the level of H3K9me3 was reduced in the absence of *Cbx3* in the $VillinCreER^{+}Cbx3^{fl/fl}$ intestinal epitheliums compared to the control intestinal epitheliums, suggesting HP1γ is involved in establishing and / or maintaining H3K9me3 in the intestinal homeostasis.

H4K20me3, another silencing heterochromatic marker, was found to be essential for proper establishment of a compact heterochromatin structure (Dambacher, Hahn and Schotta, 2013). Therefore, immunofluorescence analysis was also carried out in small intestinal tissue sections of control wildtype and $VillinCreER^{+}Cbx3^{fl/fl}$ animals and the level of H4K20me3 was found to be substantially lowered following the loss of *Cbx3*. A sequential pathway could subsequently be proposed to connect these two histone methylation systems: H3K9me3 is established by Suv39h1 and Suv39h2 enzymes (Rea *et al*., 2000). HP1γ

binds to histone methylation marks such as H4K20me3 and in turn recruit more Suv39h enzymes to maintain and propagate H3K9me3 as well as Suv4-20h methyltransferases, which then establish H4K20me3 (Schotta *et al.*, 2004). Consistent with this sequential pathway, H3K9me3 and H4K20me3 are lost in the absence of HP1γ; these findings suggest that HP1γ is involved in the establishment and maintenance of both H3K9me3 and H4K20me3 signatures at heterochromatin in intestinal homeostasis.

3.3.4. Summary

In summary, three major conclusions can be drawn from the data presented in this chapter. Firstly, *Cbx3* deficiency had no immediate effects on intestinal homeostasis and intestinal cell lineage differentiation, and epithelial *Cbx3* deficiency does not affect life span of mice up to 366 days post-induction, indicating that *Cbx3* is redundant with respect to epithelial homeostasis and survival. Secondly, *Cbx3* deficiency has no the overt effect on the majority of the intestinal stem cell markers, apart from *Ascl2*. Despite the fact that *Cbx3* deletion results in significant increase in *Ascl2* expression level, intestinal homeostasis and cell differentiation were unaltered, indicating *Cbx3*-mediated up-regulation of *Ascl2* alone might not be sufficient to alter intestinal stem cell maintenance and differentiation and therefore it has no effect on overall intestinal homeostasis. Thirdly, HP1γ plays a role in the establishment and maintenance of both H3K9me3 and H4K20me3 markers at heterochromatin in intestinal homeostasis.

Chapter Four

Investigating the effects of *Cbx3* loss in Wnt-activated small intestine

4. Investigating the effects of *Cbx3* loss in Wnt-activated small intestine

4.1. Introduction

Wnt signaling is well documented as a critical regulator of intestinal homeostasis and it is aberrantly activated in more than 90% of CRC cases (Clevers, 2006). The vast majority of mutations leading to aberrant Wnt signaling activation in CRC involve the Adenomatous polyposis poli gene (*Apc*) (Kinzler and Vogelstein, 1996). The role of activated Wnt signaling in homeostasis and tumorigenesis of the intestine has been extensively studied using murine models of *Apc* mutation (Taketo, 2006). Studies of constitutive homozygous disruption of *Apc* results in early embryonic lethality (Moser *et al.*, 1995) whereas studies of heterozygous inactivation of *Apc* using different approaches lead to tumour predisposition syndrome, reminiscent of human FAP (Moser, Pitot and Dove, 1990; Shibata *et al.,* 1997). Conditional deletion of both alleles of *Apc* in the adult intestine using the Cre-loxP system results in rapid disruption of intestinal epithelial homeostasis, observations includes hyperproliferation and attenuation of epithelial migration. Use of such model has indicated that mice following conditional deletion of *Apc* could live up to 5 days post induction (Sansom *et al.*, 2004).

Cbx3 has been reported to be frequently upregulated in various cancer cell lines (including colon cell lines) and the transient knock down of *Cbx3* inhibited cancer cell line growth (Takanashi *et al.,* 2009). Furthermore, depletion of HP1γ attenuated tumorigenesis activity in a mouse xenograft model (Sharma *et al.*, 2003), indicating that expression of HP1γ causes acceleration and progression of tumorigenesis.

To date, other than the acute up-regulation of *Cbx3* expression following Wnt signalling activation, nothing is known about the biological involvement of *Cbx3* in Wnt-activated small intestines. In this chapter, the role of *Cbx3* in Wnt-activated small intestines was investigated by studying the impact of *Cbx3* deficiency on Wnt driven carcinogenesis. Activation of Wnt signalling was achieved by conditional deletion of both copies of *Apc* using the Cre-loxP approach. Therefore, conditional homozygous deletion of *Cbx3* and *Apc* was used to examine the role of *Cbx3* loss in the context of acute Wnt driven carcinogenesis in the murine small intestinal epithelium.

4.2. Results

4.2.1. Prolonged lifespan of *Cbx3* deficient mice in the context of acute Wnt driven carcinogenesis

Before studying the immediate, acute effects of combined loss of both *Apc* and *Cbx3* on the intestinal epithelium, it is critical to examine whether *Cbx3* loss will affect the lifespan of the animals with homozygous loss of *Apc*. In order to do this, the Cre-loxP conditional transgenic system was used. Experimental animals *VillinCreER*$^{+}$*Apc*$^{fl/fl}$*Cbx3*$^{fl/fl}$ (n = 5) and controls *VillinCreER*$^{+}$*Apc*$^{fl/fl}$ (n = 5) were induced with 4 daily intraperitoneal injections of 80 mg/kg Tamoxifen and were sacrificed once ill health was observed.

Homozygous inactivation of *Apc* in the small intestinal epithelium, as previously described, induced acute aberrant Wnt activation, which results in rapid and catastrophic perturbation of epithelial homeostasis within 5 days of *Apc* loss (Sansom *et al.*, 2004b). Consistently, control cohorts (*VillinCreER*$^{+}$*Apc*$^{fl/fl}$) developed signs of ill health and had to be sacrificed by day 4 post induction (Figure 4.1, median survival 4 days). Conversely, experimental animals (*VillinCreER*$^{+}$*Apc*$^{fl/fl}$*Cbx3*$^{fl/fl}$) with additional homozygous loss of *Cbx3* displayed no signs of ill health on day 4 but survived significantly longer with some mice surviving past 7 days (Figure 4.1, median survival 7 days, Log-Rank test $p < 0.01$).

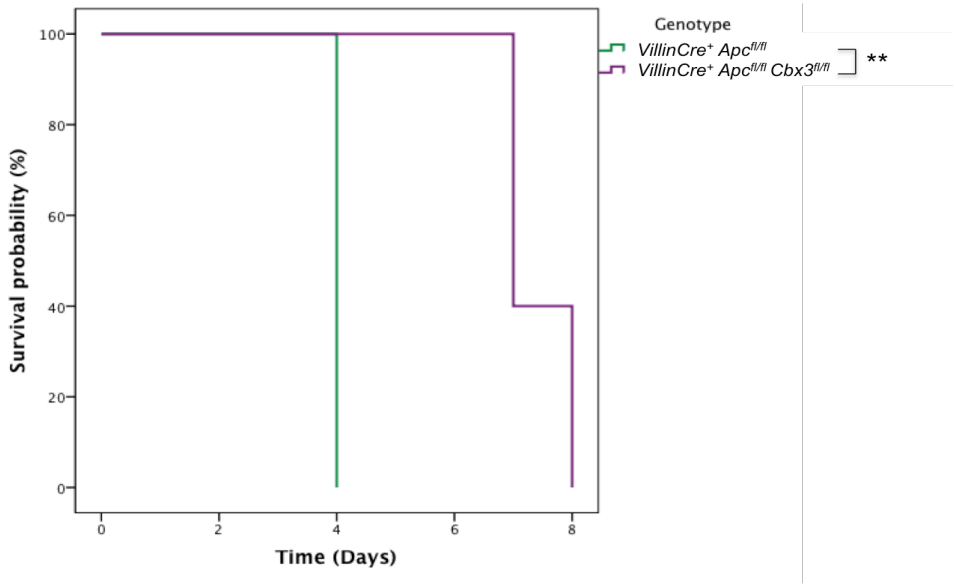

Figure 4.1. The additional loss of *Cbx3* prolonged survival of mice with homozygous *Apc* loss.
Cohort of *VillinCreER^{+}Apc$^{fl/fl}$Cbx3$^{fl/fl}$* animals were induced with four daily intraperitoneal injections of 80 mg/kg Tamoxifen along with *VillinCreER^{+}Apc$^{fl/fl}$* control animals (n = 5). Mice were closely monitored daily until signs of ill health are observed. Survival data was presented as a Kaplan-Meier plot. Analysis of survival probability revealed a significantly increased survival of *VillinCreER^{+}Apc$^{fl/fl}$Cbx3$^{fl/fl}$* mice (median survival 7 days) compared to the *VillinCreER^{+}Apc$^{fl/fl}$* control animals (median survival 4 days, Log-Rank test p = 0.003, n = 5).

4.2.2. No change in gross intestinal structure associated with *Cbx3* loss in acute Wnt activated intestinal epithelium

Considering the additional loss of *Cbx3* from the acute Wnt activated intestinal epithelium prolonged median survival by 3 days, the consequence of *Cbx3* loss in the associated phenotypes that accompany aberrant Wnt pathway activation were investigated. Experimental cohorts *VillinCreER^{+}Apc$^{fl/fl}$Cbx3$^{fl/fl}$* and *VillinCreER^{+}Apc$^{fl/fl}$*, and control wildtype were induced and culled at day 4 post induction. Intestines were removed, fixed and sectioned before being stained for histological assessment. Quantitative analysis of histological parameters (crypt and villus size, apoptosis and mitosis levels) revealed that the experimental mice shared histological features of Wnt activated intestinal epithelium and there are no significant alternations between *VillinCreER^{+}Apc$^{fl/fl}$* and double knock-out *VillinCreER^{+}Apc$^{fl/fl}$Cbx3$^{fl/fl}$* animals. The results are collated in Table 4.1.

Parameter	Genotype	Mean	± Standard Deviation	p Value		
				WT Vs $Apc^{fl/fl}$	WT Vs $Apc^{fl/fl}Cbx3^{fl/fl}$	$Apc^{fl/fl}$ Vs $Apc^{fl/fl}Cbx3^{fl/fl}$
Crypt Length (cells)	Control WT	26.62	1.21	0.001		
	$Apc^{fl/fl}$	51.87	2.59		0.001	
	$Apc^{fl/fl}Cbx3^{fl/fl}$	48.96	1.64			0.548
Villus Length (cells)	Control WT	64.37	3.59	0.005		
	$Apc^{fl/fl}$	52.70	3.09		0.024	
	$Apc^{fl/fl}Cbx3^{fl/fl}$	54.30	2.79			0.206
Apoptosis per half-crypt	Control WT	1.09	0.04	0.049		
	$Apc^{fl/fl}$	2.27	0.19		0.020	
	$Apc^{fl/fl}Cbx3^{fl/fl}$	2.52	0.23			0.875
Caspase3 positive cells per half-crypt	Control WT	0.79	0.19	0.001		
	$Apc^{fl/fl}$	3.10	0.39		0.001	
	$Apc^{fl/fl}Cbx3^{fl/fl}$	2.65	0.31			0.392
Mitosis per half-crypt	Control WT	0.70	0.20	0.013		
	$Apc^{fl/fl}$	1.60	0.42		0.041	
	$Apc^{fl/fl}Cbx3^{fl/fl}$	1.20	0.36			0.158
Ki67 positive cells per half-crypt	Control WT	24.75	1.03	0.001		
	$Apc^{fl/fl}$	55.67	3.17		0.001	
	$Apc^{fl/fl}Cbx3^{fl/fl}$	48.78	0.92			0.685

Table 4.1: Quantitative analysis of the effect of *Cbx3* loss on the histological parameters in Wnt-activated intestinal epithelium.
Quantitative analysis of histological parameters such as crypt and villus size, apoptosis and mitosis levels, in the context of Wnt activated small intestinal epithelium, showed no significant alternations between *VillinCreER^{+}Apc$^{fl/fl}$* and *VillinCreER^{+}Apc$^{fl/fl}$Cbx3$^{fl/fl}$* animals.

The size of crypt and villus were quantified as the average number of cells between the crypt base and the crypt-villus junction and between the crypt-villus junction and the tip of the villus respectively. Average number of cells (± standard deviation) per crypt was found to be significantly longer in the intestinal epithelium of *VillinCreER^{+}Apc$^{fl/fl}$* and *VillinCreER^{+}Apc$^{fl/fl}$Cbx3$^{fl/fl}$* mice compared to control wildtype animals ($p = 0.001$). On the other hand, animals from both experimental groups displayed significantly shorter villi compared to control mice ($p < 0.05$). Quantification of the crypt and villus length revealed no difference between the *Apc* deficient epithelium and animals with combined loss of *Apc* and *Cbx3* ($p = 0.548$ and $p = 0.206$ respectively, $n \geq 3$, Figure 4.2A-B).

Apoptosis and mitosis levels were scored on H&E stained sections and quantified as average number of apoptotic bodies and mitotic figures per half-crypt respectively. Quantification of apoptotic bodies within crypts was significantly increased in the experimental animals compared to controls ($p < 0.05$). Scoring of cleaved Caspase-3 positive cells revealed a similar change in apoptosis levels ($p = 0.001$). *VillinCreER^{+}Apc$^{fl/fl}$Cbx3$^{fl/fl}$* intestine displayed no significant changes of apoptotic and Caspase-3 level compared to *VillinCreER^{+}Apc$^{fl/fl}$* intestine ($p = 0.875$ and $p = 0.392$ respectively, $n \geq 3$, Figure 4.2C, E and H).

Quantification of mitotic figures revealed significant elevation of mitotic bodies in both experimental cohorts compared to control animals ($p < 0.05$). Similarly, quantification of Ki67 positive cells detected significantly higher number of proliferating cells in experimental mice compared to control mice ($p = 0.001$). However, no significant difference was observed between the *VillinCreER^{+}Apc$^{fl/fl}$Cbx3$^{fl/fl}$* intestine compared to *VillinCreER^{+}Apc$^{fl/fl}$* intestine ($p = 0.158$ and $p = 0.685$ respectively, $n \geq 3$, Figure 4.2D, F and I). Additionally, distribution of proliferating cells was assessed by scoring positions of Ki67 positive cells. Cumulative frequency analysis of Ki67 positive cell revealed significant expansion of the proliferation compartment in *VillinCreER^{+}Apc$^{fl/fl}$* and *VillinCreER^{+}Apc$^{fl/fl}$Cbx3$^{fl/fl}$* epithelium compared to control mice (Kolmogorov-Smirnov Z test $p < 0.01$, $n \geq 3$, Figure 4.2G). However, there is no significant variation in the distribution of Ki67 positive cells in the epitheliums between the two experimental groups.

Overall, these data demonstrate that loss of *Cbx3* has no effect on the associated phenotypes observed in Wnt activated small intestinal epithelium.

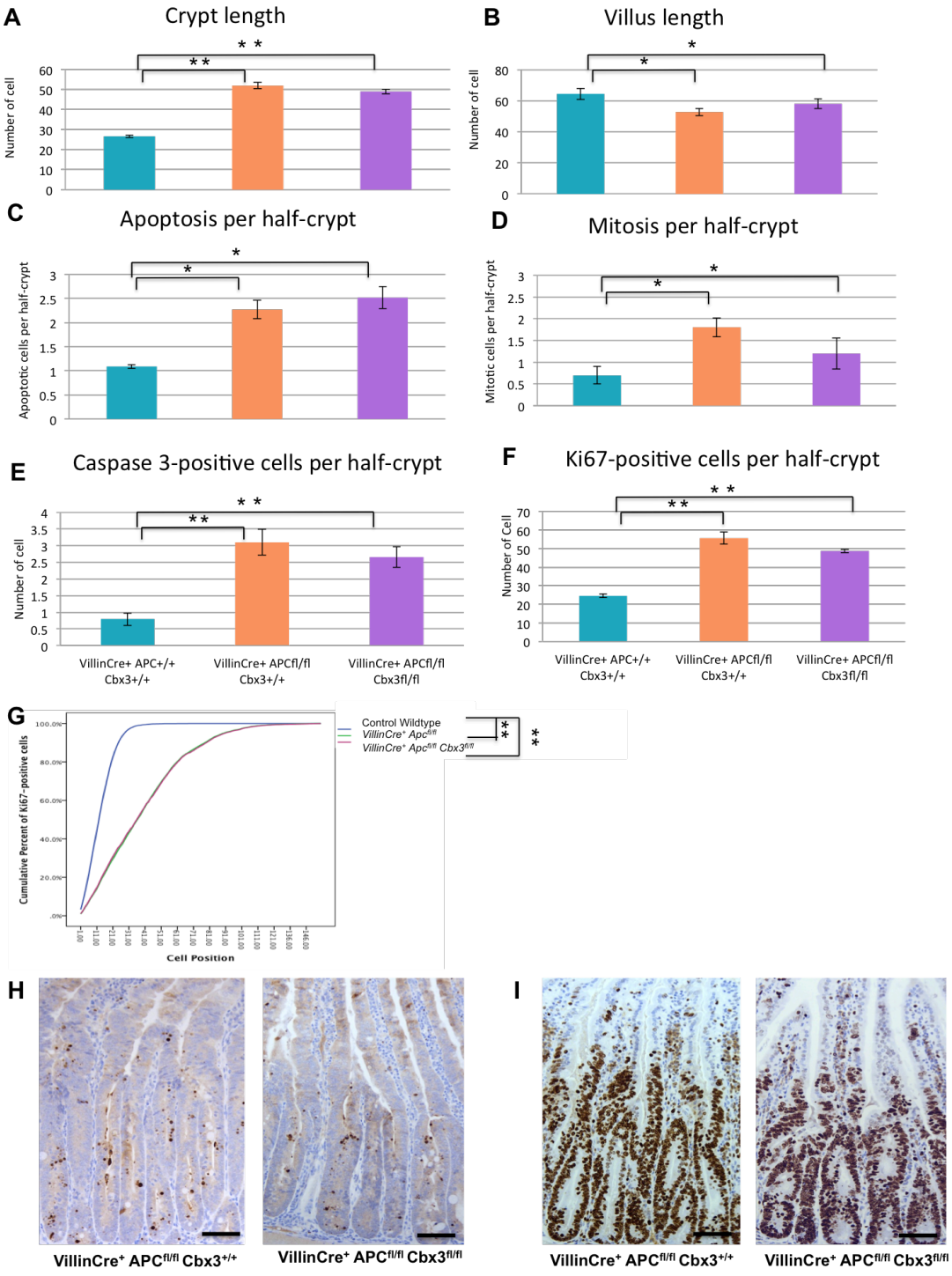

Figure 4.2: Quantification analysis of the effect of short-term *Cbx3* deficiency in Wnt-activated small intestinal epithelium.
Experimental *VillinCreER^{+}Apc$^{fl/fl}$* and *VillinCreER^{+}Apc$^{fl/fl}$Cbx3$^{fl/fl}$* mice together with control wildtype mice were induced with 4 daily i.p. injections of 80 mg/kg Tamoxifen and samples were harvested at day 4 post induction. (A-F) Histological parameters such as crypt length (A), villus length (B), apoptosis (C) and mitosis (D) were scored on H&E stained sections of small intestinal epithelium

from control, *VillinCreER^{+}Apc$^{fl/fl}$* and *VillinCreER^{+}Apc$^{fl/fl}$Cbx3$^{fl/fl}$*. The average number of cleaved Caspase-3 (E) and Ki67 (F) positive cells per half-crypt were scored on respective immunostained sections and selected representative pictures are shown (H & I). (G) Cumulative frequency analysis of Ki67 positive cells revealed an expansion of the proliferative compartment in *VillinCreER^{+}Apc$^{fl/fl}$* and *VillinCreER^{+}Apc$^{fl/fl}$Cbx3$^{fl/fl}$* mice compared to control animals (for both comparison Kolmogorov-Smirnov Z test $p < 0.001$, $n = 4$). Comparison of cumulative frequency of Ki67 positive cells between the experimental groups revealed no alteration between the two experimental groups (Kolmogorov-Smirnov Z test $p = 0.707$, $n = 4$). Scale bars represent 100 µm. Error bars represent standard deviation. A single asterisk mark statistically significant p value < 0.05 and double asterisks mark statistically significant p value < 0.01 between groups. Exact values, standard deviation, p values are provided in Table 4.1.

4.2.3. *Cbx3* loss in the context of *Apc* deficiency has no effect on cell migration

In order to investigate the effects of *Cbx3* loss on cell migration in *Apc* deficient small intestinal epithelium, BrdU was administrated at 2 hours and 24 hours prior to dissection of the mice. The positions of BrdU labelled cells 2 hours and 24 hours post labelling were quantified and compared, and cumulative frequency distributions of cell position were generated. Cumulative distribution analysis of BrdU positive cells detected an expansion of BrdU-positive cells in both experimental groups *VillinCreER^{+}Apc$^{fl/fl}$* and *VillinCreER^{+}Apc$^{fl/fl}$Cbx3$^{fl/fl}$* compared to control mice (Kolmogorov-Smirnov Z test $p < 0.001$, $n = 4$, Figure 4.3). However, the analysis of BrdU staining 24 hours post labelling displayed no significant changes in cell migration between two experimental groups *VillinCreER^{+}Apc$^{fl/fl}$* and *VillinCreER^{+}Apc$^{fl/fl}$Cbx3$^{fl/fl}$* intestines (Kolmogorov-Smirnov Z test $p > 0.05$, $n = 4$, Figure 4.3). Overall, *Cbx3* deficiency does not have any impacts on migratory ability in the intestines in the context of *Apc* deletion.

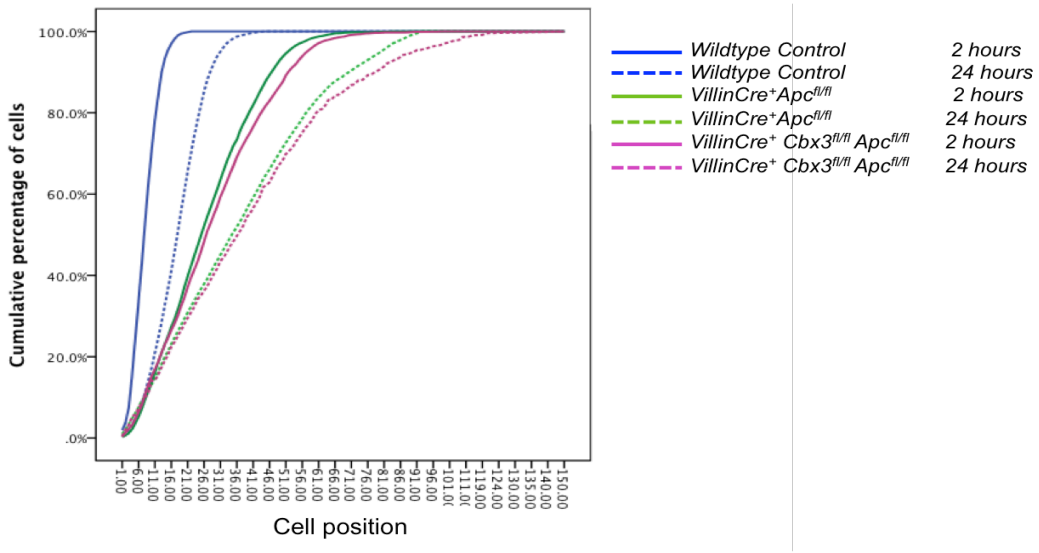

Figure 4.3: *Cbx3* loss does not affect cell migration in *Apc*-deficient small intestinal epithelium. Cumulative frequency analysis of BrdU staining 2 hours and 24 hours post-labelling detected a significant expansion of BrdU positive cells in the small intestine of the 2 experimental groups *VillinCreER^{+}Apc$^{fl/fl}$* and *VillinCreER^{+}Apc$^{fl/fl}$Cbx3$^{fl/fl}$* mice compared to control animals (for both comparisons Kolmogorov-Smirnov Z test $p < 0.001$, $n = 4$), however the analysis revealed no alteration in cell migration in *VillinCreER^{+}Apc$^{fl/fl}$Cbx3$^{fl/fl}$* intestine compared to *VillinCreER^{+}Apc$^{fl/fl}$* intestine.

4.2.4. *Cbx3* deficiency impacts on certain cell type differentiation in the context of Wnt-activated small intestinal epithelium

One of the most important signalling pathways that control cell fate decisions and differentiation in the small intestine is Wnt pathway (Fre *et al.*, 2009). Therefore, to further characterise the effects of *Cbx3* loss on cell differentiation in the context of aberrant Wnt activation, quantitative analysis of the major mature cell types present in the small intestinal epithelium of control wildtype, *VillinCreER^{+}Apc$^{fl/fl}$* and *VillinCreER^{+}Apc$^{fl/fl}$Cbx3$^{fl/fl}$* mice was undertaken (Figure 4.4 and Figure 4.5) and the results are summarised in Table 4.2.

Parameter	Genotype	Mean	± Standard Deviation	p Value		
				WT Vs $Apc^{fl/fl}$	WT Vs $Apc^{fl/fl}Cbx3^{fl/fl}$	$Apc^{fl/fl}$ Vs $Apc^{fl/fl}Cbx3^{fl/fl}$
Goblet cells per half crypt and villus	Control WT	6.98	0.57	0.016		
	$Apc^{fl/fl}$	5.09	0.22		0.192	
	$Apc^{fl/fl}Cbx3^{fl/fl}$	5.20	0.73			0.351
Enteroendocrine cells per half crypt and villus	Control WT	0.76	0.05	0.990		
	$Apc^{fl/fl}$	0.75	0.04		0.542	
	$Apc^{fl/fl}Cbx3^{fl/fl}$	0.89	0.08			0.489
Paneth cells per half crypt and villus	Control WT	4.54	1.61	0.249		
	$Apc^{fl/fl}$	5.56	0.53		0.815	
	$Apc^{fl/fl}Cbx3^{fl/fl}$	4.56	0.38			0.055

Table 4.2: Quantification analysis of *Cbx3* loss modulates cell type-specific responses to aberrant Wnt signalling activation.
Experimental *VillinCre*$^{+}$*Apc*$^{fl/fl}$ and *VillinCre*$^{+}$*Apc*$^{fl/fl}$*Cbx3*$^{fl/fl}$ mice together with control wildtype mice were induced with 4 daily i.p. 80 mg/kg Tamoxifen and samples were harvested at day 4 post-induction. Cell type-specific stains were performed to study differentiation of various mature cell types in the small intestinal epitheium. Frequency of Goblet, Enteroendocrine and Paneth cells was quantified and compared between the three groups.

Alkaline phosphatase was used to visualise the brush border of the enterocytes in small intestinal epithelium. A consistent decrease in staining was observed between *VillinCreER*$^{+}$*Apc*$^{fl/fl}$*Cbx3*$^{fl/fl}$ compared to *VillinCreER*$^{+}$*Apc*$^{fl/fl}$ epitheliums (Figure 4.4A).

Alcian blue staining was undertaken to identify Goblet cells in the small intestinal epithelium (Figure 4.4B). Scoring of the cells stained with Alcian blue showed a significant reduction in the numbers of Goblet cells per half-crypt-villus structure in the epithelium of *VillinCreER*$^{+}$*Apc*$^{fl/fl}$ mice compared to the control animals ($p < 0.01$, $n \geq 3$, Figure 4.5A). No significant changes were detected in Goblet cell numbers from *VillinCreER*$^{+}$*Apc*$^{fl/fl}$*Cbx3*$^{fl/fl}$ and *VillinCreER*$^{+}$*Apc*$^{fl/fl}$ or control epitheliums ($p > 0.05$, $n \geq 3$).

Grimelius staining was used to detect Enteroendocrine cells in the small intestinal epithelium (Figure 4.4C). Quantification of the positively stained cells revealed no differences in the number of Enteroendocrine cells per half-crypt-villus structure in control, *VillinCreER*$^{+}$*Apc*$^{fl/fl}$ and *VillinCreER*$^{+}$*Apc*$^{fl/fl}$*Cbx3*$^{fl/fl}$ animals ($p > 0.05$, $n \geq 3$, Figure 4.5B).

Lastly, immunohistochemical staining of Lysozyme expression was carried out to detect Paneth cells in the small intestinal epithelium (Figure 4.4D). Scoring of lysozyme positive cells in the intestinal epithelium of double knock out *VillinCreER*$^{+}$*Apc*$^{fl/fl}$*Cbx3*$^{fl/fl}$ mice detected a reduced number of Paneth cells compared to *VillinCreER*$^{+}$*Apc*$^{fl/fl}$ mice, however the change was not significantly different ($p = 0.055$, $n \geq 3$, Figure 4.5C). In addition, the position of the Lysozyme positive cells was scored in control, *VillinCreER*$^{+}$*Apc*$^{fl/fl}$ and *VillinCreER*$^{+}$*Apc*$^{fl/fl}$*Cbx3*$^{fl/fl}$ epithelium. Cumulative distribution analysis on Paneth cell position revealed a significant expansion of the Paneth cell population in both *VillinCreER*$^{+}$*Apc*$^{fl/fl}$ and *VillinCreER*$^{+}$*Apc*$^{fl/fl}$*Cbx3*$^{fl/fl}$ epitheliums compared to the control epithelium (Kolmogorov-Smirnov Z test, both $p < 0.001$, $n \geq 3$, Figure 4.5D). Analysis of the Paneth cell position did not differ significantly between the two experimental groups *VillinCreER*$^{+}$*Apc*$^{fl/fl}$ and *VillinCreER*$^{+}$*Apc*$^{fl/fl}$*Cbx3*$^{fl/fl}$ (Kolmogorov-Smirnov Z test, $p = 0.10$, $n \geq 3$, Figure 4.5D).

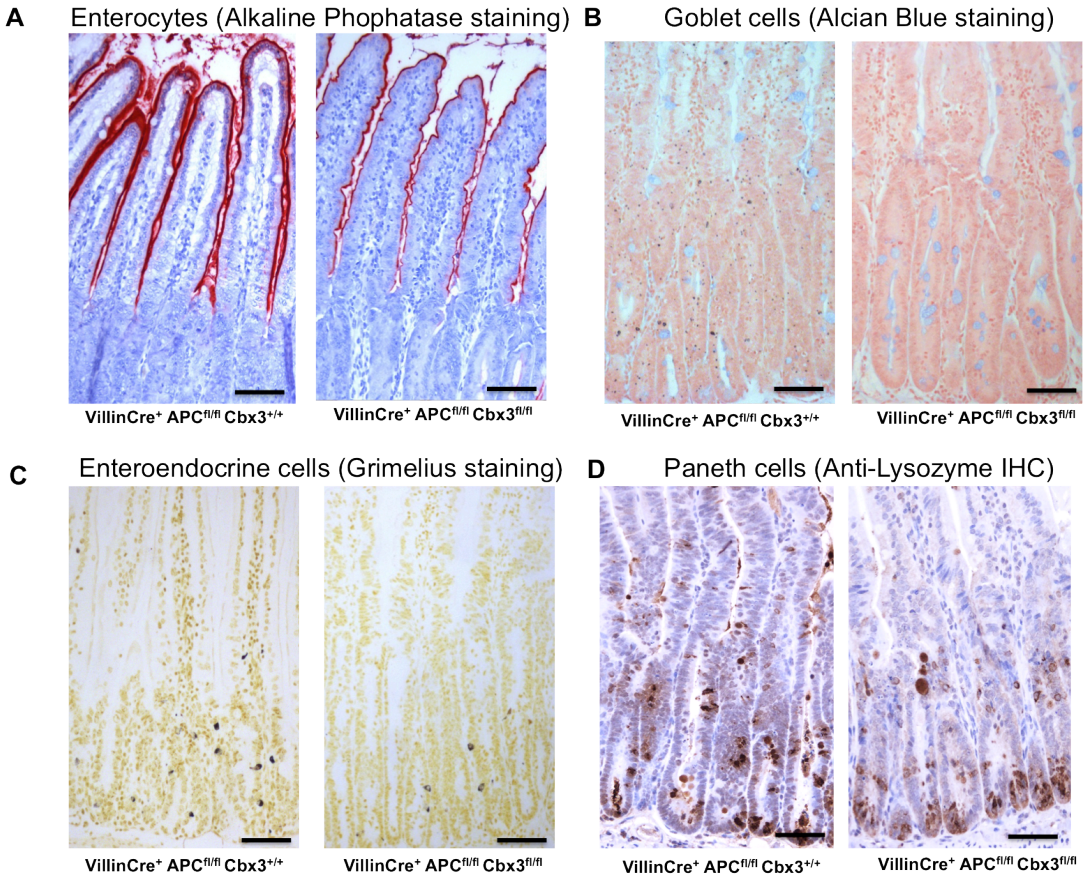

Figure 4.4: Identification of differentiated epithelial cell types upon *Cbx3* loss in Wnt activated small intestinal epithelium.
Small intestinal sections of *VillinCreER^{+}Apc$^{fl/fl}$* and *VillinCreER^{+}Apc$^{fl/fl}$Cbx3$^{fl/fl}$* mice at day 4 post induction were subjected to cell-type specific stains to visualise Enterocytes (A), Goblet cells (B), Enteroendocrine cells (C) and Paneth cells (D). Alkaline phosphatase staining revealed a slightly diminished brush border in the small intestinal epithelium of *VillinCreER^{+}Apc$^{fl/fl}$Cbx3$^{fl/fl}$* mice (A). No apparent differences were detected in differentiation of Goblet and enteroendocrine cell lineages (B and C), whereas a reduction in Paneth cell number is shown between the experimental and control cohorts. However, these changes were not significantly different (D). Scale bars indicate 100 µm.

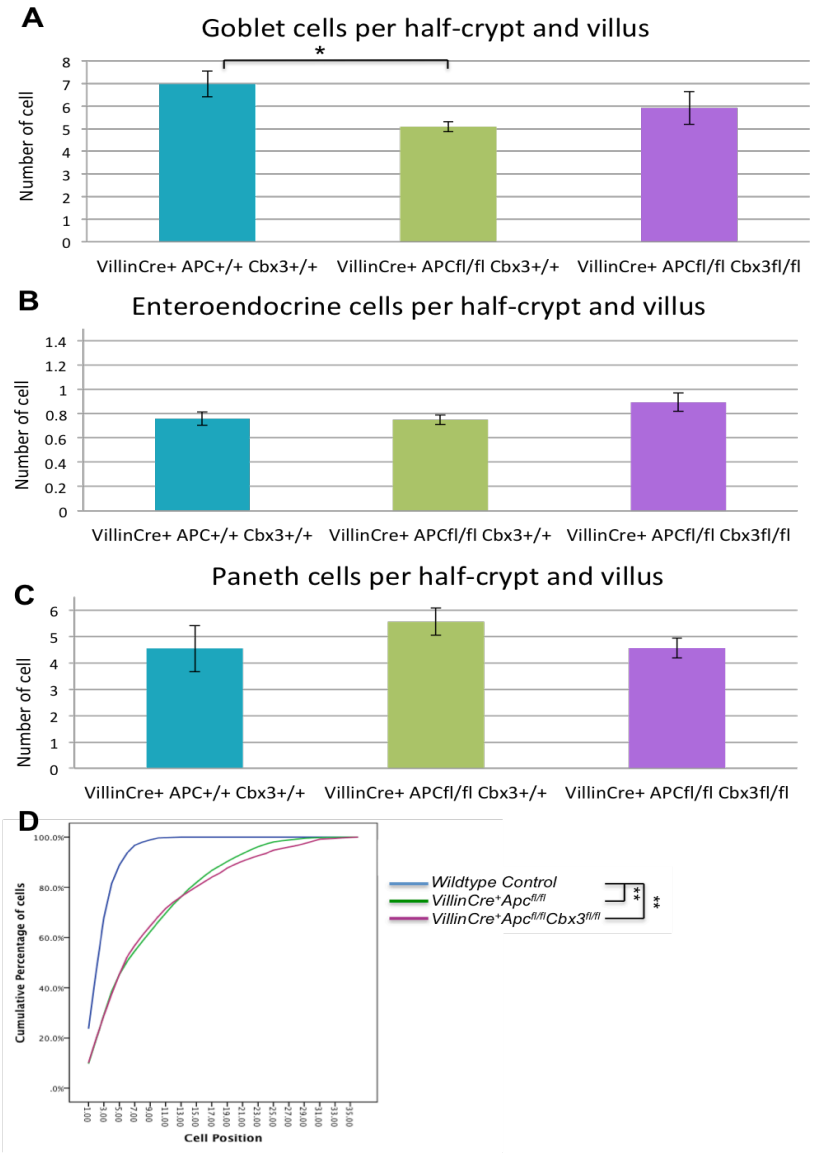

Figure 4.5: Quantification analysis of cell differentiation upon *Cbx3* loss in Wnt-activated small intestine.

The average number of Goblet (A), Enteroendocrine (B) and Paneth (C) cells per half-crypt and villus was scored in the small intestine of control, *VillinCreER^{+}Apc$^{fl/fl}$* and *VillinCreER^{+}Apc$^{fl/fl}$Cbx3$^{fl/fl}$* mice at day 4 post induction. The number of Goblet cells was significantly reduced in *VillinCreER^{+}Apc$^{fl/fl}$* mice compared to control animals ($p = 0.016$, $n \geq 3$), no changes between the groups were observed in differentiation of Enteroendocrine cells. The number of Paneth cells was found to be reduced in double knock out mice compared to *Apc* deficient animals, however the change was not significantly different ($p = 0.055$, $n \geq 3$). Error bars represent standard deviation. Exact values, standard deviations and p values are provided in Table 4.2. (D) Cumulative frequency analysis of Paneth cell distribution detected a significant expansion of Paneth cell location throughout the crypt in *VillinCreER^{+}Apc$^{fl/fl}$* and *VillinCreER^{+}Apc$^{fl/fl}$Cbx3$^{fl/fl}$* small intestine compared to control animals (Kolmogorov-Smirnov Z test, both $p < 0.001$, $n \geq 3$).

4.2.5. *Cbx3* loss shows a tendency to attenuate the expression of Wnt target genes in the Wnt activated small intestine

Down-regulation of *Cbx3* expression was previously reported to lead to growth inhibition of cancer cell lines (including colorectal cancer cell lines) (Takanashi *et al.,* 2009*b*). The dysregulation of the Wnt signalling pathway has been considered to play an important role in colorectal carcinogenesis and since little is known about the functional involvement of *Cbx3* in Wnt signalling regulation and colorectal cancer development, it was of great interest to investigate the consequence of *Cbx3* loss on Wnt target gene activation in the small intestinal epithelium.

Quantitative analysis of Wnt target gene expression was performed on intestinal samples from control, *VillinCreER*$^{+}$*Apc*$^{fl/fl}$ and *VillinCreER*$^{+}$*Apc*$^{fl/fl}$*Cbx3*$^{fl/fl}$ animals (n = 6). Total mRNA was extracted from the small intestinal epithelium and subjected to qRT-PCR analysis in order to assess the expression levels of a subset of Wnt target genes. A significantly elevated level of expression of *Axin2*, *c-Myc, CD44* and *CyclinD1* was demonstrated in the *VillinCreER*$^{+}$*Apc*$^{fl/fl}$ and *VillinCreER*$^{+}$*Apc*$^{fl/fl}$*Cbx3*$^{fl/fl}$ intestines compared to wildtype ($p < 0.05$, n = 6). Notably, the additional loss of *Cbx3* displayed a tendency to attenuate *Axin2, c-Myc, CD44, CyclinD1* and *EphB3* up-regulation although these reductions were not statistically significant (Figure 4.6).

Given that the loss of *Cbx3* has been shown to prolong survival of mice with homozygous *Apc* loss (see Section 4.2.1), and *Cbx3* loss attenuates the activation of the Wnt target genes in an *Apc* deficient intestine, an established *in vitro* Wnt-responsive Topflash analysis was performed to further study the effect of *Cbx3* loss on Wnt activity.

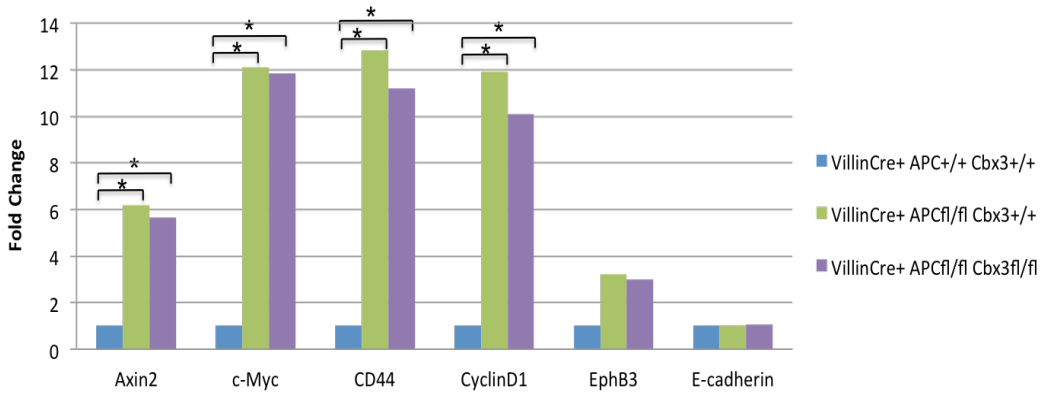

Figure 4.6: *Cbx3* loss shows a tendency to attenuate expression of the Wnt target genes.
qRT-PCR analysis of Wnt targets: *Axin2, cMyc, CD44, CyclinD1, EphB3* and *E-cadherin* revealed slight reduction of a range of Wnt target gene expression in the small intestinal epithelium of *VillinCreER^{+}Apc$^{fl/fl}$Cbx3$^{fl/fl}$* compared to *VillinCreER^{+}Apc$^{fl/fl}$* animals at day 4 post induction. Asterisks mark significant changes with p value < 0.05. For all comparisons n = 6.

4.2.6. Transient knock down of *CBX3* exhibits inhibitory effects on Wnt signalling

To investigate if *Cbx3* is a potential Wnt regulator, luciferase assays were employed in HEK-293 cells through the use of the Wnt-responsive Topflash system.

Transient knock down of *CBX3* using siRNA were performed 24 hours prior to transfection of TCF/β-catenin-responsive luciferase reporter, pTOPFLASH or its mutated variant, pFOPFLASH into HEK-293 cells in conjunction with a Wnt pathway activator, ΔNLRP6 (constitutively active LRP6 receptor) or TCF4-VP16 (constitutively active form of TCF4 transcription factor). The luciferase activities were determined from cell lysates 48 hours after transfection.

In this experiment, siRNA was used to down-regulate the expression of *CBX3* and the resulting TCF/β-catenin-dependent transcription was analysed. First, the efficiency of *CBX3* siRNA towards *CBX3* mRNA using qRT-PCR was tested (as shown in Figure 4.7A). The *CBX3* siRNA substantially reduced the levels of *CBX3* mRNA (8.7 fold reduction) compared to the control scrambled siRNA. Subsequently, the Topflash reporter plasmids were introduced using transfectin; the plasmids used include the pTOPFLASH reporter, pFOPFLASH (control) and pLacZ (transfection efficiency). To stimulate Wnt signalling the cells were co-transfected

with the ΔNLRP6 construct or the TCF4-VP16 construct. Forty-eight hours post-transfection the cells were harvested, cell lysates prepared and luciferase activity measured. *CBX3* down-regulation resulted in a reduction of ΔNLRP6 (41%) and TCF4 (27%) stimulation of TCF/β-catenin-dependent transcription or Topflash activity compared to the control cells.

Thus, the loss of *CBX3* demonstrated a reduction of Wnt activity from the receptor level to transactivation of Wnt target gene level, thereby demonstrating that *CBX3* positively contributes to Wnt signalling activation.

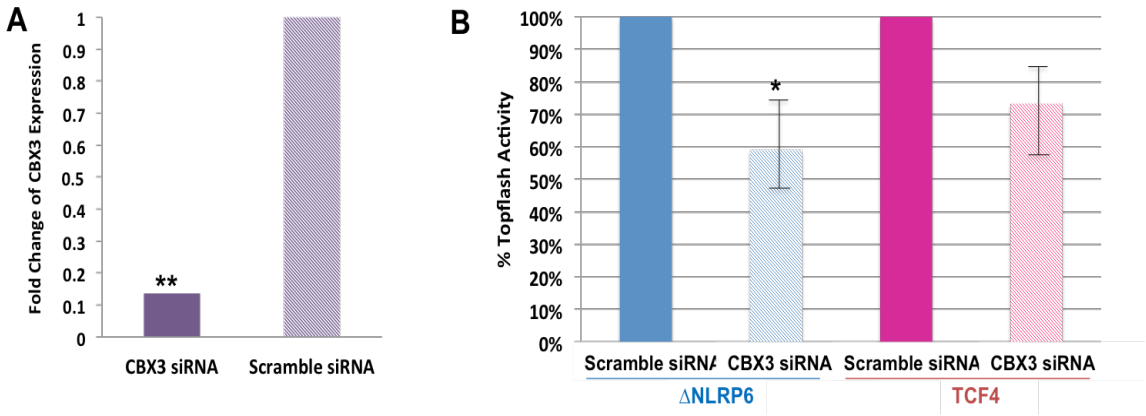

Figure 4.7: The effect of transient knock down of *CBX3* on Topflash activity.
(A) qRT-PCR was performed using human *CBX3*-specific primers on HEK-293 cells and HEK-293 cells stably transfected with siRNA toward *CBX3*. Scramble siRNA was included as control. *CBX3* transcripts were significantly reduced in cells transfected with *CBX3* siRNA compared to the Scramble siRNA control, data was collected 72 hours after siRNA transfection (8.7 fold reduction, $p < 0.01$, $n = 3$). (B) Topflash was activated by transfection of ΔNLRP6 or TCF4 in HEK-293 cells. Transient knock down of *CBX3* using *CBX3* siRNA 24 hours prior transfection of Topflash activator NLRP6 or TCF4 (plotted as percentages of the Scramble siRNA value) reduced total Topflash activity by 41% ($p = 0.04$, $n = 3$) and 27% ($p = 0.10$, $n = 3$), data collected 48 hours post-transfection. A single asterisk denotes statistically significant p value < 0.05 and double asterisks marks statistically significant p value < 0.01.

4.2.7. *Cbx3* loss does not affect Wnt-activated stem cell gene expression

Studies have shown that *Cbx3* is upregulated in various cancer cell lines including colon cell lines. Considering *Cbx3* has a potential to attenuate Wnt pathway activation in small intestinal epithelium and inactivation of *CBX3 in vitro* suppressed Wnt activation. The consequences of *Cbx3* loss on the expression levels of the intestinal stem cell genes was examined to see if *Cbx3* loss would suppress the expansion of the stem cell population in Wnt activated intestinal epithelium. In order to do this, the intestinal stem cell markers *Ascl2*, *Lgr5, Msi1, Bmi1* and *Olfm4* were analysed by qRT-PCR using RNA samples extracted from small intestinal epithelium of control, *VillinCreER^{+}Apc$^{fl/fl}$* and *VillinCreER^{+}Apc$^{fl/fl}$Cbx3$^{fl/fl}$* mice.

Expression levels of *Ascl2, Lgr5 and Msi1* were significantly increased in *VillinCreER^{+}Apc$^{fl/fl}$* and *VillinCreER^{+}Apc$^{fl/fl}$Cbx3$^{fl/fl}$* compared to control animals (Figure 4.5, for *Ascl2* $p < 0.01$ and for *Lgr5* and *Msi1* $p < 0.05$, $n = 6$), indicating the stem cell population were hugely expanded following the loss of *Apc* and acute Wnt activation. However, no significant difference was detected in the stem cell markers in *VillinCreER^{+}Apc$^{fl/fl}$Cbx3$^{fl/fl}$* epithelium compared to *VillinCreER^{+}Apc$^{fl/fl}$* epithelium ($p > 0.05$, $n = 6$), suggesting that the status of *Cbx3* does not contribute to the expansion of the stem cell population.

In addition, *In situ* hybridisation analysis of *Olfm4* was performed to further assess the effect of *Cbx3* loss on the state of the stem cell population in Wnt-activated intestinal epithelium. Small intestinal samples from *VillinCreER^{+}Apc$^{fl/fl}$* and *VillinCreER^{+}Apc$^{fl/fl}$Cbx3$^{fl/fl}$* animals harvested 4 days post induction were stained using an anti-*Olfm4* riboprobe (Figure 4.9). The small intestinal epithelium of *VillinCreER^{+}Apc$^{fl/fl}$* and *VillinCreER^{+}Apc$^{fl/fl}$Cbx3$^{fl/fl}$* animals displayed *Olfm4* staining throughout the crypt length. The additional loss of *Cbx3* in context of *Apc* deficiency revealed no alteration in the stem cell compartment in the small intestinal epithelium of *VillinCreER^{+}Apc$^{fl/fl}$Cbx3$^{fl/fl}$* compared to *VillinCreER^{+}Apc$^{fl/fl}$* animals.

Previous studies demonstrated that the loss of *Cbx3* is required for cell differentiation to occur and therefore leads to a reduction in stem cell numbers (Takanashi et al., 2009e). These observations are therefore at odds with published data, in that deletion of *Cbx3 f*rom the epithelium did not result in a reduction in stem cell markers or compartment within the Wnt-activated intestines.

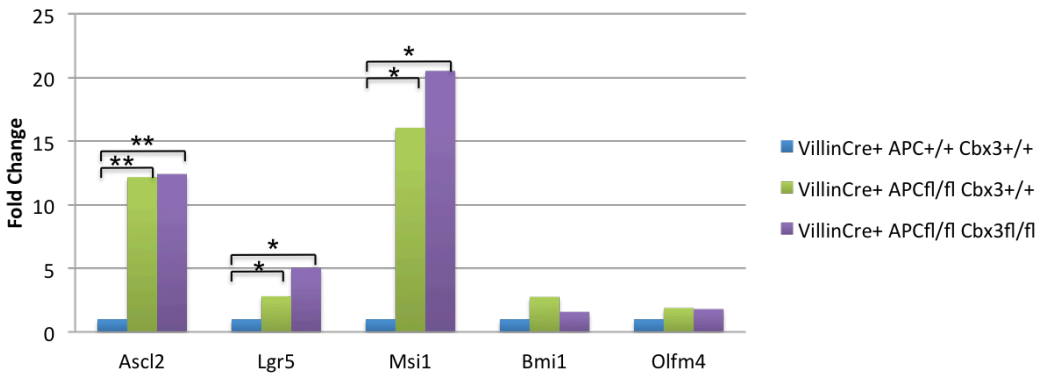

Figure 4.8: *Cbx3* loss does not attenuate Wnt-driven upregulation of small intestinal stem cell gene expression.
Quantitative RT-PCR expression analysis revealed a significant up-regulation of the stem cell markers *Ascl2, Lgr5, Msi1, Bmi1* and *Olfm4* in the small intestinal epithelium of *VillinCreER^{+}Apc$^{fl/fl}$* and *VillinCreER^{+}Apc$^{fl/fl}$Cbx3$^{fl/fl}$* mice compared to wildtype control at day 4 post-induction (for single asterisk p value < 0.05 and double asterisks p value < 0.01, n = 6). Expression levels of all stem cell markers revealed no significant differences in the small intestine of *VillinCreER^{+}Apc$^{fl/fl}$* mice compared *to VillinCreER^{+}Apc$^{fl/fl}$Cbx3$^{fl/fl}$* mice.

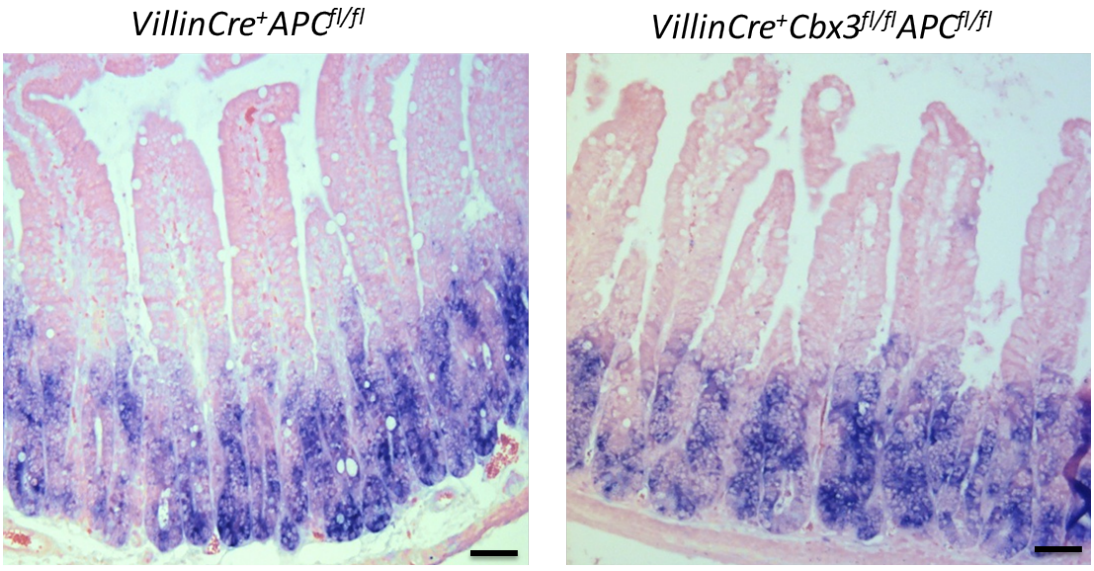

Figure 4.9: The additional *Cbx3* loss does not alter stem cell compartment.
***In situ* hybridisation analysis of *Olfm4* expression revealed no expansion or reduction of the stem cell compartment in the small intestinal epithelium of *VillinCreER^{+}Apc$^{fl/fl}$Cbx3$^{fl/fl}$* compared to *VillinCreER^{+}Apc$^{fl/fl}$* animals. Scale bars represent 100 µm.**

4.2.8. *Cbx3* loss does not affect Wnt-activated Notch target gene expression

Notch signalling pathway has been shown to be critical in driving enterocyte differentiation (Fre *et al.*, 2005). The loss of *Cbx3* was found to suppress enterocyte differentiation in *VillinCreER^{+}Apc$^{fl/fl}$Cbx3$^{fl/fl}$* compared to *VillinCreER^{+}Apc$^{fl/fl}$* epitheliums (Figure 4.4A) and therefore it can be hypothesised that *Cbx3* loss could potentially attenuate Notch signalling to a level sufficient to impair enterocyte differentiation.

In order to investigate the effects of *Cbx3* deficiency on Notch signalling in the Wnt-activated intestinal epithelium, the expression levels of a subset of Notch signalling target genes were examined. Total mRNA was extracted from the intestinal epithelium of control, *VillinCreER^{+}Apc$^{fl/fl}$* and *VillinCreER^{+}Apc$^{fl/fl}$Cbx3$^{fl/fl}$* mice at day 4 post-induction and used for qRT-PCR. Expression analysis of the Notch target genes: *Delta1, nRarp, Hes1, mTert*, *Lrig1, Jagged1* and *Jagged2* revealed significantly increased expression levels in both *VillinCreER^{+}Apc$^{fl/fl}$* and *VillinCreER^{+}Apc$^{fl/fl}$Cbx3$^{fl/fl}$* epithelium compared to wildtype control epithelium ($p < 0.05$, $n = 6$, Figure 4.10). The expression analysis of the *Cbx3* deficient epithelium demonstrated a slight decrease in *Delta1 nRarp, Hes1, Lrig1* and *Jagged2* expression compared to the *VillinCreER^{+}Apc$^{fl/fl}$* samples, and however the changes were not significantly different.

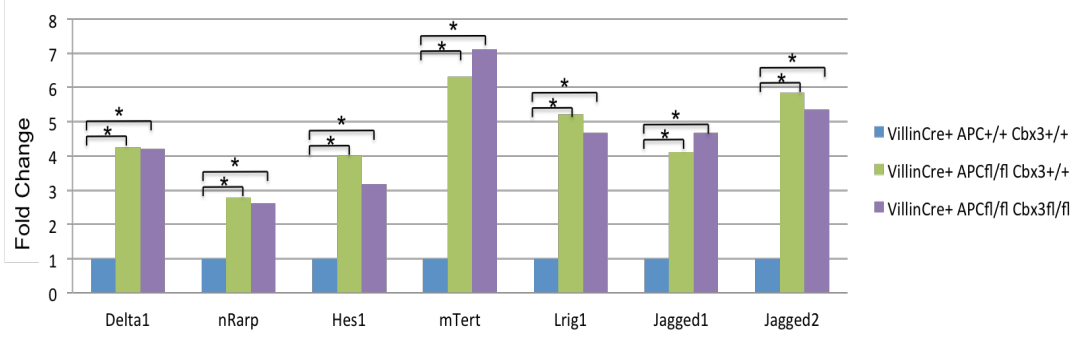

Figure 4.10： *Cbx3* loss does not affect expression of Notch target genes.
qRT-PCR analysis revealed a significant up-regulation of a range of Notch target genes (*Delta1, nRarp, Hes1, mTert, Lrig1, Jagged1 and Jagged2*) in the small intestinal epithelium of *VillinCreER^{+}Apc$^{fl/fl}$* and *VillinCreER^{+}Apc$^{fl/fl}$Cbx3$^{fl/fl}$* animals compared to control samples at day 4 post-induction. However, there is no significant change in expression of the Notch target genes between the two experimental groups. Asterisks represent the pair-wise comparisons that were found to be significantly different ($p < 0.05$, $n = 6$).

4.2.9. *Cbx3* loss alters Wnt target Splice variants but has mild effect on cell cycle gene expression in Wnt-activated intestine

The Wnt target gene, *Rac1*, was shown to be essential for tumour formation *in vivo* (Matos and Jordan, 2008) and a novel splice variant of *Rac1*, designated *Rac1b*, is expressed in a range of cancer cells including colon carcinoma cells (Singh *et al.*, 2004). *Cbx3* has been demonstrated to play a role in RNA splicing due to its interaction with splicesome (Smallwood *et al.*, 2012).

The expression levels of the Wnt target gene *Rac1* and its splice variant *Rac1b* was determined using qRT-PCR analysis. cDNA was made from RNA extracted from control, *VillinCreER*$^{+}$*Apc*$^{fl/fl}$ and *VillinCreER*$^{+}$*Apc*$^{fl/fl}$*Cbx3*$^{fl/fl}$ epithelium at day 4 post induction and used for qRT-PCR analysis.

Expression levels of the Wnt target gene *Rac1* and its splice variant *Rac1b* increased significantly in *VillinCreER*$^{+}$*Apc*$^{fl/fl}$ epithelium compared to control epithelium ($p < 0.05$, $n = 6$). Although both *Rac1* and *Rac1b* expression was reduced in the *VillinCreER*$^{+}$*Apc*$^{fl/fl}$*Cbx3*$^{fl/fl}$ epithelium compared to the *VillinCreER*$^{+}$*Apc*$^{fl/fl}$ epithelium, only expression of *Rac1b* was found to be significantly repressed following the loss of *Cbx3* in the Wnt activated intestine (Figure 4.11). This observation is consistent with the hypothesis that loss of *Cbx3* impairs RNA splicing and therefore leads to a reduced level of *Rac1b* in the small intestinal epithelium.

Previous work has demonstrated that the role of *Cbx3* on cell cycle regulation in *Caenorhabditis elegans* and human cells (Smallwood et al., 2012). It is therefore of great interest to investigate the effect of *Cbx3* loss on the expression level of a range of cell cycle genes. qRT-PCR analysis of the cell cycle genes detected a significantly reduced expression of *ATM* and a significantly elevated expression of *CDC25C* in both *VillinCreER*$^{+}$*Apc*$^{fl/fl}$ and *VillinCreER*$^{+}$*Apc*$^{fl/fl}$*Cbx3*$^{fl/fl}$ epithelium compared to the control epithelium ($p < 0.05$, $n = 6$). *Cbx3* loss shows a tendency to reduce expression of *CCNE1, PIM2* and *CAV2* in the Wnt-activated *VillinCreER*$^{+}$*Apc*$^{fl/fl}$*Cbx3*$^{fl/fl}$ intestines, although the changes are not statistically significant.

Together these observations suggest that *Cbx3* deficiency is likely to suppress RNA splicing and therefore attenuate the level of *Rac1b*, and *Cbx3* loss has mildly attenuated cell cycling gene expression in the Wnt activated intestines.

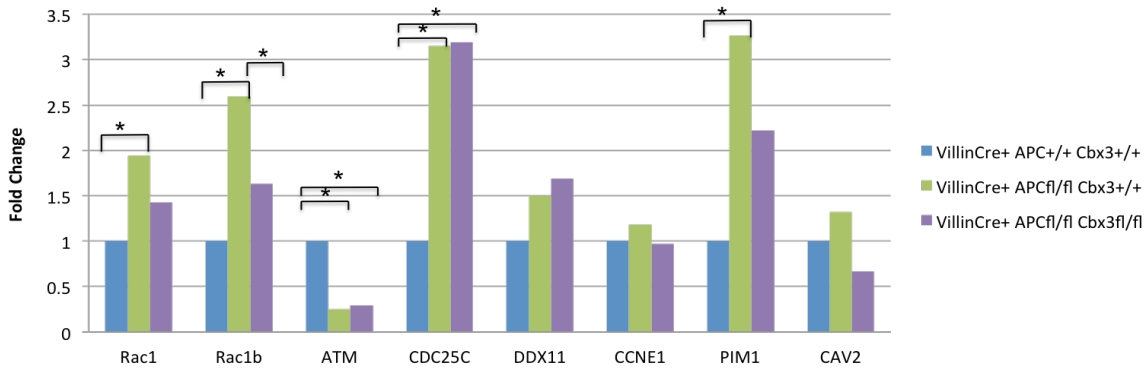

Figure 4.11: *Cbx3* loss significantly depletes the expression of Wnt target spice variant *Rac1b* in Wnt-activated intestine.
Quantitative RT-PCR analysis of the small intestinal epithelium 4 days post-induction revealed significantly increased expression levels of the Wnt-target splice gene *Rac1b*, as well as the cell cycle genes *CDC25C* and *PIM1* (apart from *ATM* which showed a reduction) in the small intestinal epithelium of *VillinCreER^{+}Apc$^{fl/fl}$* mice compared to control wildtype mice ($p < 0.05$, $n = 6$). The additional loss of *Cbx3* in the small intestinal epithelium significantly reduced expression of a Wnt target splice variant *Rac1b* in the *VillinCreER^{+}Apc$^{fl/fl}$Cbx3$^{fl/fl}$* animals compared to *VillinCreER^{+}Apc$^{fl/fl}$* animals ($p < 0.05$, $n = 6$).

4.2.10. HP1γ and H3K9me3 are mutually exclusive in normal intestinal homeostasis and acute Wnt activated intestine

HP1γ, coded by the gene *Cbx3*, differs from other members of heterochromatin protein 1 and it is present in both heterochromatin and euchromatin (Minc, Courvalin and Buendia, 2000). Previous evidence has proposed that HP1γ, bound to methylated H3K9, mediates heterochromatin formation, rendering the chromatin inaccessible for transcription (Jacobs and Khorasanizadeh, 2002b; Nielsen *et al.*, 2002b). Therefore, the association between HP1γ and methylated H3K9 marks in normal intestinal homeostasis and in acute Wnt activated intestine was investigated. Immunofluorescence co-localisation analysis was carried out in small intestinal tissue sections of control wildtype, *VillinCreER^{+}Cbx3$^{fl/fl}$*, *VillinCreER^{+}Apc$^{fl/fl}$* and *VillinCreER^{+}Apc$^{fl/fl}$Cbx3$^{fl/fl}$* animals.

Analysis of H3K9me3 expression showed nuclear localisation of H3K9me3 on the large matter of DAPI-dense facultative heterochromatin in all intestines. Staining of H3K9me3 was found to be more intense following the loss of *Apc* compared to wildtype animals. However, in contrast to the published literature no co-localisation between HP1γ and H3K9me3 was observed in all intestines (Figure 4.12, Figure 4.13). Furthermore, HP1γ and H3K9me3 also established a mutually exclusive relationship in the Wnt-activated small intestines (Figure 4.12, Figure 4.13). Interestingly, the level of H3K9me3 was substantially lowered in the absence of HP1γ in the *VillinCreER*$^{+}$*Cbx3*$^{fl/fl}$ intestinal epithelium (Chapter 3, Figure 3.12), suggesting that despite being mutually exclusive, HP1γ plays some role in establishing and / or maintaining H3K9me3 via docking on other heterochromatin marks (such as H4K20me3) to indirectly regulate H3K9me3. The lack of HP1γ-H3K9me3 co-localisation could be caused by H3S10 phosphorylation, which was reported to antagonise binding of HP1 to H3K9me3 (Fischle *et al.*, 2005). Detailed expression analysis by immunohistochemistry of H3S10 phosphorylation status is essential in future studies to determine whether the dissociation of HP1γ and H3K9me3 is caused by phosphorylation of H3S10 in the normal and Wnt-activated intestinal epithelium.

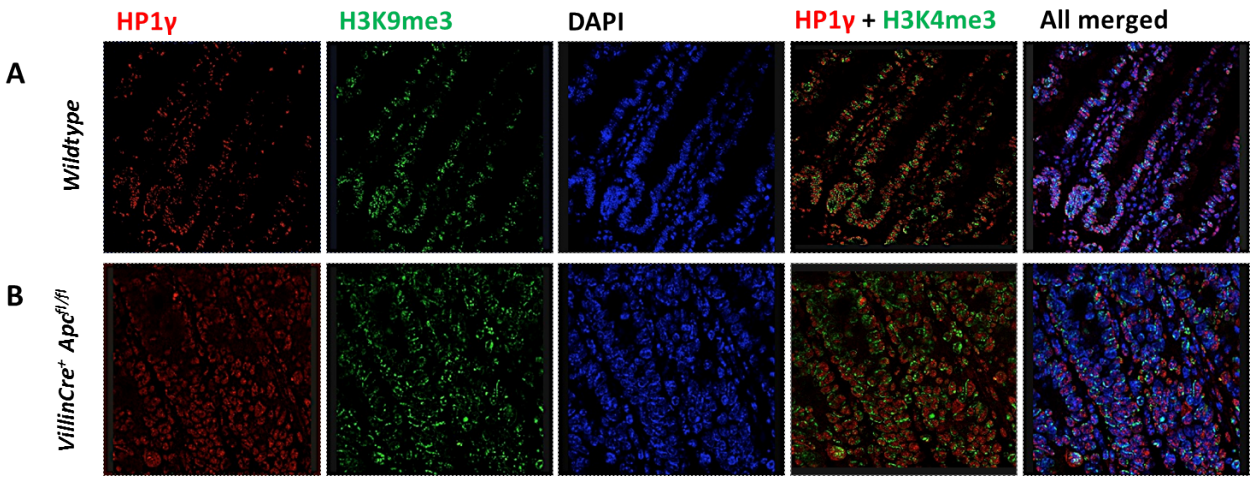

Figure 4.12: Immunofluorescence analysis of HP1γ and H3K9me3 in small intestine of wildtype and *VillinCreER*$^{+}$ *APC*$^{fl/fl}$ day 4 post-induction.
Confocal analysis of small intestines double-labelled with HP1γ antibody (Alexa 594, red) and H3K9me3 antibody (Alexa 488, green) in control wildtype (A) and *VillinCreER*$^{+}$*APC*$^{fl/fl}$ (B) intestines. These images are representative of small intestines analysed in each cohorts (n = 3). Nuclei were counterstained with DAPI (4', 6-diamidino-2-phenylindole; blue).

In order to confirm the mutually exclusive patterns observed between HP1γ and H3K9me3 in small intestinal tissues, co-localisation analysis using histograms displaying measured fluorescence intensity along a chosen distance across different cells in the small intestine was undertaken. Figure 4.13 shows representative regions that were scanned sequentially using appropriate excitation and emission settings for recordings of Alexa 594 (HP1γ in Red) and Alexa 488 (H3K9me3 in Green). The merged images of the dual-labelled HP1γ and H3K9me3 in small intestines of wildtype (Left panel) and *VillinCreER*$^{+}$*APC*$^{fl/fl}$ (Right Panel) showed distinct red and green labelling. The histograms (Figure 4.13A-H) representing the lines arbitrarily drawn upon red / green composite images across four different cells in the crypt regions of wildtype and *VillinCreER*$^{+}$*APC*$^{fl/fl}$ small intestine are consistent to our observations, the red and green fluorescence intensity peaked independently and there is no correlation between the staining patterns in both models, confirming that the immunostained HP1γ (Red) and H3K9me3 (Green) are mutually exclusive.

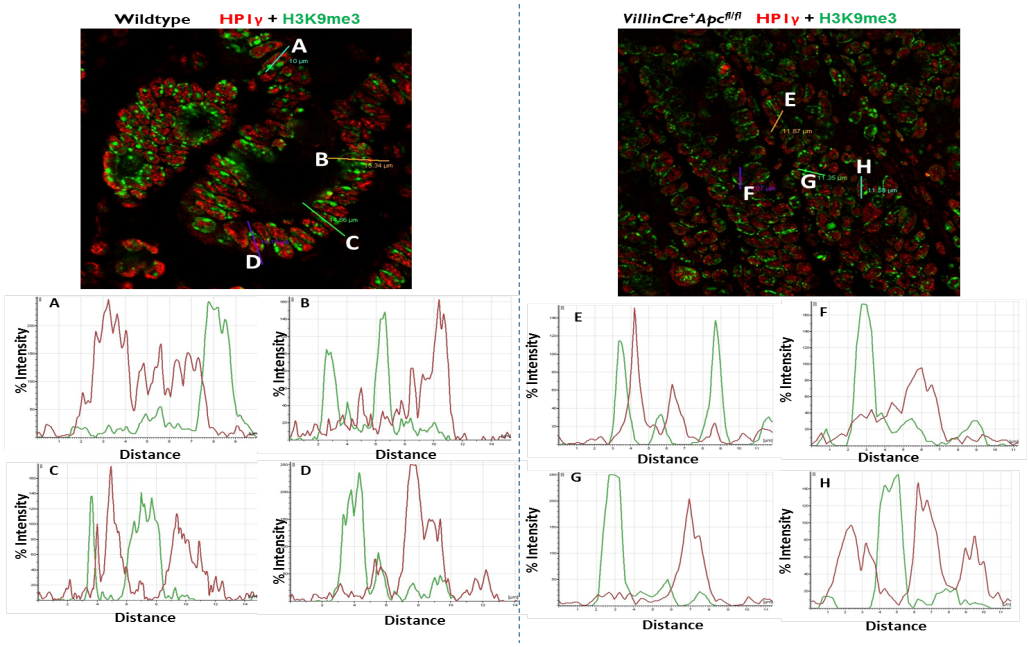

Figure 4.13: Confocal microscopic analysis of immunostained HP1γ and H3K9me3 in small intestine of wildtype and *VillinCreER*$^{+}$*APC*$^{fl/fl}$ mice day 4 post-induction.
(Top) Co-localisation of HP1γ (red) and H3K9me3 (green) in small intestines of WT and *APC*$^{fl/fl}$ mice revealed distinct patterns of staining in HP1γ and H3K9me3. (A-H) Histograms display measured fluorescence intensity along the lines marked on the top merged image. Line traces were generated with a line drawn arbitrarily upon red/green composite epithelial cells of small intestinal images.

4.2.11. Difference in HP1γ and H4K20me3 association patterns in small intestinal homeostasis and acute Wnt activated intestine

Given that the relationship between HP1γ and H3K9me3 is mutually exclusive in small intestinal homeostasis and acute Wnt activated intestines, the localisation of another heterochromatin repressive marker, H4K20me3, was also explored. H4K20me3 has been shown to have a significant correlation with HP1γ expression in normal tissue samples and a dissociation of the correlation between HP1γ expression and H4K20me3 may reflect the malfunction of epigenetic control in cancer tissues (Takanashi *et al.*, 2009). Therefore this correlation was examined in the small intestine of the wildtype animals and following *Apc* deletion in *VillinCreER*$^{+}$*Apc*$^{fl/fl}$ animals. Immunofluorescence analysis was performed on small intestinal tissue sections from wildtype and *VillinCreER*$^{+}$*Apc*$^{fl/fl}$ mice.

Immunofluorescence analysis of H4K20me3 expression showed intense staining in stromal compartments, crypts and along villi of small intestine across both the cohorts. A prominent increase in HP1γ expression was detected in the absence of *Apc* at day 4 post induction, compared to wildtype (Figure 4.14A and F), which is consistent with our preliminary data. H4K20me3 levels remained similar between *VillinCreER*$^{+}$*Apc*$^{fl/fl}$ small intestine compared to wildtype intestine, although the pattern of staining changed from more foci in wildtype to more diffuse in *VillinCreER*$^{+}$*Apc*$^{fl/fl}$ model (Figure 4.14B and G). Interestingly, the double staining (HP1γ and H4K20me3) clearly demonstrated co-localisation of HP1γ with H4K20me3 at the crypt and along the villus of the small intestine in wildtype mice in accordance to expectations (Figure 4.14D). The association of HP1γ with H4K20me3 in the small intestine of the wildtype mouse is lost in the absence of *Apc* (Figure 4.14D and I), expression of HP1γ and H4K20me3 appeared to be mutually exclusive in *VillinCreER*$^{+}$*Apc*$^{fl/fl}$ animals.

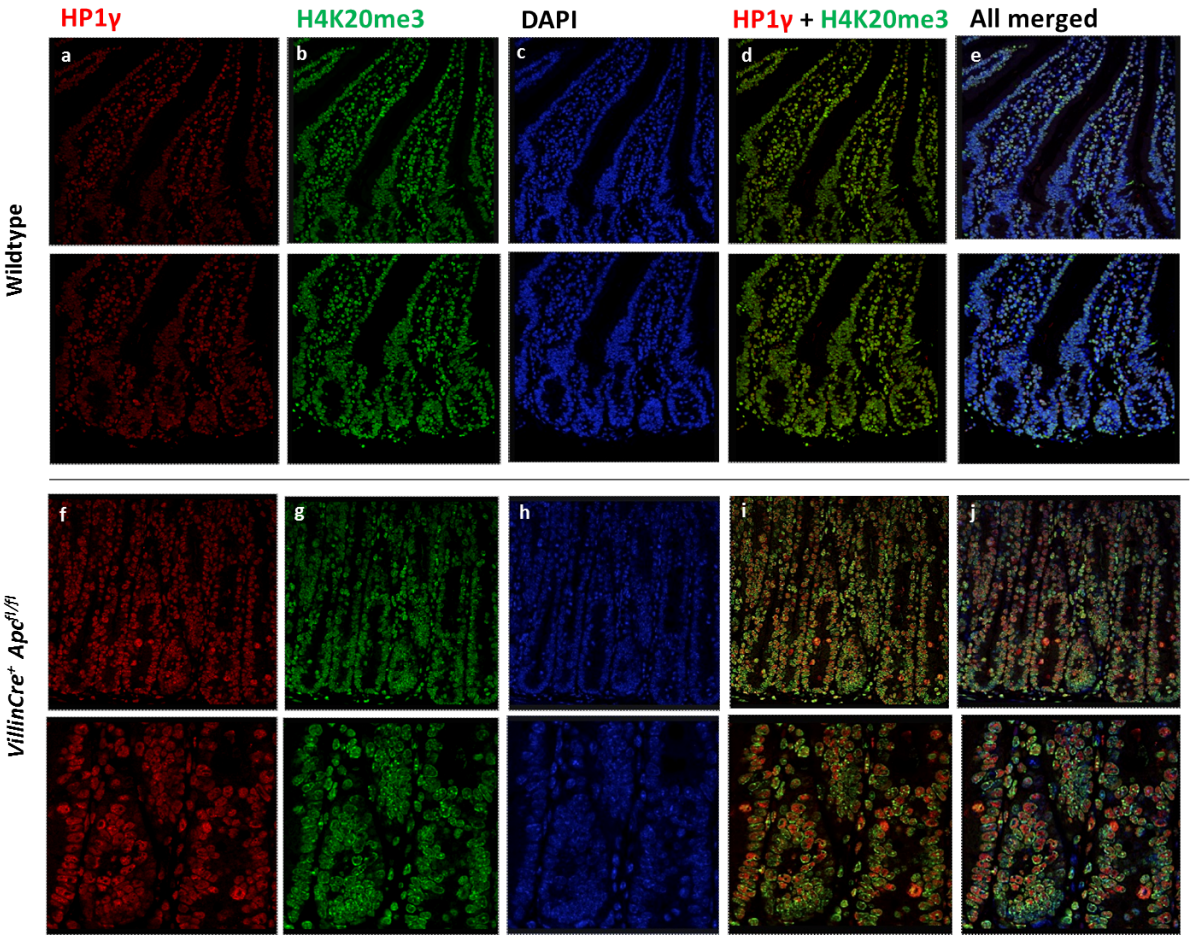

Figure 4.14: Co-localisation of HP1γ and H4K20me3 in small intestine of wildtype and *VillinCreER*$^{+}$*APC*$^{fl/fl}$ mice day 4 post-induction.
Confocal images of small intestines stained with anti-HP1γ antibody (red) and anti-H4K20me3 antibody (green). These images are representative of small intestinal tissues analysed in each cohorts (n = 3). Nuclei were stained with DAPI (4', 6-diamidino-2-phenylindole; blue).

In order to examine the co-localisation of HP1γ from H4K20me3 we examined the fluorescence intensity of HP1γ (Alexa 594, red) and H4K20me3 (Alexa 488, green) within the merged images, along the chosen distance across four different cells in the crypt and villus of small intestines, respectively. This analysis confirmed the co-localisation of HP1γ and H3K9me3 in small intestines of wildtype (Top panel,Figure 4.15) and the dissociation of the two markers following the loss of *Apc* (Bottom panel, Figure 4.15) The histograms illustrating the lines arbitrarily drawn upon red / green composite images across four different cells in the crypts (Figure 4.15A-D, I-L) and villus regions (Figure 4.15E-H, M-P) in

small intestine of wildtype and *VillinCreER*$^{+}$*Apc*$^{fl/fl}$ mice demonstrated consistent results with our previous observations. In the wildtype cohort, the red and green fluorescence intensity peaked at exact locations and the staining patterns appeared to be dependent on each other, whereas in the small intestinal tissues of *VillinCreER*$^{+}$*Apc*$^{fl/fl}$ the histograms showed that the red and green fluorescence intensity peaked independently and there was no correlation between the staining patterns. Taken together, these data suggest that HP1γ (Red) and H4K20me3 (Green) are associated in both crypt and villus of small intestine in wild-type mice. However, this association pattern is lost in the absence of *Apc* in the small intestine. This could be a potentially important mechanism by which dissociation of HP1γ and H4K20me3 are required for epigenetic malfunction in Wnt activated intestine.

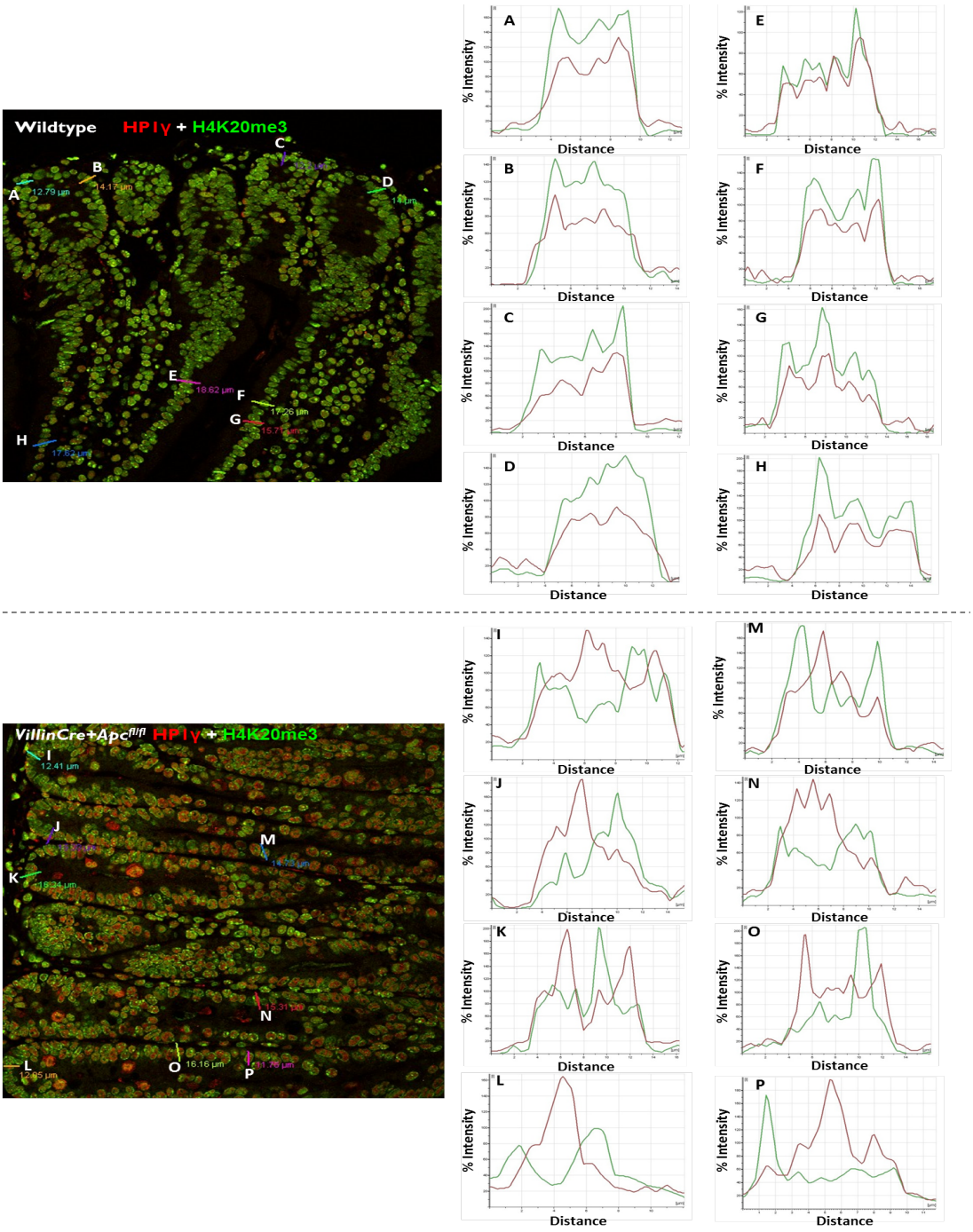

Figure 4.15: Confocal microscopy analysis of immunostained HP1γ and H4K20me3 in small intestine of wildtype *and VillinCreER^{+}APC$^{fl/fl}$* mice.
Co-localisation of HP1γ (red) and H4K20me4 (green) in small intestine of wild-type mouse is shown in the Top panels and *APC$^{fl/fl}$* mouse model is shown in the Bottom panels. Histograms display measured fluorescence intensity along the lines marked on the merged images of the wildtype mouse (A-H) and *APC$^{fl/fl}$* mouse model (I-P).

4.2.12. HP1α displaces HP1γ to the H4K20me3 marks in acute Wnt activated intestine

Considering the proposed dissociation of HP1γ and H4K20me3 as a sign for epigenetic malfunction in cancer development (Takanashi *et al.,* 2009), further investigation was undertaken to see whether this dissociation pattern was caused by displacement of other heterochromatin protein members in the Wnt activated small intestine. To this end, immunofluorescence analysis of other HP1 family members was performed on small intestinal tissue sections from wildtype and *VillinCreER*$^{+}$*Apc*$^{fl/fl}$ mice.

Immunofluorescence analysis of H4K20me3 expression showed intense staining in stromal compartments, crypts and along villi of small intestine across both the cohorts, as observed in the previous section. Expression of HP1α was detected in high level in more differentiated cells higher up along the villus of both wildtype and *VillinCreER*$^{+}$*Apc*$^{fl/fl}$ intestines (Figure 4.16). The double staining of HP1α and H4K20me3 expression demonstrated little association patterns of HP1α with H4K20me3 at the crypt and along the villus of the small intestine in wildtype mice (Figure 4.16D). Conversely, expression of HP1α with H4K20me3 in the small intestine of *VillinCreER*$^{+}$*Apc*$^{fl/fl}$ was found to be fully co-localised (Figure 4.16I).

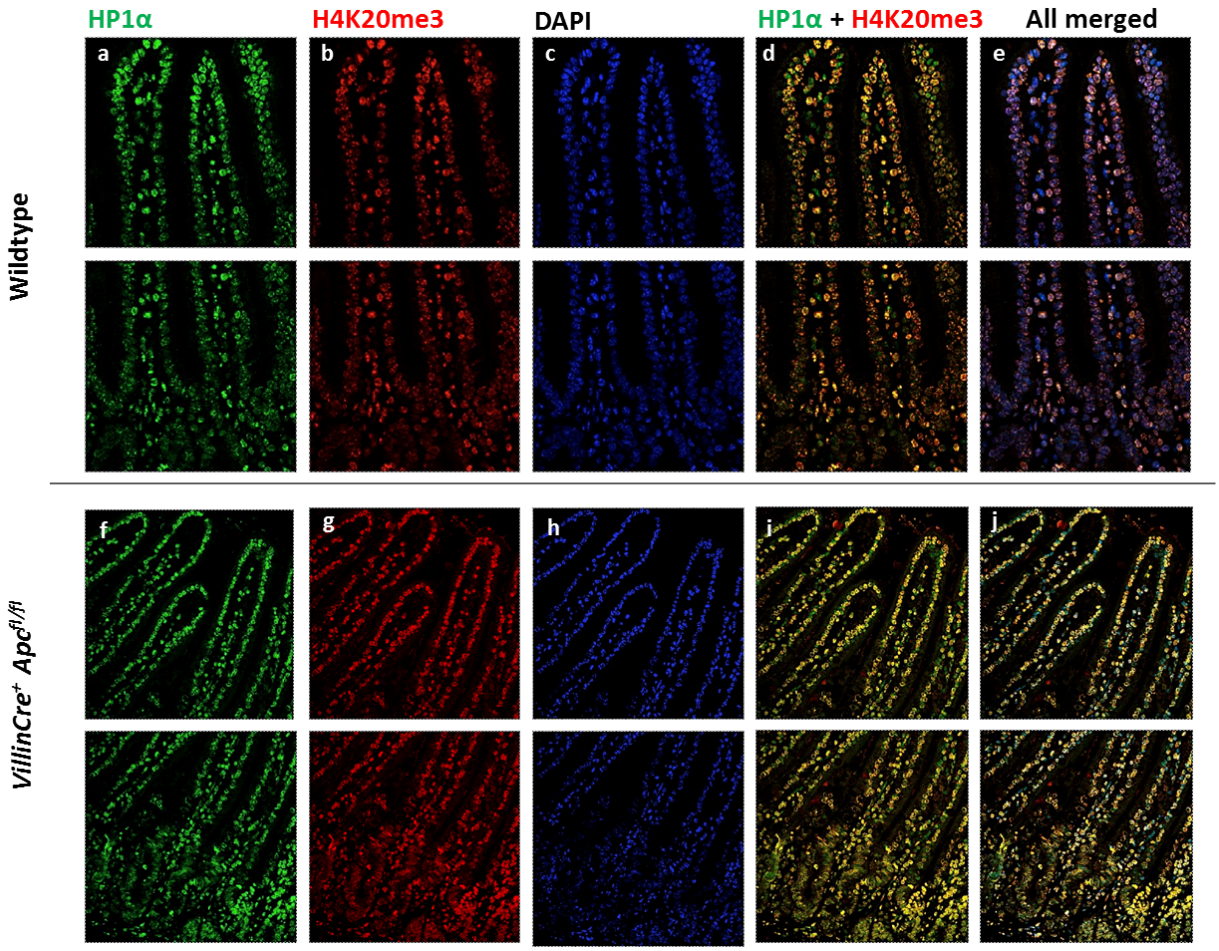

Figure 4.16: Co-localisation of HP1α and H4K20me3 in small intestine of wildtype and *VillinCreER^{+}APC$^{fl/fl}$* day 4 post-induction.
Confocal images of small intestines stained with anti-HP1α antibody (green) and anti-H4K20me3 antibody (red). These images are representative of small intestinal tissues analysed in each cohorts (n = 3). Nuclei were stained with DAPI (4', 6-diamidino-2-phenylindole; blue).

Based on these observations, the co-localisation of HP1α from H4K20me3 was examined by analysing fluorescence intensity of HP1α (Alexa 488, green) and H4K20me3 (Alexa 594, red) within the merged images, along the chosen distance across a number of cells in the crypt (Figure 4.17 Top and bottom panels, D-F) and villus (Figure 4.17 Top and bottom panels, A-C) of small intestines, respectively. This analysis confirmed the partial association pattern of HP1α and H4K20me3 in small intestines of wildtype (Top panel, Figure 4.17) and the full co-localisation of the two markers following the loss of *Apc* (Bottom panel Figure 4.17). The histograms illustrating the lines arbitrarily drawn upon red/green

composite images across four different cells in the crypts (D-F) and villus regions (A-C) in small intestine of wildtype and *VillinCreER*$^{+}$*Apc*$^{fl/fl}$ mice demonstrated consistent results with our previous observations. In the wildtype intestine, the histograms showed that the green and red fluorescence intensity partially peaked together and partially peaked independently and there was partial correlation between the staining patterns of HP1α and H4K20me3. Conversely, in the small intestinal tissues of *VillinCreER*$^{+}$*Apc*$^{fl/fl}$ the red and green fluorescence intensity peaked at exact locations and the staining patterns appeared to be dependent on each other. Collectively, these data indicate that HP1α (Green) and H4K20me4 (Red) are partially associated in both crypt and villus of small intestine in wildtype mice, whereas this association pattern become fully established in the absence of *Apc* in the small intestine. This observation, along with the dissociation of HP1γ from H4K20me3 in acute Wnt activated intestines, strongly suggests that the displacement of HP1γ by HP1α from H4K20me3 in Wnt activated small intestines.

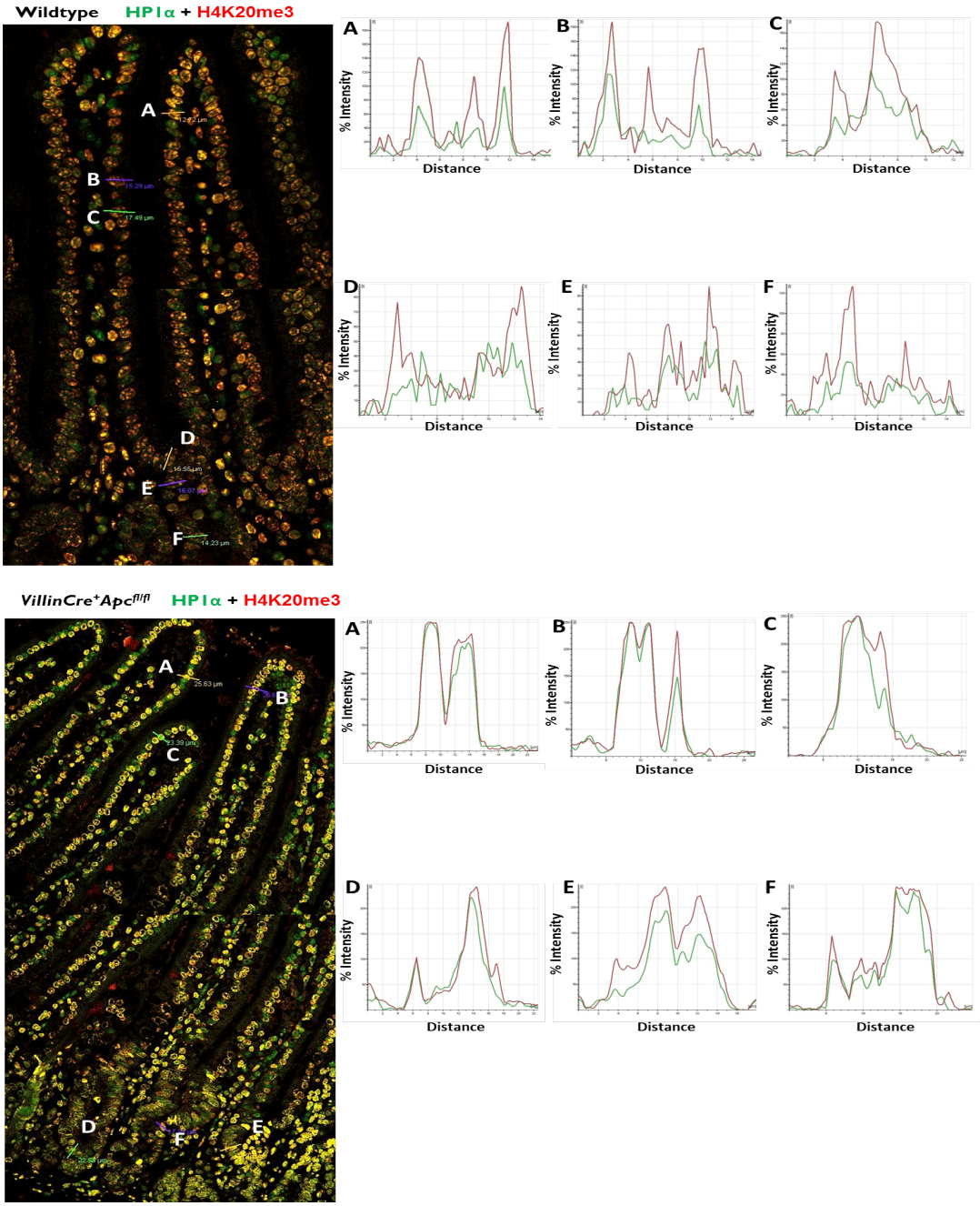

Figure 4.17: Confocal microscopy analysis of immunostained HP1α and H4K20me3 in small intestine of wildtype and *VillinCreER^{+}APC$^{fl/fl}$* small intestines.
In the top panel, co-localisation of HP1α (green) and H4K20me3 (red) in small intestines of wildtype revealed partially distinct patterns of staining in HP1α and H4K20me3. In contrast, HP1α and H4K20me3 expressions showed co-localisation in *VillinCreER^{+}APC$^{fl/fl}$* intestine. Histograms display measured fluorescence intensity along the lines marked on the top merged image. Line traces were generated with a line drawn arbitrarily upon red/green composite epithelial cells of small intestinal images (Top and bottom panels A-F).

4.2.13. Difference in HP1γ and H3K4me3 association patterns in small intestinal homeostasis and acute Wnt-activated intestine

It has been previously shown that HP1γ is fully colocalised with H4K20me3 in small intestinal homeostasis and it is dissociated from H4K20me3 in acute Wnt activated intestines. The biological significance of this association patterns was unclear and therefore the localisation of a euchromatin active marker, H3K4me3 was investigated. Histone H3K4 trimethylation (H3K4me3) is an active marker in the epigenetic code, it is enriched downstream of the active transcription start site (Hon, Hawkins and Ren, 2009). Since HP1α and HP1β are localised in heterochromatin, whereas HP1γ is present in both heterochromatin and euchromatin (Minc, Courvalin and Buendia, 2000), for it would be of great interest to determine whether HP1γ interacts with the active euchromatic marks. Therefore, immunofluorescence analysis of HP1γ and H3K4me3 was performed in the small intestine of the wildtype animals and following *Apc* deletion in *VillinCreER*$^{+}$*Apc*$^{fl/fl}$ animals.

The overall staining pattern of H3K4me3 is mostly diffuse in both wildtype and Wnt-activated intestines. Double immunofluorescence analysis of HP1γ and H3K4me3 demonstrated a partial co-localisation pattern was observed between the two markers at the crypt and along the villus of the small intestinal epithelium of the wildtype animals (Figure 4.18). On the other hand, the staining of HP1γ and H3K4me3 clearly became more fully colocalised especially at the crypt and along the villus of the small intestinal epithelium of *VillinCreER*$^{+}$*Apc*$^{fl/fl}$ animals (Figure 4.18).

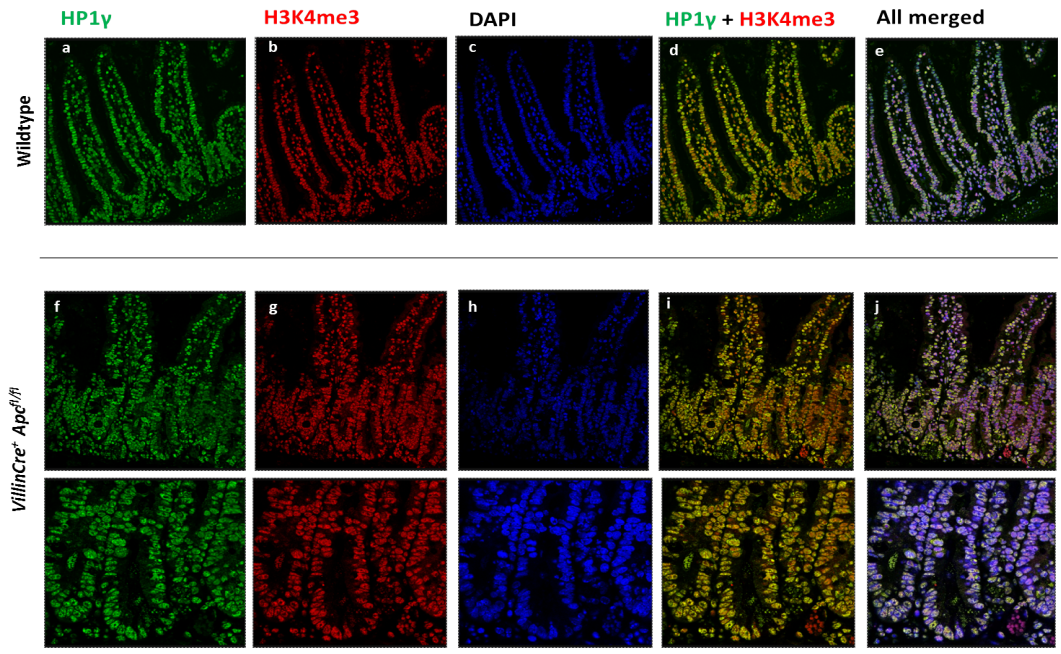

Figure 4.18: Co-localisation of HP1γ and H3K4me3 in small intestine of wildtype and *VillinCreER^{+}APC$^{fl/fl}$* mice day 4 post induction.
Confocal images of small intestines stained with anti-HP1γ antibody (green) and anti-H3K4me3 antibody (red). These images are representative of small intestinal tissues analysed in each cohort (n = 3). Nuclei were stained with DAPI (4', 6-diamidino-2-phenylindole; blue).

Having analysing the immunofluorescence images visually, the co-localisation of HP1γ from H3K4me3 was examined by analysing fluorescence intensity of HP1γ (Alexa 488, green) and H3K4me3 (Alexa 594, red) within the merged images, across a number of cells in the crypt (Figure 4.19) Top and bottom panels, A-C) and villus (Figure 4.19 Top and bottom panels, D-F) of small intestines, respectively. The histogram analysis confirmed the partial association pattern of HP1γ and H3K4me3 in small intestines of wildtype (Top panel, Figure 4.19) as the green and red fluorescence intensity partially peaked together and partially peaked independently. While in the small intestinal tissues of *VillinCreER^{+}Apc$^{fl/fl}$* mice, the green and red fluorescence intensity peaked uniformly, confirming that the co-localisation pattern seen in the Wnt-activated intestine (Bottom panel Figure 4.19). Collectively, these data indicate that HP1γ (Green) and H3K4me4 (Red) are partially associated in both crypt and villus of small intestine in wildtype mice, whereas this association pattern became fully colocalized in the absence of *Apc* in the small intestine, indicating a role of HP1γ in transcriptional activation in euchromatin.

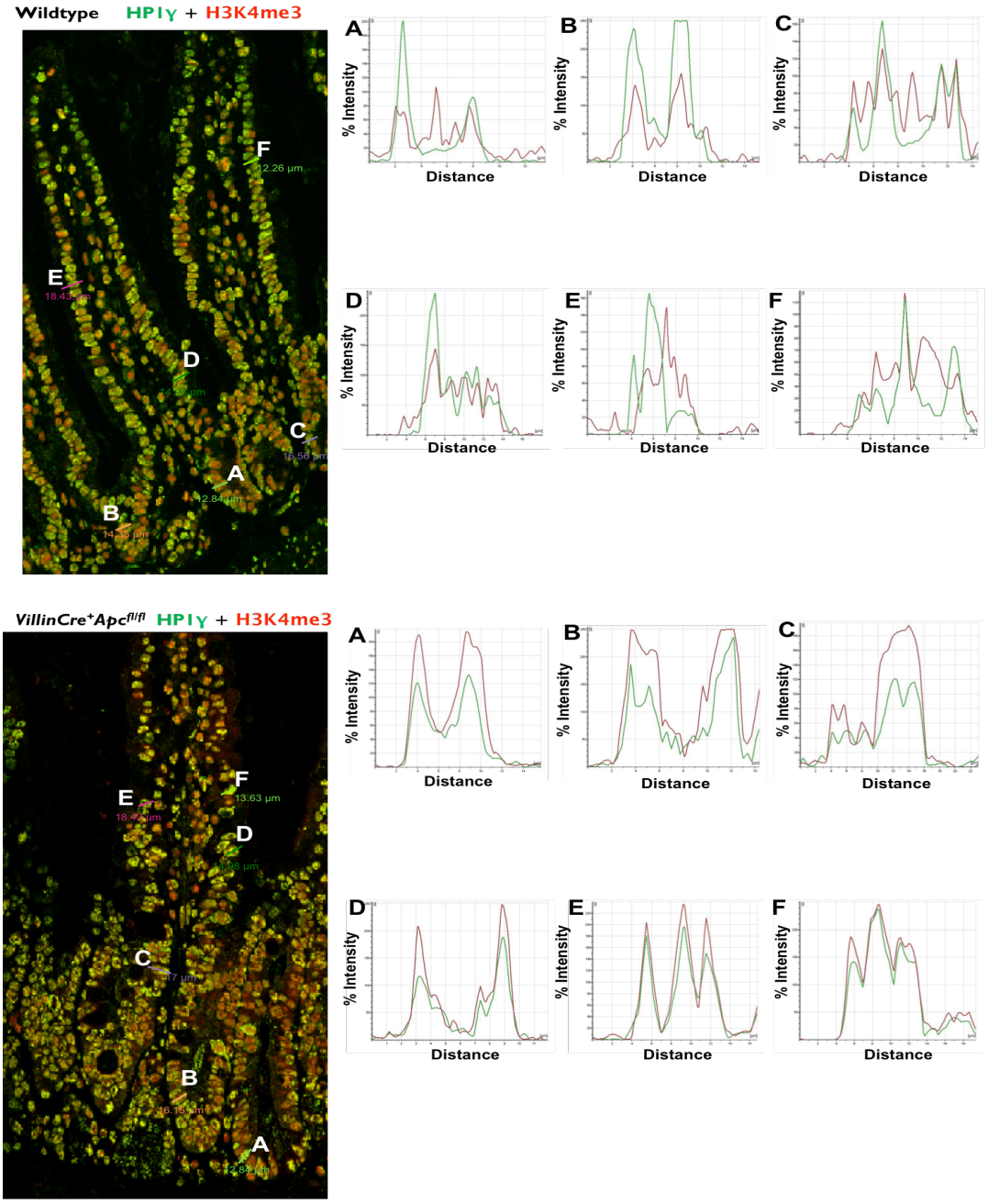

Figure 4.19 Confocal microscopy analysis of immunostained HP1γ and H3K4me3 in small intestine of wildtype and *VillinCreER^{+}APC$^{fl/fl}$* animals.
In the top panel, co-localisation of HP1γ (green) and H3K4me3 (red) in wildtype small intestines revealed partially distinct patterns of staining in HP1γ and H3K4me3. In contrast, HP1γ and H3K4me3 expressions showed more co-localisation in *VillinCreER^{+}APC$^{fl/fl}$* intestine. Histograms display measured fluorescence intensity along the lines marked on the top merged image. Line traces were generated with a line drawn arbitrarily upon red/green composite epithelial cells of small intestinal images (Top and bottom panels A-F).

4.2.14. HP1α and H3K4me3 are mutually exclusive in normal intestinal homeostasis and acute Wnt activated intestine

Having observed that the joint presence of HP1γ and H3K4me3 in the Wnt-activated intestine as a sign of gene activation in euchromatin, it would be interesting to investigate whether there is any interaction between HP1α and H3K4me3 and immunofluorescence analysis was performed on small intestinal tissue sections from wildtype and *VillinCreER*$^{+}$*Apc*$^{fl/fl}$ mice. Literature has indicated that HP1α is enriched at sites of heterochromatin, while H3K4me3 is mark of active euchromatin, therefore one would predict that there would be no association between HP1α and H3K4me3.

Consistent with our hypothesis, the double staining of HP1α and H3K4me3 demonstrated little to no association patterns between the two marks at the crypt and along the villus of the small intestine in wildtype mice (Figure 4.16D). Similarly, expression of HP1α with H3K4me3 in the small intestine of *VillinCreER*$^{+}$*Apc*$^{fl/fl}$ was also found to be mutually exclusive (Figure 4.20).

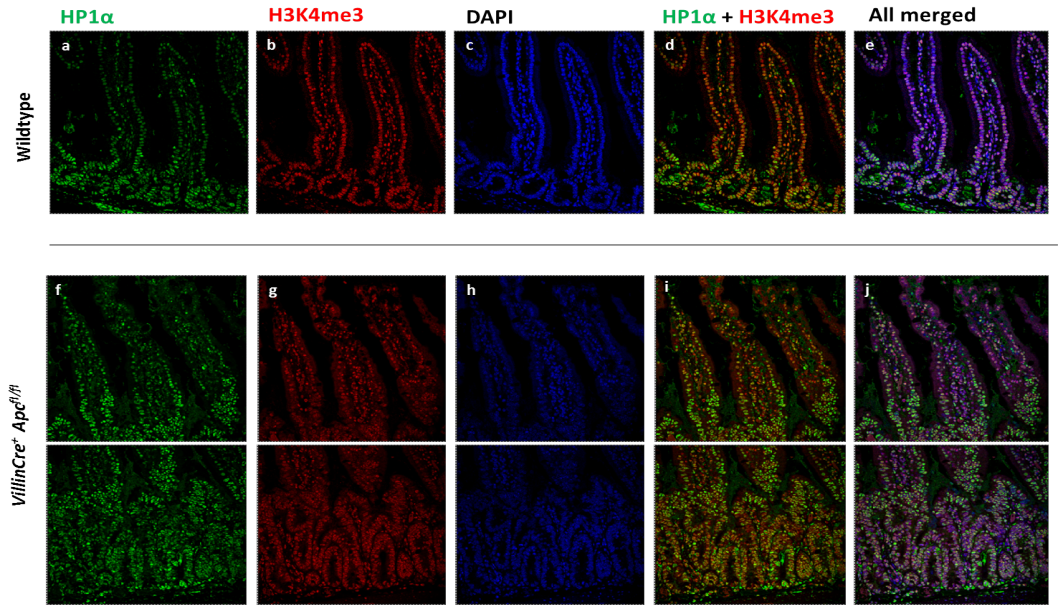

Figure 4.20: Co-localisation of HP1α and H3K4me3 in small intestine of wildtype and *VillinCreER*$^{+}$*APC*$^{fl/fl}$ Day 4 post induction.
Confocal images of small intestines stained with anti-HP1α antibody (green) and anti-H3K4me3 antibody (red). These images are representative of small intestinal tissues analysed in each cohorts (n = 3). Nuclei were stained with DAPI (4', 6-diamidino-2-phenylindole; blue).

In order to confirm the mutually exclusive patterns observed between HP1α and H3K4me3 in small intestinal tissues, co-localisation analysis using histograms displaying measured fluorescence intensity along a chosen distance across different cells in the small intestine was performed. The merged images of the dual-labelled HP1α and H3K4me3 in small intestines of wildtype (top panel) and *VillinCreER*$^{+}$*APC*$^{fl/fl}$ (bottom Panel) showed distinct red and green labelling. In the wildtype intestine, the histograms showed that the green and red fluorescence intensity peaked independently and similar pattern is observed in the small intestinal tissues of *VillinCreER*$^{+}$*Apc*$^{fl/fl}$. Taken together, these data indicate that HP1α and H3K4me3 are mutually exclusive in both crypt and villus of wildtype and Wnt-activated intestines, indicating that the two markers are localised at different nuclear locations, HP1α is enriched at sites of heterochromatin, whereas H3K4me3 is an active mark located in the euchromatin.

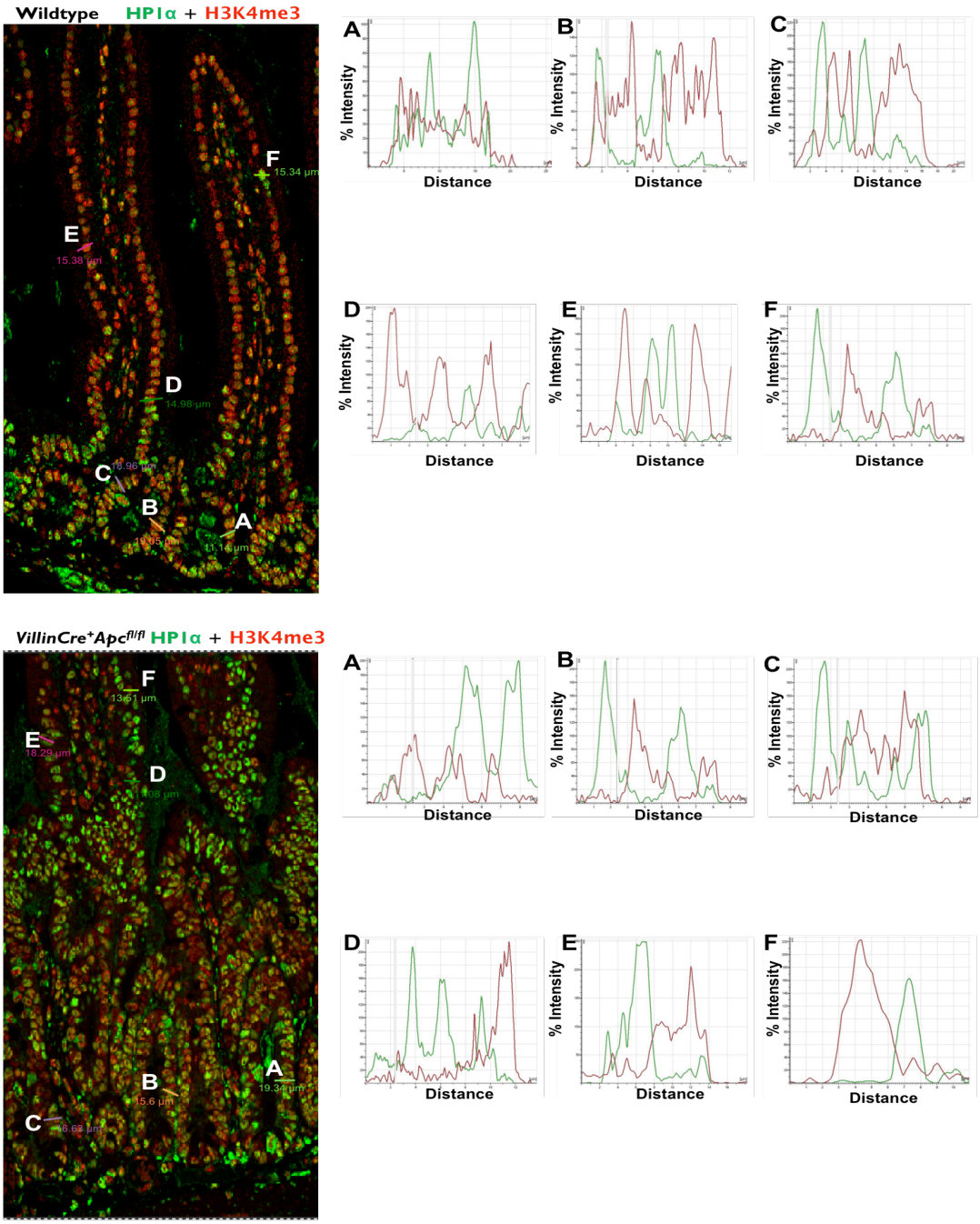

Figure 4.21: Confocal microscopy analysis of immunostained HP1α and H3K4me3 in small intestine of wildtype and *VillinCreER^{+}APC$^{fl/fl}$* animals.
In the top panel, co-localisation of HP1α (green) and H3K4me3 (red) in small intestines of wildtype revealed distinct patterns of staining in HP1α and H3K4me3. Similarly, HP1α and H3K4me3 expressions also are mutually exclusive in *VillinCreER^{+}APC$^{fl/fl}$* intestine. Histograms display measured fluorescence intensity along the lines marked on the top merged image. Line traces were generated with a line drawn arbitrarily upon red/green composite epithelial cells of small intestinal images (Top and bottom panels A-F).

4.3. Discussion

Previous work has demonstrated that epithelial deletion of *Cbx3* results in no immediate perturbation of intestinal homeostasis. Studies from the literature have shown that *Cbx3* is over-expressed in various cancer cell lines (including colon cell lines) and the deletion of *Cbx3* inhibited cancer cell line growth (Takanashi *et al.*, 2009). Furthermore, work described in our preliminary work has indicated that over-expression of *Cbx3* was observed in tumour samples of colorectal cancer patients compared to normal tissues. Consistent with this, conditional deletion of both alleles of *Apc* in the murine intestine using the Cre-loxP system results in an increased expression level of *Cbx3* and up-regulation of HP1γ protein. Taken together, these observations suggested that *Cbx3* has a role in intestinal carcinogenesis. Investigation of the effects of *Cbx3* deficiency on aberrant Wnt signaling is of importance for the understanding of the potential biological functions of *Cbx3* in cancer development. In this chapter, the effects of epithelial-specific *Cbx3* loss in the context of activated Wnt signaling was examined using conditional transgenesis with Lox-P targeted *Cbx3* and *Apc* alleles together with the inducible *VillinCreER* transgene.

4.3.1. Epithelial *Cbx3* deficiency prolongs survival but has no effect on gross intestinal structure in the context of *Apc* deficiency

The effect of *Cbx3* deletion following acute activation of Wnt signaling by deletion of both alleles of *Apc* was examined. Firstly, *VillinCreER*$^{+}$*Apc*$^{fl/fl}$*Cbx3*$^{fl/fl}$ and *VillinCreER*$^{+}$*Apc*$^{fl/fl}$ animals were generated, induced and closely monitored for signs of ill health. Intestinal deletion of both alleles of *Apc* is catastrophic for intestinal homeostasis, resulting in morbidity within 5 days (Sansom *et al*., 2004). Consistently, *VillinCreER*$^{+}$*Apc*$^{fl/fl}$ mice were sacrificed 4 days post induction due to ill health whereas *VillinCreER*$^{+}$*Apc*$^{fl/fl}$*Cbx3*$^{fl/fl}$ mice with the additional homozygous loss of *Cbx3* outlived *VillinCreER*$^{+}$*Apc*$^{fl/fl}$ mice by 3 days (with median survival 7 days). This observation is unprecedented and multiple mechanisms that might have contributed to the improved animal survival in *VillinCreER*$^{+}$*Apc*$^{fl/fl}$*Cbx3*$^{fl/fl}$ mice include the suppression of Wnt activation at the receptor level observed in the Topflash assay, the diminished enterocyte brush border and the reduction of *Rac1b* splice variant expression level. These notions would be individually discussed in the subsequent sections.

In this section, the further histological parameters were investigated in order to gain an insight to this observation.

Having established that deletion of *Cbx3* prolonged lifespan of mice with homozygous loss of *Apc*, the consequence of *Cbx3* loss on cell differentiation in the aberrant Wnt-activated intestine were investigated. Quantitative measurements of histological parameters, such as crypt length, apoptotic index, cleaved Caspase3, mitotic figures and Ki67 were all significantly increased in Wnt activated epithelium in both *Cbx3* deficient and proficient tissue compared to control mice, consistent with previous observations of conditional *Apc* deletion in the small intestine (Sansom *et al.,* 2004). No effect was observed between the two experimental cohorts *VillinCreER*$^{+}$*Apc*$^{fl/fl}$*Cbx3*$^{fl/fl}$ and *VillinCreER*$^{+}$*Apc*$^{fl/fl}$ across all these parameters. Additionally, *Cbx3* loss in the context of *Apc* deficiency exhibited no effect on cell migration.

Having observed no dramatic histological changes between *VillinCreER*$^{+}$*Apc*$^{fl/fl}$*Cbx3*$^{fl/fl}$ and *VillinCreER*$^{+}$*Apc*$^{fl/fl}$ intestines, qualitative and quantitative analysis of the normal intestinal cell differentiation was examined. Visualization of the enterocytes from the absorptive lineage in the *Cbx3* deficient Wnt activated small intestinal epithelium revealed a consistent decrease in brush border staining compared to *VillinCreER*$^{+}$*Apc*$^{fl/fl}$ intestines, indicating *Cbx3* might play a role in regulating enterocyte maturation. However, quantitative analysis of the Goblet cells, Enteroendocrine cells and Paneth cells from the secretory lineage revealed that the presence, location and frequency of these *mature* cell types was unaffected by *Cbx3* loss in the *Apc* deficient intestines. Although *Cbx3* loss did not diminish the entire absorptive lineage, the thin brush border of enterocytes were observed in *Cbx3*-deficient epithelium compared to control epithelium. Notch signaling has been reported to play a crucial role in differentiation of enterocyte, as constitutive activation of the Notch pathway substantially reduced differentiation of secretory cells and promoted differentiation of post-mitotic cells into adsorptive enterocytes (Fre *et al.,* 2005). In contrast, blockade of Notch signaling in rodent intestine with the Notch inhibitors has been found to result in expansion of secretory cells at the expense of enterocytes (Milnao *et al,* 2004). In the current study short-term *Cbx3* loss was found to perturb the development of the brush border without affecting the differentiation of other secretory cell lineages. It could be hypothesized that *Cbx3* loss does not impair

enterocyte differentiation, but rather suppresses expression of the brush border components. Expression analysis of other enterocyte-specific markers, such as Villin may be required to determine whether *Cbx3* loss suppresses enterocyte differentiation.

Taken together, theses data suggest that the immediate effect of *Cbx3* loss in the context of aberrant Wnt signaling activation is prolonged lifespan of *Apc*-deficient mice without altering the intestinal histology and cell differentiation of the secretory cell types.

4.3.2. *Cbx3* loss exhibits inhibitory effects on Wnt signaling

Evidence from the literature indicates that down regulation of *Cbx3* inhibited growth of cancer cell lines (Takanashi *et al.*, 2009). Previous data has demonstrated that *Cbx3* loss prolonged life span of Wnt-activated mice. Therefore the functional interaction between *Cbx3* and Wnt signalling *in vivo* in murine small intestinal epithelium and *in vitro* in a Wnt-responsive Topflash system was investigated.

In order to examine the consequence of *Cbx3* deficiency on Wnt target gene activation in the small intestinal epithelium, the expression levels of a number of Wnt target genes (*Axin2, c-Myc, CD44, CyclinD1, EphB3* and *E-cadherin*) was assessed. Quantitative analysis of Wnt target gene expression revealed that a subset of Wnt target genes (*Axin2, c-Myc, CD44* and *CyclinD1*) was found to be substantially upregulated following the loss of *Apc* in both *Cbx3* deficient and proficient intestinal epithelium. The Wnt target genes show a slight reduction in the small intestinal epithelium of *VillinCreER*$^{+}$*Apc*$^{fl/fl}$*Cbx3*$^{fl/fl}$ mice compared to *VillinCreER*$^{+}$*Apc*$^{fl/fl}$ mice, although these reductions were not statistically significant.

To further investigate whether *Cbx3* has a role in Wnt activity, luciferase assays were utilised in HEK-293 cells by use of the Wnt-responsive Topflash system. In order to determine at which level *Cbx3* is modulating the Wnt pathway, pathway activators (ΔNLRP6 [constitutively active LRP6 receptor] and TCF4-VP16 [constitutively active form of TCF4 transcription factor]) were used to induce Wnt signalling at distinct levels (Ewan *et al.*, 2010). Transient knock down of *CBX3* using *CBX3* siRNA 24 hours prior transfection of Topflash activator ΔNLRP6 or TCF4-VP16 reduced total Topflash activity 48 hours post-

transfection by 41% and 27%, respectively. This data suggest that *CBX3* mainly acted at LRP6 receptor level based on the observation that the loss of *CBX3* blocked TCF-dependent transcription induced by a constitutively active LRP6 receptor, but less extent of blockage observed by a constitutively active TCF-VP16 fusion protein, indicating that *CBX3* functions at receptor level within the Wnt signalling cascade.

In summary, depletion of *Cbx3* has shown a noticeable inhibitory activity against Wnt target gene expression in the epithelium of Wnt-activated intestine. Concordantly, the Topflash assay confirmed that the loss of *Cbx3* significantly suppressed Wnt activation by 41%, at the receptor level. Furthermore, the repressed Wnt activation may account for the prolonged survival observed previously in epithelial *Cbx3* deficient mice with activated Wnt signalling.

4.3.3. *Cbx3* loss in the Wnt-activated epithelium does not alter stem cell compartment

Previous evidence suggested *Cbx3* is required for cell differentiation to occur in adipocyte, male germ cell and cardiovascular system (Xiao *et al.,* 2011; Brown *et al.,* 2010b). However, *Cbx3* deficiency had no impact on cell differentiation in the Wnt-activated intestines as previously analysed. Next, the expression analysis of a range of intestinal stem cell markers (*Ascl2*, *Lgr5, Msi1, Bmi1 and Olfm4)* revealed no significant difference between *VillinCreER*$^{+}$*Apc*$^{fl/fl}$*Cbx3*$^{fl/fl}$ epithelium compared to *VillinCreER*$^{+}$*Apc*$^{fl/fl}$ epithelium. *In situ* hybridisation analysis of *Olfm4* was also performed to further assess the effect of *Cbx3* loss on the state of the stem cell population in Wnt-activated intestinal epithelium. The additional loss of *Cbx3* in context of *Apc* deficiency indicated again no alteration in the stem cell compartment in the small intestinal epithelium of *VillinCreER*$^{+}$*Apc*$^{fl/fl}$*Cbx3*$^{fl/fl}$ compared to *VillinCreER*$^{+}$*Apc*$^{fl/fl}$ animals.

These observations are compelling evidence for the fact that epithelial *Cbx3* deficiency does not modulate the stem cell genes and compartment in the intestine.

4.3.4. *Cbx3* loss has mild effect on Notch and cell cycle gene expression in Wnt-activated intestine

Notch signalling pathway also plays a critical role in intestinal homeostasis and intestinal stem cell maintenance and furthermore, Notch has been shown to be critical in driving enterocyte differentiation (Fre *et al.*, 2005). Previous data has shown that *Cbx3* was found to suppress enterocyte differentiation in *VillinCreER*$^{+}$*Apc*$^{fl/fl}$*Cbx3*$^{fl/fl}$ compared to *VillinCreER*$^{+}$*Apc*$^{fl/fl}$ epitheliums and therefore one could hypothesise that *Cbx3* loss could potentially attenuate Notch signalling to a level sufficient to impair enterocyte differentiation. Therefore the effects of *Cbx3* loss on Notch target gene expression was investigated in Wnt activated intestinal epithelium.

In order to investigate the effects of *Cbx3* deficiency on Notch signalling in the Wnt-activated intestinal epithelium, the expression levels of a subset of Notch signalling target genes were examined. Expression analysis of all examined Notch target gene: *Delta1, nRarp, Hes1, mTert*, *Lrig1, Jagged1* and *Jagged2* revealed significantly increased expression levels in both *Cbx3* deficient and proficient epithelium with *Apc* loss. The expression analysis of the *Cbx3* deficient epithelium demonstrated a trend of decrease in *Delta1 nRarp, Hes1, Lrig1* and *Jagged2* expression compared to the *VillinCreER*$^{+}$*Apc*$^{fl/fl}$ samples, however the changes did not reach statistical significance. Even though the downregulation of Notch target genes was not statistically significant, the effect of this was sufficient to be translated into cellular effect on the differentiation of secretory enterocyte.

Previous work has demonstrated that the role of *Cbx3* on cell cycle regulation in *Caenorhabditis elegans* and human cells (Black *et al*., 2010). Additionally, the involvement of *Cbx3* in cell cycle regulation is critical in controlling levels of primordial germ cells in mouse embryos (Abe *et al.*, 2011). It is therefore of great interest to investigate the effect of *Cbx3* loss on the level of a range of cell cycle genes in the Wnt-activated intestine. Expression analysis of the cell cycle genes detected a significantly reduced expression of ATM and a significantly elevated expression of *CDC25C* in both *VillinCreER*$^{+}$*Apc*$^{fl/fl}$ and *VillinCreER*$^{+}$*Apc*$^{fl/fl}$*Cbx3*$^{fl/fl}$ epithelium. However, there are no significant differences in the cell cycle gene expression levels between the two experimental groups *VillinCreER*$^{+}$*Apc*$^{fl/fl}$ and *VillinCreER*$^{+}$*Apc*$^{fl/fl}$*Cbx3*$^{fl/fl}$. A trend of reduction is observed in expression of *CCNE1*,

PIM1 and *CAV2*, which are thought to be involved in cancer progression, following the loss of *Cbx3* in the Wnt-activated intestines.

Collectively, these data indicate that *Cbx3* loss has mild modulation on Notch signalling and cell cycle regulation in the Wnt-activated intestines.

4.3.5. *Cbx3* loss alters Wnt target splice variant *Rac1b* expression in Wnt-activated intestine

Previously published data has indicated a role for *Cbx3* in aiding in efficient cotranscriptional RNA processing through recruitment of the splicing machinery. Depletion of *Cbx3* diminished the recruitment of splicing factors such as SNRNP70 and SRSF1 to gene bodies, resulting in RNA processing defect and subsequently leading to an increase in unspliced transcripts of its target genes (Saint-Andre *et al.,* 2011; Smallwood *et al.*, 2012). Alternative splicing of the tumour-related *Rac1b* is regulated by SRSF1 in colorectal cells (Goncalves *et al*., 2014). *Rac1b* was identified in malignant colorectal tumours as an alternative splice variant of *Rac1* (Schnelzer *et al.*, 2000; Fiegen *et al.,* 2004). A number of studies have reported that *Rac1b* plays an important role in tumorigenesis via augmenting Wnt signaling, promoting tumour cell survival (Matos *et al.*, 2008) and increasing the invasive and metastatic properties of colorectal cancer cells (Esufali *et al.*, 2007). However, the mechanisms of how changes in alternative splicing lead to *Rac1b* overexpression remain unclear. Since *Rac1* is a Wnt target gene which would be upregulated following *Apc* loss in the intestinal epithelium, therefore, one would predict that deletion of *Cbx3* would lead to *Rac1b* splicing defect and therefore a lower expression of *Rac1b* would be observed.

The expression levels of the Wnt target gene *Rac1* and its splice variant *Rac1b* was determined using qRT-PCR analysis. As expected, expression levels of the Wnt target gene *Rac1* and its splice variant *Rac1b* increased significantly in *Apc* deficient epithelium. The splice variant *Rac1b* was significantly repressed following the loss of *Cbx3* in the Wnt activated intestine, consistent with the hypothesis that loss of *Cbx3* impairs RNA splicing and therefore leads to a reduced level of *Rac1b* in the small intestinal epithelium. Since *Rac1b* is a product of alternative processing that can activate Wnt signalling (Esufali *et al*., 2007), a decrease in *Rac1b* level in *Cbx3* deficient epithelium would suggest an attenuation of the

Wnt target gene expression in the context of *Apc* deficiency. However, gene expression analysis of Wnt siganlling in *Cbx3* deficient epithelium was found to be unaltered compared to *Apc* deficient epithelium alone. It has been reported that the expression of *Rac1b* is controlled not only by levels of Wnt but also PI3K signalling (Goncalves, Matos and Jordan, 2009; Esufali, Charames and Bapat, 2007). Therefore, expression analysis of PI3K target genes should be explored to determine whether *Cbx3* loss plays a role in PI3K and hence the regulation of *Rac1* splicing.

4.3.6. HP1α displaces HP1γ to the Heterochromatin mark H4K20me3 in Wnt activated intestine

Previous evidence has suggested that H4K20 trimethylation (H4K20me3) is essential for the maintenance of perinatal, non-cancerous cell states and confers heterochromatin maintenance capability (Fraga *et al.*, 2005; Pogribny *et al.*, 2006; Schotta *et al.,* 2008). Trimethylation specifically requires the recruitment of the Sur4-20h enzymes by HP1 (Schotta *et al.*, 2004). H4K20me3 has been shown to have a significant correlation with HP1γ expression in normal tissue samples and a dissociation of the correlation between HP1γ expression and H4K20me3 may reflect the malfunction of epigenetic control in cancer tissues (Takanashi *et al.,* 2009). Therefore, this correlation was examined in the wildtype intestine and *Apc*-deficient intestine. Immunofluorescence analysis was performed on small intestinal tissue sections and joint presence of HP1γ with H4K20me3 was detected at the crypt and along the villus of the wildtype intestine. In accordance to expectation, this co-localisation of HP1γ with H4K20me3 is a signature of the normal intestinal homeostasis. In the Wnt-activated epithelium, the association of HP1γ with H4K20me3 is lost in the absence of *Apc*, expression of HP1γ and H4K20me3 appeared to be mutually exclusive in *VillinCreER*$^{+}$*Apc*$^{fl/fl}$ animals. These observations suggest that the co-localisation of HP1γ and H4K20me3 is important for heterochromatin maintenance required for normal intestinal homeostasis, whereas the loss of HP1γ-H4K20me3 association could be an important mechanism required for epigenetic malfunction in Wnt-activated intestine.

Considering the dissociation of the correlation between HP1γ and H4K20me3 may reflect the malfunction of epigenetic control in cancer development, further investigation

was aimed to see whether this dissociation pattern was caused by displacement of other heterochromatin protein members in the Wnt activated small intestine. Immunofluorescence analysis of the other HP1 family member HP1α was performed on small intestinal tissue sections from wildtype and Wnt-activated mice. Little association patterns between HP1α and H4K20me3 was observed in the small intestine in wildtype mice whereas the expression of HP1α with H4K20me3 in the Wnt-activated intestine was found to be fully co-localised. This observation, along with the dissociation of HP1γ from H4K20me3 in acute Wnt activated intestines, strongly suggests that the displacement of HP1γ by HP1α from H4K20me3 in Wnt activated small intestines. Studies from the literature have demonstrated that the role of HP1α in breast cancer (Takanashi *et al.,* 2009) and a correlation between HP1α and H4K20me3 levels is observed in ES cells (Wongtawan *et al.*, 2011). These observation from the literature together with our data suggest that the role of HP1α in aberrant Wnt-activated intestinal cancer.

Together, we propose that the H4K20me3 signature in heterochromatin, while bound by HP1γ contributes to maintaining normal intestinal homeostasis by providing a gene-repressive compartment in the nucleus, however when bound by HP1α it retains the dynamics to adapt to chromatin structural changes during carcinogenesis.

4.3.7. HP1γ interacts with the active Euchromatin mark H3K4me3 in Wnt activated intestine

Histone H3K4 trimethylation (H3K4me3) is an active marker in the epigenetic code, it is enriched downstream of the active transcription start site in the euchromatin (Hon, Hawkins and Ren, 2009). Since HP1γ is present in both heterochromatin and euchromatin (Minc, Courvalin and Buendia, 2000). It would be of great interest to see whether HP1γ has any interaction with the active euchromatic marks, immunofluorescence analysis of HP1γ and H3K4me3 was performed in the small intestine of the wildtype animals and following *Apc* deletion in *VillinCreER*$^{+}$*Apc*$^{fl/fl}$ animals.

Double immunofluorescence analysis of HP1γ and H3K4me3 demonstrated partial co-localising pattern is observed between the two markers in wildtype intestine whereas the association pattern of HP1γ and H3K4me3 clearly become more fully colocalised especially in the Wnt-activated intestine, indicating a role of HP1γ in transcriptional activation in euchromatin.

Immunofluorescence analysis was also performed to investigate whether there is any interaction between HP1α and H3K4me3 in small intestinal tissue sections from wildtype and *VillinCreER*$^{+}$*Apc*$^{fl/fl}$ mice. The co-localisation analysis demonstrated that HP1α and H3K4me3 are mutually exclusive in both crypt and villus of wildtype and Wnt-activated intestines, indicating that the two markers are localised at different nuclear locations, HP1α is enriched at sites of heterochromatin, whereas H3K4me3 is an active mark located in the euchromatin. This observation suggests that despite the significant degree of sequence conversation shared between the HP1 isotypes, different members of the HP1 family have distinct and non-redundant functions.

4.3.8. Summary

In summary, four major conclusions can be drawn from the data presented in this chapter. First, the loss of *Cbx3* substantially suppressed Wnt activation at the receptor level in a Topflash assay. This observation is supported by the prolonged lifespan of *Cbx3* deficient mice following the conditional loss of both alleles of *Apc* gene with no alteration in gross intestinal structure. Secondly, *Cbx3* deficiency does not impact on the stem cell compartment although the enterocyte bush border is noticeably diminished following the loss of *Cbx3* in the context of Wnt activated small intestinal epithelium. This observation could be caused by the down-regulation of Notch target genes following the epithelial Cbx3 loss in Wnt-activated intestines. Thirdly, *Cbx3* plays a crucial role in RNA splicing and upon deletion of *Cbx3* the tumour-related splice variant *Rac1b* was found to be significantly repressed in the Wnt activated intestine. Fourthly, the joint presence of HP1γ and H4K20me3 appears to be essential for heterochromatin maintenance required for normal intestinal homeostasis, whereas the loss of HP1γ-H4K20me3 association, caused by HP1α displacing HP1γ to the H4K20me3 marks, could be an important mechanism required for epigenetic malfunction in Wnt-activated intestine.

Chapter Five

Analysing the long-term consequences of *Cbx3* loss in the context of Wnt-driven tumorigenesis

5. Analysing the long-term consequences of *Cbx3* loss in the context of Wnt-driven tumorigenesis

5.1. Introduction

Previous work by others and that described in Chapter 4 indicates that *Cbx3* has the potential to regulate Wnt signalling pathway by modulating heterochromatin organisation via its association with H4K20me3 (Schotta *et al.,* 2004). Loss of *CBX3* expression has been shown to result in diminished levels of Wnt activation *in vitro* (Chapter 4). Studies have demonstrated that the deletion of mutant of HP1γ lacks tumorigenesis activity in a mouse xenograft model (Sharma e*t al., 2*003), indicating that the expression of HP1γ contributes to cancer formation.

Therefore, it is interesting to investigate the effects of *Cbx3* loss in Wnt-driven tumorigenesis. Conditional deletion of both copies of *Apc* in the adult intestine using the Cre-loxP approach resulted in rapid and catastrophic disruption of epithelial homeostasis and animals lived up to 4 days post induction (Chapter 4). Heterozygous inactivation of *Apc* is a well-established approach for induction of Wnt-driven tumorigenesis in the gastrointestinal tract (Shibata *et al.*, 1997).

In this chapter, the consequence of epithelial-specific *Cbx3* loss in the context of Wnt-activated tumorigenesis was examined utilising a mouse model possessing a heterozygous mutation of the *Apc* gene.

5.2. Results

5.2.1. *Cbx3* loss in the context of *Apc* heterozygosity has a tendency to reduce lifespan of male mice

In order to examine the effects of *Cbx3* deficiency on the survival of mice with heterozygous inactivation of *Apc*, mice from *VillinCreER*$^{+}$*Apc*$^{fl/+}$*Cbx3*$^{fl/fl}$ and *VillinCreER*$^{+}$*Apc*$^{fl/+}$*Cbx3*$^{fl/+}$ along with the control *VillinCreER*$^{+}$*Apc*$^{fl/+}$*Cbx3*$^{+/+}$ mice (for all cohorts n > 13) were induced with four daily intraperitoneal injections of 80 mg/kg Tamoxifen, were aged to 500 days and regularly inspected for signs of ill health, and sacrificed when needed. The majority of animals developed signs of ill health due to extensive tumour burden and had to be sacrificed prior to the 500 days time point. Analysis of the survival probability revealed a trend of reduced survival (but not significant) between the experimental *VillinCreER*$^{+}$*Apc*$^{fl/+}$*Cbx3*$^{fl/fl}$ cohort (median survival of 197 days post induction) and control animals (median survival of 282 days post induction, Log Rank Test: p = 0.128, n > 13, Figure 5.1).

It is known that survival rates associated with intestinal tumorigenesise can vary between the genders (Colorectal Cancer Facts & Figures 2014-2016) and given that the experimental cohorts contained animals of both genders, the survival phenomenon was further explored. The effects of *Cbx3* deficiency on survival were generated for both female and male mice with heterozygous deletion of *Apc.* Analysis of the survival probability demonstrated that the reduced survival between *VillinCreER*$^{+}$*Apc*$^{fl/+}$*Cbx3*$^{fl/fl}$ and control cohorts was more prominent in male compared to female cohorts (Figure 5.2). The median survival of the male control cohorts (n = 8) was 225 days post induction, the *VillinCreER*$^{+}$*Apc*$^{fl/+}$*Cbx3*$^{fl/+}$ cohort (n = 12) was 268 days and the *VillinCreER*$^{+}$*Apc*$^{fl/+}$*Cbx3*$^{fl/fl}$ cohort (n = 12) was reduced to 179 days, although this was not proven to be statistically significant (Log Rank Test: p = 0.082, n > 8, Figure 5.2B). On the other hand, the median survival of the female control cohort (n = 5) was 295 days, the *VillinCreER*$^{+}$*Apc*$^{fl/+}$*Cbx3*$^{fl/+}$ cohort (n = 5) was 317 days and the *VillinCreER*$^{+}$*Apc*$^{fl/+}$*Cbx3*$^{fl/fl}$ cohort (n = 8) was reduced to 260 days (Log Rank Test: p = 0.724, n > 5, Figure 5.2A). However, the Kaplan-Meier survival analysis shows a moderate reduction in median survival in male cohorts following homozygous deletion of *Cbx3* compared to control (46 days reduction), with the last survived male mouse sacrificed to 317 days post induction due to ill health.

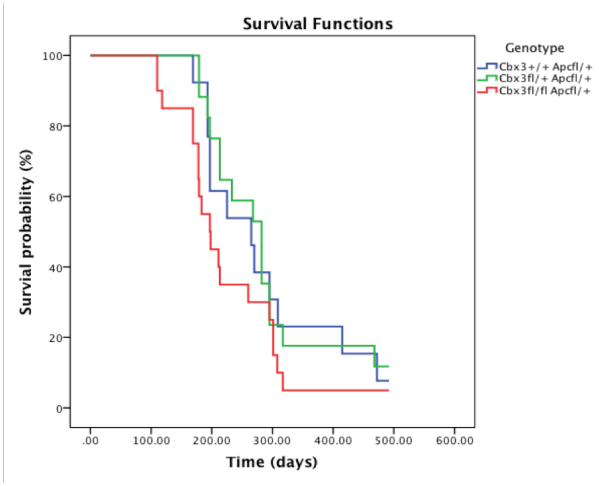

Figure 5.1: *Cbx3* deficiency moderately impairs survival of mice with heterozygous *Apc* loss.
Cohorts of *VillinCreER^{+}Apc$^{fl/+}$Cbx3$^{fl/fl}$* and *VillinCreER^{+}Apc$^{fl/+}$Cbx3$^{fl/+}$* mice were induced with 4 daily intraperitoneal injections of 80 mg/kg Tamoxifen along with *VillinCreER^{+}Apc$^{fl/+}$Cbx3$^{+/+}$* control animals (n > 13). Experimental mice were aged to 500 days post induction or sacrificed when ill health was observed. Survival data was presented as a Kaplan-Meier plot. Analysis of cumulative survival revealed a reduced survival of *VillinCreER^{+}Apc$^{fl/+}$Cbx3$^{fl/fl}$* (Median survival: 197 days) compared to control animals (265 days) (Log Rank Test: p = 0.128, n > 13). No significant difference in survival was observed between experimental and control cohorts.

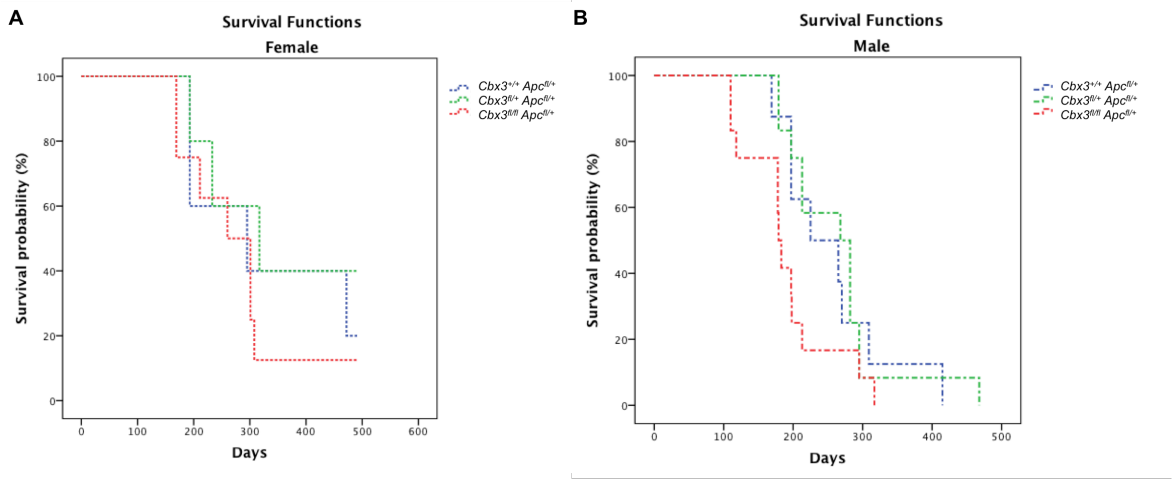

Figure 5.2: The loss of *Cbx3* shows a trend to reduce survival of male mice following heterozygous loss of *Apc*.
Experimental mice were aged to 500 days post induction or sacrificed when ill health was observed. Survival data for Female (A) and Male (B) mice were presented as Kaplan-Meier plots. Analysis of the cumulative survival of female mice demonstrated a slight reduction in the lifespan of *VillinCreER^{+}Apc$^{fl/+}$Cbx3$^{fl/fl}$* (Median survival: 260 days) compared to control animals (295 days) (Log Rank Test: p = 0.724, n > 5). On the other hand, analysis of the cumulative survival of male mice demonstrated a greater tendency to reduce survival of *VillinCreER^{+}Apc$^{fl/+}$Cbx3$^{fl/fl}$* (Median survival: 179 days) compared to control animals (225 days), although it did not reach the statistical significance (Log Rank Test: p = 0.082, n > 8).

5.2.2. Increased Wnt-driven tumorigenesis occurs in the small intestine following *Cbx3* loss

Having identified that the loss of *Cbx3* shortened the lifespan of mice with heterozygous loss of *Apc,* the incidence and rates of intestinal tumorigenesis in each cohort was investigated.

Intestines from *VillinCreER^{+}Apc$^{fl/+}$*, *VillinCreER^{+}Apc$^{fl/+}$Cbx3$^{fl/+}$* and *VillinCreER^{+}Apc$^{fl/+}$Cbx3$^{fl/fl}$* animals were dissected at the time of sacrifice and analysed for tumour burden and volume within the small and large intestines (Figure 5.3). Statistical analysis of tumour burden and size revealed significant changes in both experimental cohorts compared to control in the small intestine (for all comparisons $p < 0.05$, $n > 13$, Table 5.1). In small intestine, *VillinCreER^{+}Apc$^{fl/+}$Cbx3$^{fl/+}$* and *VillinCreER^{+}Apc$^{fl/+}$Cbx3$^{fl/fl}$* animals were found to bear significantly more tumours and larger tumours than controls at the time of dissection.

Next, the tumour number and size was also examined in both female and male Intestines from *VillinCreER^{+}Apc$^{fl/+}$Cbx3$^{fl/+}$* and *VillinCreER^{+}Apc$^{fl/+}$Cbx3$^{fl/fl}$* along with control animals (Figure 5.4). Significant increases in both tumour burden and size were observed in male mice between both experimental cohorts compared to control cohort in the small intestine, just as evident in the previous full cohort (for all comparisons $p < 0.05$, $n > 8$, Table 5.2B). Statistical analysis of tumour number in female mice also demonstrated a significant increase in tumour number in the *VillinCreER^{+}Apc$^{fl/+}$Cbx3$^{fl/fl}$* cohort compared to controls ($p < 0.05$, $n > 5$, Table 5.2A). However, note that there was no significant difference in tumour size between the experimental cohorts and controls in the small intestine of female mice.

In the full cohort and in the subgroups according to gender, there is no clear relationship between genotype and tumour number and size in the large intestine. It is therefore obvious that in the context of *Apc* heterozygosity, *Cbx3* loss increases tumour initiation and development in the small intestine, which may account for the trend in decreased survival observed in the *VillinCreER^{+}Apc$^{fl/+}$Cbx3$^{fl/fl}$* cohort.

					p Value		
	Parameter	Geneotype	Mean	Standard Deviation	$Apc^{fl/+}$ Vs $Apc^{fl/+}Cbx3^{fl/+}$	$Apc^{fl/+}$ Vs $Apc^{fl/+}Cbx3^{fl/fl}$	$Apc^{fl/+}Cbx3^{fl/+}$ Vs $Apc^{fl/+}Cbx3^{fl/fl}$
Small intestine	Tumour Number	$Apc^{fl/+}$	3.77	2.19	0.014	0.043	
		$Apc^{fl/+}Cbx3^{fl/+}$	8.59	3.94			0.852
		$Apc^{fl/+}Cbx3^{fl/fl}$	11.20	4.50			
	Tumour Size (mm^2)	$Apc^{fl/+}$	4.23	2.98	0.007	0.008	
		$Apc^{fl/+}Cbx3^{fl/+}$	10.12	4.38			0.646
		$Apc^{fl/+}Cbx3^{fl/fl}$	12.00	4.29			
Large intestine	Tumour Number	$Apc^{fl/+}$	2.15	1.71	0.726	0.564	
		$Apc^{fl/+}Cbx3^{fl/+}$	1.94	1.64			0.755
		$Apc^{fl/+}Cbx3^{fl/fl}$	2.60	2.07			
	Tumour Size (mm^2)	$Apc^{fl/+}$	2.38	2.87	0.901	0.834	
		$Apc^{fl/+}Cbx3^{fl/+}$	2.18	1.10			0.947
		$Apc^{fl/+}Cbx3^{fl/fl}$	3.00	2.28			

Table 5.1: Analysis of small and large intestinal tumour burden observed in the experimental cohorts *VillinCreER$^+$Apc$^{fl/+}$Cbx3$^{fl/+}$* and *VillinCreER$^+$Apc$^{fl/+}$Cbx3$^{fl/fl}$* along with control *VillinCreER$^+$Apc$^{fl/+}$* animals.

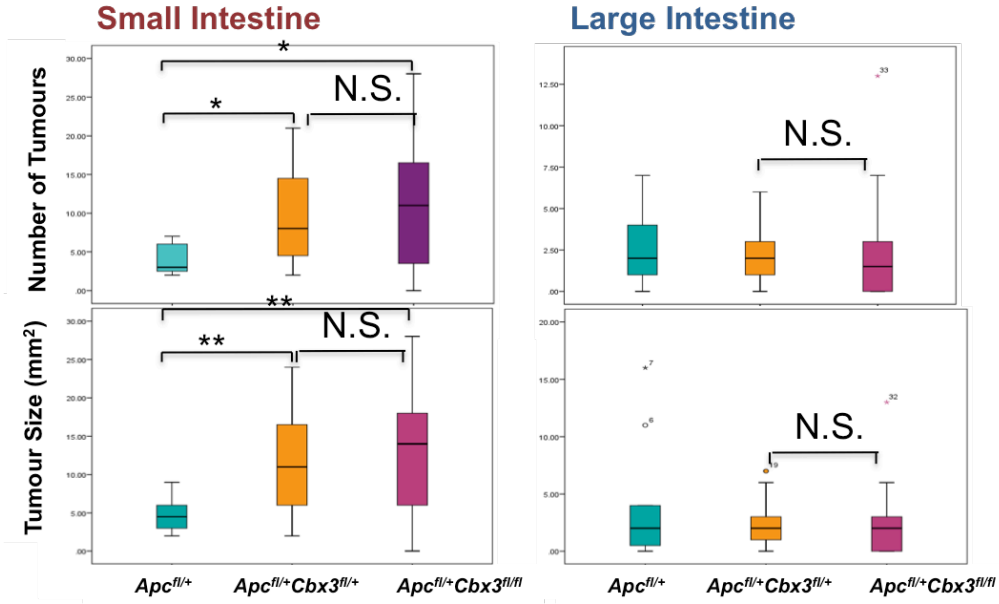

Figure 5.3: The consequence on *Cbx3* loss on intestinal tumorigenesis in mice with heterozygous loss of *Apc*.
Tumour burden was analysed in the small and large intestinal epithelium of *VillinCreER$^+$Apc$^{fl/+}$*, *VillinCreER$^+$Apc$^{fl/+}$Cbx3$^{fl/+}$* and *VillinCreER$^+$Apc$^{fl/+}$Cbx3$^{fl/fl}$* animals at the time of dissection. Tumour burden and size in the small intestine significantly increased in both the experimental cohorts compared to control animals (for all comparisons *p < 0.05, **p < 0.01, n > 13). In contrast, statistical analysis of tumour burden and size revealed no significant differences between the cohorts in large intestine. N.S. indicates 'not significant'. Exact values for tumour number, tumour size, standard deviation and p values are provided in Table 5.1.

A Female

	Parameter	Geneotype	Mean	Standard Deviation	p Value: $Apc^{fl/+}$ Vs $Apc^{fl/+}Cbx3^{fl/+}$	p Value: $Apc^{fl/+}$ Vs $Apc^{fl/+}Cbx3^{fl/fl}$	p Value: $Apc^{fl/+}Cbx3^{fl/+}$ Vs $Apc^{fl/+}Cbx3^{fl/fl}$
Small intestine	Tumour Number	$Apc^{fl/+}$	2.400	1.000	0.343	0.038	
		$Apc^{fl/+}Cbx3^{fl/+}$	5.800	1.787			0.205
		$Apc^{fl/+}Cbx3^{fl/fl}$	9.875	3.801			
	Tumour Size (mm^2)	$Apc^{fl/+}$	3.000	1.118	0.686	0.067	
		$Apc^{fl/+}Cbx3^{fl/+}$	6.200	2.007			0.257
		$Apc^{fl/+}Cbx3^{fl/fl}$	10.750	3.812			
Large intestine	Tumour Number	$Apc^{fl/+}$	0.400	0.816	0.200	0.257	
		$Apc^{fl/+}Cbx3^{fl/+}$	2.000	1.862			0.914
		$Apc^{fl/+}Cbx3^{fl/fl}$	1.375	0.983			
	Tumour Size (mm^2)	$Apc^{fl/+}$	0.333	0.816	0.114	0.067	
		$Apc^{fl/+}Cbx3^{fl/+}$	2.000	1.862			0.814
		$Apc^{fl/+}Cbx3^{fl/fl}$	1.875	1.378			

B Male

	Parameter	Geneotype	Mean	Standard Deviation	p Value: $Apc^{fl/+}$ Vs $Apc^{fl/+}Cbx3^{fl/+}$	p Value: $Apc^{fl/+}$ Vs $Apc^{fl/+}Cbx3^{fl/fl}$	p Value: $Apc^{fl/+}Cbx3^{fl/+}$ Vs $Apc^{fl/+}Cbx3^{fl/fl}$
Small intestine	Tumour Number	$Apc^{fl/+}$	4.625	1.965	0.041	0.001	
		$Apc^{fl/+}Cbx3^{fl/+}$	8.833	4.295			0.180
		$Apc^{fl/+}Cbx3^{fl/fl}$	12.714	4.540			
	Tumour Size (mm^2)	$Apc^{fl/+}$	5.000	2.455	0.007	0.001	
		$Apc^{fl/+}Cbx3^{fl/+}$	10.333	4.738			0.301
		$Apc^{fl/+}Cbx3^{fl/fl}$	13.429	5.199			
Large intestine	Tumour Number	$Apc^{fl/+}$	3.250	2.733	0.356	0.812	
		$Apc^{fl/+}Cbx3^{fl/+}$	1.917	1.835			0.635
		$Apc^{fl/+}Cbx3^{fl/fl}$	4.000	2.658			
	Tumour Size (mm^2)	$Apc^{fl/+}$	4.500	3.847	0.211	0.930	
		$Apc^{fl/+}Cbx3^{fl/+}$	2.250	1.871			0.368
		$Apc^{fl/+}Cbx3^{fl/fl}$	4.286	3.098			

Table 5.2: Analysis of small and large intestinal tumour burden observed in the female (A) and male (B) experimental cohorts *VillinCreER^{+}Apc$^{fl/+}$Cbx3$^{fl/+}$* and *VillinCreER^{+}Apc$^{fl/+}$Cbx3$^{fl/fl}$* along with control *Apc$^{fl/+}$* animals.

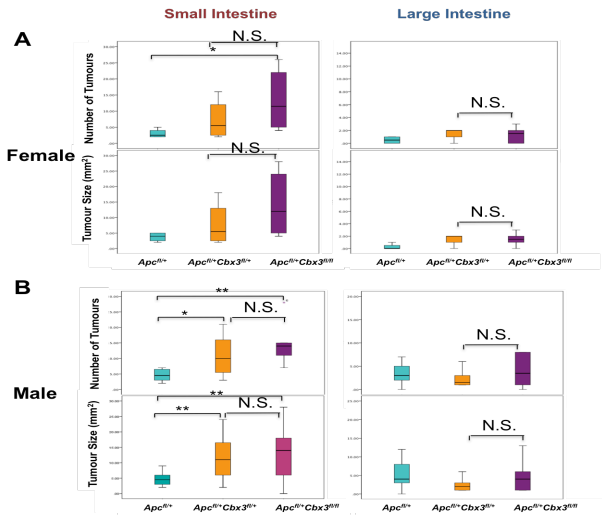

Figure 5.4: The effect of *Cbx3* loss on intestinal tumorigenesis in female and male mice with heterozygous loss of *Apc*.
(A) Tumour number in the female small intestine significantly increased in the *VillinCreER^{+}Apc$^{fl/+}$Cbx3$^{fl/fl}$* cohort compared to the control cohort ($p < 0.05$, $n > 5$). (B) Tumour burden and size in the male small intestine significantly increased in both the experimental cohorts compared to control animals (for all comparisons $*p < 0.05$, $**p < 0.01$, $n > 8$). On the contrary, no significant differences in the tumour number and size exist between the cohorts in the large intestine for both genders. N.S. indicates 'not significant'. The exact values for tumour number, tumour size, standard deviation and p values are provided in Table 5.2.

5.2.3. The tumours arising in *Cbx3*-deficient *Apc* heterozygous small intestine are more advanced compared to controls

As observed in the previous section, loss of *Cbx3* substantially increased tumour burden and tumour size in the *Apc* heterozygous small intestines. Lesions can be classified histopathologically into different categories depending on their stage and invasive qualities. Thus, the tumour morphology was examined and the number of each tumour type observed was quantified in *VillinCreER*$^{+}$*Apc*$^{fl/+}$, *VillinCreER*$^{+}$*Apc*$^{fl/+}$*Cbx3*$^{fl/+}$ and *VillinCreER*$^{+}$*Apc*$^{fl/+}$*Cbx3*$^{fl/fl}$ intestines. For the purpose of this study, five categories were classified: single crypt lesion (lesion confined to a single crypt), microadenoma (lesions confined to no more than 5 crypts), small adenoma (lesions extended up to 15 crypts), large adenoma (lesions involving more than 15 crypts) and adenocarcinoma with submucosal invasion (lesions showing clear invasion into the submucosa). Although smooth muscle invasion can also be observed in more aggressive CRC mouse models, it has not been detected in the cohorts used; therefore this category has not been included (Outlined in Figure 5.5).

In the *VillinCreER*$^{+}$*Apc*$^{fl/+}$ control cohort, 69% of lesions were found to be single crypt lesions and 19% of lesions were classed as large microadenoma. No lesions were identified as adenocarcinoma with submucosal invasion in control animals. In contrast to this, experimental animals *VillinCreER*$^{+}$*Apc*$^{fl/+}$*Cbx3*$^{fl/+}$ and *VillinCreER*$^{+}$*Apc*$^{fl/+}$*Cbx3*$^{fl/fl}$ showed a reduction in the number of lesions classified as single crypt lesion (54% and 38% respectively). An increase in the incidence of adenoma (both small and large adenoma) was observed in both experimental cohorts: 12% of all lesions in the control cohorts were adenomas compared to 23% of all lessons in the *VillinCreER*$^{+}$*Apc*$^{fl/+}$*Cbx3*$^{fl/+}$ cohort and 42% in the *VillinCreER*$^{+}$*Apc*$^{fl/+}$*Cbx3*$^{fl/fl}$ cohort (T-test $p = 0.031$ in *VillinCreER*$^{+}$*Apc*$^{fl/+}$*Cbx3*$^{fl/+}$ and $p = 0.007$ in *VillinCreER*$^{+}$*Apc*$^{fl/+}$*Cbx3*$^{fl/fl}$ tumours, $n > 13$, Figure 5.6A). Adenocarcinoma with submucosal invasion was also observed in both experimental cohorts following the deletion of *Cbx3* but absent in the control cohort (Figure 5.6A).

Subgroup analysis according to gender showed that the majority of the advanced tumours in the experimental cohorts were found mainly in male animals; while the single crypt lesion constituted a larger fraction of the tumours in female mice. Tumours with homozygous loss of *Cbx3* show a greater percentage of tumours that were graded small and large adenoma, and invasive adenocarcinomas in male mice (56%) than in the female mice

(34%) (T-test p = 0.026, n > 8, Figure 5.6 B and C). All the invasive tumours (adenocarcinomas with submucosal invasion) were found in male experimental cohorts but not in female cohorts (Figure 5.6 B and C). Taken together, these findings suggest that, in the context of *Apc* heterozygosity, additional loss of *Cbx3* resulted in more advanced progression of tumours in male mice compared to tumours arising in female mice. This suggestion is consistent with the trend for reduced survival, increased tumour number and size in the male compared with the female mice.

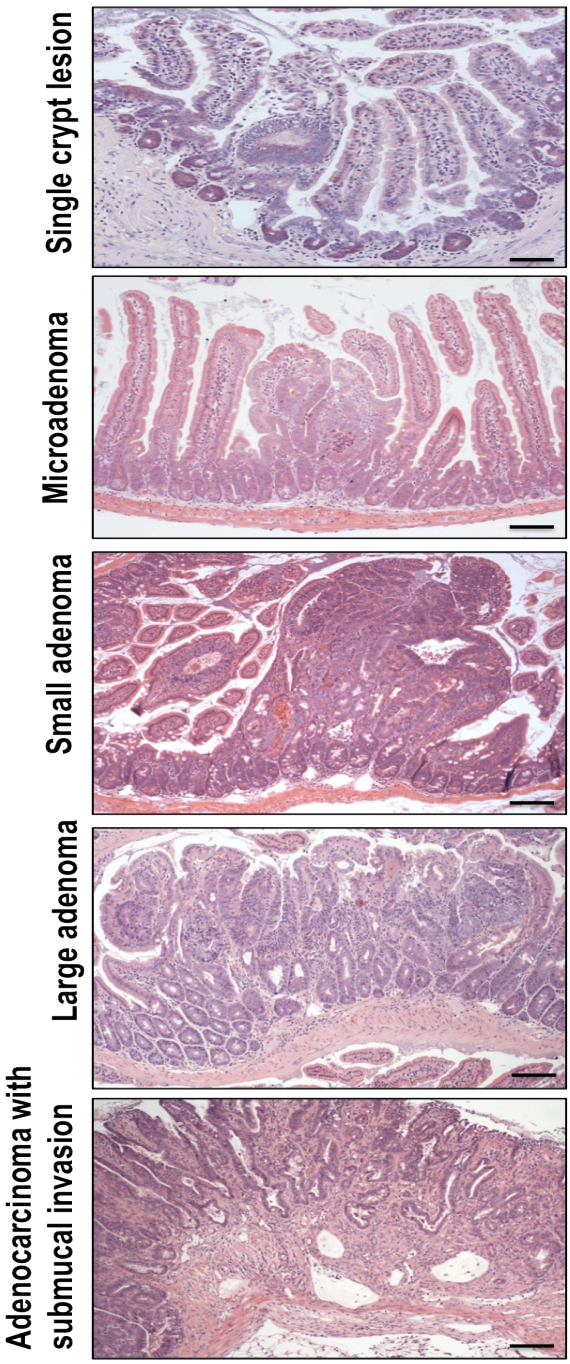

Figure 5.5: Histological categorisation of small intestinal tumour severity. Assessment of H&E stained sections of small intestinal tumours from *VillinCreER^{+}Apc$^{fl/+}$*, *VillinCreER^{+}Apc$^{fl/+}$Cbx3$^{fl/+}$* and *VillinCreER^{+}Apc$^{fl/+}$Cbx3$^{fl/fl}$* mice revealed varying grades of tumour severity. Lesions can be classified histopathologically into five categories: single crypt lesion (lesion confined to a single crypt), microadenoma (lesions confined to no more than 5 crypts), small adenoma (lesions extended up to 15 crypts), large adenoma (lesions involving more than 15 crypts) and adenocarcinoma with submucosal invasion (lesions showing clear invasion into the submucosa). Scale bars represent 100 µm.

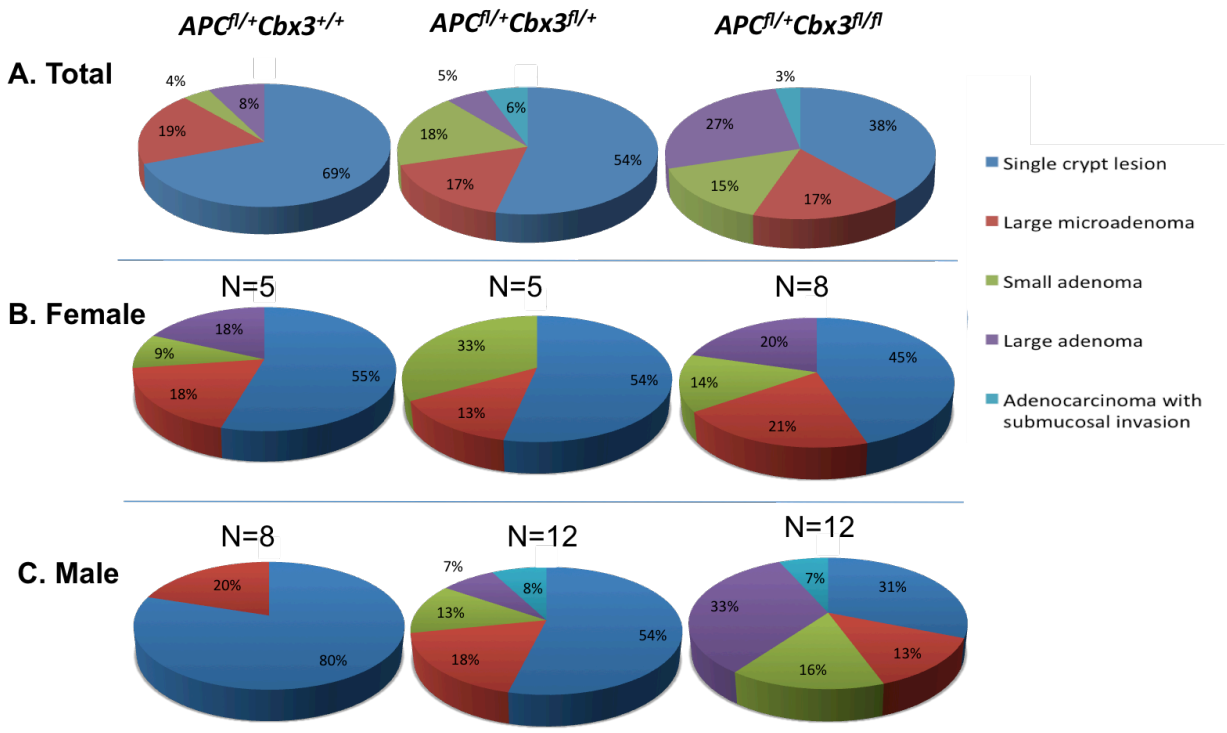

Figure 5.6: Increased severity of small intestinal tumours in mice with *Cbx3*-deficiency compared to control mice.
Intestinal tumours arising in experimental *VillinCreER^{+}Apc$^{fl/+}$Cbx3$^{fl/+}$* and *VillinCreER^{+}Apc$^{fl/+}$Cbx3$^{fl/fl}$* mice along with control *VillinCreER^{+}Apc$^{fl/+}$* mice were assessed histologically and categorised according to grade of severity of the tumour in full cohorts (A), female cohorts (B) and male cohorts (C). An increased proportion of lesions in experimental animals showed progression to small and large adenoma compared to controls (T-test p = 0.031 in *VillinCreER^{+}Apc$^{fl/+}$Cbx3$^{fl/+}$* and p = 0.007 in *VillinCreER^{+}Apc$^{fl/+}$Cbx3$^{fl/fl}$* tumours, n > 13) and a subset of lesions were also found to progress into adenocarcinoma with submucosal invasion in *VillinCreER^{+}Apc$^{fl/+}$Cbx3$^{fl/+}$* and *VillinCreER^{+}Apc$^{fl/+}$Cbx3$^{fl/fl}$* tumours in the full cohorts. Loss of *Cbx3* resulted in more advanced progression of tumours mainly in male mice compared to tumours arising in female mice in the context of *Apc* heterozygozity (More advanced tumours include small, large adenomas and adenocarcinoma, T-test p = 0.026, n > 8).

5.2.4. Limited effects on Wnt, Notch, TGF-β and PI3K signaling in *Cbx3*-deficient *Apc* heterozygous tumours

Having found that tumours arising in *VillinCreER^{+}Apc$^{fl/+}$Cbx3$^{fl/fl}$* mice show an overall increase in severity compared to that observed in the control *Apc$^{fl/+}$* mice, various signalling pathways known to govern stem cell maintenance and cell differentiation, including Wnt,

Notch, TGF-β and PI3K were examined in both control and *VillinCreER*$^{+}$*Apc*$^{fl/+}$*Cbx3*$^{fl/fl}$ tumours. Tumours (including single crypt lesion, microadenoma, small adenoma, large adenoma and adenocarcinoma with submucosal invasion) and normal tissue from control *VillinCreER*$^{+}$*Apc*$^{fl/+}$ and *VillinCreER*$^{+}$*Apc*$^{fl/+}$*Cbx3*$^{fl/fl}$ mice were subjected to immunohistochemistry against β-catenin, Notch1, PTEN, pAKT and Smad2/3.

First the normal intestinal tissues and tumours were examined using anti-β-catenin immunohistochemistry as a marker for Wnt-activation. Normal or non-tumour epithelial tissues in both control *VillinCreER*$^{+}$*Apc*$^{fl/+}$ and *VillinCreER*$^{+}$*Apc*$^{fl/+}$*Cbx3*$^{fl/fl}$ intestines was observed to have a cytoplasmic and cell-surface staining pattern of β-catenin, whereas tumours arising in both control *VillinCreER*$^{+}$*Apc*$^{fl/+}$ and *VillinCreER*$^{+}$*Apc*$^{fl/+}$*Cbx3*$^{fl/fl}$ intestines revealed both upregulation and nuclear localisation of β-catenin, consistent with activation of the Wnt pathway and indicative of loss of Apc (Figure 5.7). Furthermore, there was a site-dependent variability in the β-catenin staining patterns in small intestinal tumours. Tumours arising in *VillinCreER*$^{+}$*Apc*$^{fl/+}$ and *VillinCreER*$^{+}$*Apc*$^{fl/+}$*Cbx3*$^{fl/fl}$ intestines revealed some well-differentiated tubular epithelial structrues where weak cytoplasmic and nuclear localisation of β-catenin was observed. By contrast, strong nuclear localisaton of β-catenin was detected in the dedifferentiated epithelial cells and invasive tumour cells in the intestineal tumours in both control *VillinCreER*$^{+}$*Apc*$^{fl/+}$ and *VillinCreER*$^{+}$*Apc*$^{fl/+}$*Cbx3*$^{fl/fl}$ intestines, indicating the intratumour heterogeneity in Wnt-activated intestines. However, there is no variation in the β-catenin staining pattern between the control *VillinCreER*$^{+}$*Apc*$^{fl/+}$ and *VillinCreER*$^{+}$*Apc*$^{fl/+}$*Cbx3*$^{fl/fl}$ intestines.

Secondly, an antibody which detects the activated intracellular Notch domain produced after γ-secretase cleavage was used to determine the level of Notch pathway activation. Normal intestines and tumours from both control *VillinCreER*$^{+}$*Apc*$^{fl/+}$ and *VillinCreER*$^{+}$*Apc*$^{fl/+}$*Cbx3*$^{fl/fl}$ intestines were uniformly negative for Notch1 expression. The expression of Notch1 showed no differences across all types of tumours evaluated in both control *VillinCreER*$^{+}$*Apc*$^{fl/+}$ and *VillinCreER*$^{+}$*Apc*$^{fl/+}$*Cbx3*$^{fl/fl}$ intestines (Figure 5.7), indicating that Notch signalling was not altered following the loss of *Cbx3* in the small intestines.

Thirdly, anti-PTEN was used to confirm PTEN status *in VillinCreER*$^{+}$*Apc*$^{fl/+}$ and *VillinCreER*$^{+}$*Apc*$^{fl/+}$*Cbx3*$^{fl/fl}$ intestines. PTEN immunohistochemistry can be observed in the stromal cells of both control *VillinCreER*$^{+}$*Apc*$^{fl/+}$ and *VillinCreER*$^{+}$*Apc*$^{fl/+}$*Cbx3*$^{fl/fl}$ intestines.

Elevated level of diffuse positive cytoplasmic staining of PTEN was demonstrated in the crypt regions of intestines and single crypt lesions in *VillinCreER*$^{+}$*Apc*$^{fl/+}$*Cbx3*$^{fl/fl}$ intestines. Tumours arising in both control *VillinCreER*$^{+}$*Apc*$^{fl/+}$ and *VillinCreER*$^{+}$*Apc*$^{fl/+}$*Cbx3*$^{fl/fl}$ intestines show intense positive cytoplasmic expression for PTEN across epithelial and stromal cells, with no obvious difference between the control *VillinCreER*$^{+}$*Apc*$^{fl/+}$ and *VillinCreER*$^{+}$*Apc*$^{fl/+}$*Cbx3*$^{fl/fl}$ intestines (Figure 5.8).

Next, in order to assess the activation status of the PI3K/AKT pathway following deletion of *Apc*, sections were stained immunohistochemically against activated Phospho-AKT^{ser473} (pAKT). Weak staining of pAKT was observed at the bottom of the crypts in the normal intestines and the tumours of both control *VillinCreER*$^{+}$*Apc*$^{fl/+}$ and *VillinCreER*$^{+}$*Apc*$^{fl/+}$*Cbx3*$^{fl/fl}$ intestines. Cellular staining of pAKT was noted to be homogenously cytoplasmic, with no obvious difference between the control *VillinCreER*$^{+}$*Apc*$^{fl/+}$ and *VillinCreER*$^{+}$*Apc*$^{fl/+}$*Cbx3*$^{fl/fl}$ intestines (Figure 5.8).

Lastly, phosphorylated Smad2/3 levels were analysed in control *VillinCreER*$^{+}$*Apc*$^{fl/+}$ and *VillinCreER*$^{+}$*Apc*$^{fl/+}$*Cbx3*$^{fl/fl}$ intestines to evaluate the TGF-β growth inhibitory effects. Immunohistochemical staining of phospho-Smad2/3 was highly expressed and predominantly located in the nuclei of all normal intestinal epithelium and tumour cells in control *VillinCreER*$^{+}$*Apc*$^{fl/+}$ and *VillinCreER*$^{+}$*Apc*$^{fl/+}$*Cbx3*$^{fl/fl}$ intestines (Figure 5.8). No change in intensity of the phospho-Smad2/3 staining was observed between the two cohorts.

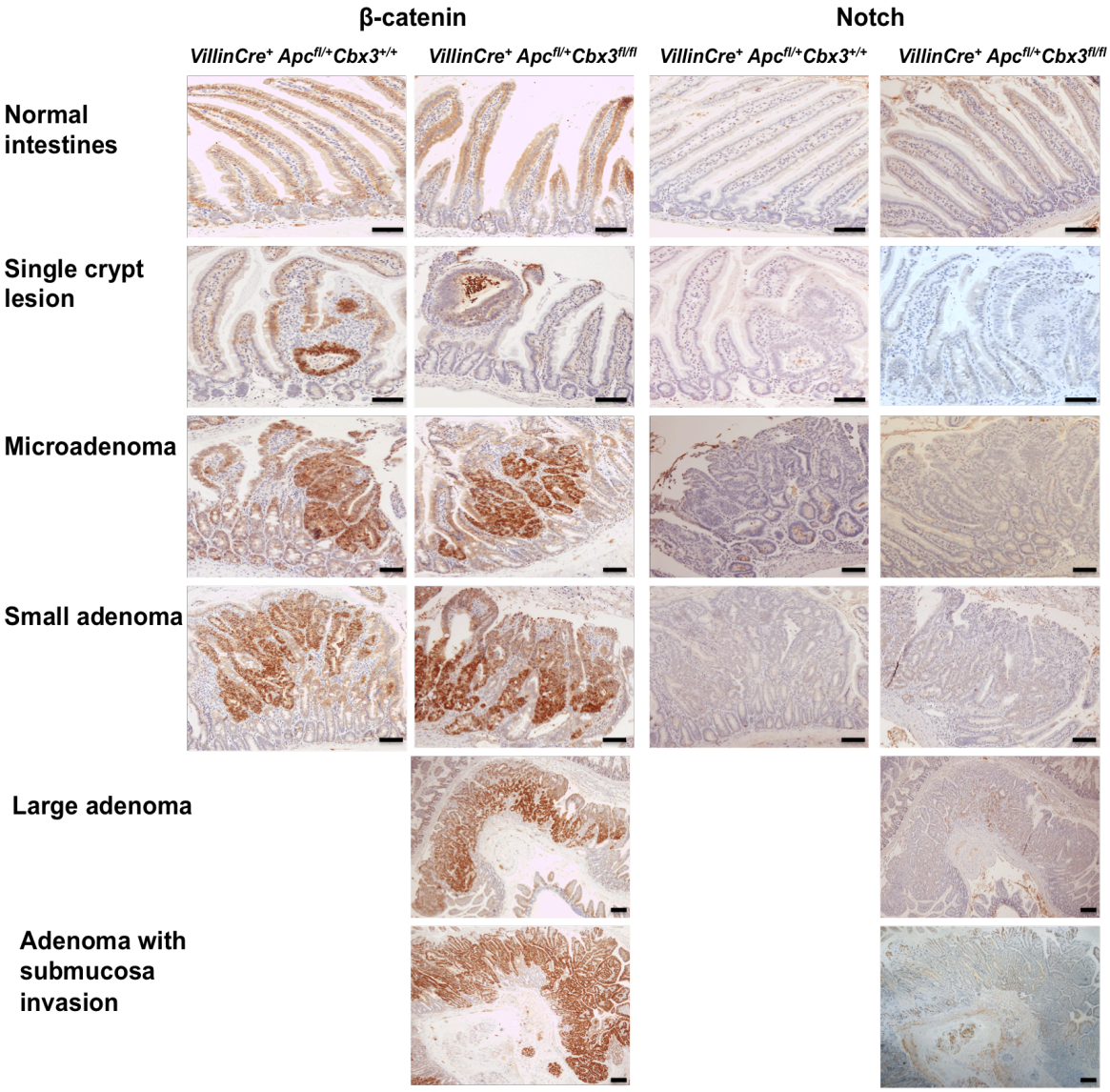

Figure 5.7: Immunohistochemical analysis of β-catenin and Notch1 in the intestines and adenomas of *VillinCreER^{+}Apc$^{fl/+}$* and *VillinCreER^{+}Apc$^{fl/+}$Cbx3$^{fl/fl}$* animals.
Anti-β-catenin immunohistochemistry revealed strong cytoplasmic staining of β-catenin in normal intestinal epithelium and nuclear localisation of β-catenin in tumours arising in both *VillinCreER^{+}Apc$^{fl/+}$* and *VillinCreER^{+}Apc$^{fl/+}$Cbx3$^{fl/fl}$* animals. Anti-Notch1 immunohistochemistry revealed little to no staining of Notch1 in both *VillinCreER^{+}Apc$^{fl/+}$* and *VillinCreER^{+}Apc$^{fl/+}$Cbx3$^{fl/fl}$* intestines and tumours. Scale bars indicate 100 µm.

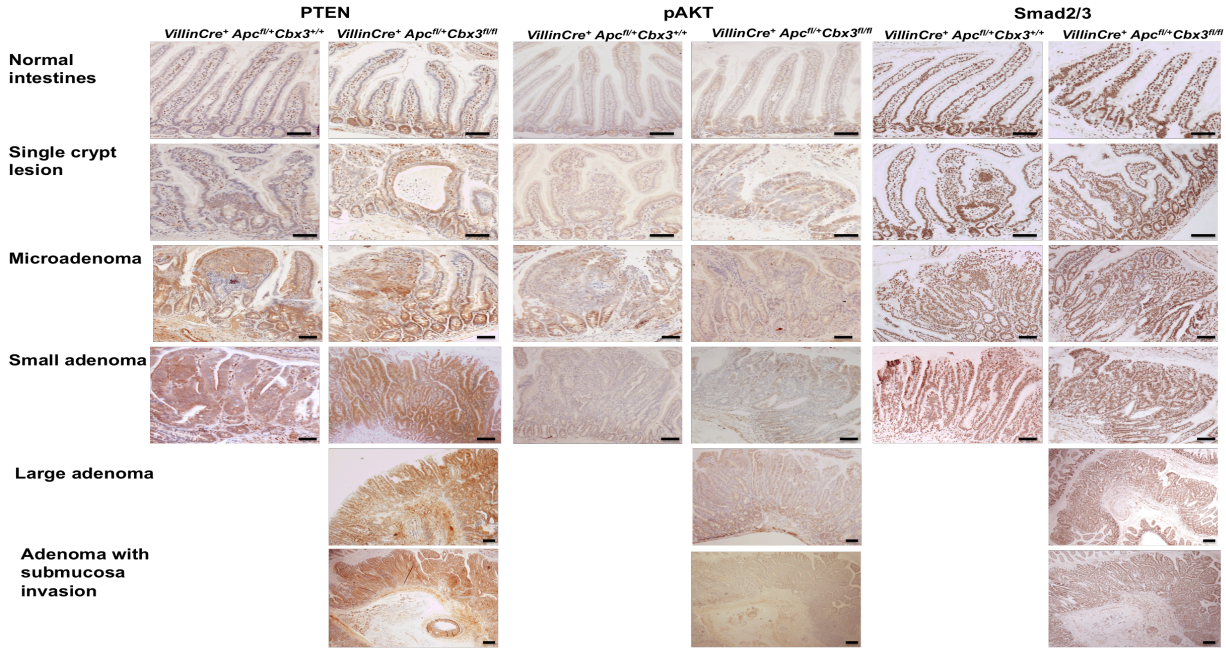

Figure 5.8: Immunohistochemical analysis of PTEN, pAKT and pSmad2/3 in intestines and adenomas of *VillinCreER^{+}Apc$^{fl/+}$* and *VillinCreER^{+}Apc$^{fl/+}$Cbx3$^{fl/fl}$* animals. Anti-PTEN immunohistochemistry detected cytoplasmic staining of PTEN in the crypt of normal intestines and single crypt lesions and intense cytoplasmic staining in tumours arising in *VillinCreER^{+}Apc$^{fl/+}$* and *VillinCreER^{+}Apc$^{fl/+}$Cbx3$^{fl/fl}$* animals. Anti-pAKT^{ser473} immunohistochemisty revealed little to no staining of pAKT in both *VillinCreER^{+}Apc$^{fl/+}$* and *VillinCreER^{+}Apc$^{fl/+}$Cbx3$^{fl/fl}$* intestines and tumours. Anti-pSmad2/3 immunohistochemistry was found ubiquitously positive in all cell nuclei of normal intestine and tumours of *VillinCreER^{+}Apc$^{fl/+}$* and *VillinCreER^{+}Apc$^{fl/+}$Cbx3$^{fl/fl}$* animals. Scale bars indicate 100 µm.

5.3. Discussion

Previous work has shown that epithelial deletion of *Cbx3* results in no immediate perturbation of intestinal homeostasis and survival (Chapter 3), but prolonged survival and repressed splice variant *Rac1b* expression in epithelial *Apc*-deficient mice (Chapter 4). Evidence has demonstrated that the deletion of HP1γ lacks tumorigenesis activity in a mouse xenograft model (Sharma *et al.*, 2003), suggesting that the expression of HP1γ contributes to cancer formation. It was therefore of great interest to examine the effects of epithelial-*Cbx3* deficiency in the context of activated Wnt signalling, achieved by conditional deletion of one alleles of *Apc*.

5.3.1. Rapid progression of Wnt-initiated tumorigenesis in the context of *Cbx3* deficiency

In order to test the long-term effects of *Cbx3* loss in the context of activated Wnt signalling, either one or both alleles of *Cbx3* were deleted in the context of *Apc* heterozygosity using the *VillinCreER* recombinase. Experimental cohorts of *VillinCreER*$^{+}$*Apc*$^{fl/+}$*Cbx3*$^{fl/fl}$ and *VillinCreER*$^{+}$*Apc*$^{fl/+}$*Cbx3*$^{fl/+}$ mice were aged along with *VillinCreER*$^{+}$*Apc*$^{fl/+}$ controls. Survival analysis of the full cohorts revealed a substantially reduced lifespan in *VillinCreER*$^{+}$*Apc*$^{fl/+}$*Cbx3*$^{fl/fl}$ animals with a medium survival of 197 days, compared to *VillinCreER*$^{+}$*Apc*$^{fl/+}$ control animals, which had a median survival time of 265 days post induction. Subgroup analysis according to gender demonstrated a more prominent reduction in median survival duration in male cohorts following homozygous deletion of *Cbx3* (179 days) compared to control (225 days), with the last survived male *VillinCreER*$^{+}$*Apc*$^{fl/+}$*Cbx3*$^{fl/fl}$ mouse lived to 317 days post induction due to ill health. Upon dissection, *VillinCreER*$^{+}$*Apc*$^{fl/+}$*Cbx3*$^{fl/fl}$ mice were found to contain remarkably more and larger lesions within the small intestine. The number and size of the tumours in the small and large intestines of the experimental animals and control animals were quantified and measured at the time of dissection. The experimental animals (*VillinCreER*$^{+}$*Apc*$^{fl/+}$*Cbx3*$^{fl/fl}$ and *VillinCreER*$^{+}$*Apc*$^{fl/+}$*Cbx3*$^{fl/+}$) were found to have a significant increase in tumour burden within the small intestine. Subgroup analysis according to gender showed that the observed

significant increase in tumour burden was mainly attributed to tumours in male mice. No difference in tumour burden was observed in the large intestine between all cohorts. Therefore, these observations indicate that additional deficiency of *Cbx3* increases predisposition of tumour formation and development in the small intestine of male mice in an *Apc* heterozygous background.

The morphology of the small intestinal tumours was examined and catergorised. Tumours arising in experimental animals *VillinCreER^{+}Apc$^{fl/+}$Cbx3$^{fl/+}$* and *VillinCreER^{+}Apc$^{fl/+}$Cbx3$^{fl/fl}$* were found to be more aggressive, with a higher number of lesions classified as small and large adenoma and also adenocarcinoma with submucosal invasion. In *VillinCreER^{+}Apc$^{fl/+}$* control animals, the majority of small intestinal lesions were found to be single crypt lesion, with a small proportion of lesions found to be microadenoma and no invasive characteristics observed. Subgroup analysis according to gender showed that this pattern was not observed in female tumours but was highly related, and even accentuated, in male tumours. This observation is consistent with the previous observed trend for reduced survival, increased tumour burden in male compared to female mice.

It is therefore clear from these data that in the context of *Apc* heterozygosity, additional epithelial deletion of *Cbx3* drives both an increase in multiplicity of small intestinal lesions and also drives progression of those lesions to a malignant phenotype in male cohorts but not female cohorts, indicating that lack of *Cbx3* is associated with a more aggressive phenotype in male mice. In male control animals, severity of intestinal tumours was not observed to equal that of *VillinCreER^{+}Apc$^{fl/+}$Cbx3$^{fl/+}$* and *VillinCreER^{+}Apc$^{fl/+}$Cbx3$^{fl/fl}$* animals, even in very aged animals. This exemplifies the dramatic acceleration of disease progression resulting from epithelial *Cbx3* loss in the context of *Apc* heterozygosity in male mice. Although the exact mechanism is currently unclear, previous evidence has shown that depletion of *Cbx3* in adult male mice resulted in a severe hypogonadism (absence of hormone secretion) associated with a loss of germ cells and defeat in spermatogenesis, therefore the observed gender differences in survival duration and incidence of tumours may be due in part to hormonal differences between male and female mice (Brown *et al.*, 2010; Cleveland *et al.,* 2009; Patman, 2015). Additionally, estrogens (female hormones) were found to induce mismatch repair gene expression in colonic epithelial cells mediated

by estrogen receptor β (ERβ) *in vitro* and *in vivo*, suggesting estrogens in female mice play a protective role against CRC initiation and progression (He *et al*, 2012; Jin *et al*, 2010; Kennelly *et al*, 2008). Thus, there is an urgent need to examine the level of ERβ using immunohistochemistry in both male and female intestinal epitheliums and such information could shed light on the tumour susceptibility observed in male mice. Another possible reason for this marked shorter survival and increased in tumour severity in *Cbx3*-deficient male mice could be genomic instability as the loss of HP1γ results in loss of gene silencing, heterochromatin structure and transcriptional repression (Eissenberg and Elgin, 2000; Ebert *et al.,* 2006; Smallwood *et al.,* 2007), which predisposes to DNA strand breakage, DNA mismatches and recombination within derepressed repetitive sequences (Ehrlich, 2002). Links between hypomethylation and genomic instability have been demonstrated for many cancer types (Tsuda *et al.,* 2002; Schulz *et al.,* 2002). The lack of HP1γ may cause a global genomic demethylation in *Cbx3* deficient epithelium and it therefore would be interesting to explore the global methylation signature of *Cbx3* deficient epithelium, in male and female subgroups, compared to control epithelium to gain an insight into the role of HP1γ in heterochromatin marks and the DNA methylation in both male and female mice of colorectal cancer.

5.3.2. Limited effects on signalling pathways in *Cbx3*-deficient Wnt-activated small intestinal tumours

Previous data has demonstrated that the deletion of *Cbx3* alone is no different from healthy wildtype, indicating that *Cbx3* loss alone is unable to induce tumorigenesis (Chapter 3). However, additional loss of *Cbx3* enhances tumour burden and progression in mice with heterozygous deletion of *Apc*, suggesting that *Cbx3* loss accelerate Wnt-driven tumour formation. Therefore the activation of several key signalling pathways was tested, including Wnt, Notch, TGF-β and PI3K, in *Apc* heterozygous tumours with or without *Cbx3* deletion. Immunohistochemistry was performed on tumour sections from all grades (single crypt lesion, microadenoma, small adenoma, large adenoma and adenocarcinoma with

submucosal invasion) and normal intestinal tissue from control *VillinCreER*$^{+}$*Apc*$^{fl/+}$ and *VillinCreER*$^{+}$*Apc*$^{fl/+}$*Cbx3*$^{fl/fl}$ mice.

In the intestine, Wnt signalling plays an important role in the proliferation and maintenance of intestinal stem cells and progenitor cells (van de Wetering *et al*., 2002). Upregulation and strong nuclear localisation of β-catenin is a sign of Wnt pathway activation by *Apc* loss within the intestine (Sansom *et al.*, 2004). Normal intestines were found to have a cytoplasmic staining pattern of β-catenin, whereas tumour tissues revealed both upregulation and nuclear localisation of β-catenin in control *VillinCreER*$^{+}$*Apc*$^{fl/+}$ and *VillinCreER*$^{+}$*Apc*$^{fl/+}$*Cbx3*$^{fl/fl}$ intestines. This observation reflects Wnt activation as a result of *Apc* loss. Furthermore, β-catenin was detected strongly in the nuclui of the dedifferentiated epithelial cells and invasive tumour cells in the intestinal tumours in both control *VillinCreER*$^{+}$*Apc*$^{fl/+}$ and *VillinCreER*$^{+}$*Apc*$^{fl/+}$*Cbx3*$^{fl/fl}$ intestines, indicating the intratumour heterogeneity in Wnt-activated intestines. However, there is no variation in the β-catenin staining pattern between the control *VillinCreER*$^{+}$*Apc*$^{fl/+}$ and *VillinCreER*$^{+}$*Apc*$^{fl/+}$*Cbx3*$^{fl/fl}$ intestines.

In the intestine, Notch signaling is a crucial element for the maintenance of intestinal stem cells and for the regulation of cell differentiation. Notch signaling was thought to be oncogenic by positively regulating the proliferation of intestinal progenitors and imitating tumour formation in the intestine (Fre *et al*., 2011). Previously published data has demonstrated that the dual roles of Notch signaling in both enhancing tumour initiation and suppressing tumour progression. Furthermore, Notch signaling particularly has a suppressive role in *Apc* deficient tumours, suggesting that there is a negative correlation between Wnt and Notch signaling activation (Kim *et al*., 2012). As described above, I previously observed a dramatic increase in activation status of Wnt, as assessed by immunohistochemical staining for β-catenin, following heterozygous loss of *Apc* in both *Cbx3*-proficient and deficient intestines. Therefore, the activation status of Notch was examined in tumours arising in both *VillinCreER*$^{+}$*Apc*$^{fl/+}$ *control* and *VillinCreER*$^{+}$*Apc*$^{fl/+}$*Cbx3*$^{fl/fl}$ intestines. The immunohistochemistry was performed using anti-activated Notch1 as a marker of Notch activation. Normal intestines and tumours from both control *VillinCreER*$^{+}$*Apc*$^{fl/+}$ and *VillinCreER*$^{+}$*Apc*$^{fl/+}$*Cbx3*$^{fl/fl}$ intestines were uniformly negative for

Notch1 expression, suggesting that a very low levels of Notch activation in the Wnt-activated intestines. However, Notch signalling was not altered following the loss of *Cbx3* in the small intestines.

PTEN is an important tumour suppressor that negatively regulates the PI3K-AKT signalling pathway and it is frequency mutated in a wide range of human cancers and is associated with the apoptosis, proliferation and metastasis of tumour cells (Sansal and Sellers, 2004; Tamura *et al.*, 1998). I then examined the normal intestinal tissues and tumours using anti-PTEN immunohistochemistry as a marker for PTEN status. Tumours arising in both control *VillinCreER*$^{+}$*Apc*$^{fl/+}$ and *VillinCreER*$^{+}$*Apc*$^{fl/+}$*Cbx3*$^{fl/fl}$ intestines show intense positive cytoplasmic expression for PTEN across epithelial and stromal cells, indicating that PI3K-AKT may not yet be activated.

The PI3K/AKT signalling pathway plays an important role in cell proliferation, tumour growth and metastasis and activation of PI3K/AKT pathway promotes cancer formation through a variety of mechanisms (Liu *et al.*, 2009; Xue *et al*., 2012; Engelman, 2009). PTEN is a negative regulator of PI3K/AKT signalling, and its inactivation is a common cause of increased PI3K activity in cancers (Di Cristofano and Pandolfi, 2000). As described previously, intense PTEN expression by PTEN immunostaining was detected in tumours of both control *VillinCreER*$^{+}$*Apc*$^{fl/+}$ and *VillinCreER*$^{+}$*Apc*$^{fl/+}$*Cbx3*$^{fl/fl}$ intestines, suggesting that PI3K/AKT pathway may not be activated. Sections were then stained immunohistochemically against activated Phospho-AKT^{ser473} (pAKT) to assess the activation status of the PI3K/AKT pathway. Low levels of cytoplasmic pAKT staining were detected at the crypt regions in the normal intestines and across tumours of both control *VillinCreER*$^{+}$*Apc*$^{fl/+}$ and *VillinCreER*$^{+}$*Apc*$^{fl/+}$*Cbx3*$^{fl/fl}$ intestines, consistent with the suggestion that PI3K/AKT pathway may not yet be activated in the tumours.

The TGF-β signalling pathway has dual roles in exerting tumour suppressor effects by regulating cell growth, apoptosis and immortalisation in normal cells and early carcinomas and exerting prometastatic effects by promoting cancer progression, invasion, and tumour metastasis in more advanced tumours (Yingling, Blanchard and Sawyer, 2004; Siegel and Massague, 2003; Dumont and Arteaga, 2003). Given that no distant metastasis

was observed in both of control *VillinCreER*$^{+}$*Apc*$^{fl/+}$ and *VillinCreER*$^{+}$*Apc*$^{fl/+}$*Cbx3*$^{fl/fl}$ animals, evaluation of the tumor suppressive activity of TGF-β would be more relevant in this case. Since accumulated evidences suggests that the phosphorylation of Smad2/3 at its C-terminal region correlates with the growth inhibition mediated by TGF-β pathway, the phosphorylated Smad2/3 levels were analysed in control *VillinCreER*$^{+}$*Apc*$^{fl/+}$ and *VillinCreER*$^{+}$*Apc*$^{fl/+}$*Cbx3*$^{fl/fl}$ intestines to evaluate the TGF-β grwoth inhibitory effects. Immunohistochemical staining of phospho-Smad2/3 was highly expressed and predominantly located in the nuclei of all normal intestinal epithelium and tumour cells in control *VillinCreER*$^{+}$*Apc*$^{fl/+}$ and *VillinCreER*$^{+}$*Apc*$^{fl/+}$*Cbx3*$^{fl/fl}$ intestines, suggesting a role of Smad complex in transcriptional regulation. This ubiquitous phospho-Smad2/3 staining indicates that tumour repressive arm of TGF-β pathway is activated in Wnt-activated intestines.

5.3.3. Summary

In summary, the findings presented in this chapter demonstrated for the first time that *Cbx3* loss accelerates Wnt-driven tumour progression and reduces survival of mice, particularly in male mice, with heterozygous loss of *Apc*.

These data also indicate that the advanced Wnt-driven tumorigenesis in *Cbx3* deficient intestines do not show increased activation of Wnt, Notch, PI3K and TGF-β compared to the *Cbx3* proficient Wnt-activated intestines. The exact nature and mechanism by which *Cbx3* deficiency influences tumour formation and progression remains unclear, but it is clear that that the phenomenon is influenced by gender, as *Cbx3* deficiency is strongly associated with shortened survival and more aggressive phenotypes in male but not female mice.

Chapter Six

General Discussion

6. General Discussion

"The important thing in science is not so much to obtain new facts as to discover new ways of thinking about them."

Sir William Bragg 1862 – 1942

Colorectal cancer (CRC) is the third most common cancer in men and the second in women worldwide (International Agency for Research on Cancer 2014). It is estimated that 110 new cases of CRC are diagnosed each day in the U.K. alone and the 5-year survival rate is as low as 50% (Cancer Research U.K. 2013).

The stepwise model of CRC initiation and progression implicates the requirement for the accumulation of multiple genetic and epigenetic mutations to drive the transformation of the normal epithelium to invasive adenocarcinoma (Fearon and Vogelstein, 1990). The first mutation in this process is often the inactivation of the tumour suppressor gene, *Apc*.

Although genetic mutations have been the focus of cancer research for many years, epigenetic alterations have been increasingly recognised as playing an important role in tumorigenesis. Members of the heterochromatin protein 1 (HP1) family have been implicated in various functions, including heterochromatin formation, gene silencing, RNAi mediated silencing, telomere stability, DNA replication and repair, and positive regulation of gene expression (Hediger and Gasser, 2006; Kwon *et al.,* 2010; Dinant and Luijsterburg, 2009; Zeng *et al.,* 2013). Compared to the wealth of studies conducted on HP1α and HP1β, much less is known about HP1γ.

Growing evidence suggest that HP1γ plays an important role in the epigenetic regulation of cancer development, via regulating cell proliferation, differentiation (Takanashi *et al.,* 2009), telomere maintenance (Sharma *et al.,* 2003) and DNA damage repair (Luijsterburg *et al.*, 2009). What is more the level of HP1γ is frequently up-regulated in many cancer cell lines, including the colon (Takanashi e*t al.,* 2009). Loss of *Cbx3*, the gene encoding HP1γ, in selected cancer cell lines has also been reported to inhibit cancer cell growth and colony formation, while further evidence indicates that the deletion mutant of

HP1γ lacks tumorigenesis activity in a mouse xenograft model (Zhou *et al.*, 2014; Sharma *et* al., 2003). These observations provide evidence that *Cbx3* functions as a driver in cancer cell growth and the over-expression of HP1γ in cancer is therefore important in the process of tumorigenesis, at least in the tumour initiation stage.

Since these observations were made in cell lines and xenographs, the role of *Cbx3* in the small intestinal epithelium has not yet been explored. Although not reported to be directly involved in intestinal homeostasis, *Cbx3* has been implicated as a key regulator in cell differentiation via the molecular interaction with histone H4K20, and the loss of *Cbx3* is required for cell differentiation to occur (Takanashi *et al.*, 2009). Bearing in mind the role of Wnt pathway in intestinal homeostasis and intestinal stem cell maintenance, one could speculate that *Cbx3* might be involved in regulating the trans-activation of Wnt target gene expression epigenetically.

In my PhD project, I set about investigating the effects of *Cbx3* loss in normal intestinal homeostasis and in the context of aberrant Wnt signalling activation. Furthermore, I investigated the long-term consequences of *Cbx3* deletion upon Wnt-driven intestinal tumour initiation and progression.

The main findings from this PhD thesis are:

- *Cbx3* in the intestinal epithelium is redundant with regards to intestinal homeostasis as *Cbx3* deficiency has no effects on intestinal homeostasis, cell lineage differentiation and survival
- *Cbx3* deficiency prolongs survival of mice with acute Wnt-activated intestines potentially via attenuation of Wnt activation at the receptor level and RNA splicing defects
- *Cbx3* deficiency promotes Wnt-driven tumour progression and reduces survival of male mice with heterozygous loss of *Apc* in the long term
- The multifaceted roles of HP1γ maintain a gene-repressive environment in heterochromatin for normal intestinal homeostasis, and provide a gene-permissive environment in euchromatin for carcinogenesis

6.1. The redundant role of *Cbx3* in normal intestinal homeostasis

The literature has indicated that *Cbx3* has a role in stem cell maintenance and cell differentiation in adipocytes, male germ cells and cardiovascular system (Xiao *et al.*, 2011; Brown *et al.*, 2010). However, little is known about the nature of *Cbx3* in intestinal epithelial cell differentiation and homeostasis. In Chapter 3, the effects of epithelial-specific deletion of *Cbx3* from the murine small intestine were investigated.

The proposed role of *Cbx3* on stem cell maintenance leads to the prediction that *Cbx3* loss would result in diminished stem cell compartment and increased cell lineage differentiation in the small intestinal epithelium. In contrast to this hypothesis, histological and quantitative analysis of the small intestinal epithelium following *Cbx3* loss has no dramatic effect upon homeostasis. No changes to the gross histology or structure of the intestine and survival up to 366 days following *Cbx3* loss were detected, and no alterations in crypt and villus size, proliferative, apoptosis and cell migration were observed in the *Cbx3* deficient small intestine. Furthermore, there was no enhancement in cell differentiation and no alteration in the majority of the stem cell markers in the intestinal epithelium in the absence of *Cbx3*. Despite the fact that *Cbx3* deletion results in a significant increase in one of the CBC stem cell markers, *Ascl2*, which is a transcriptional target of Wnt signalling and is often upregulated in colorectal neoplasms (Jubb *et al.*, 2006), intestinal homeostasis and cell differentiation were unaltered. This suggests that *Cbx3*-mediated up-regulation of *Ascl2* alone might not be sufficient to alter intestinal stem cell maintenance and differentiation and therefore no effect on the overall intestinal homeostasis was observed. The findings presented in this study therefore indicate that homozygous loss of *Cbx3* in the intestinal epithelium has no detrimental effect on the normal intestinal homeostasis, suggesting that *Cbx3* acts redundantly in normal intestinal homeostasis and intestinal cell lineage differentiation.

There appears to be a discrepancy between the data presented here and in the literature on the proposed role of *Cbx3* as a safety lock for the transition to cell differentiation and stem cell maintenance (Takanashi *et al*., 2009). In order to further understand the functional role of *Cbx3* in maintenance of the small intestinal stem cells, the

Lgr5-EGFP-Cre transgene could be incorporated into the wild type and *VillinCre*$^{+}$*Cbx3*$^{fl/fl}$ mice for further analysis of the stem cell enriched populations of epithelial cells. Furthermore, single cell suspension from Lgr5-EGFP-Cre*ER*$^{+}$ *Cbx3*$^{fl/fl}$ small intestine could be enriched for GFP expressing cells and grown in organoid culture system in the presence or absence of tamoxifen to investigate if *Cbx3* loss directly targets stem cells. Finally, genome-wide expression analysis of *Cbx3* deficient small intestinal epithelium should be performed to further elucidate the role of *Cbx3* in regulation of intestinal stem cell maintenance, differentiation and other potential physiological functions, by analysing the transcriptional effects of *Cbx3* loss in the entire intestinal epithelium.

6.2. The role of *Cbx3* in Wnt signalling and RNA splicing

Cbx3 has been previously reported to be up-regulated in human colorectal cancer tumours and multiple cancer cell lines. Furthermore, down-regulation of *Cbx3* expression was previously reported to lead to growth inhibition of cancer cell lines (including colorectal cancer cell lines) suggesting a role of *Cbx3* in carcinogenesis and as a therapeutic target for various types of cancers (Takanashi *et al*., 2009). It is well established that appropriate regulation of the Wnt signalling pathway is critical for intestinal homeostasis and active Wnt signalling has been extensively reported to play a pivotal role in intestinal tumorigenesis (Clevers, 2006). However, very little is known about the functional involvement of *Cbx3* in Wnt signalling regulation and colorectal cancer development. Thus, it was of great interest to investigate the consequence of *Cbx3* loss in the context of activated Wnt signalling. Activation of Wnt signalling was achieved by conditional deletion of both alleles of the *Apc* gene within the intestinal epithelium (Sansom *et al*., 2004).

Analysis of the effects of *Cbx3* deficiency in Wnt-activated intestines revealed a significant increase in lifespan of mice with homozygous loss of *Apc*. The impact of *Cbx3* deficiency on prolonged animal survival suggested that the loss of *Cbx3* alleviates the oncogenic effects in the context of Wnt activation. The expression of Wnt target genes was examined to investigate the feasibility of *Cbx3* as a potential therapeutic target in Wnt-activated intestines. *Cbx3* loss slightly reduced the Wnt target gene up-regulation in Wnt-

activated small intestine but the attenuation of Wnt target gene expression did not reach statistical significance, it is possible that the slight reduction of Wnt target genes was sufficient to repress the enterocyte differentiation in *Cbx3* deficient epithelium and therefore lower its oncogenic potential leading to an increase in survival. In order to further investigate the mechanism behind the attenuated Wnt target gene expression of *Apc* loss in *Cbx3* deficient epithelium, luciferase assays were performed in HEK-293 cells by the use of Wnt-responsive Topflash system. Transient knockdown of *CBX3* reduced ΔNLRP6–mediated Topflash activity by 41% and TCF4-VP16–mediated Topflash activity by 27%, suggesting that *CBX3* mainly acted at the LRP6 receptor level. This suggestion is based on the observation that the loss of *CBX3* blocked TCF-dependent transcription induced by a constitutively active LRP6 receptor, but a lower extent of blockage was observed by a constitutively active TCF-VP16 fusion protein, indicating that *Cbx3* does function at the receptor level within the Wnt signalling cascade. Together these data provide evidence that *Cbx3* deficiency attenuates Wnt signalling by suppressing its receptors and thus causes a suboptimal level of Wnt activation. This observation also explains that the loss of *Cbx3* had little effect on Wnt target gene expression in *Apc*-deficient intestine, as the activation of Wnt signalling in the *Apc* mutants were downstream of the receptor. However, the exact mechanism underlying the regulation of Wnt signalling by *Cbx3* remains to be elucided. It is tempting to speculate that a positive feedback loop exists in the presence of *Cbx3*, in which initial Wnt pathway activation induces expression of a subset of gene products which in turn function in an autocrine or paracrine manner to induce further activation of Wnt signalling. In the absence of *Cbx3*, the positive feedback loop may be abolished and this resulted in a suboptimal level of Wnt activation. Whether such a feedback loop exists warrants future investigation. Furthermore, it is worth investigating further at which distinct levels *Cbx3* is acting within the Wnt signalling cascade. Further Topflash assays could be performed using the mutant plasmids Axin-GID (which acts to titrate GSK-3 from the endogenous Axin complex) (Fraser *et al.,* 2002) and ΔN-89-β-catenin (which is a non-degradable form of β-catenin) (Munemitsu *et al*., 1996).

Accumulated evidence indicates a role for *Cbx3* in aiding in efficient RNA processing through the recruitment or stabilisation of the splicing machinery. Depletion of *Cbx3* leads

to a decrease in recruitment of the RNA splicing factors SNRNP70 and SRSF1 to gene bodies, resulting in RNA splicing defects and subsequently leading to an increase in unspliced RNA species (Saint-Andre *et al.*, 2011; Smallwood *et al.,* 2012). It has been documented that the splicing factor SRSF1 regulates the expression of the tumour-related gene *Rac1b*, which is an alternative splice variant of *Rac1* and it is frequently overexpressed in a subset of tumour samples (Goncalves *et al*., 2014; Schnelzer *et al.,* 2000; Fiegen *et al.,* 2004). Numerous studies have reported that *Rac1b* plays a critical role in tumorigenesis via augmenting Wnt signaling, promoting tumour cell survival (Matos *et al.,* 2008) and increasing the invasive and metastatic properties of colorectal cancer cells (Esufali *et al.*, 2007). However, the mechanisms of how changes in alternative splicing lead to *Rac1b* overexpression remain unclear. Gene expression analysis was performed to determine if *Cbx3* affects the splicing of *Rac1b* gene. Following the loss of *Cbx3* in the Wnt activated intestine, the splice variant *Rac1b* was significantly repressed. This was consistent with the hypothesis that loss of *Cbx3* impairs RNA splicing and therefore leads to a reduced level of *Rac1b* in the small intestinal epithelium. This further confirmed the role of *Cbx3* in influencing alternative splicing through its recruitment of the splicing machinery and splicing factors like SRSF1.

The deletion of *Cbx3* in the Topflash assay resulted in marked repression of Wnt activity, together with the repressed alternative splicing of *Rac1b* gene *in vivo*, resulting in a prolonged lifespan of mice with homozygous loss of *Apc*. Collectively, the initial data presented portray *Cbx3* as a positive regulator of Wnt signalling at the receptor level and as a positive regulator of alternative splicing in *Rac1* gene. A more comprehensive insight into the role of *Cbx3* could be gained by performing chromatin immunoprecipitation (ChIP) analysis of the Wnt-activated small intestinal epithelium to verify whether *Cbx3* occupies promoter regions of Wnt target genes, as previous evidence suggested that *Cbx3* binding is strongly correlated with the level of gene expression (Smallwood *et al*., 2012). Furthermore, we are planning to carry out a high-throughput RNA sequencing (RNA-seq) using total nuclear RNA of Wnt-activated small intestinal epithelium with or without *Cbx3* loss to fully characterise the functional role of *Cbx3* on alternative splicing.

6.3. *Cbx3* loss promotes Wnt-driven tumour progression

Previous work has established that the deletion of *Cbx3,* in the context of homozygous *Apc* loss in the intestinal epithelium, prolonged survival of mice with diminished level of Wnt activation and reduced expression of the tumour-related splice variant *Rac1b*. These data indicates the oncogenic potential of *Cbx3* on aberrant Wnt-activated intestines.

Homozygous loss of *Apc* alleles in the adult intestine resulted in rapid and catastrophic disruption of epithelial homeostasis and animals only survive up to 4 days post induction. In order to investigate the consequences of *Cbx3* deletion in Wnt-driven tumorigenesis, the delayed phenotype study was achieved through the deletion of one allele of the *Apc* gene within the intestinal epithelium, which has been previously reported as an intestinal tumour-prone model (Shibata *et al*., 1997).

Although *Cbx3* deletion has been reported to inhibit the growth of various cancer-derived cell lines (Takanashi *et al.,* 2009), my data indicated that the survival probability of *Cbx3*-deficient mice was shortened in the context of *Apc* heterozygosity due to a dramatic increase in tumour number and size in the small intestine, particularly in male mice. In addition, the loss of *Cbx3* accelerated tumour progression, resulting in more advanced tumours compared to mice with heterozygous loss of *Apc* alone. The advanced Wnt-driven tumours in *Cbx3* deficient intestines showed no changes in the characteristic patterns of Wnt, Notch, PI3K and TGF-β signalling compared to the *Cbx3* proficient Wnt-activated tumours. Unprecedentedly, these observations suggest that *Cbx3* deletion confers cancer susceptibility and accelerate tumour progression in male mice with Wnt-activated intestines over long period of time. Previous studies have shown that deletion of *Cbx3* in adult male mice resulted in a dramatic reduction in hormone secretion that is associated with the reduced number of germ cells and a severe impairment of spermatogenesis (Brown *et al.*, 2010b). Together these findings not only suggest an important role for *Cbx3* in colorectal carcinogenesis and progression, but also add support to the accumulating evidence that sex hormones are relevant to the development of colorectal cancer (Slattery *et al*., 2001).

The underlying mechanism for the long-term *Cbx3* loss in the context of *Apc* heterozygosity on the intestinal epithelium is currently inadequately understood. Tumours arising from *Cbx3*-deficient mice demonstrated invasive potential, which is unprecedented in $Apc^{fl/+}$ mice. It was unknown how *Cbx3* deficiency may contribute to invasive potential of Wnt-driven tumorigenesis. However, an increasing number of investigations suggest the role of *Cbx3* in cell differentiation and stem cell maintenance (Wang *et al.,* 2012; Xiao *et al.,* 2011). It is possible that *Cbx3*-deficient tumours became progressively more undifferentiated with higher proliferative, invasive and metastatic potential. Although this explanation, however, may be undermined by the results from previous chapters, which demonstrated *Cbx3* deficiency resulted in no alteration to cell differentiation and stem cell compartment in intestines with or without homozygous loss of *Apc*. It is still worth investigating whether *Cbx3* has a role in tumour cell differentiation, invasion and metastasis. Further insight into the nature of *Cbx3* and cell differentiation could be gained by investigating the expression of tumour cancer stem cell markers (such as *CD133, CD24* and *CD44v6*) in $Apc^{fl/+}$ tumours with or without *Cbx3* (Choi *et al.*, 2009; Todaro *et al.,* 2014). Furthermore, the accelerated tumour progression caused by *Cbx3* deficiency in Wnt-driven tumorigenesis is being further investigated to address the ability of Wnt-activated tumours to progress and invade upon *Cbx3* loss. A more invasive model of colorectal cancer is currently being generated, by incorporating with a *PTEN* gene deletion. By using $Apc^{fl/+}$ mice with conditional deletion of the tumour suppressor *PTEN* in the epithelium with or without *Cbx3*, the role of *Cbx3* in facilitating tumours to acquire increased invasiveness and metastatic potential could be further characterised.

6.4. The functional versatility of HP1γ in normal intestinal homeostasis and tumorigenesis

Work to date has yet to clarify the multifaceted roles of *Cbx3* in intestinal homeostasis and tumorigenesis. The findings of this study demonstrate the functional versatility of HP1γ in different contexts (Figure 6.1).

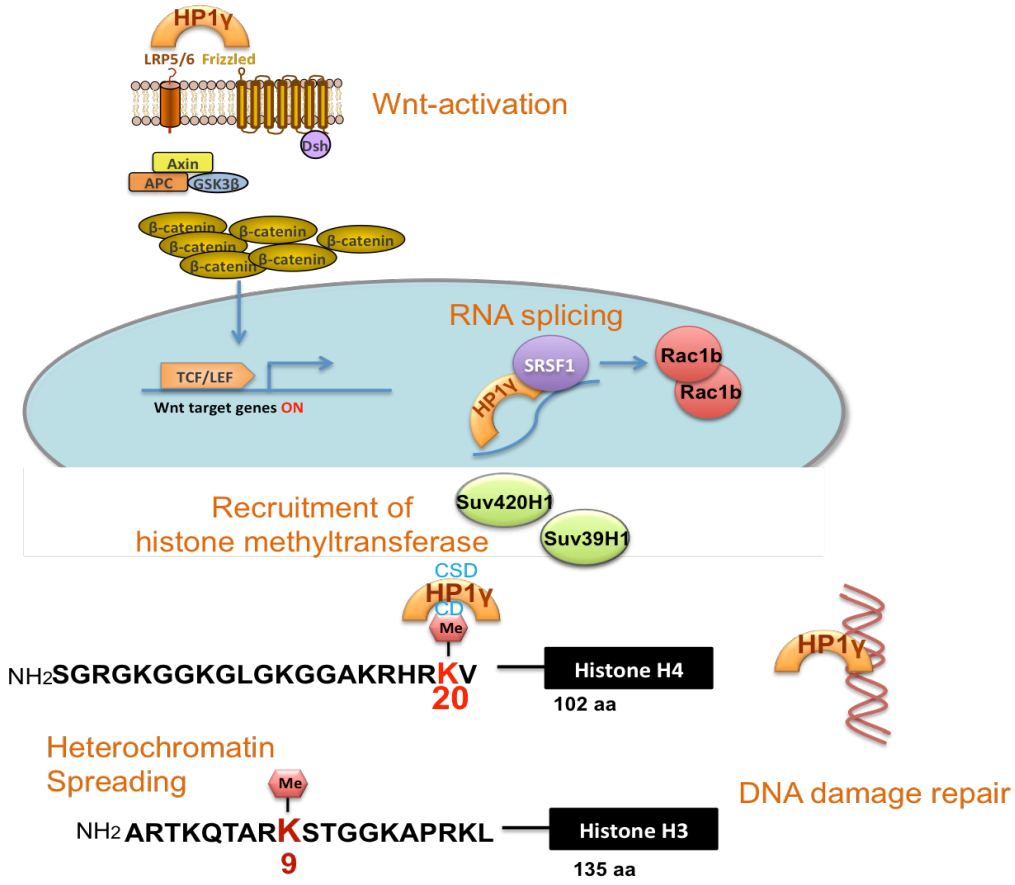

Figure 6.1: Simplified proposed multifaceted functional model of HP1γ in intestine. We proposed that HP1γ acts as a positive regulator of Wnt signalling at the LRP5/6 receptor level and a suboptimal level of Wnt activation was observed in the absence of *Cbx3* (encoding the HP1γ protein) *in vitro* and *in vivo*. Secondly, HP1γ is proposed to aid efficient RNA processing through recruitment / stabilisation of the splicing machinery SRSF1 which mediates *Rac1b* splicing. *Cbx3* loss resulted in a dramatic decrease in level of *Rac1b* in aberrant Wnt-activated intestine. Thirdly, H4K20me3 is proposed to serve as a docking site for HP1γ, which in turn recruits histone methyltransferases Suv420h1 (to methylate H4K20me3) and Suv39h1 (to methylate H3K9me3), and results in heterochromatin spreading. HP1γ is required to maintain a gene-repressive environment via formation and maintenance of heterochromatin marks in Wnt-driven tumourigenesis. Lastly, HP1γ has a potential role in regulating DNA double strand break repair.

Normal healthy intestines do not seem to require Cbx3 for homeostasis, as long-term loss of Cbx3 did not perturb normal intestinal homeostasis and survival, suggesting the redundant nature of Cbx3 in intestinal homeostasis under physiological conditions. Upon aberrant Wnt-activation, *Cbx3* deficiency suppressed Wnt-activation and reduced splicing of the tumour-associated gene *Rac1b*, leading to an increase in survival probability of mice with homozygous loss of *Apc*. In this context, *Cbx3* is therefore thought to be a positive regulator of Wnt-signalling and RNA splicing. Consistently, a number of studies have shown that *Cbx3* is widely associated with euchromatin and localized to active genes (Vakoc et al., 2005; Smallwood *et al.,* 2007; Mateescu *et al*., 2008) and evidence has suggested a role for *Cbx3* in alternative splicing (Saint-Andre *et al.*, 2011). Together, these observations suggest an oncogenic nature of *Cbx3* in aberrant Wnt-activated intestine (Figure 6.1).

In the long-term, deletion of *Cbx3* accelerated Wnt-driven tumour progression, leading to a reduced lifespan of mice, particularly in male mice with heterozygous loss of *Apc*. Exactly how *Cbx3* loss is involved in tumour progression has yet to be determined. Previous evidence has shown that *Cbx3* loss depleted hormone secretion in adult male mice resulted in a severe hypogonadism, leading a loss of germ cells and defeat in spermatogenesis (Brown *et al.,* 2010; Cleveland *et al.*, 2009). Furthermore, the female hormone estrogen have been widely regonised to play a protective role against CRC formation and progression via aiding efficient DNA mismatch repair mediated by estrogen receptor β (ERβ) (He *et al,* 2012; Jin *et al*, 2010; Kennelly *et al*, 2008). It is therefore tempting to speculate that the diminished level of DNA mismatch repair in male mice resulted in more severe tumour progression and decreased survival of male mice. Detailed immunohistochemical analysis of ERβ expression in both male and female intestinal epitheliums is essential to verify this speculation. Another potential way that *Cbx3* deficiency leads to more aggressive tumours could be by abolishing apoptosis. A previously published report demonstrated that *Cbx3* has a role in regulating apoptosis through binding and sequestering the pro-apoptotic Bax and GADD45a proteins (Zhou *et al.*, 2014), suggesting a potential role of *Cbx3* in assisting cancer cells to escape from apoptosis. It would therefore be interesting to investigate the level of caspase-3 cleavage using

immunohistochemistry and to assess the binding of *Cbx3* to the apoptotic proteins by co-immunoprecipitation analysis in the *Cbx3*-proficent and deficient tumours, in both male and female cohorts. Another potential mechanism that *Cbx3* loss leads to more severe tumour progression could be by disrupting heterochromatin formation and gene silencing (Maison and Almouzni, 2004; Haldar *et al*., 2011; Smallwood *et al*., 2012; Larson *et al.,* 2012). Concordant with this notion, a reduced level of heterochromatic mark H4K20me3 was consistently observed following *Cbx3* loss in the small intestinal epithelium, suggesting a role of *Cbx3* as a ''gatekeeper'' of epigenetic gene silencing in establishing, maintaining and spreading of H4K20me3. Similar scenarios are reported in the literature proposing that HP1 protein is necessary to establish H4K20me3 in heterochromatin (Kourmouli *et al.,* 2004; Schotta *et al*., 2004) (Figure 6.1).

Previous evidence has suggested that H4K20 trimethylation (H4K20me3) is essential for the maintenance of perinatal, non-cancerous cell states and confers heterochromatin maintenance capability (Fraga *et al.*, 2005; Pogribny *et al.,* 2006; Schotta *et al.*, 2008). Trimethylation specifically requires the recruitment of the Sur4-20h enzymes by HP1 (Schotta *et al.*, 2004). H4K20me3 has been shown to have a significant correlation with HP1γ expression in normal tissue samples and a dissociation of the correlation between HP1γ expression and H4K20me3 may reflect the malfunction of epigenetic control in cancer tissues (Takanashi *et al.*, 2009). These studies from the literature are consistent with our observation that co-localisation of HP1γ to H4K20me3, which is essential for heterochromatin maintenance, is observed in normal intestinal homeostasis. Whereas in Wnt-activated intestine the HP1γ-H4K20me3 association is lost, caused by HP1α displacing HP1γ to the H4K20me3 marks. The relationship between HP1α and H4K20me3 remains to be determined but some early evidence has shown a dynamic correlation between HP1α and H4K20me3 levels in ES cells (Wongtawan *et al.*, 2011), suggesting an important mechanism required for epigenetic malfunction in Wnt-activated intestine. Our findings are in agreement with the previous conclusion that HP1γ binding at H4K20me3 is implicated to maintain the transcriptionally repressed state of heterochromatin. It is possible that *Cbx3* deficiency leads to the disruption of heterochromatin formation and therefore induces widespread genomic instability, which allows further DNA double stranded breaks and

mutations aiding tumour progression and malignant transformation in Wnt-driven tumorigenesis.

Further investigation is required to establish the mechanism behind the loss of *Cbx3* on chromatin compaction and heterochromatin formation. This could be achieved by examining levels of other heterochromatin (H3K27me3) or euchromatin (H3K36me3 and H3K79me3) histone marks. However, altered heterochromatin levels may not be the only contributor to genome instability in *Cbx3* deficient intestines. Given that *Cbx3* has been implicated to play a role in DNA repair pathways (review in Luijsterburg and van Attikum, 2011), deletion of *Cbx3* may result in higher levels of DNA damage. This could be investigated through examining levels of DNA damage markers, such as the histone variant γH2AX, as an indicator of DNA double-strand breaks. Preliminary immunohistochemical analysis of DNA double-strand breaks demonstrated that γH2AX expression level was markedly increased in *Cbx3*-deficient tumours (data not shown). It would also be interesting to analyse the level of γH2AX expression separately in male and female tumours to determine whether there is a male-specific susceptibility to DNA damage. Furthermore, it would also be imperative to investigate RNA splicing (e.g. level of *Rac1b*, the tumour-specific splice variant of *Rac1*) in male and female tumour samples to determine whether there is a male-specific sensitivity towards HP1γ-mediated *Rac1b* splicing in colorectal tumours.

In order to fully understand the relationships between nucleosome organisation, *Cbx3* and gene expression in normal intestinal homeostasis and Wnt-activated tumorigenesis, nucleosome positioning could be performed in intestinal epithelial genome with or without *Cbx3* to gain a detailed picture of how *Cbx3* influence nucleosome positioning in euchromatin and heterochromatin and subsequently facilitate or inhibit gene transcription. To identify genes that are either up-regulated or down-regulated in the absence of *Cbx3*, total RNA from the intestinal epithelium could be extracted and subjected to transcriptome analysis using Next Generation Sequencing. Once the genes with altered expression in the absence of *Cbx3* are identified, *Cbx3*-targeted chromatin immunoprecipitation sequencing (ChIP-seq) analysis could be performed to further investigate the evidence of direct regulation of target genes by *Cbx3*.

Despite the fact that the results of this study are preliminary, current data indicates for the first time that *Cbx3* plays multifaceted roles in intestinal homeostasis and tumorigenesis. *Cbx3* has been implicated to play a novel role in positive regulation of Wnt signalling and RNA splicing in aberrant Wnt-activated intestine and a role in heterochromatin formation and gene silencing in long-term Wnt-activated tumorigenesis. Further phenotypic and mechanistic investigations as outlined previously would provide an increased understanding of the multifaceted roles of *Cbx3* in aberrant Wnt-activation, RNA splicing, tumour progression and invasion, and its interaction with histone marks in our mouse models of colorectal cancer. Such knowledge has the potential to bring about the development of novel prognostic marker or therapeutic agent targeted *Cbx3* in different stages of colorectal cancer, leading to more effective treatment regimes and ultimately resulting in improved patient outcomes.

"Today we are learning the language in which God created life."

US President Bill Clinton

Bibliography

Aasland, R. and Stewart, A.F. (1995) The chromo shadow domain, a second chromo domain in heterochromatin-binding protein 1, HP1. *Nucleic acids research,* 23 (16), pp. 3168-3173.

Abad, A., Massuti, B., Anton, A., Vega, M.E., Yuste, A.L., Marcuello, E., Manzano, J.L., Alonso, V., Carrato, A., Martinez-Villacampa, M., Tabernero, J., Aranda, E., Rivera, F., Diaz-Rubio, E. and Spanish Cooperative Group for Digestive Tumor Therapy (2008) Colorectal cancer metastasis resectability after treatment with the combination of oxaliplatin, irinotecan and 5-fluorouracil. Final results of a phase II study. *Acta Oncologica (Stockholm, Sweden),* 47 (2), pp. 286-292.

Abe, K., Naruse, C., Kato, T., Nishiuchi, T., Saitou, M. and Asano, M. (2011a) Loss of heterochromatin protein 1 gamma reduces the number of primordial germ cells via impaired cell cycle progression in mice. *Biology of reproduction,* 85 (5), pp. 1013-1024.

Abremski, K. and Hoess, R. (1984) Bacteriophage P1 site-specific recombination. Purification and properties of the Cre recombinase protein. *The Journal of biological chemistry,* 259 (3), pp. 1509-1514.

Akhtar, A., Zink, D. and Becker, P.B. (2000) Chromodomains are protein-RNA interaction modules. *Nature,* 407 (6802), pp. 405-409.

Amit, S., Hatzubai, A., Birman, Y., Andersen, J.S., Ben-Shushan, E., Mann, M., Ben-Neriah, Y. and Alkalay, I. (2002) Axin-mediated CKI phosphorylation of beta-catenin at Ser 45: a molecular switch for the Wnt pathway. *Genes & development,* 16 (9), pp. 1066-1076.

Andreu, P., Colnot, S., Godard, C., Gad, S., Chafey, P., Niwa-Kawakita, M., Laurent-Puig, P., Kahn, A., Robine, S., Perret, C. and Romagnolo, B. (2005) Crypt-restricted proliferation and commitment to the Paneth cell lineage following Apc loss in the mouse intestine. *Development (Cambridge, England),* 132 (6), pp. 1443-1451.

Archbold, H.C., Yang, Y.X., Chen, L. and Cadigan, K.M. (2012) How do they do Wnt they do?: regulation of transcription by the Wnt/beta-catenin pathway. *Acta physiologica (Oxford, England),* 204 (1), pp. 74-109.

Artavanis-Tsakonas, S., Rand, M.D. and Lake, R.J. (1999) Notch signaling: cell fate control and signal integration in development. *Science (New York, N.Y.),* 284 (5415), pp. 770-776.

Aucott, R., Bullwinkel, J., Yu, Y., Shi, W., Billur, M., Brown, J.P., Menzel, U., Kioussis, D., Wang, G., Reisert, I., Weimer, J., Pandita, R.K., Sharma, G.G., Pandita, T.K., Fundele, R. and Singh, P.B.

(2008) HP1-beta is required for development of the cerebral neocortex and neuromuscular junctions. *The Journal of cell biology,* 183 (4), pp. 597-606.

Ayoub, N., Jeyasekharan, A.D., Bernal, J.A. and Venkitaraman, A.R. (2008) HP1-beta mobilization promotes chromatin changes that initiate the DNA damage response. *Nature,* 453 (7195), pp. 682-686.

Badugu, R., Shareef, M.M. and Kellum, R. (2003) Novel Drosophila heterochromatin protein 1 (HP1)/origin recognition complex-associated protein (HOAP) repeat motif in HP1/HOAP interactions and chromocenter associations. *The Journal of biological chemistry,* 278 (36), pp. 34491-34498.

Bagchi,A.; Papazoglu,C.; Wu,Y.; Capurso,D.; Brodt,M.; Francis,D.; Bredel,M.; Vogel,H.; Mills,A.A.(2007) CHD is a tumor suppressor at human 1p36. *Cell*, 128, 3, pp. 459-475.

Ball, L.J., Murzina, N.V., Broadhurst, R.W., Raine, A.R., Archer, S.J., Stott, F.J., Murzin, A.G., Singh, P.B., Domaille, P.J. and Laue, E.D. (1997) Structure of the chromatin binding (chromo) domain from mouse modifier protein 1. *The EMBO journal,* 16 (9), pp. 2473-2481.

Bannister, A.J., Zegerman, P., Partridge, J.F., Miska, E.A., Thomas, J.O., Allshire, R.C. and Kouzarides, T. (2001a) Selective recognition of methylated lysine 9 on histone H3 by the HP1 chromo domain. *Nature,* 410 (6824), pp. 120-124.

Barker, N. (2014) Adult intestinal stem cells: critical drivers of epithelial homeostasis and regeneration. *Nature reviews.Molecular cell biology,* 15 (1), pp. 19-33.

Barker, N., van Es, J.H., Kuipers, J., Kujala, P., van den Born, M., Cozijnsen, M., Haegebarth, A., Korving, J., Begthel, H., Peters, P.J. and Clevers, H. (2007a) Identification of stem cells in small intestine and colon by marker gene Lgr5. *Nature,* 449 (7165), pp. 1003-1007.

Bartkova, J., Moudry, P., Hodny, Z., Lukas, J., Rajpert-De Meyts, E. and Bartek, J. (2011) Heterochromatin marks HP1gamma, HP1alpha and H3K9me3, and DNA damage response activation in human testis development and germ cell tumours. *International journal of andrology,* 34 (4 Pt 2), pp. e103-13.

Betz, U.A., Vosshenrich, C.A., Rajewsky, K. and Muller, W. (1996) Bypass of lethality with mosaic mice generated by Cre-loxP-mediated recombination. *Current biology : CB,* 6 (10), pp. 1307-1316.

Bevins, C.L. and Salzman, N.H. (2011) Paneth cells, antimicrobial peptides and maintenance of intestinal homeostasis. *Nature reviews.Microbiology,* 9 (5), pp. 356-368.

Bjerknes, M. and Cheng, H. (1981) Methods for the isolation of intact epithelium from the mouse intestine. *The Anatomical Record,* 199 (4), pp. 565-574.

Black, J.C., Allen, A., Van Rechem, C., Forbes, E., Longworth, M., Tschop, K., Rinehart, C., Quiton, J., Walsh, R., Smallwood, A., Dyson, N.J. and Whetstine, J.R. (2010) Conserved antagonism between JMJD2A/KDM4A and HP1gamma during cell cycle progression. *Molecular cell,* 40 (5), pp. 736-748.

Bodmer, W.F., Bailey, C.J., Bodmer, J., Bussey, H.J., Ellis, A., Gorman, P., Lucibello, F.C., Murday, V.A., Rider, S.H. and Scambler, P. (1987) Localization of the gene for familial adenomatous polyposis on chromosome 5. *Nature,* 328 (6131), pp. 614-616.

Bos, J.L. (1989) Ras Oncogenes in Human Cancer: a Review. *Cancer research,* 49 (17), pp. 4682-4689.

Brasher, S.V., Smith, B.O., Fogh, R.H., Nietlispach, D., Thiru, A., Nielsen, P.R., Broadhurst, R.W., Ball, L.J., Murzina, N.V. and Laue, E.D. (2000) The structure of mouse HP1 suggests a unique mode of single peptide recognition by the shadow chromo domain dimer. *The EMBO journal,* 19 (7), pp. 1587-1597.

Brown, J.P., Bullwinkel, J., Baron-Luhr, B., Billur, M., Schneider, P., Winking, H. and Singh, P.B. (2010a) HP1gamma function is required for male germ cell survival and spermatogenesis. *Epigenetics & chromatin,* 3 (1), pp. 9-8935-3-9.

Buczacki, S.J., Zecchini, H.I., Nicholson, A.M., Russell, R., Vermeulen, L., Kemp, R. and Winton, D.J. (2013) Intestinal label-retaining cells are secretory precursors expressing Lgr5. *Nature,* 495 (7439), pp. 65-69.

Cammas, F., Herzog, M., Lerouge, T., Chambon, P. and Losson, R. (2004) Association of the transcriptional corepressor TIF1beta with heterochromatin protein 1 (HP1): an essential role for progression through differentiation. *Genes & development,* 18 (17), pp. 2147-2160.

Cammas, F., Oulad-Abdelghani, M., Vonesch, J.L., Huss-Garcia, Y., Chambon, P. and Losson, R. (2002) Cell differentiation induces TIF1beta association with centromeric heterochromatin via an HP1 interaction. *Journal of cell science,* 115 (Pt 17), pp. 3439-3448.

Canzio, D., Chang, E.Y., Shankar, S., Kuchenbecker, K.M., Simon, M.D., Madhani, H.D., Narlikar, G.J. and Al-Sady, B. (2011) Chromodomain-mediated oligomerization of HP1 suggests a nucleosome-bridging mechanism for heterochromatin assembly. *Molecular cell,* 41 (1), pp. 67-81.

Cedar, H. and Bergman, Y. (2009) Linking DNA methylation and histone modification: patterns and paradigms. *Nature reviews.Genetics,* 10 (5), pp. 295-304.

Cheng, H. (1974) Origin, differentiation and renewal of the four main epithelial cell types in the mouse small intestine. II. Mucous cells. *The American Journal of Anatomy,* 141 (4), pp. 481-501.

Cheng, H. and Leblond, C.P. (1974) Origin, differentiation and renewal of the four main epithelial cell types in the mouse small intestine. V. Unitarian Theory of the origin of the four epithelial cell types. *The American Journal of Anatomy,* 141 (4), pp. 537-561.

Cheng, H., Merzel, J. and Leblond, C.P. (1969) Renewal of Paneth cells in the small intestine of the mouse. *The American Journal of Anatomy,* 126 (4), pp. 507-525.

Choi, D., Lee, H.W., Hur, K.Y., Kim, J.J., Park, G.S., Jang, S.H., Song, Y.S., Jang, K.S. and Paik, S.S. (2009) Cancer stem cell markers CD133 and CD24 correlate with invasiveness and differentiation in colorectal adenocarcinoma. *World journal of gastroenterology : WJG,* 15 (18), pp. 2258-2264.

Chow, E. and Macrae, F. (2005) A review of juvenile polyposis syndrome. *Journal of gastroenterology and hepatology,* 20 (11), pp. 1634-1640.

Clarke, A.R., Cummings, M.C. and Harrison, D.J. (1995) Interaction between murine germline mutations in p53 and APC predisposes to pancreatic neoplasia but not to increased intestinal malignancy. *Oncogene,* 11 (9), pp. 1913-1920.

Cleveland, A.G., Oikarinen, S.I., Bynote, K.K., Marttinen, M., Rafter, J.J., Gustafsson, J.A., Roy, S.K., Pitot, H.C., Korach, K.S., Lubahn, D.B., Mutanen, M. and Gould, K.A. (2009) Disruption of estrogen receptor signaling enhances intestinal neoplasia in Apc(Min/+) mice. *Carcinogenesis,* 30 (9), pp. 1581-1590.

Clevers, H. (2006) Wnt/beta-catenin signaling in development and disease. *Cell,* 127 (3), pp. 469-480.

Cowieson, N.P., Partridge, J.F., Allshire, R.C. and McLaughlin, P.J. (2000) Dimerisation of a chromo shadow domain and distinctions from the chromodomain as revealed by structural analysis. *Current biology : CB,* 10 (9), pp. 517-525.

Crane, R. (1968) Digestive-absorptive surface of the small bowel mucosa. *Annual Review of Medicine,* 19, pp. 57-68.

Cryderman, D.E., Grade, S.K., Li, Y., Fanti, L., Pimpinelli, S. and Wallrath, L.L. (2005) Role of Drosophila HP1 in euchromatic gene expression. *Developmental dynamics : an official publication of the American Association of Anatomists,* 232 (3), pp. 767-774.

Dambacher, S., Hahn, M. and Schotta, G. (2013) The compact view on heterochromatin. *Cell cycle (Georgetown, Tex.),* 12 (18), pp. 2925-2926.

Daniels, D.L. and Weis, W.I. (2005) Beta-catenin directly displaces Groucho/TLE repressors from Tcf/Lef in Wnt-mediated transcription activation. *Nature structural & molecular biology,* 12 (4), pp. 364-371.

Dawson, M.A., Bannister, A.J., Gottgens, B., Foster, S.D., Bartke, T., Green, A.R. and Kouzarides, T. (2009) JAK2 phosphorylates histone H3Y41 and excludes HP1alpha from chromatin. *Nature,* 461 (7265), pp. 819-822.

de Wit, E., Greil, F. and van Steensel, B. (2007) High-resolution mapping reveals links of HP1 with active and inactive chromatin components. *PLoS genetics,* 3 (3), pp. e38.

Di Cristofano, A. and Pandolfi, P.P. (2000) The multiple roles of PTEN in tumor suppression. *Cell,* 100 (4), pp. 387-390.

Dialynas, G.K., Terjung, S., Brown, J.P., Aucott, R.L., Baron-Luhr, B., Singh, P.B. and Georgatos, S.D. (2007) Plasticity of HP1 proteins in mammalian cells. *Journal of cell science,* 120 (Pt 19), pp. 3415-3424.

Dinant, C. and Luijsterburg, M.S. (2009) The emerging role of HP1 in the DNA damage response. *Molecular and cellular biology,* 29 (24), pp. 6335-6340.

Dumont, N. and Arteaga, C.L. (2003) Targeting the TGF beta signaling network in human neoplasia. *Cancer cell,* 3 (6), pp. 531-536.

Ebert, A., Lein, S., Schotta, G. and Reuter, G. (2006) Histone modification and the control of heterochromatic gene silencing in Drosophila. *Chromosome research : an international journal*

on the molecular, supramolecular and evolutionary aspects of chromosome biology, 14 (4), pp. 377-392.

Ehrlich, M. (2002) DNA methylation in cancer: too much, but also too little. *Oncogene,* 21 (35), pp. 5400-5413.

Eissenberg, J.C. (2001) Molecular biology of the chromo domain: an ancient chromatin module comes of age. *Gene,* 275 (1), pp. 19-29.

Eissenberg, J.C. and Elgin, S.C. (2000) The HP1 protein family: getting a grip on chromatin. *Current opinion in genetics & development,* 10 (2), pp. 204-210.

Eissenberg, J.C., James, T.C., Foster-Hartnett, D.M., Hartnett, T., Ngan, V. and Elgin, S.C. (1990) Mutation in a heterochromatin-specific chromosomal protein is associated with suppression of position-effect variegation in Drosophila melanogaster. *Proceedings of the National Academy of Sciences of the United States of America,* 87 (24), pp. 9923-9927.

el Marjou, F., Janssen, K.P., Chang, B.H., Li, M., Hindie, V., Chan, L., Louvard, D., Chambon, P., Metzger, D. and Robine, S. (2004a) Tissue-specific and inducible Cre-mediated recombination in the gut epithelium. *Genesis (New York, N.Y.: 2000),* 39 (3), pp. 186-193.

Engelman, J.A. (2009) Targeting PI3K signalling in cancer: opportunities, challenges and limitations. *Nature reviews.Cancer,* 9 (8), pp. 550-562.

Esufali, S., Charames, G.S. and Bapat, B. (2007) Suppression of nuclear Wnt signaling leads to stabilization of Rac1 isoforms. *FEBS letters,* 581 (25), pp. 4850-4856.

Esufali, S., Charames, G.S., Pethe, V.V., Buongiorno, P. and Bapat, B. (2007) Activation of tumor-specific splice variant Rac1b by dishevelled promotes canonical Wnt signaling and decreased adhesion of colorectal cancer cells. *Cancer research,* 67 (6), pp. 2469-2479.

Ewan, K., Pajak, B., Stubbs, M., Todd, H., Barbeau, O., Quevedo, C., Botfield, H., Young, R., Ruddle, R., Samuel, L., Battersby, A., Raynaud, F., Allen, N., Wilson, S., Latinkic, B., Workman, P., McDonald, E., Blagg, J., Aherne, W. and Dale, T. (2010) A useful approach to identify novel small-molecule inhibitors of Wnt-dependent transcription. *Cancer research,* 70 (14), pp. 5963-5973.

Fanti, L. and Pimpinelli, S. (2008) HP1: a functionally multifaceted protein. *Current opinion in genetics & development,* 18 (2), pp. 169-174.

Farin, H.F., Van Es, J.H. and Clevers, H. (2012) Redundant sources of Wnt regulate intestinal stem cells and promote formation of Paneth cells. *Gastroenterology,* 143 (6), pp. 1518-1529.e7.

Fazeli, A., Dickinson, S.L., Hermiston, M.L., Tighe, R.V., Steen, R.G., Small, C.G., Stoeckli, E.T., Keino-Masu, K., Masu, M., Rayburn, H., Simons, J., Bronson, R.T., Gordon, J.I., Tessier-Lavigne, M. and Weinberg, R.A. (1997) Phenotype of mice lacking functional Deleted in colorectal cancer (Dcc) gene. *Nature,* 386 (6627), pp. 796-804.

Fearon, E.R. and Vogelstein, B. (1990a) A genetic model for colorectal tumorigenesis. *Cell,* 61 (5), pp. 759-767.

Feil, R., Brocard, J., Mascrez, B., LeMeur, M., Metzger, D. and Chambon, P. (1996) Ligand-activated site-specific recombination in mice. *Proceedings of the National Academy of Sciences of the United States of America,* 93 (20), pp. 10887-10890.

Fevr, T., Robine, S., Louvard, D. and Huelsken, J. (2007) Wnt/beta-catenin is essential for intestinal homeostasis and maintenance of intestinal stem cells. *Molecular and cellular biology,* 27 (21), pp. 7551-7559.

Fiegen, D., Haeusler, L.C., Blumenstein, L., Herbrand, U., Dvorsky, R., Vetter, I.R. and Ahmadian, M.R. (2004) Alternative splicing of Rac1 generates Rac1b, a self-activating GTPase. *The Journal of biological chemistry,* 279 (6), pp. 4743-4749.

Fischle, W., Tseng, B.S., Dormann, H.L., Ueberheide, B.M., Garcia, B.A., Shabanowitz, J., Hunt, D.F., Funabiki, H. and Allis, C.D. (2005) Regulation of HP1-chromatin binding by histone H3 methylation and phosphorylation. *Nature,* 438 (7071), pp. 1116-1122.

Flint, N., Cove, F.L. and Evans, G.S. (1991) A low-temperature method for the isolation of small-intestinal epithelium along the crypt-villus axis. *The Biochemical journal,* 280 (Pt 2) (Pt 2), pp. 331-334.

Fraga, M.F., Ballestar, E., Villar-Garea, A., Boix-Chornet, M., Espada, J., Schotta, G., Bonaldi, T., Haydon, C., Ropero, S., Petrie, K., Iyer, N.G., Perez-Rosado, A., Calvo, E., Lopez, J.A., Cano, A., Calasanz, M.J., Colomer, D., Piris, M.A., Ahn, N., Imhof, A., Caldas, C., Jenuwein, T. and Esteller, M. (2005) Loss of acetylation at Lys16 and trimethylation at Lys20 of histone H4 is a common hallmark of human cancer. *Nature genetics,* 37 (4), pp. 391-400.

Fraser, E., Young, N., Dajani, R., Franca-Koh, J., Ryves, J., Williams, R.S., Yeo, M., Webster, M.T., Richardson, C., Smalley, M.J., Pearl, L.H., Harwood, A. and Dale, T.C. (2002) Identification of the

Axin and Frat binding region of glycogen synthase kinase-3. *The Journal of biological chemistry,* 277 (3), pp. 2176-2185.

Fre, S., Bardin, A., Robine, S. and Louvard, D. (2011) Notch signaling in intestinal homeostasis across species: the cases of Drosophila, Zebrafish and the mouse. *Experimental cell research,* 317 (19), pp. 2740-2747.

Fre, S., Huyghe, M., Mourikis, P., Robine, S., Louvard, D. and Artavanis-Tsakonas, S. (2005) Notch signals control the fate of immature progenitor cells in the intestine. *Nature,* 435 (7044), pp. 964-968.

Fre, S., Pallavi, S.K., Huyghe, M., Lae, M., Janssen, K.P., Robine, S., Artavanis-Tsakonas, S. and Louvard, D. (2009) Notch and Wnt signals cooperatively control cell proliferation and tumorigenesis in the intestine. *Proceedings of the National Academy of Sciences of the United States of America,* 106 (15), pp. 6309-6314.

Gerbe, F., Brulin, B., Makrini, L., Legraverend, C. and Jay, P. (2009) DCAMKL-1 expression identifies Tuft cells rather than stem cells in the adult mouse intestinal epithelium. *Gastroenterology,* 137 (6), pp. 2179-80; author reply 2180-1.

Gerber, M. and Shilatifard, A. (2003) Transcriptional elongation by RNA polymerase II and histone methylation. *The Journal of biological chemistry,* 278 (29), pp. 26303-26306.

Goldberg, A.D., Allis, C.D. and Bernstein, E. (2007) Epigenetics: a landscape takes shape. *Cell,* 128 (4), pp. 635-638.

Goncalves, V., Henriques, A., Pereira, J., Neves Costa, A., Moyer, M.P., Moita, L.F., Gama-Carvalho, M., Matos, P. and Jordan, P. (2014) Phosphorylation of SRSF1 by SRPK1 regulates alternative splicing of tumor-related Rac1b in colorectal cells. *RNA (New York, N.Y.),* 20 (4), pp. 474-482.

Goncalves, V., Matos, P. and Jordan, P. (2009) Antagonistic SR proteins regulate alternative splicing of tumor-related Rac1b downstream of the PI3-kinase and Wnt pathways. *Human molecular genetics,* 18 (19), pp. 3696-3707.

Grewal, S.I. and Jia, S. (2007) Heterochromatin revisited. *Nature reviews.Genetics,* 8 (1), pp. 35-46.

Groden, J., Thliveris, A., Samowitz, W., Carlson, M., Gelbert, L., Albertsen, H., Joslyn, G., Stevens, J., Spirio, L. and Robertson, M. (1991a) Identification and characterization of the familial adenomatous polyposis coli gene. *Cell,* 66 (3), pp. 589-600.

Guyton A.C., H.J.E. (1996) *Textbook of Medical Physiology.* 9th Edition ed. London: W.B. Saunders.

Haldar, S., Saini, A., Nanda, J.S., Saini, S. and Singh, J. (2011) Role of Swi6/HP1 self-association-mediated recruitment of Clr4/Suv39 in establishment and maintenance of heterochromatin in fission yeast. *The Journal of biological chemistry,* 286 (11), pp. 9308-9320.

Hall, P.A., Coates, P.J., Ansari, B. and Hopwood, D. (1994) Regulation of cell number in the mammalian gastrointestinal tract: the importance of apoptosis. *Journal of cell science,* 107 (Pt 12) (Pt 12), pp. 3569-3577.

Hammoudi, A., Song, F., Reed, K.R., Jenkins, R.E., Meniel, V.S., Watson, A.J., Pritchard, D.M., Clarke, A.R. and Jenkins, J.R. (2013) Proteomic profiling of a mouse model of acute intestinal Apc deletion leads to identification of potential novel biomarkers of human colorectal cancer (CRC). *Biochemical and biophysical research communications,* 440 (3), pp. 364-370.

Han, S.S., Kim, W.J., Hong, Y., Hong, S.H., Lee, S.J., Ryu, D.R., Lee, W., Cho, Y.H., Lee, S., Ryu, Y.J., Won, J.Y., Rhee, H., Park, J.H., Jang, S.J., Lee, J.S., Choi, C.M., Lee, J.C., Lee, S.D. and Oh, Y.M. (2014) RNA sequencing identifies novel markers of non-small cell lung cancer. *Lung cancer (Amsterdam, Netherlands),* 84 (3), pp. 229-235.

Harada, N., Tamai, Y., Ishikawa, T., Sauer, B., Takaku, K., Oshima, M. and Taketo, M.M. (1999) Intestinal polyposis in mice with a dominant stable mutation of the beta-catenin gene. *The EMBO journal,* 18 (21), pp. 5931-5942.

Haramis, A.P., Begthel, H., van den Born, M., van Es, J., Jonkheer, S., Offerhaus, G.J. and Clevers, H. (2004) De novo crypt formation and juvenile polyposis on BMP inhibition in mouse intestine. *Science (New York, N.Y.),* 303 (5664), pp. 1684-1686.

Hart, M., Concordet, J.P., Lassot, I., Albert, I., del los Santos, R., Durand, H., Perret, C., Rubinfeld, B., Margottin, F., Benarous, R. and Polakis, P. (1999) The F-box protein beta-TrCP associates with phosphorylated beta-catenin and regulates its activity in the cell. *Current biology : CB,* 9 (4), pp. 207-210.

He, X.C., Zhang, J., Tong, W.G., Tawfik, O., Ross, J., Scoville, D.H., Tian, Q., Zeng, X., He, X., Wiedemann, L.M., Mishina, Y. and Li, L. (2004) BMP signaling inhibits intestinal stem cell self-renewal through suppression of Wnt-beta-catenin signaling. *Nature genetics,* 36 (10), pp. 1117-1121.

He,Y.Q.; Sheng,J.Q.; Ling,X.L.; Fu,L.; Jin P.; Yen,L.; Rao,J. (2012) Estradiol regulates miR-135b and mismatch repair gene expressions via estrogen receptor-beta in colorectal cells. *Exp.Mol.Med*, 44(12), pp. 723-732.

Hediger, F. and Gasser, S.M. (2006) Heterochromatin protein 1: don't judge the book by its cover! *Current opinion in genetics & development,* 16 (2), pp. 143-150.

Helton, E.S. and Chen, X. (2007) p53 modulation of the DNA damage response. *Journal of cellular biochemistry,* 100 (4), pp. 883-896.

Heyer, J., Yang, K., Lipkin, M., Edelmann, W. and Kucherlapati, R. (1999) Mouse models for colorectal cancer. *Oncogene,* 18 (38), pp. 5325-5333.

Hirota, T., Lipp, J.J., Toh, B.H. and Peters, J.M. (2005) Histone H3 serine 10 phosphorylation by Aurora B causes HP1 dissociation from heterochromatin. *Nature,* 438 (7071), pp. 1176-1180.

Hocker, M. and Wiedenmann, B. (1998) Molecular mechanisms of enteroendocrine differentiation. *Annals of the New York Academy of Sciences,* 859, pp. 160-174.

Hoess, R.H., Ziese, M. and Sternberg, N. (1982) P1 site-specific recombination: nucleotide sequence of the recombining sites. *Proceedings of the National Academy of Sciences of the United States of America,* 79 (11), pp. 3398-3402.

Hon, G.C., Hawkins, R.D. and Ren, B. (2009) Predictive chromatin signatures in the mammalian genome. *Human molecular genetics,* 18 (R2), pp. R195-201.

Howe, J.R., Sayed, M.G., Ahmed, A.F., Ringold, J., Larsen-Haidle, J., Merg, A., Mitros, F.A., Vaccaro, C.A., Petersen, G.M., Giardiello, F.M., Tinley, S.T., Aaltonen, L.A. and Lynch, H.T. (2004) The prevalence of MADH4 and BMPR1A mutations in juvenile polyposis and absence of BMPR2, BMPR1B, and ACVR1 mutations. *Journal of medical genetics,* 41 (7), pp. 484-491.

Huang, H.C. and Klein, P.S. (2004) The Frizzled family: receptors for multiple signal transduction pathways. *Genome biology,* 5 (7), pp. 234.

Iacopetta, B. (2003) TP53 mutation in colorectal cancer. *Human mutation,* 21 (3), pp. 271-276.

Ireland, H., Houghton, C., Howard, L. and Winton, D.J. (2005) Cellular inheritance of a Cre-activated reporter gene to determine Paneth cell longevity in the murine small intestine. *Developmental dynamics : an official publication of the American Association of Anatomists,* 233 (4), pp. 1332-1336.

Ireland, H., Kemp, R., Houghton, C., Howard, L., Clarke, A.R., Sansom, O.J. and Winton, D.J. (2004) Inducible Cre-mediated control of gene expression in the murine gastrointestinal tract: effect of loss of beta-catenin. *Gastroenterology,* 126 (5), pp. 1236-1246.

Ishizuya-Oka, A. (2005) Epithelial-connective tissue cross-talk is essential for regeneration of intestinal epithelium. *Journal of Nippon Medical School = Nippon Ika Daigaku zasshi,* 72 (1), pp. 13-18.

Jacobs, S.A. and Khorasanizadeh, S. (2002a) Structure of HP1 chromodomain bound to a lysine 9-methylated histone H3 tail. *Science (New York, N.Y.),* 295 (5562), pp. 2080-2083.

Jacobs, S.A., Taverna, S.D., Zhang, Y., Briggs, S.D., Li, J., Eissenberg, J.C., Allis, C.D. and Khorasanizadeh, S. (2001) Specificity of the HP1 chromo domain for the methylated N-terminus of histone H3. *The EMBO journal,* 20 (18), pp. 5232-5241.

James, T.C., Eissenberg, J.C., Craig, C., Dietrich, V., Hobson, A. and Elgin, S.C. (1989) Distribution patterns of HP1, a heterochromatin-associated nonhistone chromosomal protein of Drosophila. *European journal of cell biology,* 50 (1), pp. 170-180.

James, T.C. and Elgin, S.C. (1986) Identification of a nonhistone chromosomal protein associated with heterochromatin in Drosophila melanogaster and its gene. *Molecular and cellular biology,* 6 (11), pp. 3862-3872.

Jass, J.R., Young, J. and Leggett, B.A. (2002) Evolution of colorectal cancer: change of pace and change of direction. *Journal of gastroenterology and hepatology,* 17 (1), pp. 17-26.

Jenuwein, T. and Allis, C.D. (2001) Translating the histone code. *Science (New York, N.Y.),* 293 (5532), pp. 1074-1080.

Joslyn, G., Carlson, M., Thliveris, A., Albertsen, H., Gelbert, L., Samowitz, W., Groden, J., Stevens, J., Spirio, L. and Robertson, M. (1991) Identification of deletion mutations and three new genes at the familial polyposis locus. *Cell,* 66 (3), pp. 601-613.

Jubb, A.M., Chalasani, S., Frantz, G.D., Smits, R., Grabsch, H.I., Kavi, V., Maughan, N.J., Hillan, K.J., Quirke, P. and Koeppen, H. (2006) Achaete-scute like 2 (ascl2) is a target of Wnt signalling and is upregulated in intestinal neoplasia. *Oncogene,* 25 (24), pp. 3445-3457.

Keino-Masu, K., Masu, M., Hinck, L., Leonardo, E.D., Chan, S.S., Culotti, J.G. and Tessier-Lavigne, M. (1996) Deleted in Colorectal Cancer (DCC) encodes a netrin receptor. *Cell,* 87 (2), pp. 175-185.

Kellum, R. (2003) HP1 complexes and heterochromatin assembly. *Current topics in microbiology and immunology,* 274, pp. 53-77.

Kemp, R., Ireland, H., Clayton, E., Houghton, C., Howard, L. and Winton, D.J. (2004) Elimination of background recombination: somatic induction of Cre by combined transcriptional regulation and hormone binding affinity. *Nucleic acids research,* 32 (11), pp. e92.

Kennelly,R.; Kavanagh,D.O.; Hogan,A.M.; Winter,D.C. (2008) Oestrogen and the colon: potential mechanisms for cancer prevention. *Lancet Oncol.,* 2008, 9, 4, 385-391

Kim, H.A., Koo, B.K., Cho, J.H., Kim, Y.Y., Seong, J., Chang, H.J., Oh, Y.M., Stange, D.E., Park, J.G., Hwang, D. and Kong, Y.Y. (2012) Notch1 counteracts WNT/beta-catenin signaling through chromatin modification in colorectal cancer. *The Journal of clinical investigation,* 122 (9), pp. 3248-3259.

Kim, J.J., Baek, M.J., Kim, L., Kim, N.G., Lee, Y.C., Song, S.Y., Noh, S.H. and Kim, H. (1999) Accumulated frameshift mutations at coding nucleotide repeats during the progression of gastric carcinoma with microsatellite instability. *Laboratory investigation; a journal of technical methods and pathology,* 79 (9), pp. 1113-1120.

Kinzler, K.W. and Vogelstein, B. (1996) Lessons from hereditary colorectal cancer. *Cell,* 87 (2), pp. 159-170.

Kirschmann, D.A., Lininger, R.A., Gardner, L.M., Seftor, E.A., Odero, V.A., Ainsztein, A.M., Earnshaw, W.C., Wallrath, L.L. and Hendrix, M.J. (2000) Down-regulation of HP1Hsalpha expression is associated with the metastatic phenotype in breast cancer. *Cancer research,* 60 (13), pp. 3359-3363.

Knudson, A.G. (2001) Two genetic hits (more or less) to cancer. *Nature reviews.Cancer,* 1 (2), pp. 157-162.

Ko, M., Sohn, D.H., Chung, H., Seong, R.H., (2008) Chromatin remodeling, development and disease. *Mutat. Res.*, 647, pp59-67.

Korinek, V., Barker, N., Moerer, P., van Donselaar, E., Huls, G., Peters, P.J. and Clevers, H. (1998) Depletion of epithelial stem-cell compartments in the small intestine of mice lacking Tcf-4. *Nature genetics,* 19 (4), pp. 379-383.

Korinek, V., Barker, N., Morin, P.J., van Wichen, D., de Weger, R., Kinzler, K.W., Vogelstein, B. and Clevers, H. (1997) Constitutive transcriptional activation by a beta-catenin-Tcf complex in APC-/- colon carcinoma. *Science (New York, N.Y.),* 275 (5307), pp. 1784-1787.

Kourmouli, N., Jeppesen, P., Mahadevhaiah, S., Burgoyne, P., Wu, R., Gilbert, D.M., Bongiorni, S., Prantera, G., Fanti, L., Pimpinelli, S., Shi, W., Fundele, R. and Singh, P.B. (2004) Heterochromatin and tri-methylated lysine 20 of histone H4 in animals. *Journal of cell science,* 117 (Pt 12), pp. 2491-2501.

Kourmouli, N., Theodoropoulos, P.A., Dialynas, G., Bakou, A., Politou, A.S., Cowell, I.G., Singh, P.B. and Georgatos, S.D. (2000) Dynamic associations of heterochromatin protein 1 with the nuclear envelope. *The EMBO journal,* 19 (23), pp. 6558-6568.

Kouzarides, T. (2007a) Chromatin modifications and their function. *Cell,* 128 (4), pp. 693-705.

Kuehn, M.R., Bradley, A., Robertson, E.J. and Evans, M.J. (1987) A potential animal model for Lesch-Nyhan syndrome through introduction of HPRT mutations into mice. *Nature,* 326 (6110), pp. 295-298.

Kwon, O.H., Park, J.L., Baek, S.J., Noh, S.M., Song, K.S., Kim, S.Y. and Kim, Y.S. (2013) Aberrant upregulation of ASCL2 by promoter demethylation promotes the growth and resistance to 5-fluorouracil of gastric cancer cells. *Cancer science,* 104 (3), pp. 391-397.

Kwon, S.H., Florens, L., Swanson, S.K., Washburn, M.P., Abmayr, S.M. and Workman, J.L. (2010) Heterochromatin protein 1 (HP1) connects the FACT histone chaperone complex to the phosphorylated CTD of RNA polymerase II. *Genes & development,* 24 (19), pp. 2133-2145.

Lachner, M., O'Carroll, D., Rea, S., Mechtler, K. and Jenuwein, T. (2001) Methylation of histone H3 lysine 9 creates a binding site for HP1 proteins. *Nature,* 410 (6824), pp. 116-120.

Larson, K., Yan, S.J., Tsurumi, A., Liu, J., Zhou, J., Gaur, K., Guo, D., Eickbush, T.H. and Li, W.X. (2012) Heterochromatin formation promotes longevity and represses ribosomal RNA synthesis. *PLoS genetics,* 8 (1), pp. e1002473.

Levy, D.B., Smith, K.J., Beazer-Barclay, Y., Hamilton, S.R., Vogelstein, B. and Kinzler, K.W. (1994) Inactivation of both APC alleles in human and mouse tumors. *Cancer research,* 54 (22), pp. 5953-5958.

Li, F.P., Fraumeni, J.F.,Jr, Mulvihill, J.J., Blattner, W.A., Dreyfus, M.G., Tucker, M.A. and Miller, R.W. (1988) A cancer family syndrome in twenty-four kindreds. *Cancer research,* 48 (18), pp. 5358-5362.

Li, W.H., Yi, S. and Makova, K. (2002) Male-driven evolution. *Current opinion in genetics & development,* 12 (6), pp. 650-656.

Lin, R.J., Nagy, L., Inoue, S., Shao, W., Miller, W.H.J., Evans, R.M. (1998) Role of the histone deacetylase complex in acute promyelocytic leukaemia. *Nature*, 391 (6669), pp. 811-814.

Liu, C., Li, Y., Semenov, M., Han, C., Baeg, G.H., Tan, Y., Zhang, Z., Lin, X. and He, X. (2002) Control of beta-catenin phosphorylation/degradation by a dual-kinase mechanism. *Cell,* 108 (6), pp. 837-847.

Liu, P., Cheng, H., Roberts, T.M. and Zhao, J.J. (2009) Targeting the phosphoinositide 3-kinase pathway in cancer. *Nature reviews.Drug discovery,* 8 (8), pp. 627-644.

Livak, K.J. and Schmittgen, T.D. (2001) Analysis of relative gene expression data using real-time quantitative PCR and the 2(-Delta Delta C(T)) Method. *Methods (San Diego, Calif.),* 25 (4), pp. 402-408.

Lomberk, G., Bensi, D., Fernandez-Zapico, M.E. and Urrutia, R. (2006) Evidence for the existence of an HP1-mediated subcode within the histone code. *Nature cell biology,* 8 (4), pp. 407-415.

Lomberk, G., Wallrath, L. and Urrutia, R. (2006) The Heterochromatin Protein 1 family. *Genome biology,* 7 (7), pp. 228.

Luger, K., Mader, A.W., Richmond, R.K., Sargent, D.F. and Richmond, T.J. (1997) Crystal structure of the nucleosome core particle at 2.8 A resolution. *Nature,* 389 (6648), pp. 251-260.

Luijsterburg, M.S., Dinant, C., Lans, H., Stap, J., Wiernasz, E., Lagerwerf, S., Warmerdam, D.O., Lindh, M., Brink, M.C., Dobrucki, J.W., Aten, J.A., Fousteri, M.I., Jansen, G., Dantuma, N.P., Vermeulen, W., Mullenders, L.H., Houtsmuller, A.B., Verschure, P.J. and van Driel, R. (2009) Heterochromatin protein 1 is recruited to various types of DNA damage. *The Journal of cell biology,* 185 (4), pp. 577-586.

Luijsterburg, M.S. and van Attikum, H. (2011) Chromatin and the DNA damage response: the cancer connection. *Molecular oncology,* 5 (4), pp. 349-367.

Madison, B.B., Braunstein, K., Kuizon, E., Portman, K., Qiao, X.T. and Gumucio, D.L. (2005) Epithelial hedgehog signals pattern the intestinal crypt-villus axis. *Development (Cambridge, England),* 132 (2), pp. 279-289.

Maison, C. and Almouzni, G. (2004a) HP1 and the dynamics of heterochromatin maintenance. *Nature reviews.Molecular cell biology,* 5 (4), pp. 296-304.

Marshman, E., Booth, C. and Potten, C.S. (2002) The intestinal epithelial stem cell. *BioEssays : news and reviews in molecular, cellular and developmental biology,* 24 (1), pp. 91-98.

Mateescu, B., Bourachot, B., Rachez, C., Ogryzko, V. and Muchardt, C. (2008) Regulation of an inducible promoter by an HP1beta-HP1gamma switch. *EMBO reports,* 9 (3), pp. 267-272.

Mateescu, B., England, P., Halgand, F., Yaniv, M. and Muchardt, C. (2004) Tethering of HP1 proteins to chromatin is relieved by phosphoacetylation of histone H3. *EMBO reports,* 5 (5), pp. 490-496.

Matos, P. and Jordan, P. (2008) Increased Rac1b expression sustains colorectal tumor cell survival. *Molecular cancer research : MCR,* 6 (7), pp. 1178-1184.

Matos, P., Oliveira, C., Velho, S., Goncalves, V., da Costa, L.T., Moyer, M.P., Seruca, R. and Jordan, P. (2008) B-Raf(V600E) cooperates with alternative spliced Rac1b to sustain colorectal cancer cell survival. *Gastroenterology,* 135 (3), pp. 899-906.

May, R., Riehl, T.E., Hunt, C., Sureban, S.M., Anant, S. and Houchen, C.W. (2008) Identification of a novel putative gastrointestinal stem cell and adenoma stem cell marker, doublecortin and CaM kinase-like-1, following radiation injury and in adenomatous polyposis coli/multiple intestinal neoplasia mice. *Stem cells (Dayton, Ohio),* 26 (3), pp. 630-637.

Miller, J.R. and Moon, R.T. (1996) Signal transduction through beta-catenin and specification of cell fate during embryogenesis. *Genes & development,* 10 (20), pp. 2527-2539.

Minc, E., Courvalin, J.C. and Buendia, B. (2000) HP1gamma associates with euchromatin and heterochromatin in mammalian nuclei and chromosomes. *Cytogenetics and cell genetics,* 90 (3-4), pp. 279-284.

Morin, P.J., Sparks, A.B., Korinek, V., Barker, N., Clevers, H., Vogelstein, B. and Kinzler, K.W. (1997) Activation of beta-catenin-Tcf signaling in colon cancer by mutations in beta-catenin or APC. *Science (New York, N.Y.),* 275 (5307), pp. 1787-1790.

Moser, A.R., Pitot, H.C. and Dove, W.F. (1990a) A dominant mutation that predisposes to multiple intestinal neoplasia in the mouse. *Science (New York, N.Y.),* 247 (4940), pp. 322-324.

Moser, A.R., Shoemaker, A.R., Connelly, C.S., Clipson, L., Gould, K.A., Luongo, C., Dove, W.F., Siggers, P.H. and Gardner, R.L. (1995) Homozygosity for the Min allele of Apc results in disruption of mouse development prior to gastrulation. *Developmental dynamics : an official publication of the American Association of Anatomists,* 203 (4), pp. 422-433.

Muller, P.A., Caswell, P.T., Doyle, B., Iwanicki, M.P., Tan, E.H., Karim, S., Lukashchuk, N., Gillespie, D.A., Ludwig, R.L., Gosselin, P., Cromer, A., Brugge, J.S., Sansom, O.J., Norman, J.C. and Vousden, K.H. (2009) Mutant p53 drives invasion by promoting integrin recycling. *Cell,* 139 (7), pp. 1327-1341.

Muncan, V., Sansom, O.J., Tertoolen, L., Phesse, T.J., Begthel, H., Sancho, E., Cole, A.M., Gregorieff, A., de Alboran, I.M., Clevers, H. and Clarke, A.R. (2006) Rapid loss of intestinal crypts upon conditional deletion of the Wnt/Tcf-4 target gene c-Myc. *Molecular and cellular biology,* 26 (22), pp. 8418-8426.

Munemitsu, S., Albert, I., Rubinfeld, B. and Polakis, P. (1996) Deletion of an amino-terminal sequence beta-catenin in vivo and promotes hyperphosporylation of the adenomatous polyposis coli tumor suppressor protein. *Molecular and cellular biology,* 16 (8), pp. 4088-4094.

Murphy, T.K., Calle, E.E., Rodriguez, C., Kahn, H.S. and Thun, M.J. (2000) Body mass index and colon cancer mortality in a large prospective study. *American Journal of Epidemiology,* 152 (9), pp. 847-854.

Neutra, M.R., Frey, A. and Kraehenbuhl, J.P. (1996) Epithelial M cells: gateways for mucosal infection and immunization. *Cell,* 86 (3), pp. 345-348.

Nielsen, A.L., Oulad-Abdelghani, M., Ortiz, J.A., Remboutsika, E., Chambon, P. and Losson, R. (2001a) Heterochromatin formation in mammalian cells: interaction between histones and HP1 proteins. *Molecular cell,* 7 (4), pp. 729-739.

Nielsen, A.L., Sanchez, C., Ichinose, H., Cervino, M., Lerouge, T., Chambon, P. and Losson, R. (2002a) Selective interaction between the chromatin-remodeling factor BRG1 and the heterochromatin-associated protein HP1alpha. *The EMBO journal,* 21 (21), pp. 5797-5806.

Nielsen, P.R., Nietlispach, D., Mott, H.R., Callaghan, J., Bannister, A., Kouzarides, T., Murzin, A.G., Murzina, N.V. and Laue, E.D. (2002b) Structure of the HP1 chromodomain bound to histone H3 methylated at lysine 9. *Nature,* 416 (6876), pp. 103-107.

Nielsen, S.J., Schneider, R., Bauer, U.M., Bannister, A.J., Morrison, A., O'Carroll, D., Firestein, R., Cleary, M., Jenuwein, T., Herrera, R.E. and Kouzarides, T. (2001b) Rb targets histone H3 methylation and HP1 to promoters. *Nature,* 412 (6846), pp. 561-565.

Norat, T., Lukanova, A., Ferrari, P. and Riboli, E. (2002) Meat consumption and colorectal cancer risk: dose-response meta-analysis of epidemiological studies. *International journal of cancer.Journal international du cancer,* 98 (2), pp. 241-256.

Park, Y., Hunter, D.J., Spiegelman, D., Bergkvist, L., Berrino, F., van den Brandt, P.A., Buring, J.E., Colditz, G.A., Freudenheim, J.L., Fuchs, C.S., Giovannucci, E., Goldbohm, R.A., Graham, S., Harnack, L., Hartman, A.M., Jacobs, D.R.,Jr, Kato, I., Krogh, V., Leitzmann, M.F., McCullough, M.L., Miller, A.B., Pietinen, P., Rohan, T.E., Schatzkin, A., Willett, W.C., Wolk, A., Zeleniuch-Jacquotte, A., Zhang, S.M. and Smith-Warner, S.A. (2005) Dietary fiber intake and risk of colorectal cancer: a pooled analysis of prospective cohort studies. *JAMA : the journal of the American Medical Association,* 294 (22), pp. 2849-2857.

Parry, L., Young, M., El Marjou, F. and Clarke, A.R. (2013) Evidence for a crucial role of paneth cells in mediating the intestinal response to injury. *Stem cells (Dayton, Ohio),* 31 (4), pp. 776-785.

Patman, G. (2015) Colorectal cancer: Male hormones increase the incidence of colonic adenomas. *Nature reviews.Gastroenterology & hepatology,* 12 (1), pp. 4.

Paulsson, M. (1992) The role of laminin in attachment, growth, and differentiation of cultured cells: a brief review. *Cytotechnology,* 9 (1-3), pp. 99-106.

Pearce, J.J., Singh, P.B. and Gaunt, S.J. (1992) The mouse has a Polycomb-like chromobox gene. *Development (Cambridge, England),* 114 (4), pp. 921-929.

Peng, J.C. and Karpen, G.H. (2009) Heterochromatic genome stability requires regulators of histone H3 K9 methylation. *PLoS genetics,* 5 (3), pp. e1000435.

Peng, J.C. and Karpen, G.H. (2007) H3K9 methylation and RNA interference regulate nucleolar organization and repeated DNA stability. *Nature cell biology,* 9 (1), pp. 25-35.

Petitjean, A., Mathe, E., Kato, S., Ishioka, C., Tavtigian, S.V., Hainaut, P. and Olivier, M. (2007) Impact of mutant p53 functional properties on TP53 mutation patterns and tumor phenotype: lessons from recent developments in the IARC TP53 database. *Human mutation,* 28 (6), pp. 622-629.

Piacentini, L., Fanti, L., Berloco, M., Perrini, B. and Pimpinelli, S. (2003) Heterochromatin protein 1 (HP1) is associated with induced gene expression in Drosophila euchromatin. *The Journal of cell biology,* 161 (4), pp. 707-714.

Pinson, K.I., Brennan, J., Monkley, S., Avery, B.J. and Skarnes, W.C. (2000) An LDL-receptor-related protein mediates Wnt signalling in mice. *Nature,* 407 (6803), pp. 535-538.

Pinto, D., Gregorieff, A., Begthel, H. and Clevers, H. (2003) Canonical Wnt signals are essential for homeostasis of the intestinal epithelium. *Genes & development,* 17 (14), pp. 1709-1713.

Pitman, R.S. and Blumberg, R.S. (2000) First line of defense: the role of the intestinal epithelium as an active component of the mucosal immune system. *Journal of gastroenterology,* 35 (11), pp. 805-814.

Pogribny, I.P., Ross, S.A., Tryndyak, V.P., Pogribna, M., Poirier, L.A. and Karpinets, T.V. (2006) Histone H3 lysine 9 and H4 lysine 20 trimethylation and the expression of Suv4-20h2 and Suv-39h1 histone methyltransferases in hepatocarcinogenesis induced by methyl deficiency in rats. *Carcinogenesis,* 27 (6), pp. 1180-1186.

Popova, E.Y., Claxton, D.F., Lukasova, E., Bird, P.I. and Grigoryev, S.A. (2006) Epigenetic heterochromatin markers distinguish terminally differentiated leukocytes from incompletely differentiated leukemia cells in human blood. *Experimental hematology,* 34 (4), pp. 453-462.

Potten, C.S. (1974) The epidermal proliferative unit: the possible role of the central basal cell. *Cell and tissue kinetics,* 7 (1), pp. 77-88.

Potten, C.S., Booth, C., Tudor, G.L., Booth, D., Brady, G., Hurley, P., Ashton, G., Clarke, R., Sakakibara, S. and Okano, H. (2003) Identification of a putative intestinal stem cell and early lineage marker; musashi-1. *Differentiation; research in biological diversity,* 71 (1), pp. 28-41.

Potten, C.S. and Loeffler, M. (1990) Stem cells: attributes, cycles, spirals, pitfalls and uncertainties. Lessons for and from the crypt. *Development (Cambridge, England),* 110 (4), pp. 1001-1020.

Purdie, C.A., O'Grady, J., Piris, J., Wyllie, A.H. and Bird, C.C. (1991) P53 Expression in Colorectal Tumors. *The American journal of pathology,* 138 (4), pp. 807-813.

Rajagopalan, H., Bardelli, A., Lengauer, C., Kinzler, K.W., Vogelstein, B. and Velculescu, V.E. (2002) Tumorigenesis: RAF/RAS oncogenes and mismatch-repair status. *Nature,* 418 (6901), pp. 934.

Ramalho-Santos, M., Melton, D.A. and McMahon, A.P. (2000) Hedgehog signals regulate multiple aspects of gastrointestinal development. *Development (Cambridge, England),* 127 (12), pp. 2763-2772.

Rea, S., Eisenhaber, F., O'Carroll, D., Strahl, B.D., Sun, Z.W., Schmid, M., Opravil, S., Mechtler, K., Ponting, C.P., Allis, C.D. and Jenuwein, T. (2000) Regulation of chromatin structure by site-specific histone H3 methyltransferases. *Nature,* 406 (6796), pp. 593-599.

Reed, K.R., Athineos, D., Meniel, V.S., Wilkins, J.A., Ridgway, R.A., Burke, Z.D., Muncan, V., Clarke, A.R. and Sansom, O.J. (2008a) B-catenin deficiency, but not Myc deletion, suppresses the immediate phenotypes of APC loss in the liver. *Proceedings of the National Academy of Sciences of the United States of America,* 105 (48), pp. 18919-18923.

Reed, K.R., Meniel, V.S., Marsh, V., Cole, A., Sansom, O.J. and Clarke, A.R. (2008b) A limited role for p53 in modulating the immediate phenotype of Apc loss in the intestine. *BMC cancer,* 8, pp. 162-2407-8-162.

Reed, K.R., Tunster, S.J., Young, M., Carrico, A., John, R.M. and Clarke, A.R. (2012) Entopic overexpression of Ascl2 does not accelerate tumourigenesis in ApcMin mice. *Gut,* 61 (10), pp. 1435-1438.

Rijsewijk, F., Schuermann, M., Wagenaar, E., Parren, P., Weigel, D. and Nusse, R. (1987) The Drosophila homolog of the mouse mammary oncogene int-1 is identical to the segment polarity gene wingless. *Cell,* 50 (4), pp. 649-657.

Roose, J., Molenaar, M., Peterson, J., Hurenkamp, J., Brantjes, H., Moerer, P., van de Wetering, M., Destree, O. and Clevers, H. (1998) The Xenopus Wnt effector XTcf-3 interacts with Groucho-related transcriptional repressors. *Nature,* 395 (6702), pp. 608-612.

Rubinfeld, B., Albert, I., Porfiri, E., Fiol, C., Munemitsu, S. and Polakis, P. (1996) Binding of GSK3beta to the APC-beta-catenin complex and regulation of complex assembly. *Science (New York, N.Y.),* 272 (5264), pp. 1023-1026.

Saini, V., Hose, C.D., Monks, A., Nagashima, K., Han, B., Newton, D.L., Millione, A., Shah, J., Hollingshead, M.G., Hite, K.M., Burkett, M.W., Dolosh, R.M., Silvers, T.E., Scudiero, D.A.,

Shoemaker, R.H. (2012) Identification of CBX3 and ABCA5 as putative biomarkers for tumor stem cells in osteosarcoma. *PLoS One*, 7, 8, e41401

Saint-Andre, V., Batsche, E., Rachez, C. and Muchardt, C. (2011) Histone H3 lysine 9 trimethylation and HP1gamma favor inclusion of alternative exons. *Nature structural & molecular biology,* 18 (3), pp. 337-344.

Sancho, E., Batlle, E. and Clevers, H. (2004) Signaling pathways in intestinal development and cancer. *Annual Review of Cell and Developmental Biology,* 20, pp. 695-723.

Sangiorgi, E. and Capecchi, M.R. (2008) Bmi1 is expressed in vivo in intestinal stem cells. *Nature genetics,* 40 (7), pp. 915-920.

Sansal, I. and Sellers, W.R. (2004) The biology and clinical relevance of the PTEN tumor suppressor pathway. *Journal of clinical oncology : official journal of the American Society of Clinical Oncology,* 22 (14), pp. 2954-2963.

Sansom, O.J., Meniel, V., Wilkins, J.A., Cole, A.M., Oien, K.A., Marsh, V., Jamieson, T.J., Guerra, C., Ashton, G.H., Barbacid, M. and Clarke, A.R. (2006) Loss of Apc allows phenotypic manifestation of the transforming properties of an endogenous K-ras oncogene in vivo. *Proceedings of the National Academy of Sciences of the United States of America,* 103 (38), pp. 14122-14127.

Sansom, O.J., Reed, K.R., Hayes, A.J., Ireland, H., Brinkmann, H., Newton, I.P., Batlle, E., Simon-Assmann, P., Clevers, H., Nathke, I.S., Clarke, A.R. and Winton, D.J. (2004a) Loss of Apc in vivo immediately perturbs Wnt signaling, differentiation, and migration. *Genes & development,* 18 (12), pp. 1385-1390.

Sato, A. (2007) Tuft cells. *Anatomical science international,* 82 (4), pp. 187-199.

Sato, T., van Es, J.H., Snippert, H.J., Stange, D.E., Vries, R.G., van den Born, M., Barker, N., Shroyer, N.F., van de Wetering, M. and Clevers, H. (2011a) Paneth cells constitute the niche for Lgr5 stem cells in intestinal crypts. *Nature,* 469 (7330), pp. 415-418.

Sato, T., Vries, R.G., Snippert, H.J., van de Wetering, M., Barker, N., Stange, D.E., van Es, J.H., Abo, A., Kujala, P., Peters, P.J. and Clevers, H. (2009) Single Lgr5 stem cells build crypt-villus structures in vitro without a mesenchymal niche. *Nature,* 459 (7244), pp. 262-265.

Sawan, C. and Herceg, Z. (2010) Histone modifications and cancer. *Advances in Genetics,* 70, pp. 57-85.

Sawan, C., Vaissiere, T., Murr, R. and Herceg, Z. (2008) Epigenetic drivers and genetic passengers on the road to cancer. *Mutation research,* 642 (1-2), pp. 1-13.

Schnelzer, A., Prechtel, D., Knaus, U., Dehne, K., Gerhard, M., Graeff, H., Harbeck, N., Schmitt, M. and Lengyel, E. (2000) Rac1 in human breast cancer: overexpression, mutation analysis, and characterization of a new isoform, Rac1b. *Oncogene,* 19 (26), pp. 3013-3020.

Schotta, G., Lachner, M., Sarma, K., Ebert, A., Sengupta, R., Reuter, G., Reinberg, D. and Jenuwein, T. (2004a) A silencing pathway to induce H3-K9 and H4-K20 trimethylation at constitutive heterochromatin. *Genes & development,* 18 (11), pp. 1251-1262.

Schotta, G., Sengupta, R., Kubicek, S., Malin, S., Kauer, M., Callen, E., Celeste, A., Pagani, M., Opravil, S., De La Rosa-Velazquez, I.A., Espejo, A., Bedford, M.T., Nussenzweig, A., Busslinger, M. and Jenuwein, T. (2008) A chromatin-wide transition to H4K20 monomethylation impairs genome integrity and programmed DNA rearrangements in the mouse. *Genes & development,* 22 (15), pp. 2048-2061.

Schulz, W.A., Elo, J.P., Florl, A.R., Pennanen, S., Santourlidis, S., Engers, R., Buchardt, M., Seifert, H.H. and Visakorpi, T. (2002) Genomewide DNA hypomethylation is associated with alterations on chromosome 8 in prostate carcinoma. *Genes, chromosomes & cancer,* 35 (1), pp. 58-65.

Sharma, G.G., Hwang, K.K., Pandita, R.K., Gupta, A., Dhar, S., Parenteau, J., Agarwal, M., Worman, H.J., Wellinger, R.J. and Pandita, T.K. (2003a) Human heterochromatin protein 1 isoforms HP1(Hsalpha) and HP1(Hsbeta) interfere with hTERT-telomere interactions and correlate with changes in cell growth and response to ionizing radiation. *Molecular and cellular biology,* 23 (22), pp. 8363-8376.

Sharma, S., Kelly, T.K. and Jones, P.A. (2010) Epigenetics in cancer. *Carcinogenesis,* 31 (1), pp. 27-36.

Shechter, D., Dormann, H.L., Allis, C.D. and Hake, S.B. (2007) Extraction, purification and analysis of histones. *Nature protocols,* 2 (6), pp. 1445-1457.

Shi, Y. and Massague, J. (2003) Mechanisms of TGF-beta signaling from cell membrane to the nucleus. *Cell,* 113 (6), pp. 685-700.

Shibata, H., Toyama, K., Shioya, H., Ito, M., Hirota, M., Hasegawa, S., Matsumoto, H., Takano, H., Akiyama, T., Toyoshima, K., Kanamaru, R., Kanegae, Y., Saito, I., Nakamura, Y., Shiba, K. and Noda, T. (1997) Rapid colorectal adenoma formation initiated by conditional targeting of the Apc gene. *Science (New York, N.Y.),* 278 (5335), pp. 120-123.

Shoemaker, A.R., Luongo, C., Moser, A.R., Marton, L.J. and Dove, W.F. (1997) Somatic mutational mechanisms involved in intestinal tumor formation in Min mice. *Cancer research,* 57 (10), pp. 1999-2006.

Siegel, P.M. and Massague, J. (2003) Cytostatic and apoptotic actions of TGF-beta in homeostasis and cancer. *Nature reviews.Cancer,* 3 (11), pp. 807-821.

Singh, A., Karnoub, A.E., Palmby, T.R., Lengyel, E., Sondek, J. and Der, C.J. (2004) Rac1b, a tumor associated, constitutively active Rac1 splice variant, promotes cellular transformation. *Oncogene,* 23 (58), pp. 9369-9380.

Singh, G., Kaur, S., Stock, J.L., Jenkins, N.A., Gilbert, D.J., Copeland, N.G. and Potter, S.S. (1991) Identification of 10 murine homeobox genes. *Proceedings of the National Academy of Sciences of the United States of America,* 88 (23), pp. 10706-10710.

Slattery, M.L., Potter, J.D., Curtin, K., Edwards, S., Ma, K.N., Anderson, K., Schaffer, D. and Samowitz, W.S. (2001) Estrogens reduce and withdrawal of estrogens increase risk of microsatellite instability-positive colon cancer. *Cancer research,* 61 (1), pp. 126-130.

Slezak, J., Truong, M., Huang, W. and Jarrard, D. (2013) HP1gamma expression is elevated in prostate cancer and is superior to Gleason score as a predictor of biochemical recurrence after radical prostatectomy. *BMC cancer,* 13, pp. 148-2407-13-148.

Smallwood, A., Esteve, P.O., Pradhan, S. and Carey, M. (2007) Functional cooperation between HP1 and DNMT1 mediates gene silencing. *Genes & development,* 21 (10), pp. 1169-1178.

Smallwood, A., Hon, G.C., Jin, F., Henry, R.E., Espinosa, J.M. and Ren, B. (2012) CBX3 regulates efficient RNA processing genome-wide. *Genome research,* 22 (8), pp. 1426-1436.

Smith, M.W. (1992) Diet effects on enterocyte development. *The Proceedings of the Nutrition Society,* 51 (2), pp. 173-178.

Snippert, H.J., van Es, J.H., van den Born, M., Begthel, H., Stange, D.E., Barker, N. and Clevers, H. (2009) Prominin-1/CD133 marks stem cells and early progenitors in mouse small intestine. *Gastroenterology,* 136 (7), pp. 2187-2194.e1.

Soriano, V. (1999) Prevalence of drug resistance mutations in Spain among both naive and pretreated patients. *Antiviral Therapy,* 4 Suppl 3, pp. 57-63.

Sternberg, N. and Hamilton, D. (1981) Bacteriophage P1 site-specific recombination. I. Recombination between loxP sites. *Journal of Molecular Biology,* 150 (4), pp. 467-486.

Stoffel, E.M. (2010) Lynch Syndrome/Hereditary Non-polyposis Colorectal Cancer (HNPCC). *Minerva gastroenterologica e dietologica,* 56 (1), pp. 45-53.

Su, L.K., Kinzler, K.W., Vogelstein, B., Preisinger, A.C., Moser, A.R., Luongo, C., Gould, K.A. and Dove, W.F. (1992) Multiple intestinal neoplasia caused by a mutation in the murine homolog of the APC gene. *Science (New York, N.Y.),* 256 (5057), pp. 668-670.

Takaku, K., Oshima, M., Miyoshi, H., Matsui, M., Seldin, M.F. and Taketo, M.M. (1998) Intestinal tumorigenesis in compound mutant mice of both Dpc4 (Smad4) and Apc genes. *Cell,* 92 (5), pp. 645-656.

Takanashi, M., Oikawa, K., Fujita, K., Kudo, M., Kinoshita, M. and Kuroda, M. (2009a) Heterochromatin protein 1gamma epigenetically regulates cell differentiation and exhibits potential as a therapeutic target for various types of cancers. *The American journal of pathology,* 174 (1), pp. 309-316.

Taketo, M.M. (2006) Wnt signaling and gastrointestinal tumorigenesis in mouse models. *Oncogene,* 25 (57), pp. 7522-7530.

Tamai, K., Zeng, X., Liu, C., Zhang, X., Harada, Y., Chang, Z. and He, X. (2004) A mechanism for Wnt coreceptor activation. *Molecular cell,* 13 (1), pp. 149-156.

Tamura, M., Gu, J., Matsumoto, K., Aota, S., Parsons, R. and Yamada, K.M. (1998) Inhibition of cell migration, spreading, and focal adhesions by tumor suppressor PTEN. *Science (New York, N.Y.),* 280 (5369), pp. 1614-1617.

Thiagalingam, S., Lengauer, C., Leach, F.S., Schutte, M., Hahn, S.A., Overhauser, J., Willson, J.K., Markowitz, S., Hamilton, S.R., Kern, S.E., Kinzler, K.W. and Vogelstein, B. (1996) Evaluation of candidate tumour suppressor genes on chromosome 18 in colorectal cancers. *Nature genetics,* 13 (3), pp. 343-346.

Thiru, A., Nietlispach, D., Mott, H.R., Okuwaki, M., Lyon, D., Nielsen, P.R., Hirshberg, M., Verreault, A., Murzina, N.V. and Laue, E.D. (2004) Structural basis of HP1/PXVXL motif peptide interactions and HP1 localisation to heterochromatin. *The EMBO journal,* 23 (3), pp. 489-499.

Thyagarajan, B., Guimaraes, M.J., Groth, A.C. and Calos, M.P. (2000) Mammalian genomes contain active recombinase recognition sites. *Gene,* 244 (1-2), pp. 47-54.

Tian, H., Biehs, B., Warming, S., Leong, K.G., Rangell, L., Klein, O.D. and de Sauvage, F.J. (2011) A reserve stem cell population in small intestine renders Lgr5-positive cells dispensable. *Nature,* 478 (7368), pp. 255-259.

Todaro, M., Gaggianesi, M., Catalano, V., Benfante, A., Iovino, F., Biffoni, M., Apuzzo, T., Sperduti, I., Volpe, S., Cocorullo, G., Gulotta, G., Dieli, F., De Maria, R. and Stassi, G. (2014) CD44v6 is a marker of constitutive and reprogrammed cancer stem cells driving colon cancer metastasis. *Cell stem cell,* 14 (3), pp. 342-356.

Trojer, P. and Reinberg, D. (2007) Facultative heterochromatin: is there a distinctive molecular signature? *Molecular cell,* 28 (1), pp. 1-13.

Troughton, W.D. and Trier, J.S. (1969) Paneth and goblet cell renewal in mouse duodenal crypts. *The Journal of cell biology,* 41 (1), pp. 251-268.

Tsuda, H., Takarabe, T., Kanai, Y., Fukutomi, T. and Hirohashi, S. (2002) Correlation of DNA hypomethylation at pericentromeric heterochromatin regions of chromosomes 16 and 1 with histological features and chromosomal abnormalities of human breast carcinomas. *The American journal of pathology,* 161 (3), pp. 859-866.

Vakoc, C.R., Mandat, S.A., Olenchock, B.A. and Blobel, G.A. (2005a) Histone H3 lysine 9 methylation and HP1gamma are associated with transcription elongation through mammalian chromatin. *Molecular cell,* 19 (3), pp. 381-391.

van de Wetering, M., Sancho, E., Verweij, C., de Lau, W., Oving, I., Hurlstone, A., van der Horn, K., Batlle, E., Coudreuse, D., Haramis, A.P., Tjon-Pon-Fong, M., Moerer, P., van den Born, M., Soete, G., Pals, S., Eilers, M., Medema, R. and Clevers, H. (2002) The beta-catenin/TCF-4 complex imposes a crypt progenitor phenotype on colorectal cancer cells. *Cell,* 111 (2), pp. 241-250.

van den Brink, G.R. (2007) Hedgehog signaling in development and homeostasis of the gastrointestinal tract. *Physiological Reviews,* 87 (4), pp. 1343-1375.

van der Flier, L.G., Haegebarth, A., Stange, D.E., van de Wetering, M. and Clevers, H. (2009a) OLFM4 is a robust marker for stem cells in human intestine and marks a subset of colorectal cancer cells. *Gastroenterology,* 137 (1), pp. 15-17.

van der Flier, L.G., van Gijn, M.E., Hatzis, P., Kujala, P., Haegebarth, A., Stange, D.E., Begthel, H., van den Born, M., Guryev, V., Oving, I., van Es, J.H., Barker, N., Peters, P.J., van de Wetering, M. and Clevers, H. (2009b) Transcription factor achaete scute-like 2 controls intestinal stem cell fate. *Cell,* 136 (5), pp. 903-912.

van Engeland, M., Roemen, G.M., Brink, M., Pachen, M.M., Weijenberg, M.P., de Bruine, A.P., Arends, J.W., van den Brandt, P.A., de Goeij, A.F. and Herman, J.G. (2002) K-ras mutations and RASSF1A promoter methylation in colorectal cancer. *Oncogene,* 21 (23), pp. 3792-3795.

van Es, J.H., van Gijn, M.E., Riccio, O., van den Born, M., Vooijs, M., Begthel, H., Cozijnsen, M., Robine, S., Winton, D.J., Radtke, F. and Clevers, H. (2005) Notch/gamma-secretase inhibition turns proliferative cells in intestinal crypts and adenomas into goblet cells. *Nature,* 435 (7044), pp. 959-963.

Varambally,S.; Dhanasekaran,S.M.; Zhou,M.; Barrette,T.R.; KumarSinha,C.; Sanda,M.G.; Ghosh,D.;Pienta,K.J.; Sewalt,R.G.; Otte,A.P.; Rubin,M.A.; Chinnaiyan,A.M.(2002) The polycomb group protein EZH2 is involved in progression of prostate cancer. Nature, 419 (6907), pp 624-629.

Vousden, K.H. and Lane, D.P. (2007) P53 in Health and Disease. *Nature reviews.Molecular cell biology,* 8 (4), pp. 275-283.

Waddington, C.H. (1939) Preliminary Notes on the Development of the Wings in Normal and Mutant Strains of Drosophila. *Proceedings of the National Academy of Sciences of the United States of America,* 25 (7), pp. 299-307.

Wang, G., Xiao, Q., Luo, Z., Ye, S. and Xu, Q. (2012) Functional impact of heterogeneous nuclear ribonucleoprotein A2/B1 in smooth muscle differentiation from stem cells and embryonic arteriogenesis. *The Journal of biological chemistry,* 287 (4), pp. 2896-2906.

Waterman, M.L. (2002) Expression of lymphoid enhancer factor/T-cell factor proteins in colon cancer. *Current opinion in gastroenterology,* 18 (1), pp. 53-59.

Williams, L. and Grafi, G. (2000) The retinoblastoma protein - a bridge to heterochromatin. *Trends in plant science,* 5 (6), pp. 239-240.

Wilson, A. and Radtke, F. (2006) Multiple functions of Notch signaling in self-renewing organs and cancer. *FEBS letters,* 580 (12), pp. 2860-2868.

Wolin, K.Y., Yan, Y. and Colditz, G.A. (2011) Physical activity and risk of colon adenoma: a meta-analysis. *British journal of cancer,* 104 (5), pp. 882-885.

Wongtawan, T., Taylor, J.E., Lawson, K.A., Wilmut, I. and Pennings, S. (2011) Histone H4K20me3 and HP1alpha are late heterochromatin markers in development, but present in undifferentiated embryonic stem cells. *Journal of cell science,* 124 (Pt 11), pp. 1878-1890.

Xiao, Q., Wang, G., Yin, X., Luo, Z., Margariti, A., Zeng, L., Mayr, M., Ye, S. and Xu, Q. (2011) Chromobox protein homolog 3 is essential for stem cell differentiation to smooth muscles in vitro and in embryonic arteriogenesis. *Arteriosclerosis, Thrombosis, and Vascular Biology,* 31 (8), pp. 1842-1852.

Xue, G., Restuccia, D.F., Lan, Q., Hynx, D., Dirnhofer, S., Hess, D., Ruegg, C. and Hemmings, B.A. (2012) Akt/PKB-mediated phosphorylation of Twist1 promotes tumor metastasis via mediating cross-talk between PI3K/Akt and TGF-beta signaling axes. *Cancer discovery,* 2 (3), pp. 248-259.

Yan, K.S., Chia, L.A., Li, X., Ootani, A., Su, J., Lee, J.Y., Su, N., Luo, Y., Heilshorn, S.C., Amieva, M.R., Sangiorgi, E., Capecchi, M.R. and Kuo, C.J. (2012) The intestinal stem cell markers Bmi1 and Lgr5 identify two functionally distinct populations. *Proceedings of the National Academy of Sciences of the United States of America,* 109 (2), pp. 466-471.

Yan, S.J., Lim, S.J., Shi, S., Dutta, P. and Li, W.X. (2011) Unphosphorylated STAT and heterochromatin protect genome stability. *FASEB journal : official publication of the Federation of American Societies for Experimental Biology,* 25 (1), pp. 232-241.

Ye, Q. and Worman, H.J. (1996) Interaction between an integral protein of the nuclear envelope inner membrane and human chromodomain proteins homologous to Drosophila HP1. *The Journal of biological chemistry,* 271 (25), pp. 14653-14656.

Yingling, J.M., Blanchard, K.L. and Sawyer, J.S. (2004) Development of TGF-beta signalling inhibitors for cancer therapy. *Nature reviews.Drug discovery,* 3 (12), pp. 1011-1022.

Zeng, A., Li, Y.Q., Wang, C., Han, X.S., Li, G., Wang, J.Y., Li, D.S., Qin, Y.W., Shi, Y., Brewer, G. and Jing, Q. (2013) Heterochromatin protein 1 promotes self-renewal and triggers regenerative proliferation in adult stem cells. *The Journal of cell biology,* 201 (3), pp. 409-425.

Zhang, C.L., McKinsey, T.A. and Olson, E.N. (2002) Association of class II histone deacetylases with heterochromatin protein 1: potential role for histone methylation in control of muscle differentiation. *Molecular and cellular biology,* 22 (20), pp. 7302-7312.

Zhao, T., Heyduk, T. and Eissenberg, J.C. (2001) Phosphorylation site mutations in heterochromatin protein 1 (HP1) reduce or eliminate silencing activity. *The Journal of biological chemistry,* 276 (12), pp. 9512-9518.

Zhou, J., Bi, H., Zhan, P., Chang, C., Xu, C., Huang, X., Yu, L., Yao, X. and Yan, J. (2014) Overexpression of HP1gamma is associated with poor prognosis in non-small cell lung cancer cell through promoting cell survival. *Tumour biology : the journal of the International Society for Oncodevelopmental Biology and Medicine,* 35 (10), pp. 9777-9785.